



HAL
open science

Organic electrografted thin films based nano-devices

Florian Lebon

► **To cite this version:**

Florian Lebon. Organic electrografted thin films based nano-devices. Material chemistry. Université Paris Saclay (COMUE), 2019. English. NNT : 2019SACLS286 . tel-02317642

HAL Id: tel-02317642

<https://theses.hal.science/tel-02317642v1>

Submitted on 16 Oct 2019

HAL is a multi-disciplinary open access archive for the deposit and dissemination of scientific research documents, whether they are published or not. The documents may come from teaching and research institutions in France or abroad, or from public or private research centers.

L'archive ouverte pluridisciplinaire **HAL**, est destinée au dépôt et à la diffusion de documents scientifiques de niveau recherche, publiés ou non, émanant des établissements d'enseignement et de recherche français ou étrangers, des laboratoires publics ou privés.

Nano-composants à base de films minces organiques électrogreffés : Fabrication, caractérisation, étude du transport électronique et intégration

Organic electrografted thin films based nano-devices

Thèse de doctorat de l'Université Paris-Saclay
préparée à l'Université Paris-Sud

Ecole doctorale n°571 Sciences Chimiques : Molécules, Matériaux, Instrumentation
et Biosystèmes (2MIB)
Spécialité de doctorat : Chimie

Thèse présentée et soutenue à Gif-sur-Yvette, le 30 Septembre 2019, par

FLORIAN LEBON

Composition du Jury :

Dominique Vuillaume Directeur de Recherche, CNRS	Rapporteur
Jalal Ghilane Chargé de Recherche, Université Paris Diderot	Rapporteur
Caroline Cannizzo Maître de Conférence, Université Evry Val d'Essonne	Examinatrice
Jean-Christophe Lacroix Professeur, Université Paris Diderot	Président du jury
Vincent Derycke Chercheur CEA, CEA Saclay	Co-encadrant
Bruno Jousselme Chercheur CEA, CEA Saclay	Directeur de thèse

Remerciements

Je tiens à commencer par remercier mes deux encadrants, Bruno et Vincent, qui ont su me supporter pendant 3 ans. Énormément de choses les différencient, notamment leur façon de travailler, de me relire ainsi que leur domaine de prédilection, mais ils ont réussi à s'accorder à peu près sur mon encadrement, et ils ont ainsi toujours pu apporter l'aide dont j'ai eu besoin pour l'avancée de mes recherches. Évidemment, chacun a ses petits défauts, et ce ne fût pas tous les jours facile de gérer ceux-ci ! Malgré ça, ils ont toujours en confiance en mes choix, même si ceux-ci ne leur paraissaient pas convaincants au début. De plus, ils ont réussi à s'adapter à mon optimisme impressionnant, et j'espère qu'ils ne sont pas marqués à vie par mes arrivées dans leurs bureaux avec des résultats corrects et comme phrase d'introduction : "Bon, c'est pas fufou, mais voici ce que j'ai eu".

J'aimerais aussi remercier Serge Palacin, le chef du NIMBE, qui a toujours su rester très impliqué dans les activités du LICSEN et, aussi, très intéressé par mon sujet. Le reste de l'équipe administrative du NIMBE m'a aussi beaucoup assisté dans toutes les tâches administratives auxquelles j'ai dû faire face.

Ensuite, je tiens à rappeler que beaucoup de mes connaissances de lithographie et d'électrogreffage m'ont été enseignées par les deux précédents étudiants sur ce sujet : Hugo et surtout Yu-Pu. Je me souviendrai souvent de nos petites compétitions de démineur et de Freecell lors de séances d'électrogreffage intenses ! Dans le même ordre d'idée, Pief m'a énormément assisté pour toute la lithographie optique, et son aide m'a été bien précieuse à de nombreuses reprises.

Je tiens aussi à remercier toutes les personnes qui ont pu passer dans mon bureau : Caue au tout début, puis Andrea et son parrain durant mon stage. Ensuite, de nouvelles têtes m'ont rejoint dans ce magnifique bureau, et m'ont accompagnées pendant un moment : Thomas, avec qui nous avons mis en place un magnifique aquarium qui a subi une première apocalypse (en espérant qu'il n'y en aura pas une seconde !); Sarah, dont le franc-parler légendaire a permis d'avoir de nombreuses discussions sympathiques et intéressantes et Robin, qui était bien souvent l'un de mes compagnons d'arrivée de bonne heure et qui était toujours de bonne humeur malgré ses déboires avec l'administration française ! Je remercie évidemment tous les autres qui ont pu passer par mon bureau, mais dont ma mémoire à très court terme ne m'a pas permis de nommer lors de l'écriture de ces remerciements.

Je remercie aussi tous les membres du laboratoire qui m'ont accompagné, notamment Kévin et Aurélien, arrivés en thèse en même temps que moi. Je n'oublierai jamais les discussions que j'ai eues avec eux, ainsi que les techniques de gitan forain de Kévin pour beaucoup de manips et les déboires d'Aurélien dans un bâtiment qui ne devrait plus être. J'en profite pour remercier rapidement les permanents et non-permanents

avec qui j'ai eu de nombreuses discussions intéressantes sur des sujets plus ou moins professionnels : Maud, la meilleure technicienne, Julie, dont on se demande toujours où est sa main droite, Guy, aussi appelé père Castor, Renaud aux 253 SECM, Fanny au rire tonitruant, et plein d'autres.

Finalement, mes derniers remerciements se dirigent vers mes amis proches et ma famille, qui ont su me supporter pendant 3 ans, notamment Cédric, avec qui j'ai eu l'occasion d'avoir de nombreuses discussions extrêmement intéressantes et qui a suivi mon évolution de très près. J'ai énormément apprécié son soutien, ainsi que les nombreux moments passés ensemble autour d'une table et de jeux de société de qualité plus ou moins douteuse. Enfin, je ne peux que conclure par Estelle, ma jeune demoiselle qui arrive encore et toujours à supporter mon humour douteux et mon honnêteté extrême, et qui va malheureusement devoir continuer encore un bon moment !

Contents

Contents	6
Introduction	7
I Context and positioning	11
I.1 Transistors	12
I.1.1 Channel material in organic and nano-material based transistors	12
I.1.2 Organic gate-dielectrics in transistors	15
I.2 Two-terminal memory devices and memristors	20
I.2.1 Metal-Insulator-Metal memristors	21
I.2.2 Organic memristors	22
I.2.3 Aim of the work in this context	24
II Diazonium salt electrografting on patterned micrometer sized electrodes	29
II.1 Diazonium electrografting	29
II.2 Electrografting of the diazonium salts	33
II.3 Physico-chemical characterization of the layers grafted	36
II.4 Control of the thickness of the layer grafted	42
II.4.1 TBPF _e electrografting	44
II.4.2 DzF ₈ and Thio electrografting	49
III Double layer electrografting	53
III.1 Electrochemical grafting of the double layer	54
III.2 Physical characterization of the grafted double layers	58
IV Printed gold nanoparticle top electrode	65
IV.1 State of the art	65
IV.2 Printing a gold nanoparticle top electrode	67
IV.2.1 Printing process and analysis of printed gold nanoparticle electrodes	67
IV.2.2 Printed gold electrodes deposited on ECG layers	75
V Electronic devices using ECG layers	79
V.1 Electrical properties of the ECG layers in vertical metal-molecules-metal junctions with evaporated metal as top electrodes	79
V.1.1 Conductivity of the ECG layers	79
V.1.2 Breakdown voltage of the ECG layers	82
V.1.3 Capacitance of the ECG layers	84
V.2 MoS ₂ transistors with ECG dielectrics	86

CONTENTS

Conclusion	93
Experimental	97
SI	98
References	114
Notations	115
Résumé	117

Introduction

Modern electronics relies on the use of a huge number of transistors on the same chip. In 1971, the first Intel computers used processors with 2 300 transistors, while it has risen to more than 23 billions on the GC2 IPU from Graphcore, commercialized in 2018. The size of a single transistor transitioned from 10 μm to only 16 nm in less than 50 years. While the progress is astonishing, it was predicted in 1965 in what is commonly referred as Moore's law [1]. It states that the number of transistors in a circuit would double every two years. However, the increase of the number of transistors in chips is slowing down [2]. In the same time, electronics have found new uses : while it was mostly aimed for high-end technologies, such as computers and phones, it is now spreading in a lot of low-end technologies, such as wearable devices, disposable bio-sensors, etc. This is due to the rise of the Internet of Things (IoT), which corresponds to the trend towards connecting everyday objects in a near future. While the maturity and the performances of silicon electronics qualify it to be naturally used in this domain, there are limitation to its exclusive prevalence : silicon based chips are rigid, fragile, and too costly for their use in certain classes of applications. Moreover, some applications require the combination of functionalities that cannot all be addressed with a single technology, such as analog sensing, RFIDs, flexible displays, etc. Thus, opportunities for new combinations of materials and processes are opening.

Among the considered strategies to perform innovative electronic functions, organic and molecular electronics is a particularly active field. This domain was pioneered by various teams starting in the 1970s. It was early envisioned that molecules could one day be used in electronics and proposed that the richness and the variety of these compounds could be exploited to build efficient functions and devices. After more than 40 years of research in this domain, some industrial applications are getting standard, such as the organic light emitting diode (OLED) for high-brightness, low-power consumption displays. Since their first appearance on the market in 2003 in Kodak's digital cameras, more and more products use this technology, in particular an increasing proportion of smartphones. With the emergence of commercial flexible displays, the role of organics will keep growing.

Organic electronics combine interesting properties : different types of organic films can be conducting, semiconducting, insulating, emit or detect light, react to chemical changes, etc. Some can even be printed in roll-to-roll processes, while some can be produced at low cost and processed at low temperature. Devices using molecules or polymers are also expected to require less energy than conventional materials which is a key asset.

Organic electronics can be studied using different configurations. What is mostly used is multi-layered organic films, which consists in forming stacks of organic layers with different properties. This is the basis of OLEDs, organic photovoltaic cells and organic

thin film transistors (OTFTs). It usually results in layers thicker than 100 nm. Conversely, many groups also studied the electronic properties of organic materials at the single molecule level. STM measurements of a single molecule and molecular break junction measurements, have been used to probe the behavior of individual molecules. They considerably increased the general knowledge of how molecules transport current. However, these setups are not compatible with commercial devices. Another way to use molecules in electronic devices is by using self-assembled monolayers (SAMs). While it forms the thinnest possible molecular layers, being able to use them in electronic device is a hard feat to achieve and requires a particular care in the selection of the molecule/metal and molecule/substrate couples. Thus, a fourth way of forming organic layers for organic electronics that would combine both the ease of integration in devices shown by organic thin layers and thicknesses similar to the ones of SAMs would be particularly interesting.

Electrochemical grafting, which will be referred as electrografting through the rest of this document, could be an interesting alternative. It leads to the formation of organic thin layers of thickness between 5 and 100 nm. Their grafting is straightforward : the conducting or semi-conducting material that needs an organic coating just has to be used as a working electrode in an electrochemical setup. One other significant advantage of electrografting is that it grafts locally on the working electrode, and thus can be used to selectively graft different electrodes of the same chip with different molecules. At LICSEN, two devices using electrografted (ECG) layers in special configurations were previously studied : transistors using such layers as gate-dielectric and memristors using such layers as the memristive element [3, 4]. While it showed that ECG can be used for organic electronics, further studies are needed in order to better assess their potential. This notably supposed to considerably improve both the grafting protocols and the device performances.

In this PhD thesis, the main objective is to improve the ECG process in terms of quality, adjustability and reliability and then to use this improved control to evaluate the potential of ECG layers in vertical metal-molecules-metal junctions for electronics.

This work is presented through 5 chapters.

The first chapter presents examples of organic electronic devices. Two devices are specifically chosen when reviewing the state of the art : transistors and memristors. The main objective of this chapter is to recall the configurations of these devices using organic layers, and their main advantages and drawbacks. Then, the chapter includes a short presentation of the two devices using ECG previously made in the laboratory, with a particular focus on the limitations that should be addressed.

In the second chapter, a short review of the state of the art on electrografting is first presented. Then, the three diazonium salts used in this thesis are introduced and analyzed : one is a derivative from the tris-bipyridine iron (II) complex (**TBPFe**), one is a diazonium salt with a long fluorinated chain (**DzF8**) and the last one is a diazonium salt with a thiol function (**Thio**). Their behavior in a classic electrochemical cell is also studied, first by using classic macroscopic gold working electrodes, then on micro-sized patterned gold electrode. In this last part, a particular care is taken to shine light on the various parameters controlling the final thickness of the grafted layers.

The third chapter aims at presenting an original way of using electrografting for the sequential formation of organic films composed of two different layers. The process is first

described and studied by using macroscopic gold electrodes, with a focus on the ECG process and the electrochemical behavior of the resulting layer. Then, these layers are characterized using the same physico-chemical measurements than in the previous chapter. Finally, this process is performed on microsized patterned gold electrodes to verify its compatibility with such configuration and open the way to their integration in junctions.

The fourth chapter presents the work done on printing solution of metal nanoparticles to make metallic electrodes, first by showing what has already been done in the literature, then by presenting what has been achieved in this thesis. In order to get micrometer sized gold top electrodes on micrometer sized ECG electrodes, a novel way of combining inkjet printing of an aqueous gold nanoparticle solution with optical lithography is presented. Then, the compatibility of these printed gold electrodes with ECG layers as top electrodes on ECG layers is probed by doing electrical measurements.

The last chapter is devoted to vertical metal-molecules-metal junctions made using ECG layers as the molecular layer. In this chapter, the top electrodes are made using direct metal evaporation above the ECG layers. After showing which metal is the best choice for the top electrodes, the first part of this chapter tries to elucidate the different electrical behavior of each ECG layers. After careful examination of these results, the best candidate is chosen to be integrated as gate-dielectric in field-effect transistors where the channel material is a MoS₂ single layer flake made in the laboratory. The performances of the resulting FETs is studied, and the potential of ECG layers as a gate-dielectric for transistors is determined.

The conclusion propose an assessment of the various achievements of this thesis. It seeks to answer to the problematic exposed above, and proposes various perspectives opened by this work on ECG layers.

Chapter I

Context and positioning

Organic and molecular electronics originated in the 70s with the seminal works of Mann and Kuhn [5], Aviram and Ratner [6], Heeger and co-workers [7], Sagiv and co-workers [8]. They, and others, envisioned that, one day, the electronic properties of small molecules or polymers would be used to build devices and to process information. Almost fifty years later, this vision has not yet been fully realized but important knowledge has been gained on the transport properties of organic materials. Many types of organic devices have been demonstrated and a few successful commercial applications have even emerged.

Many devices showed interesting behavior when made using organic molecules : OLED [9, 10], diodes [11, 12], photodetectors [13], capacitors [14, 15], transistors [16], memristors [17, 18], etc. Since the first commercial application of OLEDs in 2003 with Kodak's EasyShare LS633 digital camera, this technology became more and more important, and is now widely used in screens. However, most of the other domains are still mostly studied at the laboratory scale.

While organic electronics has been studied for more than 40 years, its development was shadowed by the exceptional success of the mainstream silicon electronics branch. But nowadays, silicon starts meeting a few limitations, such as its incompatibility with flexible devices. Also, the increase in the number of transistors in chips using silicon electronics begins to slow down and departs from the Moore's law [1]. While it obviously does not invalidate the power of silicon electronics, it only highlights that future electronics could welcome additional combinations of materials and types of devices to fill the ever-growing needs of the "electronic-in-everything" era. Organic electronics is particularly adapted for flexible, all-substrate, low-cost and large surface devices. Its first widely used commercial application, OLEDs, is a strong indicator of its potential. A future where organic and silicon electronics could work together is foreseeable.

Organic electronics can be subdivided in different categories, depending of the way the molecules are studied. The most fundamental one is the single molecule electronics, where the electrical behavior of a single molecule is probed. While these are not compatible with the fabrication of devices, it gives a lot of information on how the electrons flow through molecules, and help the understanding of the behavior of more scalable organic devices. Another type of organic electronic devices uses self-assembled monolayers (SAMs), and gives interesting results. However, the molecules used for SAMs must have anchoring groups specific for the metal electrodes on which they will be used, meaning that this group must be changed when the metal is different. Finally, the most common organic devices, especially for applications, use thin layers of

evaporated or spin-coated molecules, which can be small molecules or polymers. The thickness of the resulting films are usually above 100 nm. This method fits the need of having large surface devices, but could be improved, notably in term of scalability by making thinner layers.

In the laboratory, an alternative to these layer deposition methods is studied : the electrochemical grafting of organic layers. Its main advantages are the formation of covalently bounded thin layers, giving access to thickness between 5 to 100 nm and the possibility to selectively graft different electrodes on the same chips with different molecules or thickness. Two types of devices using ECG layers have already been studied at LICSEN. The first one is a transistor using ECG layers as gate-dielectric and multilayer MoS₂ as the semiconducting channel, which showed good characteristics but also severe limitations [3]. The second one is a memristor using an ECG layer as the memristive element, and was used in a functional neuromorphic device [4].

This is the reason why the current state of transistors will first be presented, with a particular focus on organic transistors and transistors using nanoscaled materials. The different types of recent semi-conductors and dielectrics used for organic field effect transistors (OFETs) will be briefly described and compared. Then, two different types of memristors devices will be presented. Finally, two devices made in the laboratory using a novel way of doing organic thin layers for electronics are introduced : electrografted (ECG) layer.

I.1 Transistors

Organic transistors were first demonstrated in 1986 by the group of Tsumura et al [19]. Since then, many groups studied the interest of small molecules and polymers for transistors by changing the nature of two main parts of the transistors : the semi-conducting channel and the gate-dielectric layer [20]. More studies have been done on organic semi-conductors, with the most well-known being pentacene for the single molecules or polythiophene [16] for polymers, in combination with classic inorganic dielectric, usually SiO₂.

While they cannot be considered as organic electronic devices, it is interesting to consider here some other types of transistors that share some similarities with organic transistors : transistors made from semiconducting nanomaterials through a bottom-up approach. Indeed, some of these materials can be combined with organic dielectrics, a strategy that is particularly relevant to this thesis.

With the rise of studies on carbon nanotubes, transistors using those carbon materials [21, 22], including graphene [23], were studied starting in 1998 [24, 25]. More recently, two dimensional materials, such as phosphrene [26], WS₂ and MoS₂ [27], have been found to be of great interest as semi-conductors in transistors. Another type of materials that was used in a similar way are nanowires, such as silicon or indium phosphide nanowires [28, 29]. A table regrouping various semi-conductors used in transistors and their respective charge mobility is presented in table I.1.

I.1.1 Channel material in organic and nano-material based transistors

Semi-conductor	Polythiophene	Sexithiophene	Pentacene	Crystalline pentacene
$\mu(\text{cm}^2 \cdot (\text{V.s})^{-1})$	0.12	10^{-3}	2.17	40
Year	2004	1989	2012	2007
Semi-conductor	Single CNT	Arrays of CNTs	MoS ₂ multi-layers	MoS ₂ monolayer
$\mu(\text{cm}^2 \cdot (\text{V.s})^{-1})$	79 000	100-200	200-500	54
Year	2004	2014	1967	2013

Table I.1: Data table for the charge mobility measured for various semi-conductors.

Organic materials

The first organic field effect transistors (OFETs) were demonstrated between 1983 and 1986 by various Japanese teams [30, 31, 19]. Their associated mobility was extremely low, between 10^{-7} and $10^{-5} \text{ cm}^2 \cdot (\text{V.s})^{-1}$, but they paved the way to future OFETs. These devices were based on spin-coated polymers. An alternative option was found later, and was based on using thin films of small molecules, such as the works of Fichou et al in 1989 [32]. Then, new polymers and molecules were designed, and the charge mobility most commonly obtained nowadays is usually between 1 to $10 \text{ cm}^2 \cdot (\text{V.s})^{-1}$ [33, 34]. Some recent record mobility of $40 \text{ cm}^2 \cdot (\text{V.s})^{-1}$ have been obtained by using highly crystalline layer of pentacene [35] or rubrene [36], but it is still far away from those of the silicon ($1\,400 \text{ cm}^2 \cdot (\text{V.s})^{-1}$ for electron mobility and $400 \text{ cm}^2 \cdot (\text{V.s})^{-1}$ for hole mobility). All these organic semi-conductors were either spin coated for the case of polymers or evaporated under vacuum for the small molecules, for thin layers of thickness above 100 nm.

Usually, organic semi-conductor leads to P-type OFET, such as pentacene [33]. However, molecules leading to N-type OFETs has been developed, but the measured charge mobility for these devices usually is lower than for their P-type counterpart [37, 38, 39, 40].

Carbon nanotubes

Carbon nanotubes (CNTs) were first synthesized by the groups of Iijima and Bethune in 1993 [41, 42]. They consist in a graphene sheet rolled on itself to form a hollow cylinder. CNTs can be either metallic or semi-conducting depending of the way the graphene sheet is rolled relative to the tube axis, which is also called chirality of the CNTs. The interest of CNTs for nanoelectronics was twofolds : metallic CNTs could be used as good contacts, while the semi-conducting CNTs could be used as a channel material in FETs [22, 24, 25].

The first architecture demonstrated for carbon nanotube based FETs used a single nanotube as a channel [24, 25]. While record charge mobility of $79\,000 \text{ cm}^2 \cdot (\text{V.s})^{-1}$ have been demonstrated in 2004 [43], the synthesis process of these devices is still too complicated for use in commercial devices. This is mostly due to the fact that it is not possible to place individual CNTs exactly where they should be in complex circuits.

Thus, an alternative way of using CNTs as a channel material is to use them in a dense networks of nanotubes. This is compatible with the coating of CNTs solutions

on the substrate, but can also be made using CVD [44]. However, the mobility and conductivity of such devices is always inferior to the one of single CNT due to the resistance between each tubes. When using CVD grown CNTs, a mobility of up to $100 \text{ cm}^2 \cdot (\text{V} \cdot \text{s})^{-1}$ has been measured, which is way lower than what a single CNT can do [44]. This low value is due to the high number of contact resistance between all the CNTs, but can also be due to the fact that all CNTs do not have the same chirality, meaning that the current does not propagate homogeneously in the entire channel and is limited by the more resistive current pathways.

Two dimensional materials

Another carbonated material had interesting electronic properties : graphene. High quality graphene was measured for the first time by the team of A. Geim in 2004 using graphened prepared by the "scotch tape" technique which consists in the mechanical exfoliation of graphene sheets from highly oriented pyrolytic graphite [45]. It showed the potential of graphene for electronics with a first measurement of its charge mobility : $10\,000 \text{ cm}^2 \cdot (\text{V} \cdot \text{s})^{-1}$. Few years later, a record mobility of $100\,000 \text{ cm}^2 \cdot (\text{V} \cdot \text{s})^{-1}$ has been measured at room temperature [46]. However, graphene is a semi-metal material, which means that it cannot be ideally used for FETs structures.

While graphene is not ideal in its most basic form for transistors, it opened up the way of 2D materials for electronic. Thus, many materials were studied, including hBN, graphene oxide or 2D chalcogenides (such as MoS_2 or WS_2).

2D chalcogenides' formula is MX_2 , where M is a transition metal and X is a chalcogenide, namely sulfur, selenium or tellure. In this part, MoS_2 will be used as an example of this category. This material is studied in two different configurations : in single layer flakes, mostly synthesized by CVD; or in multilayer extracted from a MoS_2 crystal by using the scotch-tape method. In the latter case, mobility as high as $200\text{-}500 \text{ cm}^2 \cdot (\text{V} \cdot \text{s})^{-1}$ have been measured [47].

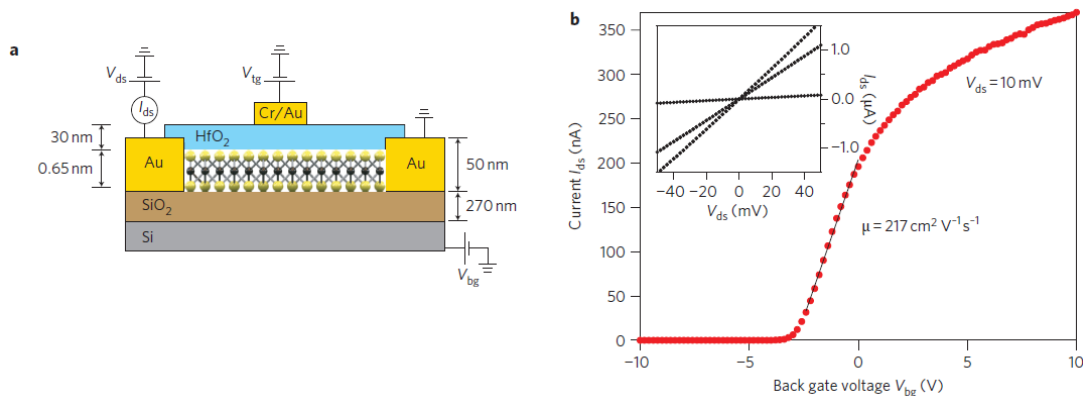


Figure I.1: (a) Schematic view of double gated FET with exfoliated MoS_2 as semiconductor (b) Transfer characteristics at $V_{DS} = 10 \text{ mV}$ by applying potential at the back-gate while the top gate is disconnected. Inset : $I_{DS}-V_{DS}$ curve acquired for V_{BG} value of 0, 1 and 5 V. Figures and captions from [48].

However, single crystal MoS_2 was shown to have lower charge mobility. In 2011, the team of Kis et al. managed to make high-performance transistors [48] using a single exfoliated layer of MoS_2 on top of a silicon wafer with a 270 nm SiO_2 . This serves as a

backgate for the setup. On top of the MoS₂, HfO₂ is deposited and serves as both an encapsulating layer for the flake and as a dielectric for the top gate. A scheme of the setup is shown in figure I.1.

Without using the top gate, the charge mobility of a single layer MoS₂ was found to be between 0.1 and 10 cm².(V.s)⁻¹ [49], which is fairly low. However, when using the top gate and the HfO₂ insulator, the mobility value was 217 cm².(V.s)⁻¹. While these results have been confirmed by various studies [50, 48], it has been demonstrated that the values were overestimated due the fact that the backgate is coupled with the topgate as was shown by M. Fuhrer et al [51]. Thus, after taking into account these considerations, the team of A. Kis reestimated the mobility of their devices to be around 50 cm².(V.s)⁻¹ [52].

I.1.2 Organic gate-dielectrics in transistors

SAMs thin films as a dielectric

Organic field-effect transistors (OFET) using relatively thick layers requires high operating voltage. One of the solutions for this problem is to tune the thickness of the dielectric in order to get a thinner one. By using the thinnest dielectric films available, one should be able to have very low operating voltage. SAMs are a great choice for that, since they are only a few nanometer thick and can form spontaneously monolayers on some of the most interesting surfaces for electronics, namely SiO₂.

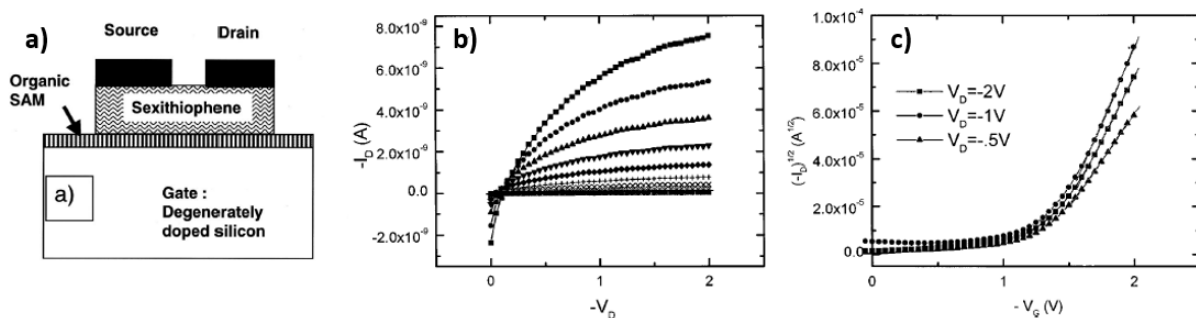


Figure I.2: (a) Schematic view of the isolated OTFT. Sexithiophene region (45 nm thick) is vacuum evaporated and patterned by e-beam lithography and lift-off. The gate insulator is made of a SAM of alkyl chains (2 nm thick). Source and drain contacts (Au 50 nm thick) were defined by e-beam lithography and lift-off. (b) Output current-voltage (I_D - V_D) and (c) transfer $I_D^{1/2}$ - V_G characteristics of a 500 nm channel length OTFT (V_G from -2 V, top curve, to -0.7 V, step 0.1 V). Figures and captions from [53].

Vuillaume et al. was the first group to evidence this fact [54, 53]. In their device shown in 2000 [53], they used SAM of an alkyltrichlorosilane as a gate dielectric in a transistor using evaporated sexithiophene as its semi-conductor (figure I.2). The source and drain electrodes were evaporated gold electrodes patterned using e-beam lithography. With this device, a channel length of 500 nm and good performances at the time, such as a subthreshold slope of 350 mV/decade, leakage currents at 4 MV/cm and charge mobility of $6.3 \cdot 10^{-4}$ cm².(V.s)⁻¹ were measured. This article also demonstrated that the channel length could be reduced down to 30 nm in this configuration.

Another example of a nearly fully organic transistor device was shown by Park et al. in 2005 [55]. The transistor made is composed of a heavily doped Si wafer as a gate.

On top of it, a SAM layer of docosyltrichlorosilane (DCTS) is deposited by simply immersing a cleaned Si wafer in a solution containing the molecules to form a SAM. Then, the semi-conductor used is poly(3-hexylthiophene), and the source and drain are printed droplets of poly(3,4-ethylenedioxythiophene) doped with polystyrene sulfonic acid (PEDOT-PSS). The resulting device is shown figure I.3.

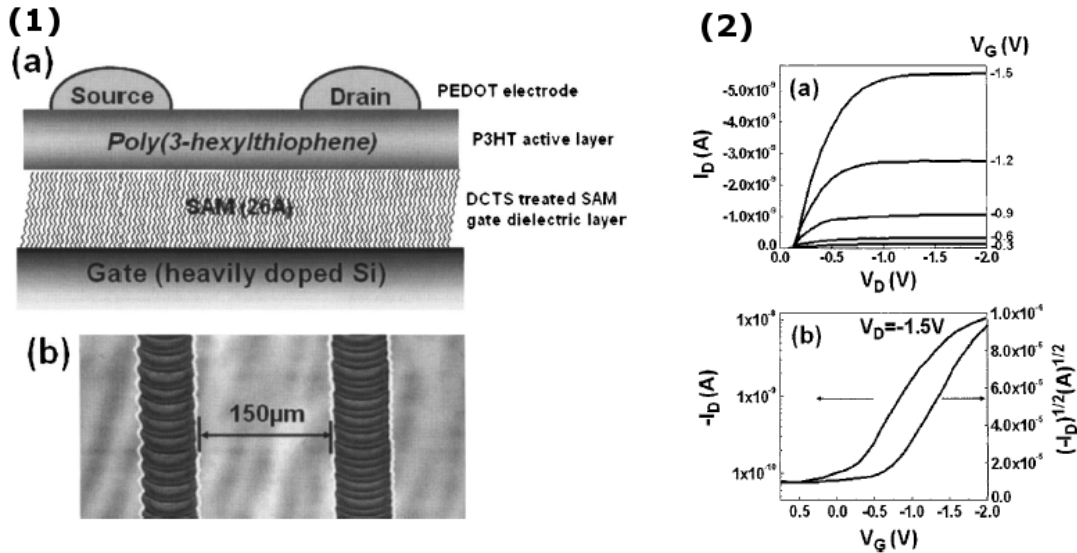


Figure I.3: (1)(a) Schematic view of the P3HT transistor with a SAM dielectric (b) Optical micrograph of inkjet printed source and drain electrodes. (2)(a) Typical output current-voltage characteristics of a 150 μm channel length and 1000 μm width OFET. (b) Transfer characteristics [$-I_{DS}$ vs V_G at $V_{DS} = -1.5$ V] and [$(-I_{DS})^{1/2}$ vs V_G at $V_{DS} = -1.5$ V]. Figures and captions from [55].

The resulting device is a p-type transistor. The channel length is 150 μm and channel width is 1000 μm . The resulting device had a measured capacitance of 457 $\text{nF}\cdot\text{cm}^{-2}$ for a dielectric thickness of 2.6 nm, which is as good as a 10 nm thick SiO_2 layer (407 $\text{nF}\cdot\text{cm}^{-2}$). Also, the device works at really low voltage, with its onset voltage at -0.3 V, its OFF state voltage at 0.5 V and its ON state voltage at -2 V. However, while this device solves the needs of low operating voltage, its other parameters are still not ideal : the on/off current ratio is only 200, the field-effect mobility is around $0.005 \text{ cm}^2\cdot(\text{V}\cdot\text{s})^{-1}$ and the subthreshold slope is 630 mV/decade, which is high when compared with the theoretical minimum at room temperature of 60 mV/decade.

More recently, the group of Zschiechang et al. illustrated the impact of the dielectric on the resulting device performances [56]. In their study, they use two different semi-conductors : pentacene, a p-type semi-conductor, and hexadecafluorocopperphthalocyanine (F_{16}CuPc). The dielectric used is a mix of two different SAMs : an alkyl SAMs, the octadecylphosphonic acid, and its fluoroalkyl counterpart, the pentadecylfluoro-octadecylphosphonic acid. In previous studies [57, 58], the electronegativity of fluoroalkyl SAMs reduced the electron density in the semi-conductor, leading to a shift of the threshold voltage of the device to more positive values. In order to confirm this hypothesis on both types of semi-conductor, the dielectric used in Zschiechang's study is thus a pure alkyl SAM, a pure fluoroalkyl SAM or a 50/50 mix of both SAMs. The resulting transistors are shown figure I.4, and are made by simply evaporating all the metals used, and functionalizing the gate by immersing it in a solution containing the molecules to form the SAMs.

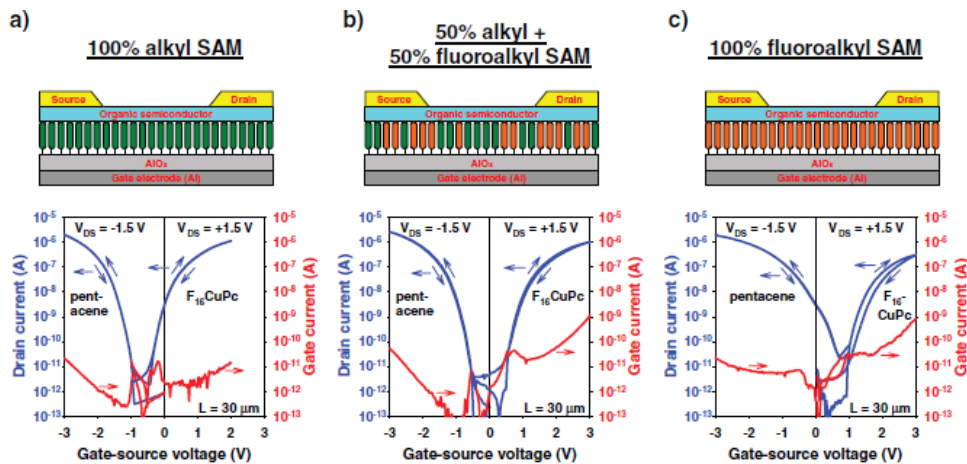


Figure I.4: Schematic cross-sections and transfer characteristics of pentacene p-channel TFTs and $F_{16}CuPc$ n-channel TFTs with three different SAMs as the gate dielectric : SAM of 100% alkyl phosphonic acid, mixed SAM of 50% fluoroalkyl and 50% alkyl phosphonic acid, and SAM of 100% of fluoroalkyl phosphonic acid, and their respective transfer characteristics. Figures and captions from [56].

By changing the nature of the surface, they managed to change the V_T of their transistors for both type. Also, when the SAM layer is a mix of both the alkyl and the fluoroalkyl molecules, the V_T measured is indeed between those measured when the layers are 100% alkyl or 100% fluoroalkyl SAM. V_T was tuned on a range of 1.6 V for the alkyl and 1.4 V for the fluoroalkyl SAM, while the transistor works in a range of 4 V, meaning that the tuning effect is important. However, the other properties of the channels also changed with the dielectric : for example, the hole mobility of the pentacene p-channel FET diminished from $0.75 \text{ cm}^2 \cdot (\text{V} \cdot \text{s})^{-1}$ to $0.25 \text{ cm}^2 \cdot (\text{V} \cdot \text{s})^{-1}$ when the dielectric is changed from the alkyl SAM to the fluoroalkyl SAM. Thus, this work clearly illustrates that organic dielectrics can be used to finely tune the properties of OFETs.

Further studies have been done on the impact of the dielectric layer on the semiconductor properties. As shown by Kraft et al. [59], the same alkyl and fluoroalkyl SAMs as in Zschieschang study can improve the properties of p-type and n-type OFETs respectively. A high mobility of $4.2 \text{ cm}^2 \cdot (\text{V} \cdot \text{s})^{-1}$ was notably measured. Also, this study shows the compatibility of fully organic FET with flexible plastic substrates. However, one point that was raised in the study is that SAM cannot be used to make different areas of dielectric in the same sample, and thus having access to high quality OTFT of the two types in the same sample remains difficult when using only SAM layers.

Finally, more complex SAM deposition processes can lead to higher capacitance for the dielectrics. For example, a 4 step synthesis of a dielectric by first functionalizing a doped silica sample with an anchoring SAM group, then adding a fully capped push-pull molecule, a capacitance of 710 nF/cm^2 is successfully achieved by the group of T.Marks [60] (figure I.5). Another way of increasing the capacitance of the layers is to use mixed organic-inorganic layers, such as hafnium oxide-organic self-assembled nanodielectric (Hf-SAND). By topping an organic SAM layer with a nanometer sized HfO_x layer, an extremely high capacitance of 1100 nF/cm^2 is achieved, with on/off ratio as high as 10^5 and subthreshold swing of 150 mV/decade , which puts such device by Facchetti, Marks and co-workers among the best devices made using SAM layers [61]

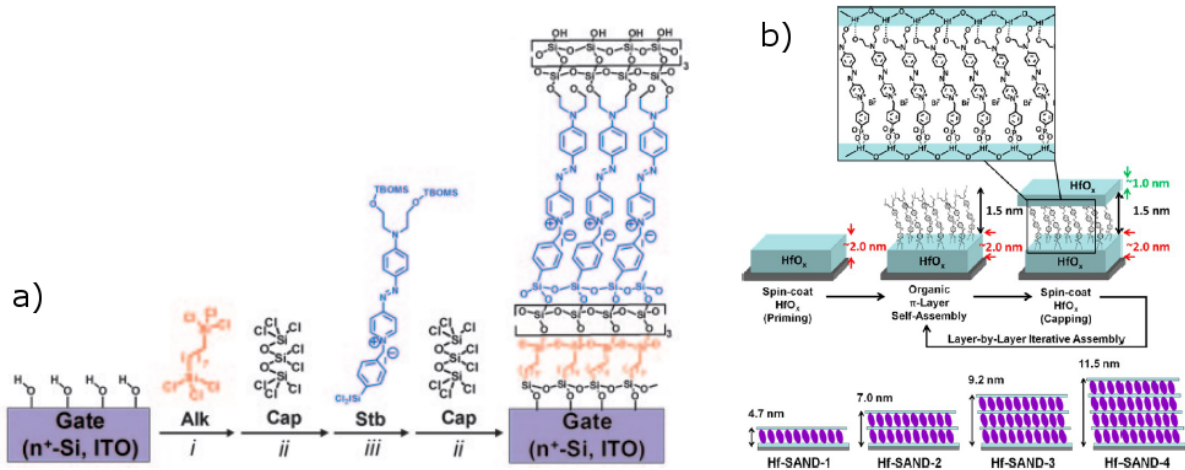


Figure I.5: **a)** Schematic of the self-assembly of the nanodielectric Alk+Cap+Stb+Cap. Conditions were as follows: 5 mM Alk in dry toluene at 0°C in N₂ for 1 h (I), 34 mM Cap in dry pentane at RT in N₂ for 25 min (II), or 10 mM Stb in dry tetrahydrofuran at 60°C in N₂ for 15 min (III), followed by hydrolysis with acetone–H₂O solution. **b)** (Top) Solution-based Hf-SAND self-assembly procedure. (Bottom) Schematic of the various Hf-SAND multilayers produced including the corresponding X-ray reflectivity derived thicknesses (Hf-SAND-1, -4) and estimated thicknesses (Hf-SAND-2, -3). Figures and captions from [60, 61].

(figure I.5).

Thin films of small molecules or polymers

Another way to prepare gate insulators for OTFTs is by using insulating organic thin films. These films are usually spin coated, and have a thickness superior than 100 nm. Thus, in order to have a similar capacitance as what SAM can offer, there is a need for thin layers with high k , as illustrated by the equation I.1, where k is the relative permittivity and d is the thickness.

$$C_i = \epsilon_0 \frac{k}{d} \quad (I.1)$$

Most of the dielectrics in this type of devices are made by spin-coating a polymer in solution. Thus, most of the studies are mostly focused on the polymer's structure and functional groups in order to optimize the gate-dielectric of the resulting transistors. Also, it is often used with organic semi-conductors in order to do fully organic OFETs, with the more common being pentacene.

An example of a typical study of the influence of the dielectric layer on the semi-conductor can be found in Baek et al.'s work [62]. Three different polymers were used and spin-coated for the dielectric layer : BFPDA-PDA-PDA polyimide (PI), a PI without fluorinated carbons, and two other similar polymers with different quantity of fluorinated carbons 6FDA-PDA-PDA PI and 6FDA-CF₃Bz-PDA PI, with the latter having more fluorinated carbons than the former. The idea behind adding fluorine in the polymers is that it should result in a more hydrophobic surface, which should lead to less charges

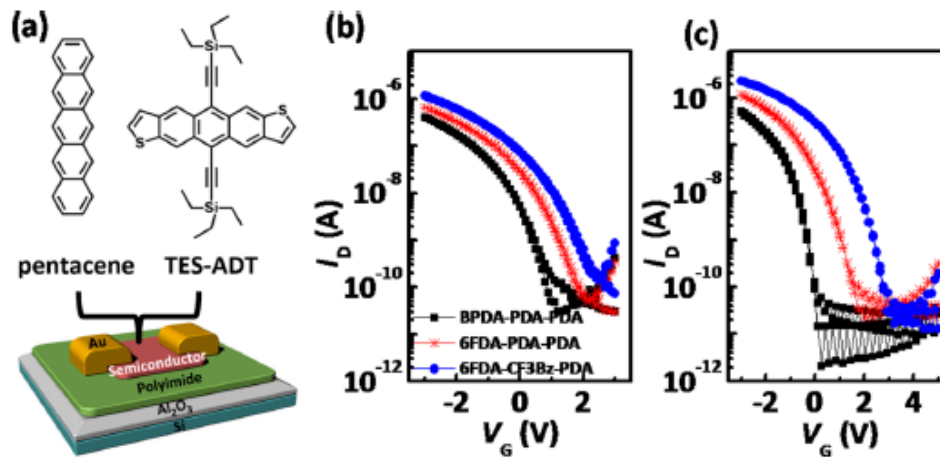


Figure I.6: (a) Schematic diagram of the top-contact OFETs. (b and c) Drain current-gate voltage (I_D - V_G) transfer characteristics of (b) pentacene and (c) TES-ADT based OFETs containing BPDA-PDA-PDA PI, 6FDA-PDA-PDA PI and 6FDA-CF3Bz-PDA PI and after and applied gate bias stress of $V_G = -3$ V ($V_D = 0$) for 3h in N_2 . Figures from [62].

trapped on the dielectric layer and thus a better dielectric-semiconductor interface. Usually, trapped charges on the dielectric layer lead to hysteresis in the transfer characteristics of the transistors. Baek et al. assembled the different types of transistors by using these three dielectrics and pentacene as a p-type semiconductor or TES-ADT as a n-type semiconductor. Their results are summarized figure I.6.

All transistors made this way had similar mobility, around $0.2 \text{ cm}^2 \cdot (\text{V}\cdot\text{s})^{-1}$, similar ON/OFF ratio around 10^4 and subthreshold slope above 180 mV/decade. However, V_T was at -0.05 V and -0.38 V for the BFPDA-PDA-PDA PI dielectric, 0.36 and 0.74 V for the 6FDA-PDA-PDA Pi and 0.64 and 2.21 V for the 6FDA-CF3Bz-PDA PI with pentacene or TES-ADT as a semiconductor respectively. Thus, the threshold voltage was increased with the quantity of fluorines in the polymers. Various studies show the same tendency [63], confirming the fact that the threshold voltage can be finely tuned in this way. However, the capacitance of the dielectrics used in this study did not change much between each structures, and was between 76.8 and 78.4 nF/cm^2 , which is low compared to what SAMs or thin SiO_2 can achieve.

Most of the organic thin layer dielectrics used in literature have a low capacitance, even though a high k was sometimes obtained. The table I.2 displays a list of some dielectrics used in the literature and various measured parameters. What is notable is that all the charge mobility values are between 10^{-3} and $1 \text{ cm}^2 \cdot (\text{V}\cdot\text{s})^{-1}$, which is due to the organic semiconductor used. High ON/OFF ratio around 10^4 or 10^5 are common. Working potentials of the devices are usually in the 100 V range, while some dielectrics have been made that allow working at low potential, such as CPVP- C_6 or PVA.

However, most capacitance values measured are quite low. This is due to the fact that the layers are usually too thick, and the capacitance could be upgraded easily by thinning the layers by a factor 10 or 100, provided that the gate leakage current can be kept low. The work of Yoon et al. shows that pretty clearly by managing to spin-coat a thin layer of CPVP- C_6 of 18 nm, which results in a capacitance of 225 nF/cm^2 [60].

Dielectric	h (nm)	Semi-conductor	C (nF/cm ²)	I _{ON} /I _{OFF}	μ _T (cm ² /(V.s))	V _G (V)	Ref
PI	540	Pentacene	6.4	900	1	-100/40	[33]
PS	660	P(NDI2OD-T2)	0.35	10 ⁶	0.62	-20/60	[64]
PMMA	630	P(NDI2OD-T2)	0.51	-	0.39	-20/60	[64]
P4VP	420	P(NDI2OD-T2)	0.69	10 ⁴	0.3	-20/60	[64]
PVA	810	P(NDI2OD-T2)	0.85	-	0.05	-20/60	[64]
P4VP-co-PMMA	630	P(NDI2OD-T2)	0.69	-	0.3	-20/60	[64]
CPVP-C ₆	18	Pentacene	225	10 ⁴	0.1	-4/4	[60]
CPS-C ₆	10	Pentacene	300	10 ⁴	0.08	-4/4	[60]
PVA/P(MMA-GMA)	1015	Pentacene	0.723	10 ⁵	2.17	-6/6	[34]
PVA	860	Pentacene	0.854	10 ⁴	1.48	-6/6	[34]
P(MMA-GMA)/PCA	920	Pentacene	0.798	2.10 ³	1.51	-6/6	[34]

Table I.2: Data table for some OTFT using organic thin layer as a dielectric.

Recently, a new way of doing organic insulator for transistors called ion gel electrolytes was developed. It roughly consists in gelating ionic liquids. Record capacitance of 41 000 nF/cm² have been obtained at 10 Hz or 2 000 nF/cm² at 1 kHz [65]. The technique is still under investigation, and the resulting layers are presently thick (around 100 μm) and hard to implement in an electronic device due to the synthesis conditions.

To summarize, organic thin layers can be used as efficient gate-dielectric for transistors. The coating process is straightforward and fast, and does not require any particular condition, which qualifies these layers as promising for industrial uses. However, their coating is not selective on the surface, which is a point to work on. Also, the layers still have low capacitance, mostly due to their thickness. Reducing the thickness of the spin-coated layers would lead to higher capacitance and lower working potential. Yet, controlling precisely the thickness by spin coating for very thin films is challenging, and raises the question of potential current leakages.

I.2 Two-terminal memory devices and memristors

Almost all complex information processing systems work on the basis of separated computing elements (arrays of logic gates made of transistors) and memory elements. Memory elements are also usually composed of transistors (and capacitors). However, there exists many possibilities to store information in two-terminal devices, which could be an important advantage in terms of integration density. In addition, memory elements usually only relies on two conductivity states (ON/OFF) to store data. With the initial impulsion of the HP Labs in 2008 [66], more and more attention was devoted to analog two-terminal memory devices taking benefit of a continuum of conductivity states. It was notably postulated that such devices, combined with transistors, could help mixing the computing and storage functionalities within the same arrays of devices [67, 68]. A large variety of 2-terminal memory devices exists. It includes magnetic devices, phase-transition devices, and others which presentation is outside the scope

of this work. Hereafter, two different families of memristors are presented : the first one is the Metal-Insulator-Metal memristor, which consists simply in using an insulator, organic or inorganic, between two electrodes. The second one concerns organic memristors that use active molecules as memristive layer.

I.2.1 Metal-Insulator-Metal memristors

The physical explanation of memristive behaviors in the MIM systems can be ascribed to different effects that combine each others : electrochemical effects, thermal effects and electrical effects [69, 70, 68].

The most common device with electrochemical effect is the metal-TiO₂-metal junction, made for the first time by Argall et al. [71], where the top metal could be Au, Cu, Al, Ti or Bi and the TiO₂ layer is 100 nm thick. Then, multiple studies on TiO₂ for memristors have been done. The mechanism was elucidated by an article from Kwon et al. in 2010 [72].

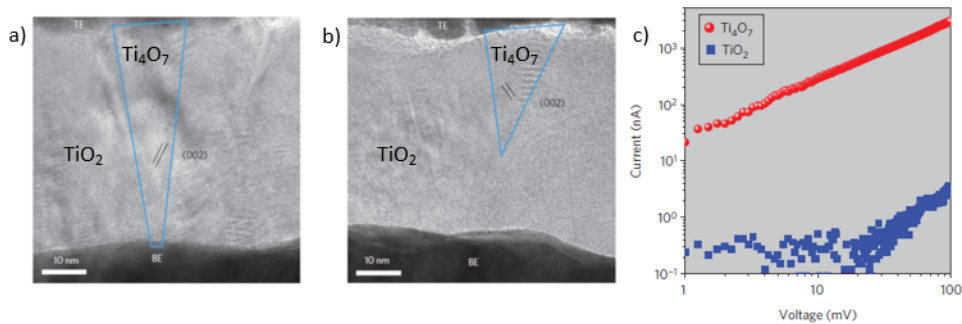


Figure I.7: a) High resolution TEM image of a Ti₄O₇ nanofilament. b) High resolution TEM image of a disconnected Ti₄O₇ nanofilament. c) Local I-V curves measured on the Ti₄O₇ structure and 50 nm away from this structure, on top of insulating TiO₂. Figures from [72].

In this study, vertical Pt-TiO₂-Pt are made, with the memristive layer being 40 nm thick and the contact having a surface of $2.8 \cdot 10^5 \mu\text{m}^2$. After applying a potential between the two electrodes, the oxygen vacancies in the TiO₂ migrates following the current flow. This leads to the formation of small filament of Ti₄O₇, poor in oxygen and thus more conducting than the pure TiO₂ layer, and the device is turned ON. The OFF state is obtained by applying a reverse potential, which makes the oxygen vacancies move in the TiO₂ layer and break the conduction path. A TEM study of these different states is shown figure I.7.

Thermal effects also plays an important role. When the current flows through localized conductive paths within an insulating matrix material, it can destroy them due to phononic excitation. The conductivity then drops, and the device is turned OFF. In order to bring the device back to its ON state, a different bias needs to be applied in order to reform the filament.

Electronic effects can be illustrated with an example from Bozano et al. [73]. The device is composed of multiple layers of Alq₃/Al/Alq₃ evaporated under vacuum, where Alq₃ is an aluminum metal complexe, between Al electrodes. An example of the I-V characteristic obtained is showed in figure I.8. In this setup, the Al serves as a

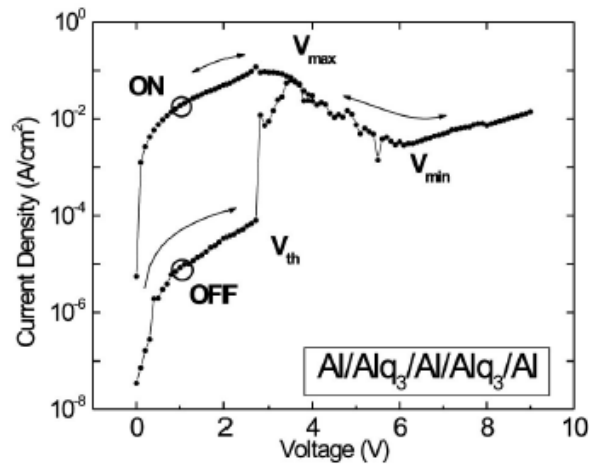


Figure I.8: I-V characteristic of an Al/Alq₃/Al/Alq₃/Al device. Figure from [73].

charge trapping layer while the Alq₃ is a semi-conducting material. Initially, the device is conducting. When the potential is increased, charges begins to get trapped in the Al layers. If the potential is reduced sufficiently fast to 0 V, the conductivity of the whole layer is changed due to the negative charges trapped in the Al layers.

I.2.2 Organic memristors

Organic memristors are divided in two families : redox-based memristors and fully organic memristors [17]. Their main differences are their switching mechanism. These devices are usually done with SAMs, and their different conduction properties are due to a change of the interface between the SAM and the electrodes, notably by a small shift on the SAM between the different position available for binding [17] or a change of its molecular structure [74]. These can result to low I_{ON}/I_{OFF} ratio between 1.5 and 5.5 [74].

Redox-based memristors have been more studied. They are usually made from metal complexes, such as Fe [4] or Ru [75]. Miyamachi et al. [76] demonstrated this by measuring the conductivity of single Fe-Phen molecules on CuN/Cu(100) with an STM (Figure I.9). After proving the presence of two different states of the Fe-Phen on the substrate, they managed to switch between the two types by only varying the potential applied on one molecule, resulting in a $I(V)$ hysteresis as shown in figure I.9 (b).

Then, the memristive behavior was further probed by doing potential pulses in order to check the robustness of the device. The memristor was switched between its on state, with a current measured at +0.5 V equal to 150 pA, and its off state, with a current measured at +0.5 V equal to 130 pA, in a repeated and reversible way. However, the I_{ON}/I_{OFF} ratio is very low (1.15) and the time of the pulses for writing or erasing the layer is between 0.1 and 5 s, which is way too slow for future uses in electronics.

Single molecular layers of memristor active compound can be done by adding a thiol function, for example, in order to bond the molecules to the surface of a metal electrode and then evaporate an electrode on top of it. This would result in a bigger contact area, which lead to the response of an ensemble of molecules instead of only a single one. Lee et al [18] managed to demonstrate that by using a bis-tripyridine ruthenium complex and adding a carbonated chain ended by a thioacetate function used for bind-

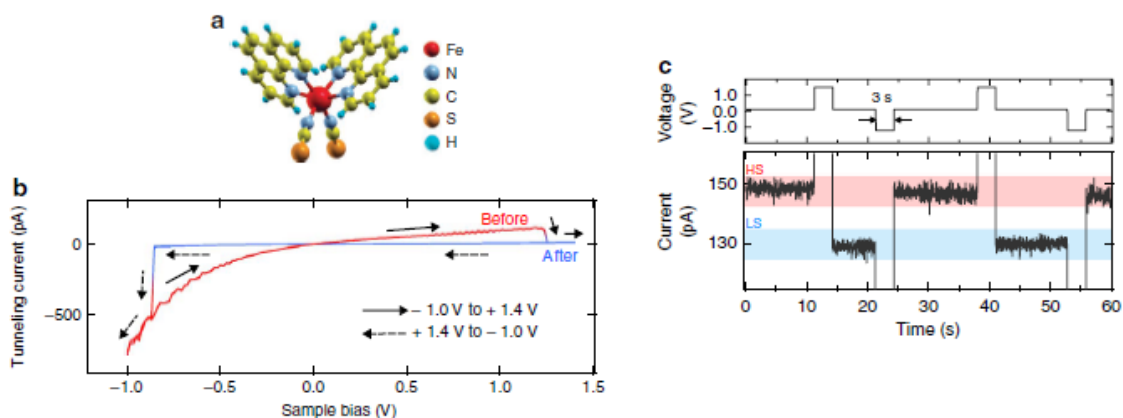


Figure I.9: a) Three dimensional model of a Fe-phen molecule. b) I(V) curves of isolated Fe-phen molecules on the CuN/Cu(100) surface. c) Reversible switching by voltage pulses of +1.5 V inducing high spin to low spin switching and -1.2 V inducing low spin to high spin switching. Figures and caption from [76].

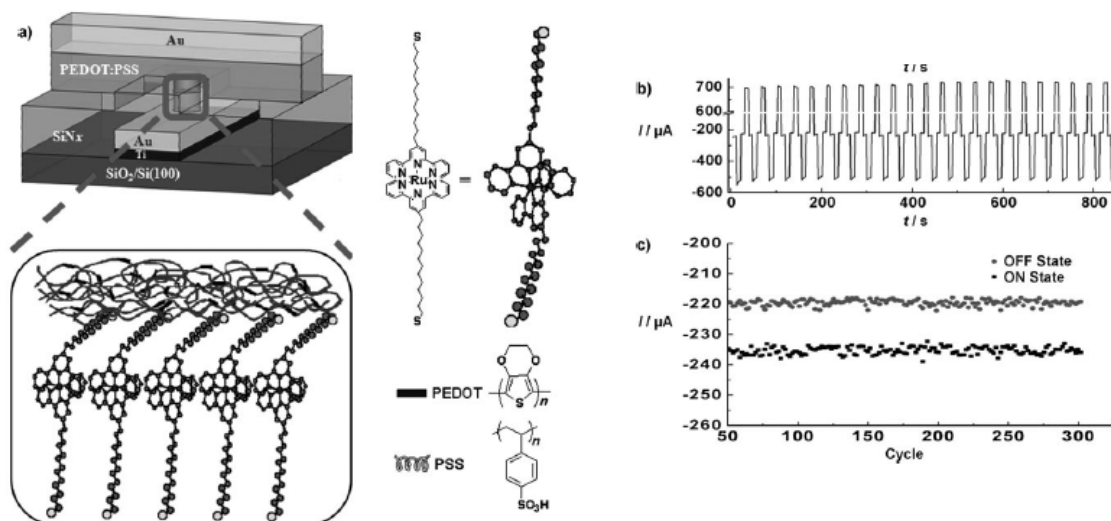


Figure I.10: a) Schematic representation of the cross section of the device layout of PEDOT:PSS on the ruthenium complex SAMs. b) Write-multiple read-erase-multiple read (WREM) cycles of a molecular monolayer device containing Ru^{II} complex for a rewritable data storage application. The writing, reading, erasing and reading voltages were -1.5, -1, +1.5 and -1 V respectively. c) Current in the ON and OFF states as a function of the number of WREM cycles. Figures and caption from [18].

ing the molecule to the gold electrode. After functionalizing the bottom gold electrode with this SAM, the top electrode was fabricated by first spin-coating PEDOT:PSS, in order to prevent the penetration of the evaporated metal through the SAM layer, and then evaporating gold on top of the device (Figure I.10).

The I(V) curve of the resulting device show a memristor behavior with only a I_{ON}/I_{OFF} ratio of 1.07. However, the top electrode fabrication leads to a high percentage of working device after optimizing the structure of the molecule and the process of the formation of the SAM layer (from 4 to 81 % of working junction of 490 μm^2). Additionally, the main advantage of this device is its high cyclability, with no degradation of the

current measured after more than 300 cycles. Another interesting information is that the molecule used in these devices can lead to a I_{ON}/I_{OFF} ratio of 10^4 when the layer is 60 nm thick, meaning that attaining an intermediate thickness could lead to high I_{ON}/I_{OFF} ratios.

As with transistors, organic thin films of thickness around 100 nm can be used for memristors. These layers come with two advantages against single molecule electronics : these devices have less short-circuit, and the resulting memristive properties have higher ON/OFF ratios and better defined states. For example, an ITO glass substrate is spin-coated with a thin film of 80 nm of bis(2,2'-bipyridyl)(triazolopyridyl)Ru(II), then the top contact is an Al electrode. The I-V characteristic of the final device is shown figure I.11. It is bipolar, meaning that the writing and erasing voltage occur at opposite polarity.

The I_{ON}/I_{OFF} ratio of the device is 10^3 , which is higher than for single layer of molecules but still lower than what have been attained with inorganic memristors. When the stability of the written or erased state is probed, Pradhan et al. showed that the resulting device can keep their state for more than 5 000 s.

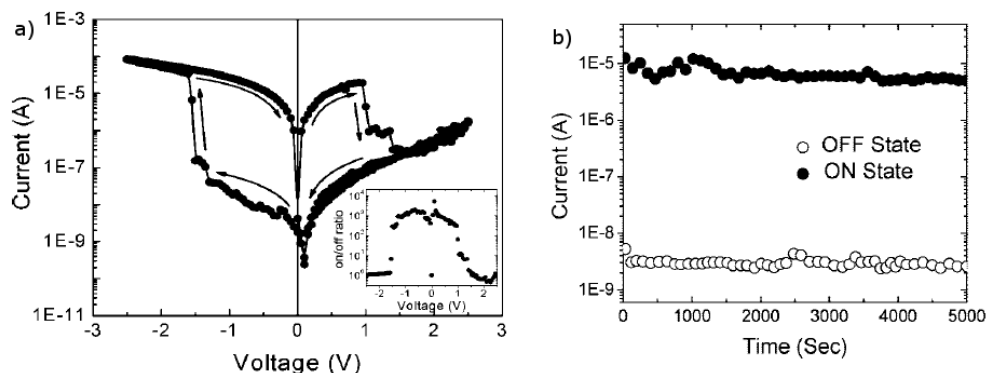


Figure I.11: a) I-V characteristics of a device based on spin-cast film of turthenium complex for two sweep directions in log scale. b) Long time response of the ON and OFF state as probed by device current under -0.8 V. Figures and caption from [77].

More recently, Barman et al. demonstrated that a fully organic molecule could be used to obtain similar results. By spin-coating pyrene-affixed triazoles on an ITO substrate and evaporating an Al electrode on top of it, they managed to get a similar I_{ON}/I_{OFF} ratio of 10^3 as Pradhan, and demonstrated a higher retention time of 6 500 s [78].

In this part, different example of memristive under study were presented. While the most successful ones were mostly based on inorganic compounds, organic molecules showed great promises for the future. The main challenges notably include the improvement of the I_{ON}/I_{OFF} ratio, the stability of the stored state, the write and erase potentials, the variability between devices and, for certain class of applications, the accessibility and stability of intermediate conductivity states.

I.2.3 Aim of the work in this context

As shown above on selected samples, many devices that uses either single layer of molecules or organic thin films have been developed in view of their future use in electronics. Both strategies have their advantages and drawbacks : single layers are

extremely thin (1 to 5 nm thick) but requires a particular care to the choice of the electrodes used and robustness could be a long term issue, while organic spin-coated layers are compatible with every type of conductors or semi-conductors, but results in thicker layer (usually above 100 nm) and are harder to miniaturize. There exists a gap between 5 and 100 nm in which fewer devices were studied, would it be by spin-coating or by using multiple processes starting with SAMs layer. Having access to thin layers of thickness in this range combine the thin thickness of SAMs layers and the high compatibility properties of the spin-coated layers. Thus, another type of organic layers that fulfills such requirements is being considered by different groups : electrochemically grafted thin layers [79]. It notably led to successful examples of intergration in electronic devices by the groups of J.C. Lacroix at university Paris-Diderot and R. McCreery at University of Alberta [80, 81, 82, 83, 84, 85].

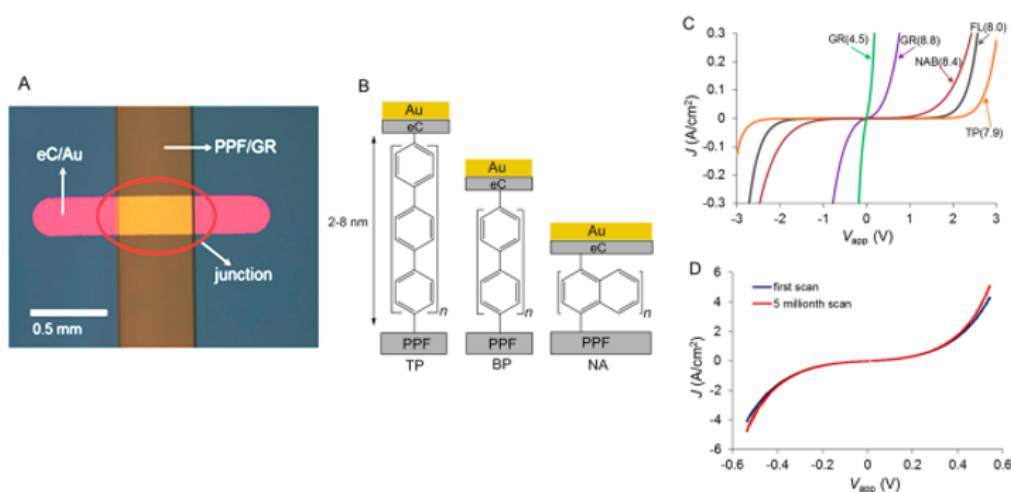


Figure I.12: (A) Photograph of a device made on Si/SiO_x chip. (B) Molecular junctions of singly bonded layers of TP, BP and NA generated by electroreduction of their diazonium ions on PPF for comparison with doubly bonded graphene ribbon. (C) JV curves for graphene nanoribbon electrografted, NA, BP and TP junctions with indicated molecular layer thickness in nanometers. (D) Overlay of JV curves of graphene nanoribbon junction (4.6) before and after the 5 million cycles in air at 1000 V/s. Figures and captions from [85].

A recent example of a device using an ECG layer fabricated by the team of McCreery is shown figure I.12. Here, the organic layer used is graphene ribbon made by electrografting diazonium salts on a PPF electrode. Then, the top electrode is made by electron beam deposition of carbon and gold. Thanks to this structure, they manage to get a graphene ribbon junction that could withstand more than 10⁶ JV cycles at 1000 V/s without any degradation. Another keypoint of this study is that the surface of the junction is around 0.1 mm² and does not show any sign of current leakage, which illustrates quite well the covering properties of ECG layers. Also, they showed that the resulting behavior depends on the nature and the thickness of the ECG layer, as illustrated by the JV curve in figure I.12.

ECG layers have multiple advantages, the most notable being that the same sample can have different ECG layers. It is a local process, and thus should allow the selective functionalization of different electrodes, as shown in figure I.13. This allows the formation of various devices on the same chip, which is a great advantage against the

different organic layers showed previously. Also, those electrodes can be patterned at the micrometric scale using classic lithography techniques. The resulting layer is covalently grafted with the substrate with a strength similar to what can be achieved with SAMs on gold ($D_{C-Au} \approx 262$ kJ/mol vs $D_{S-Au} \approx 254$ kJ/mol [86]), and is compatible with lithography techniques.

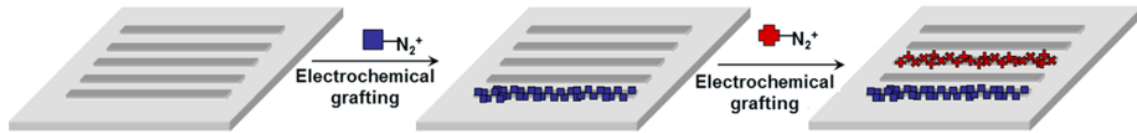


Figure I.13: Scheme of an ECG process on patterned electrodes with different diazonium salts.

In the recent years, the laboratory studied two types of devices incorporating these ECG layers. The first one is a device combining both an organic dielectric and a 2D semi-conductor. Casademont et al [3] demonstrated in 2016 transistors using an exfoliated multi-layers of MoS_2 as the semiconductor channel and ECG thin layer as the gate dielectric. The grafted molecules, 4-heptadecafluorobenzene diazonium, were insulating and hydrophobic. An SEM image of such final MoS_2 -FET with ECG gate-dielectric and its transfer characteristics are shown in figure I.14. The transistors looked promising, with a low subthreshold slope of 145 mV/dec, low working voltage between -0.25 and 1.75 V and relatively high I_{ON}/I_{OFF} ratio of $3 \cdot 10^3$. However, this device was studied using a double back-gate configuration, which is not the optimal setup since it requires 4 contacts and a high static potential must be continuously applied on the global back-gate electrode.

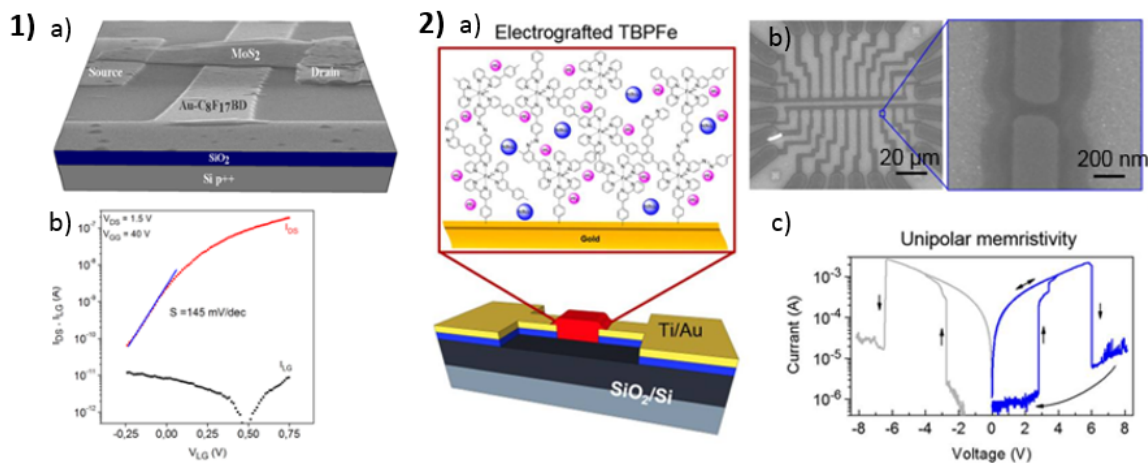


Figure I.14: 1)(a) Schematic representation and SEM image (scale bar = 500 nm) of a MoS_2 FET with a local-gate electrode electrografted with $C_8F_{17}BD$. (b) Transfer characteristics $I_D(V_{LG})$ and gate-leakage current I_{LG} measured at $V_{DS} = 1.5$ V and $V_{GG} = 40$ V for an organic dielectric thickness of 7 nm. 2)(a) Schematic representation of the metal/organic/metal memristor and the organic composing layer. (b) SEM image of the horizontal devices. (c) Electrical characteristics of the memristor under voltage sweeps. Figures from [3] and [4].

The second type of device recently studied at LICSEN are memristors using ECG material as memristive part. They were used to build an elementary prototype of circuit

able to learn its function in a supervised manner [4]. They mostly studied horizontal metal-ECG layer-metal junctions. These junctions were made by first evaporating under vacuum all the metal electrodes through an E-beam lithography mask in order to have the smallest gap possible between two electrodes as shown in the image **2**(b) of figure I.14. Then, the electrografting of the active molecule, a tris-bipyridine iron (II) derivative (**TBPFe**), was performed on each electrodes to grow a bridging organic layer. Even though such junctions could be used in small circuits and show appreciable stability and moderate variability, the strategy suffers from limitations : circuits based on horizontal junctions are not scalable and each individual devices required a "forming step" (a first programming cycle performed at high bias), which complicated the analysis of the physics governing the switching.

Both these devices are limited in terms of miniaturization. For the MoS₂ transistor, miniaturization is limited by the special care taken not to evaporate the source and drain electrodes directly above the gate electrode. For the memristive device, the main problem comes from the fact that the junctions are horizontal. The reason for these scaling issues is that evaporating metals directly on top of ECG layers usually lead to high percentage of leaking devices. Thus, the work that will be presented in this PhD notably aims to solve this problem, by working along two different paths : the first one is trying to master the electrografting process in order to have a better control over the growth of the ECG layer, and obtaining a denser layer than what was previously done; the second one is by trying to get the best top contact possible by using various ways to make top electrodes. To achieve such goals, a fine control over the thickness and the nature of the ECG layers must be demonstrated in order to obtain highly tunable ECG layers.

Chapter II

Diazonium salt electrografting on patterned micrometer sized electrodes

This chapter begins with a review of the state of the art on the ECG of diazonium salts. Then, the ECG of the three diazonium salts used in this PhD is investigated. First, ECG is done on classic macroscopic gold electrodes, in order to determine the behavior of the ECG and the nature of the resulting layer grafted. Then, ECG performed on patterned micrometer sized gold electrodes is studied. In order to be able to use those layers in micro-sized devices, a good control over the growth and the final thickness of the ECG layer is needed. Thus, the influence of different parameters of the ECG on the resulting thickness of the grafted layers on these electrodes are investigated : the concentration of the active species in solution, the time and the potential of the ECG. A process to obtain higher quality layers is then shown. These results will lead to a high degree of control over the thickness of the resulting layer, which allows a fine tuning of the physical properties of the ECG layer.

II.1 Diazonium electrografting

Electrografting (ECG) is a process consisting in reducing or oxidizing a redox active molecule on a conductive or semi-conductive electrode in a classic electrochemical setup. When this redox center is activated, the resulting molecule becomes more reactive and can be covalently grafted on the surface of the working electrode, resulting in the formation of a thin organic layer. Various redox functions can be used for ECG, such as amine [87, 88] or carboxylate [89, 90] in oxidation or vinylic [91, 92, 93] and diazonium [94, 95, 96] in reduction. ECG layers have various advantages over spin coated thin layers or SAMs : it is compatible with any conductive or semi-conductive substrate, it can be used to do localized grafting on a sample (as shown in figure I.13) and can be used with a high variety of molecules.

Diazonium ECG was first studied at the start of the 80s by the group of Parker et al, and has numerous advantages over other electrografting processes [97]. First, their reduction potential is low and between -0.45 V/SCE and $+0.25$ V/SCE [98]. This property allows them to be used on a lot of different materials without any risk of oxidation : conductors or semi-conductors, such as iron [92], gold [95] or doped silica [99], and even insulators in specific setups, like PTFE [100] for example.

One of the other advantages is that the diazonium function can be stable in presence of water and even in aqueous solution at pH 2-3 [101]. When the pH increases, the

diazonium function is oxidized in diazohydroxydes (Ar-N=N-OH) or diazoates (Ar-N=N-O^-). However, these oxidized forms can also be reduced, but at a slower rate.

Diazonium salts can be synthesized from nearly any aromatic amine. It is usually done in aprotic solvent, such as acetonitrile (ACN). The arylamine molecule is solubilized at the lowest temperature possible, which can be as low as just above the freezing point of acetonitrile (-45°C). Nitrosium tetrafluoroborate (NOBF_4) is then added to the solution, and the reaction takes place according to the mechanism in figure II.1. The resulting diazonium salt is then precipitated by adding diethyl ether (Et_2O) to the solution, and then is filtrated. Another way of synthesizing diazonium salts from amine derivative is by performing the synthesis in aqueous acidic solution and by adding NaNO_2 .

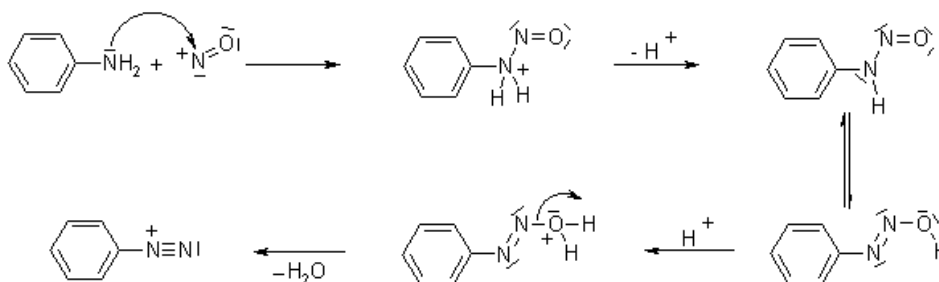


Figure II.1: Synthesis mechanism for a diazonium salt.

The mechanism of the ECG of diazonium salts is shown figure II.2. The diazonium function of the molecule is reduced by the working electrode to a radical, which will then react to the closest molecule or material, which is usually the surface of the electrode to graft. The next reduced molecules will then react with either the substrate or the molecules grafted to the substrate, resulting in the formation of multilayers. However, non reduced diazonium salts can also react with radicals that can be found in the growing multilayer to form azo bounds, after oxidation and the loss of dihydrogen. Thus, the resulting layers are composed of monomers linked by both C-C and N=N bonds [102].

The diazonium salt that was the most studied is the 4-nitrobenzene diazonium salt (NBD). Its ECG on glassy carbon (GC) (figure II.3) shows two peaks during the first reduction cycle : one around 0.36 V and another around -0.05 V vs SCE. Both are attributed to the reduction of the diazo function, and are signs of the ECG of the molecule on the surface of the electrode. On the second cycle, no peaks are visible, and the current measured is lower than during the first cycle, which indicates the formation of a passivating layer on the GC electrode.

The presence of two peaks instead of only one is still under investigation. Benedetto et al. [104] showed evidences that these two peaks are due to the ECG taking places on different crystallites of the gold electrode. These two peaks being visible even on GC could also be attributed to the reduction of the diazonium salt on different carbon planes. Cline et al. [105] confirmed that by showing that the pretreatment, and thus the surface state of the GC influences the presence and the intensity of the peak at the highest voltage. Hypothesis for this difference are the presence of different sites on GC, and more precisely a difference of terminal group on the surface of the electrode. More recently, Lee et al. [103] showed that the two peaks are due to the ECG of the NBD in a catalytic or non-catalytic manner, leading to a loosely or dense packed final

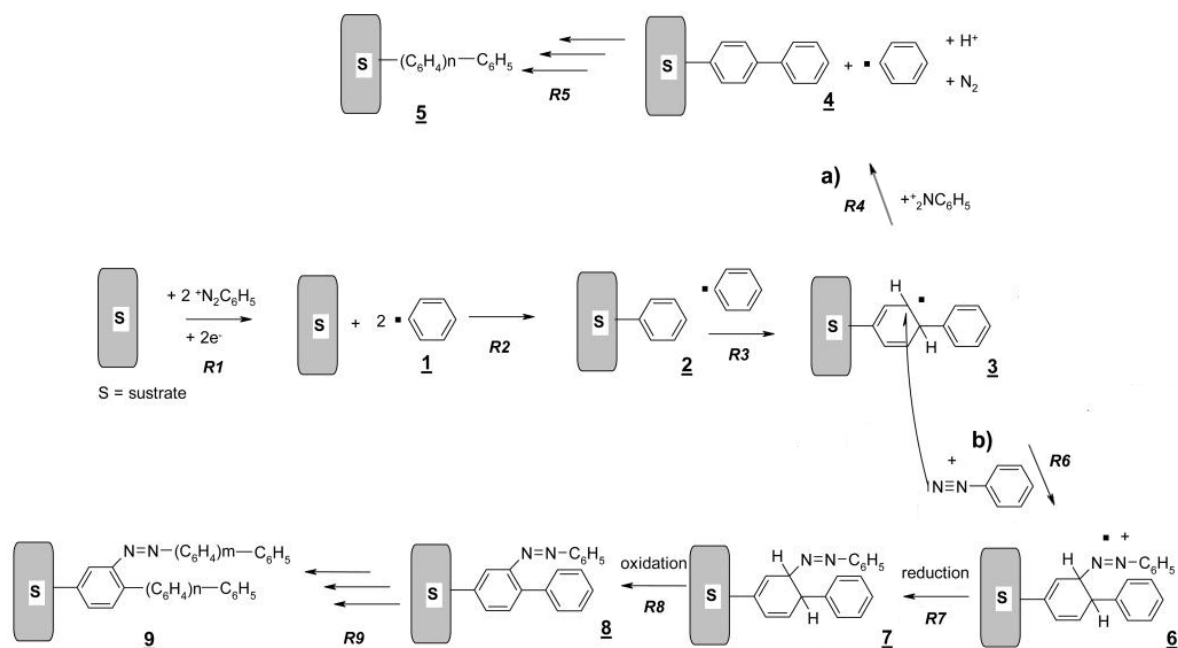


Figure II.2: ECG mechanism for a diazonium salt. Path a) forms carbon bounds only chains, while path b) forms both azo and carbon bounds chains. Figure from [102].

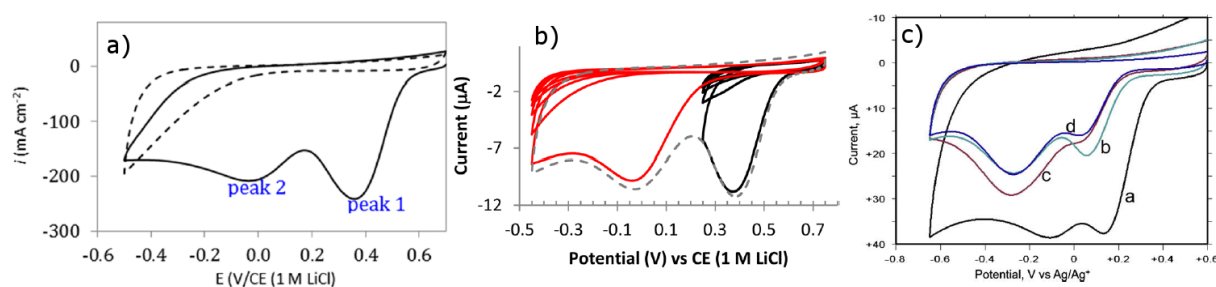


Figure II.3: **a)** CVs obtained at glassy carbon in a solution of 1 mM NBD in 0.1 M [Bu₄N]BF₄-ACN at (a, b) $v = 0.02 \text{ V s}^{-1}$ (1), 0.05 V s^{-1} (2), 0.08 V s^{-1} (3), 0.1 V s^{-1} (4), 0.2 V s^{-1} (5), 0.3 V s^{-1} ; **b)** CVs ($v = 0.1 \text{ V s}^{-1}$) obtained in 1 mM NBD in 0.1 M [Bu₄N]BF₄-ACN. Black lines: five repeat scans, 0.75 to 0.25 V, at freshly polished glassy carbon; red lines: scans 6-10, 0.75 to -0.45 V, recorded immediately after scans 1-5; gray dashed line: one scan, 0.75 to -0.45 V, at freshly polished GC. Figures from [103] **c)** CVs of NBD ion (product solution diluted to ca. 2 mM with 0.1 M TBABF₄ in acetonitrile) on GC (a) electrochemically oxidized in 1 M H₂SO₄; (b) Al₂O₃/H₂O polished and sonicated in activated charcoal/isopropanol, then H₂O; (c) polished and sonicated in cyclohexane; (d) Al₂O₃/H₂O polished and sonicated in H₂O. Scan rate = 200 mV/s.

organic multilayer.

The compacity of the layer formed is usually measured by using redox probes [106, 107, 108]. The grafted layer is used as a working electrode in a classical electrochemical setup, with a known redox probe, such as ferrocene, solubilized in the electrolyte. For example, Cannizzo et al. demonstrated that they grafted calix[6]arene diazonium salt by using the ECG electrode as the working electrode in a solution containing K₃Fe(CN)₆. They then compared the results with a non grafted electrode [106]. In the case of [103], ferrocene and dopamine were used to probe the compacity of NBD

layers made using different process. (Figure II.4) Dopamine was used as an inner-sphere probe, which means that it needs to diffuse to the surface of the electrode to be reduced, while ferrocene can be reduced by tunneling effect. The results show that the NBD layers made could be divided in two groups : when ECG is done before the second reduction peak, the formed layer is loose but impairs the diffusion of species between the GC electrode and the solution; when the second peak is met during the ECG, there is no response of dopamine, and the ferrocene peaks are less intense and has higher ΔV , showing that the layer made is thicker and more densely packed than the previous one.

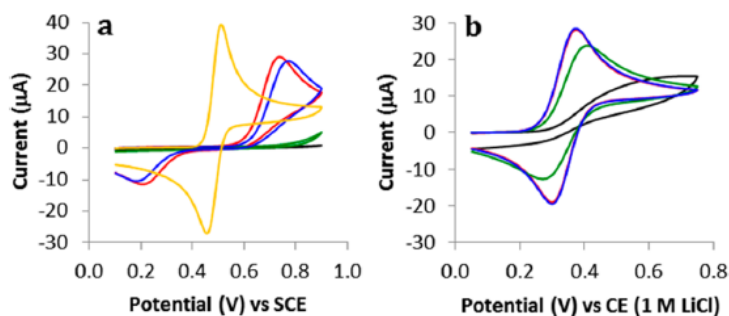


Figure II.4: CVs ($v = 0.1 \text{ V s}^{-1}$) obtained in (a) 1 mM dopamine in 0.1 M H₂SO₄; (b) 1 mM ferrocene in 0.1 M [Bu₄N]BF₄-ACN at a GC electrode after modification in a solution of 1 mM NBD (in 0.1 M [Bu₄N]BF₄-ACN) by five cycles from 0.75 to 0.25 V followed by five cycles from 0.75 to -0.45 V (black lines); one cycle from 0.75 to -0.45 V (green line); five cycles from 0.75 to 0.25 V (red line); applying 0.45 V for 300 s (blue line). Yellow line is 1 mM dopamine in 0.1 M H₂SO₄ at polished GC. Figure and caption from [103].

While ECG of diazonium salts usually leads to multilayers, single layers can be made using this method. The most common way is to use radical scavenger during the ECG process, such as the 2,2-diphenyl-1-picrylhydrazyl (DPPH) [109]. The CV of NBD on GC with and without DPPH are shown figure II.5. On the CV of the ECG with DPPH, the reduction of DPPH into DPPH^{•-} is seen at -0.06V, at the same potential as the diazonium reduction peak. The most notable difference with the classic CV behavior of NBD is the fact that the electrochemical response of all the species in solution, NBD and DPPH, can be seen after the first cycle when the radical scavenger is present.

When electrochemical quartz crystal microbalance (EQCM) is done (figure II.5), the frequency stays the same after 20s during the ECG of NBD with DPPH, while it continues to diminish without DPPH, showing the formation of a thicker multilayer. The measured surface coverage of the modified GC electrode were also calculated, and were constant whatever the potential applied was or during multiple CV, which was attributed to the fact that the layer formed was a monolayer [109]. Another way of obtaining a monolayer with diazonium ECG is to use bulky molecules, such as the 3,5-bis-*tert*-butylbenzenediazonium [96].

Additionally, the diazonium salts to be grafted can also be synthesized *in situ* from its amine derivative and ECG in the same solution, resulting in a one pot electrochemical grafting process [94, 110]. Finally, since the reduction potential of diazonium salts is pretty low, grafting of these molecules can be done directly in solution by using chemical reduction processes or even reductive surfaces [111]. For the former process,

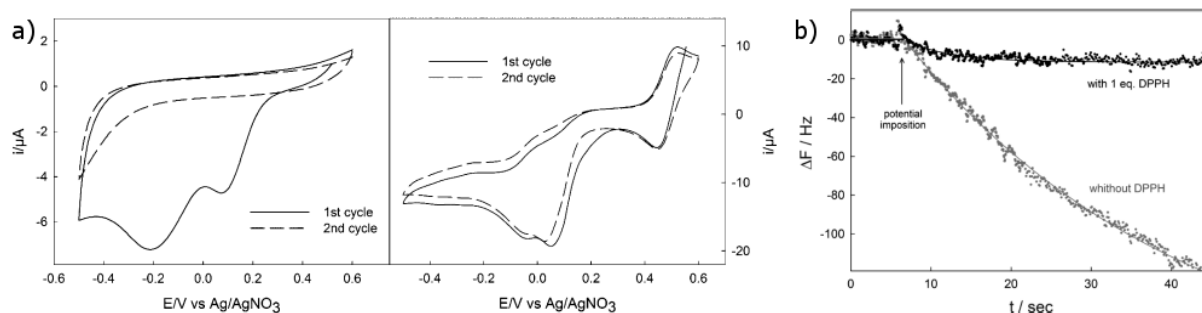


Figure II.5: **a)** First and second CV cycle recorded in CH_3CN 0.1 nBu_4NPF_6 containing 1 mM of 4-nitrobenzenediazonium on GC at 50 mV/s without DPPH (left) and with 1 mM of DPPH (right); **b)** Frequency variation vs time on a carbon quartz measured by EQCM for the electrochemical grafting using 4-nitrobenzenediazonium (1 mM) at a fixed potential of -0.5 V without DPPH (gray plot) and with 1 mM DPPH (black plot). Data are fitted using the Langmuir model (solid lines). Figure and caption from [109].

a particular focus has been done on using both vinylics and diazonium salts for grafting thin layer on any type of surface in aqueous solution [112, 113].

Thus, diazonium salt is an interesting material for the formation of organic thin layers for electronic. However, there are only few studies on the control of its thickness [114, 115], and even less on the growth of ECG layers on patterned gold electrode, which would be the most interesting for future use in electronics as was shown in our laboratory's works [3, 4].

II.2 Electrografting of the diazonium salts

Three different diazonium salts were studied : a derivative from the tris-bipyridine iron (II) (**TBPFe**), the 4-heptafluorobenzene diazonium (**DzF8**) and the 4-thiophenol diazonium (**Thio**). Their chemical structures are shown figure II.6. The first one has redox properties in addition to its diazonium centers, and has shown memristive properties when used in devices made in the laboratory [4]. The other two, however, only have their diazonium functions as their redox active center. The main interest for the **DzF8** molecule is its long fluorinated chain, which can interact with the chains of other **DzF8** molecules to form denser layers in order to get good dielectric. On the other hand, the **Thio** has a smaller carbonated chain but possesses a thiol function, which is known for having a great affinity with gold as shown in [116, 117].

All diazonium salts were synthesized in the laboratory starting with their amine derivative. The synthesis is further detailed in the experimental section. The infrared spectra of each molecules showed similar bands (figure II.7) : one sharp and low intensity band around 3100 cm^{-1} corresponding to the C-H bending of a carbon sp^2 ; one sharp and intense band around 1550 cm^{-1} corresponding to the stretching of a C=C bond; one broad and intense band between 1000 and 1100 cm^{-1} corresponding to the bending of the C=C bond, each of those corresponding to the different bonds in the aromatic ring of the benzene ring; one sharp band around 2250 cm^{-1} corresponding to the $\text{N}\equiv\text{N}$ bending vibration of the diazonium function of the compounds. The main difference between each compounds are multiple sharp and intense bands between 1150 and 1250 cm^{-1} correspond to the bending of the C-F bonds in the **DzF8** molecules. Some

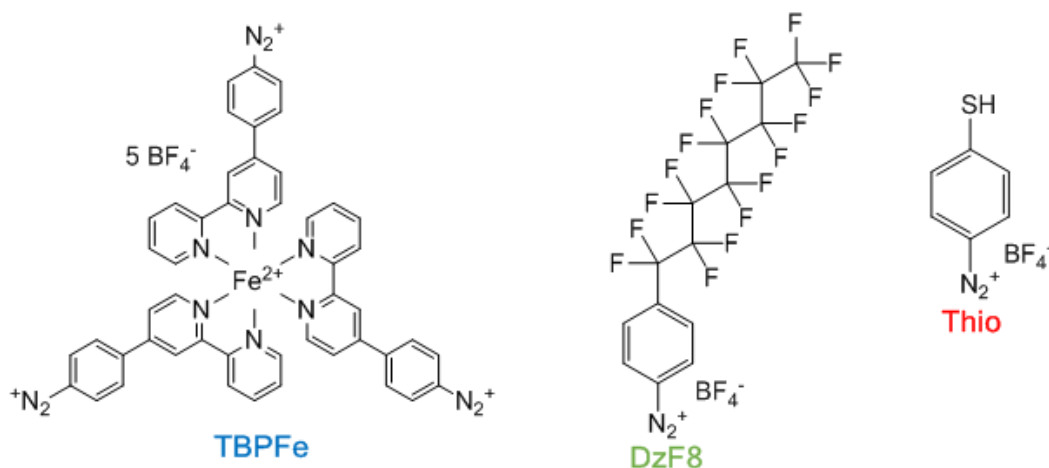


Figure II.6: Chemical structures of the tris-bipyridine iron(II) diazonium derivative (**TBPFe**), the 4-heptadecafluorobenzene diazonium salt (**DzF8**) and the 4-thiophenol diazonium salt (**Thio**).

of the bands around 1000 cm^{-1} could also be indicators of the presence of BF_4^- in the diazonium salts, which is not surprising since it is needed to keep the neutrality of the compound.

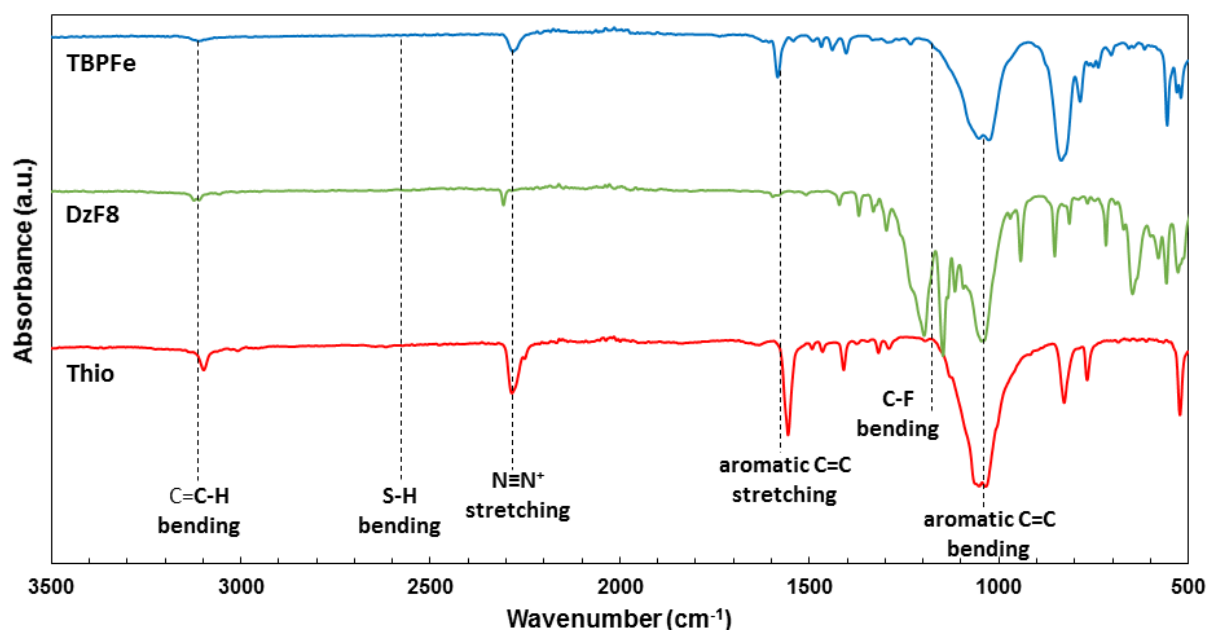


Figure II.7: Infrared spectra of **TBPFe**, **DzF8** and **Thio** powder.

The electrolyte used for probing the electrografting of the three salts was a solution of 0.1 M tetrabutylammonium hexafluorophosphate (TBAPF_6) in which the concentration of the diazonium redox molecule is set (28 μM for **TBPFe**, 1 mM for **DzF8** and 0.5 mM for **Thio**) in acetonitrile (ACN). In order to probe the electrografting behavior of each salts, cyclic voltammetry (CV) on gold was performed in a glove box by using a classic electrochemical setup where the working electrode was a gold electrode, the counter electrode was a platinum wire and the reference electrode was a silver wire in a solution of AgNO_3 at 10 mM and TBAPF_6 at 0.1 M in acetonitrile.

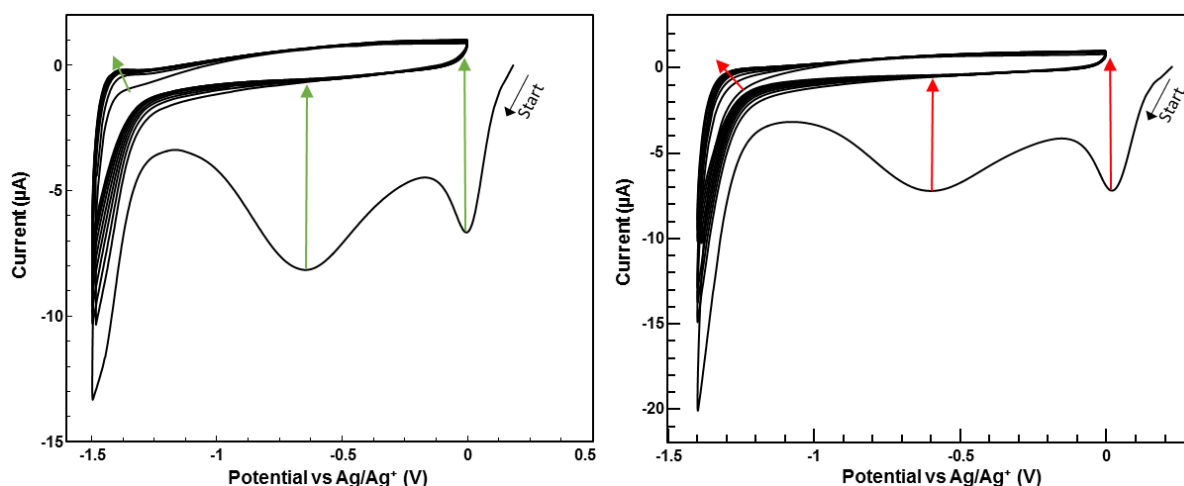


Figure II.8: CV (10 cycles) at 50 mV/s of a solution of 1 mM **DzF8** (left) or 0.5 mM **Thio** in 0.1M TBAPF₆ in ACN on gold.

The CV behavior of **DzF8** was first probed (figure II.8 left). During the first reduction cycle, two peaks at 0 V and -0.6 V vs Ag/Ag⁺ are observed, corresponding to the reduction of the diazonium function of the molecule. As mentioned previously, the presence of two peaks was tentatively attributed to different effects : the reduction of the diazonium function on different crystalline orientation of gold [104], the pretreatment of the substrate [103] or two different reactions, one catalyzed and another uncatalyzed [105]. During the next cycles, these peaks disappear, showing that they are irreversible, and the current diminishes meaning that the surface of the working electrode is more and more insulating and that the reduction process of the **DzF8** is stopped. This result is coherent with the fact that **DzF8** layers were observed to be insulating [3]. The CV behavior of **Thio** (figure II.8 right) shows a similar behavior as **DzF8** : two irreversible peaks are visible during the first cycle at 0 V and -0.6 V vs Ag/Ag⁺, and then the current diminishes during the following cycle, showing the formation of an insulating layer. This is in agreement with the lack of redox active species on **Thio** and **DzF8**.

TBPFe shows a different behavior than the two precedent molecules (figure II.9). Multiple reversible peaks are present : one at +0.9 V corresponding to the reversible oxidation of the iron(II) core, and two between -1.5 V and -2 V corresponding to the successive reversible reduction of two bipyridine ligands. The third one is at lower potential than what was probed in this experiment, and thus is not visible. The fact that there is multiple redox signals for the ligands is due to the fact that the reduction of one ligand also changes the structure of the molecule and its stability, and thus changes the energy required to reduce another ligand. A last set of two additional peaks centered at -1 V and +0.7 V can be seen. These reversible peaks with a huge overpotential, still under investigation and dependant on each other, can be attributed to charges trapped within the growing film or the redox properties of the various azo bonds that are formed during the formation of the layer.

Compared to **DzF8** or **Thio**, two molecules with only their diazonium function as a redox center, the intensity of the peaks increases during the electrografting of **TBPFe**. This comes from the fact that the quantity of active species that are oxidized or reduced increases during the cycles, which means that more active molecules are located in the neighbourhood of the gold electrode. Since ECG leads to the formation of an organic

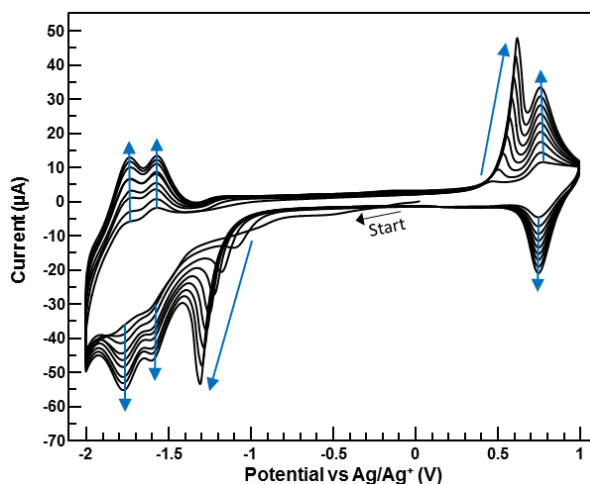


Figure II.9: CV (10 cycles) at 50 mV/s of a solution of 50 μM **TBPFe** in 0.1M TBAPF_6 in ACN on gold.

layer, this result is the proof that more and more **TBPFe** is grafted on the electrode surface. Also, it illustrates the fact that, since **TBPFe** is an electroactive molecule, its ECG layer keeps those properties. Thus, the ECG process of **TBPFe** and the growth of the organic layer is not self-limiting, contrary to **Thio** or **DzF8**.

II.3 Physico-chemical characterization of the layers grafted

The electrografted layers were investigated using various surface characterization tools. First, the infrared spectra of all grafted layers were done on gold electrodes (figure II.7). The bands of the C-H stretching vibration around 3100 cm^{-1} are not visible. Moreover the bands corresponding to the C=C stretching vibration at 1550 cm^{-1} and the bands corresponding to the C=C bending vibration between 950 and 1100 cm^{-1} are less intense than the bands observed in figure II.7. The band at 1200 cm^{-1} corresponding to the C-F bending vibration on the **DzF8** grafted layer spectra cannot be seen in this spectra. However, a band at 2550 cm^{-1} can barely be seen on the **Thio** spectra, corresponding to the bending of the S-H bond. That means that either the layers are not grafted or they are too thin to be seen by IR spectroscopy.

In order to have a better idea of the presence or absence of a grafted layer in addition to get informations on the structure of the ECG layer, X-ray photoelectron spectroscopy (XPS) has been used on the grafted working electrodes. The XPS analysis of the **TBPFe** grafted layer is shown figure II.11 and in table II.1. On the survey, peaks for fluor, carbon, nitrogen, oxygen, iron, phosphorous and gold can be seen. The intensity of the Au 4f peak is really low, indicating that the grafted layer is dense, but not thick or dense enough to block all the x-rays from getting to the gold substrate. The fluor and phosphorous peaks can be associated to PF_6^- that are inside the grafted **TBPFe** layers and required for the electroneutrality of the compound.

The experimental determination of the relative concentration of iron, carbon and nitrogen in the **TBPFe** layer are in good agreement with the theory : according to the XPS spectra, there is 5 times more nitrogen than iron (6% of one of N 1s peak versus 1.2% for both Fe 2p peaks; 6 N atoms versus 1 Fe atom in theory), and there is a lot more

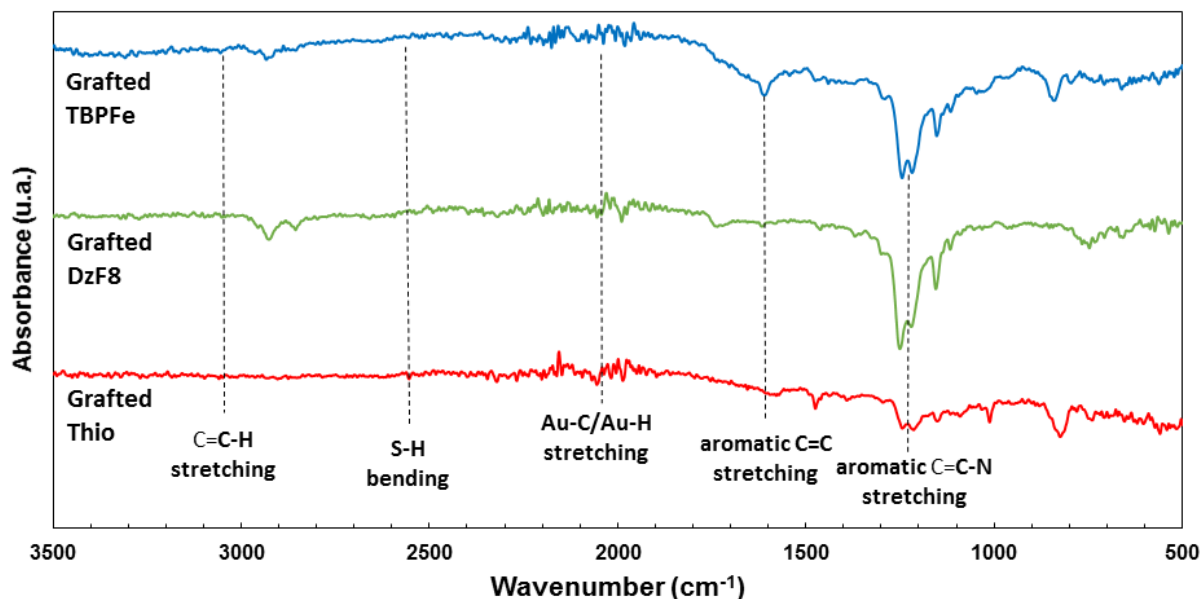


Figure II.10: Infrared spectra of **TBPFe**, **DzF8** and **Thio** grafted layers on gold

carbon (74.8%) than iron. The second N 1s peak at 402.2 eV (2 eV higher than the N 1s peak of the pyridines of the **TBPFe** molecule) can be attributed to N=N bonds that cannot be avoided when doing electrografting with diazonium salts. However, the calculated value is 1.6% and would mean that there is on average 1.3 N=N bond per molecule. It could also be attributed to the tetrabutyl ammonium of the electrolyte that could be inside the organic layer.

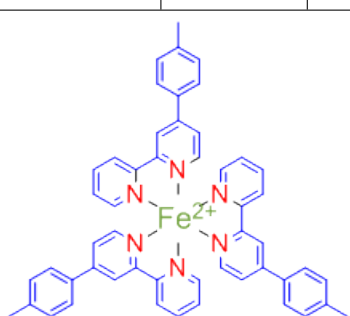
Atom and Orbital	Fe 2p	Fe 2p	C 1s	N 1s	N 1s	P 2p	F 1s
Peak position (eV)	716.2 / 708.5	722 / 711.5	285.1 to 292	400.1	402.2	136.6 / 134	687
Concentration (% atom)	0.3	0.9	74.8	6	1.6	3.8	12.7
Concentration (Theory)	1.4		69.6	8.7	0	2.9	17.4
Attribution					N=N	PF ₆	

Table II.1: XPS data table for a grafted layer of **TBPFe** on gold.

The XPS analysis of **DzF8** is shown figure II.12 and table II.2. On the survey, peaks for fluor, gold, oxygen and carbon can be seen. The Au 4d peaks are way more visible than with the **TBPFe** layer, showing that the **DzF8** layer is either more porous or thinner than the **TBPFe** layer. However, since the grafting of **DzF8** is self limited, the second

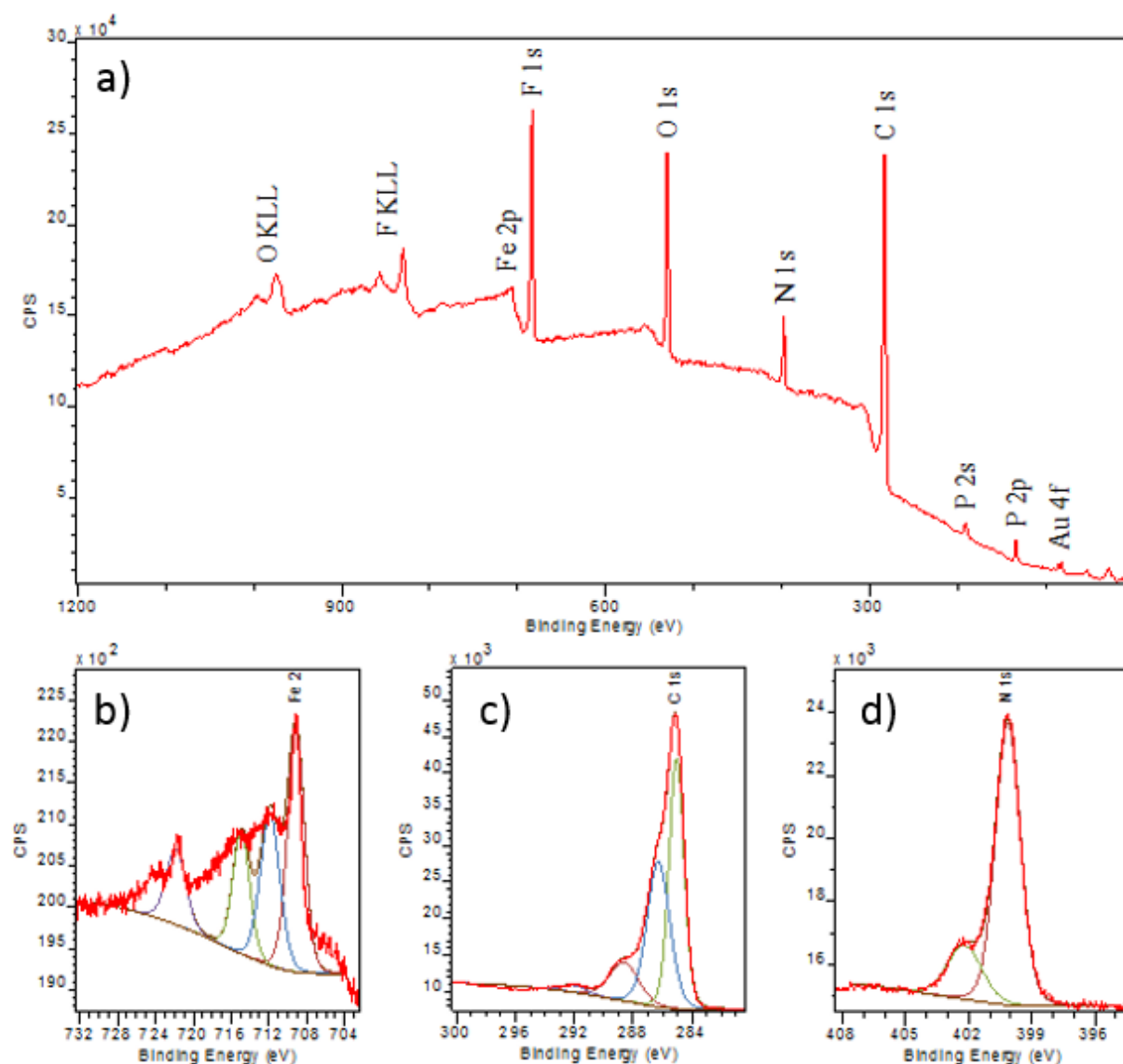


Figure II.11: XPS survey spectra (a) and high resolution spectra of the Fe 2p region (b), the C 1s region (c) and the N 1s region (d) of a **TBPF8** grafted layer on gold.

explanation seems more plausible. The high resolution spectra of the C 1s peaks shows 3 well defined different areas at 284 eV, 290.2 eV and 292.2 eV, which is in agreement with the three different types of carbon in the **DzF8** molecule. The relative atomic concentration ratio are also really close to the theory : the calculated relative concentrations are 3.1% for the terminal C, 22.3% for the C-F₂ molecules and 15.6% for the aromatic carbon, which is really close to the theoretical ratio. Moreover, there is 15.8 times more fluor than the carbon at 290.2 eV, attributed to the terminal carbon of the fluorinated chain, which is only 1.2 times less than what should have been measured. However, no nitrogen peaks are observed, meaning that the formed layer have no N=N bonds.

The XPS analysis of **Thio** is shown figure II.13 and table II.3. On the survey, the peaks for oxygen, gold, nitrogen, carbon and sulfur are visible. The Au 4d peaks are as visible as for the **DzF8** case, and even have the same calculated relative concentration. That could mean that the layer grafted is similar for both molecules, but could also mean that one of the two layers is thinner and denser than the other one. The S 2p high

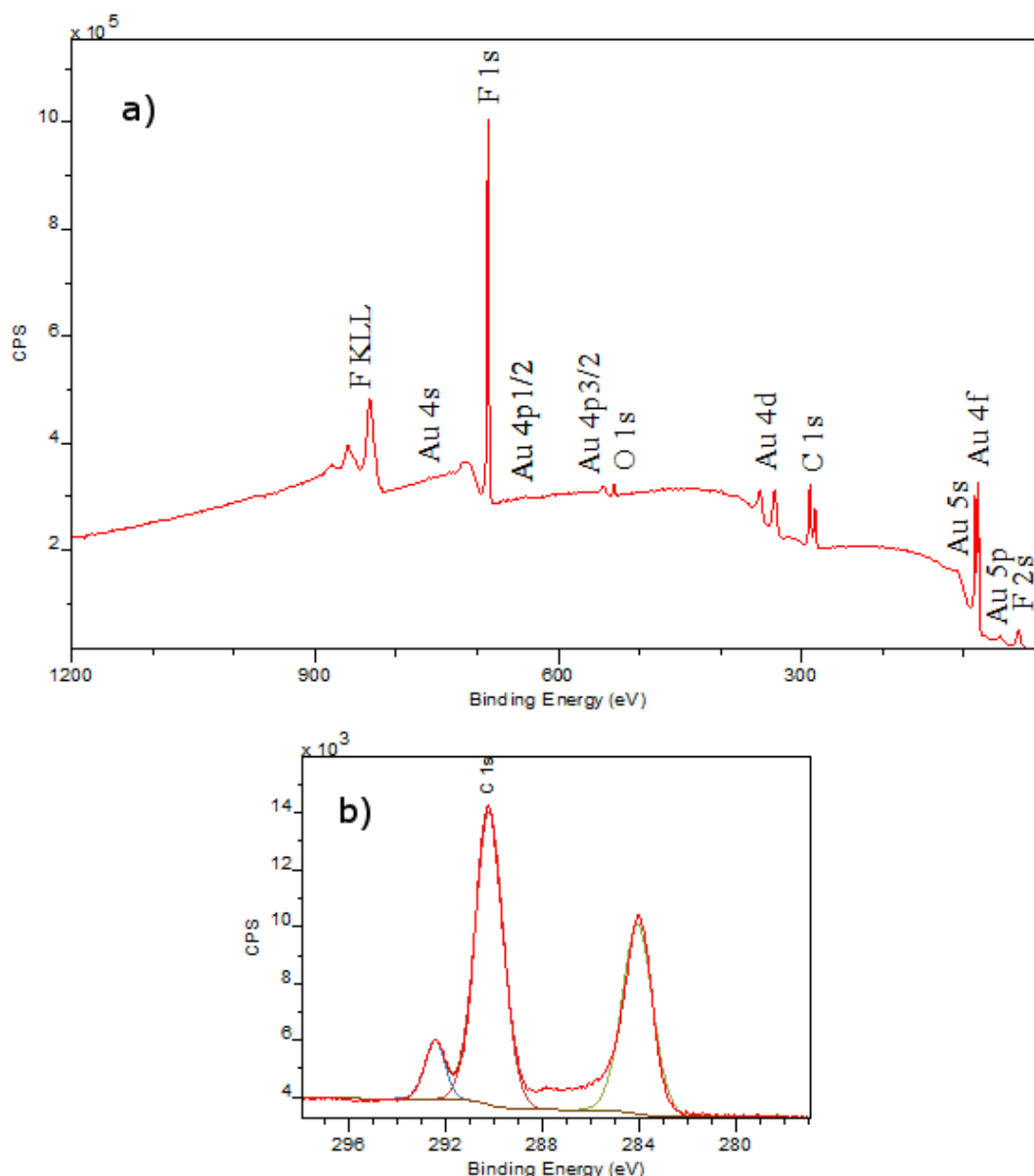


Figure II.12: XPS survey spectra (a) and high resolution spectra of the C 1s region (b) of a **DzF8** grafted layer on gold

Atom and Orbital	Au 4f	F 1s	C 1s	C 1s	C 1s
Peak position (eV)	81.7/85.4	687.5	290.2	292.2	284
Concentration (% atom)	10	49	3.1	22.3	15.6
Concentration (Theory)	0	54.8	3.2	22.6	19.4
Attribution	Substrate				

Table II.2: XPS data table for a grafted layer of **DzF8** on gold.

resolution spectra show a well defined peak, meaning that all sulfur atoms contained in the layer have the same neighbourhood. According to tables, an energy of 164 eV

for a S 2p peak means that these sulfur are part of a thiol function, when an energy of 161.5 eV means that the sulfur is linked to a metal. Here, an energy of 164 eV is measured after calibration of the spectra, meaning that the sulfur seen with XPS are part of the thiol function of **Thio**. Then, most of the sulfur are not part of an Au-S bond, which proves that the electrografting managed to fix **Thio** molecules with their sulfur site available for further deposition of gold on top of it. Also, the ratio of sulfur versus carbon (10.5% versus 67%) is really close to the theoretical one (1 versus 6). There is also traces of N=N bonds with the nitrogen peaks.

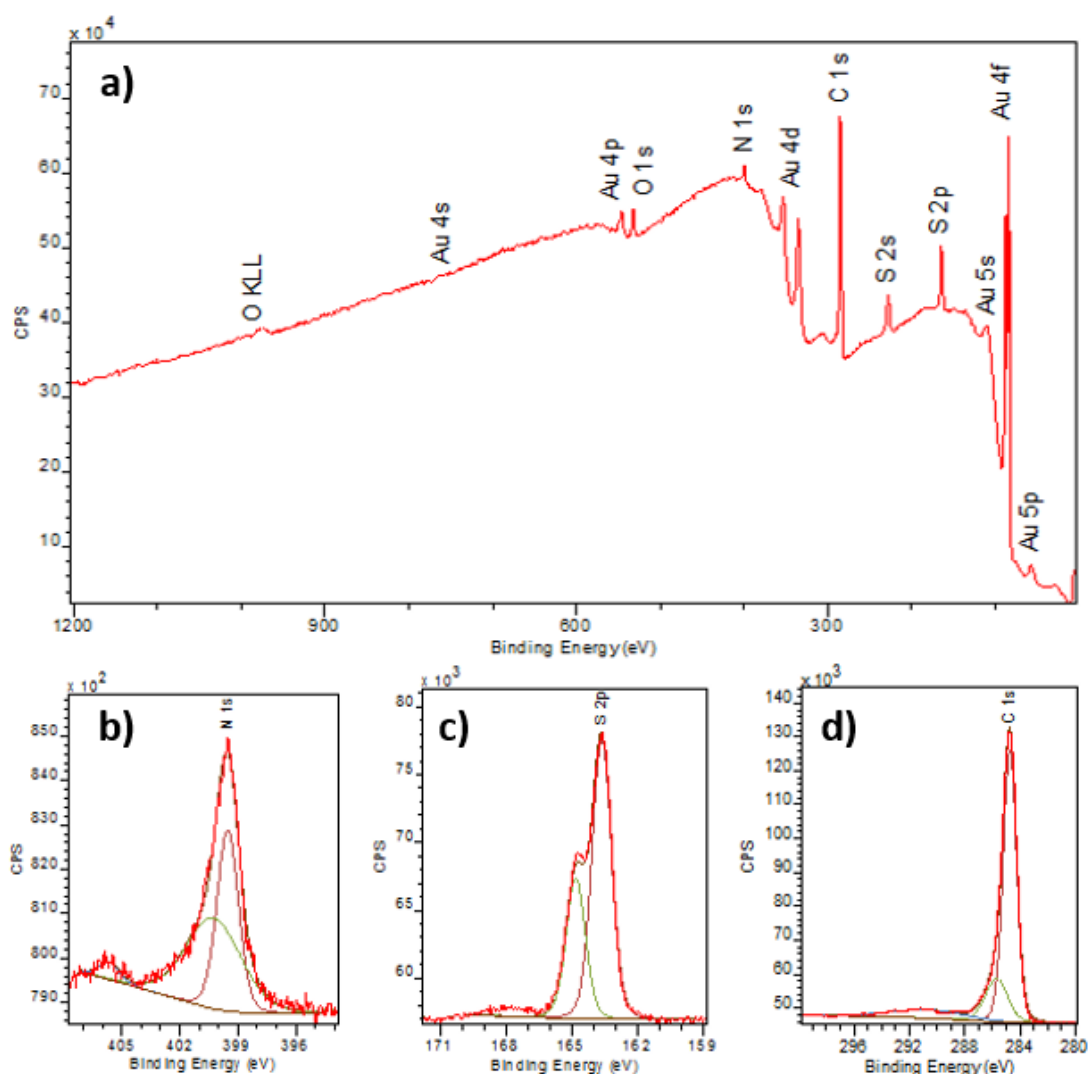


Figure II.13: XPS survey spectra (a) and high resolution spectra of the N 1s region (b), the S 2p region (c) and the C 1s region (d) of a **Thio** grafted layer on gold

The hydrophobic character of the grafted layers is probed by using contact angle measurements with a water droplet. The results are summed up in table II.4. All layers are more hydrophobic than gold. Not surprisingly, the **DzF8** layer is highly hydrophobic (106.8°), which is in agreement with the presence of the long fluorinated chain, followed closely by the **Thio** layer (91.5°) which is surprising considering the affinity of water with thiol [118]. The **TBPF** layer is not really hydrophobic (66.5°) which could be due to the fact that the layer is charged with the iron(II) cores.

The compacity of the layer was probed using a redox agent, here ferrocene, in acetoni-

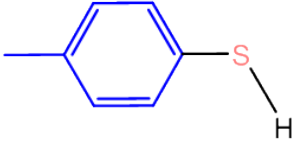
Atom and Orbital	Au 4f	S 2p	C 1s	C 1s	N 1s
Peak position (eV)	87.7/84	164.8/163.6	285.7/284.7	290.6	400/405.7
Concentration (% atom)	10	10.5	67	8.5	4
Concentration (Theory)	0	14.3	85.7	0	0
Attribution	Substrate			Contamination	N=N

Table II.3: XPS data table for a grafted layer of **Thio** on gold.

Nature of the layer	Substrate (gold)	TBPF ₆	DzF8	Thio
Contact angle (°)	48.4	66.5	106.8	91.5

Table II.4: Contact angle measured on gold grafted with **TBPF₆**, **DzF8** or **Thio**.

trile. All three layers should inflate when put inside an acetonitrile solution due to their affinity with this solvent, which would make them more porous. If the signal of the redox probe is still lower than when a non-grafted probe electrode is used, the grafted layer is compact and insulating. The results are shown figure II.14. The reversible peaks centered at 0.1 V vs Ag/Ag⁺ correspond to the oxidoreduction of ferrocene. The measured overpotential is around 0.2 V for every measurement, meaning that the electron transfer is slower than when using a pure gold or carbon electrode which shows that the grafted layer impairs the transfer of electron from the electrode to the solution, even with the **TBPF₆** layer. However, this overpotential does not change with the different layers.

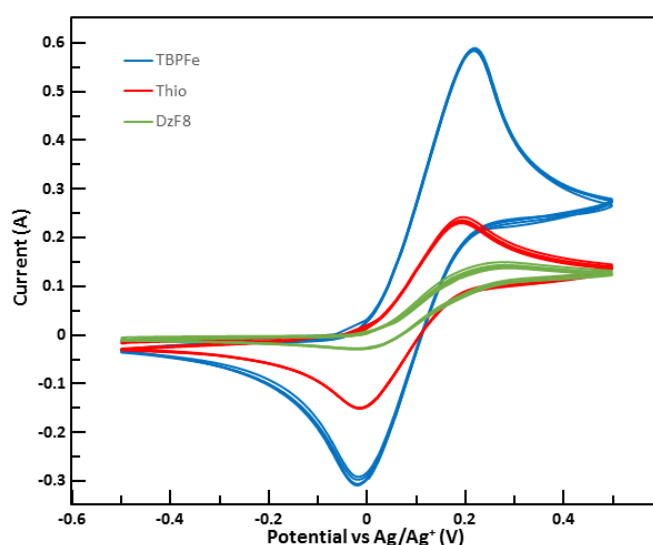


Figure II.14: CV (5 cycles) at 50 mV/s of a solution of 10 mM ferrocene in 0.1M TBAPF₆ in ACN on gold grafted with **TBPF₆**, **DzF8** or **Thio**.

The ratio between the intensity of the oxidation and the reduction peak of the ferrocene

on the **TBPF**e grafted electrode is around 2, which is a sign of a good diffusion of the redox probe to the electrode. This could be due both by the fact that the **TBPF**e layer is conducting and thus behave as the conducting electrode on which the ferrocene probe is reduced or by the fact that the diffusion of the ferrocene probe to the surface of the gold electrode is not limited by the **TBPF**e layer. This would mean that the diffusion coefficient is the same in the solution as in the **TBPF**e layer. For the **DzF8** and **Thio** layer, however, the shape of the peaks is closer to what is obtained when the diffusion coefficient of the layer is lower than the diffusion coefficient of the solution, as seen in [119]. This means that the two layers act as an insulator to the ferrocene probe, with **DzF8** being a better hindrance to ferrocene diffusion than **Thio**. This could be due to the fact that the **Thio** layer has a higher affinity with acetonitrile than **DzF8** or that the **DzF8** molecules are more closely packed, notably due to interactions between the long fluorinated chains.

II.4 Control of the thickness of the layer grafted

In this part, the working electrode used is a patterned gold electrode of a few micrometers width made using e-beam lithography and metal evaporation on oxidized silica wafers. In order to electrograft each electrodes individually, the sample is put inside the diazonium solution. The electrical contact of each electrodes is done individually by using a tungstene tip. The setup is illustrated in figure II.15. All the electrografting are done in a glove box.

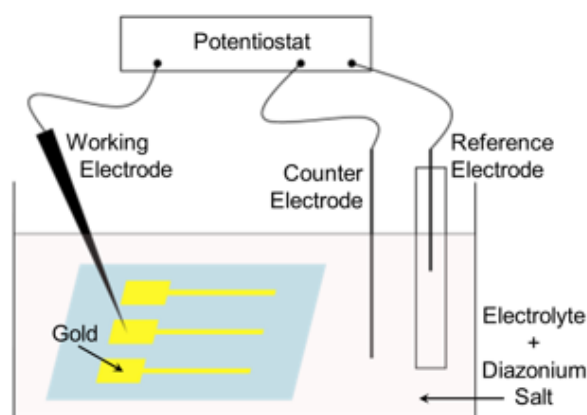


Figure II.15: Scheme of the setup used for electrografting on microelectrodes.

The different conditions of electrografting are studied by electrografting each individual electrodes using various conditions. However, in order to have a better control over the electrografting process, cyclic voltammetry will not be used in order to avoid the oxidation or reduction of the various redox center that can be found on the diazonium salt to be grafted. The process is divided in three steps : (1) a first linear sweep voltammetry (LSV) step that starts from the open circuit voltage (OCP) to the grafting potential at 50 mV/s; (2) a second step of chronoamperometry (CA) at the grafting potential during a set time; (3) a last step of LSV from the grafting potential to 0 V vs Ag/Ag⁺ at 50 mV/s. The CA process allows the formation of a stationary regimen and thus a continuous reduction of diazonium salt at the surface of the electrode. The resulting curves of this process are shown figure II.16. Another advantage of this process is that the grafting potential is chosen in order to reduce only the diazonium part of the solution, meaning

that the molecule to be grafted will not be stressed during the ECG process due to oxidation or reduction of its redox centers.

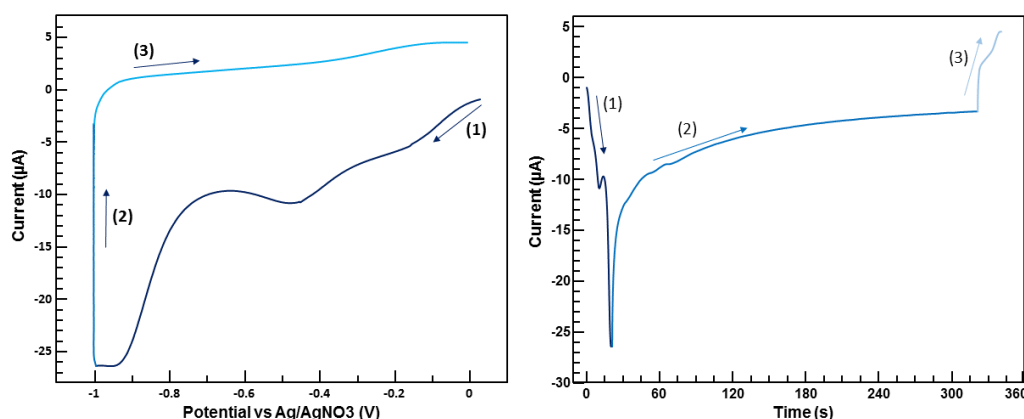


Figure II.16: Current measured versus the potential applied (left) and current applied versus time (right) of a typical electrochemical controlled grafting process. (1) LSV at 50 mV/s from OCP to grafting potential, (2) CA at grafting potential, (3) LSV at 50 mV/s from grafting potential to 0 V vs Ag/Ag⁺.

Before studying the various electrochemical conditions on the electrografting process, a first study on the impact of the geometry of the electrode on the resulting layer thickness have been done using the **TBPFe** (figure II.17). An electrode of different width is made using a mask made from e-beam lithography and metal evaporation, and is then grafted with **TBPFe** using the previous setup. The thickness of the grafted layer is measured by using AFM. On the profile of figure II.17, the thickness of the grafted layer is higher on the side of the electrode than on the middle. This effect will be called the edge effect for the rest of this document.

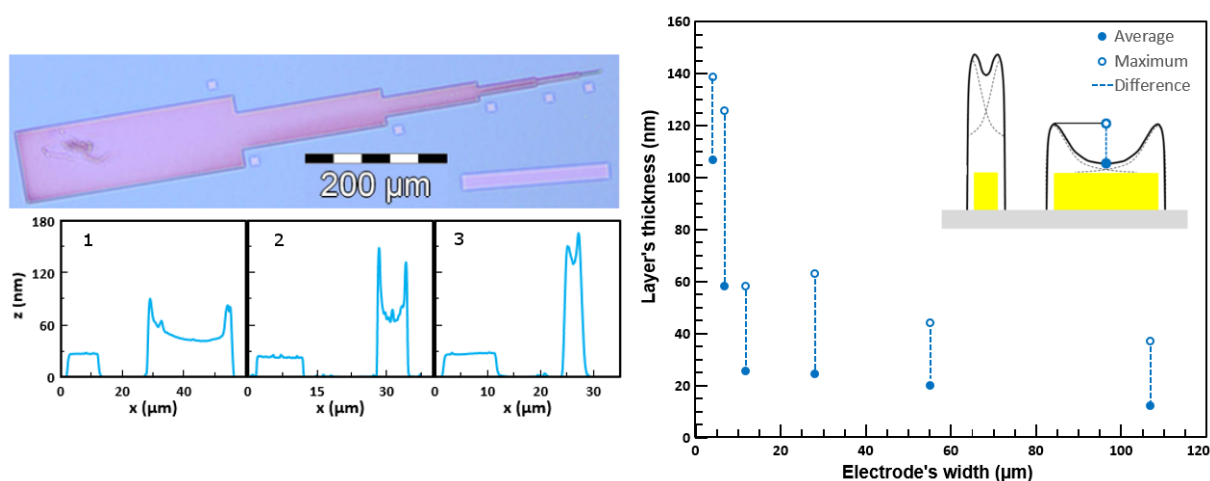


Figure II.17: Optical microscope image of a **TBPFe** electrografted electrode and profile along the red lines corresponding to an electrode width of 28 µm (1), 7 µm (2) and 4 µm (3) respectively (left). Results of the different layers' thickness and illustration of the impact of the edge effect (dotted black lines) on the final thickness of the grafted **TBPFe** layer (red line) with the reduction of the width of the patterned gold electrode (yellow) (right).

The width of the electrode impacts strongly the ratio of the maximum thickness mea-

sured and the average, which is the thickness measured in the middle of the electrode. The thinner the electrode is, the higher this ratio is, until the tendency is reversed after a critical width, here 7 μm . However, the edge effect is still present even after this critical width. In fact, it may be due to the fact that the edge effect of both side of the electrode combines themselves, and thus increase the average thickness of the layer (20 nm at 12 μm versus 105 nm at 4 μm) while diminishing the difference between the average and the maximum thickness, such as illustrated in the inset of figure II.17. In order to have a high density of electrodes and a low edge effect, a width of 2 μm is set for the electrodes for the following study.

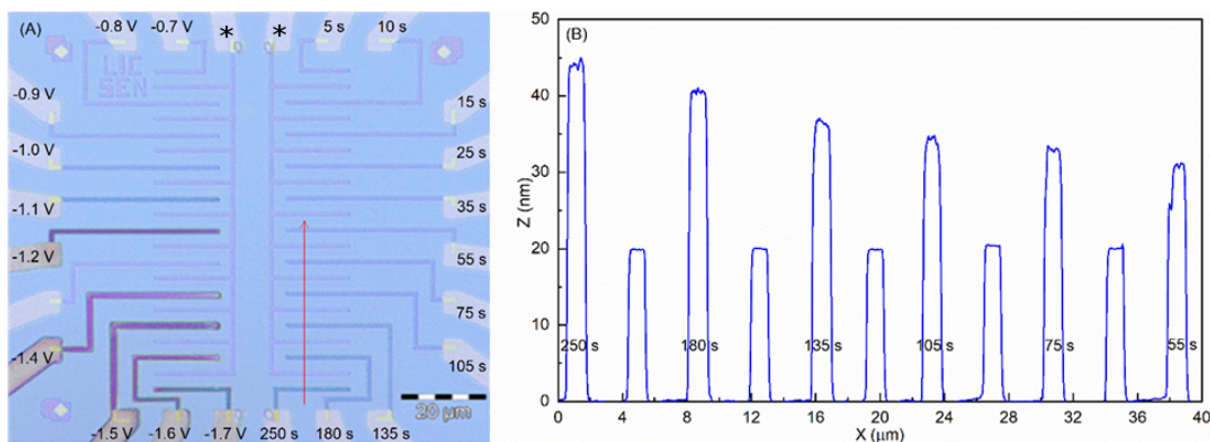


Figure II.18: Optical microscope image (left) and AFM height profile (right) along the red arrow of a sample electrografted with **TBPFe** using different grafting potentials for the left side and different times for the right side. The non grafted electrodes are indicated by a *.

A typical set of results obtained after electrografting **TBPFe** on various electrodes with different conditions is shown figure II.18. Only two electrodes are not grafted, indicated by a *. These two electrodes are used as a reference electrode, and the resulting thickness of the grafted layer is calculated by doing the difference between the total thickness of each grafted electrode and the thickness of the non-grafted reference electrodes. Differences between grafted electrodes can already be seen : on the left side, the different potential used lead to different looking grafted layer, while on the right side, the time only impacted the final thickness of the layers.

In the following part, the electrografting of **TBPFe** on one side and of **DzF8** and **Thio** on the other side is studied. Three different parameters of the CA are probed : the time, the grafting potential and the concentration of the active species.

II.4.1 TBPFe electrografting

Influence of the concentration

The concentration of the **TBPFe** diazonium molecule on the final thickness of the grafted layer was first investigated. The grafting process was performed at -1 V vs Ag/Ag⁺ for 120 s. Figure II.19 displays the final thickness of **TBPFe** (determined by AFM) as a function of the concentration of **TBPFe** in solution. A sharp increase between 1 μM to 15 μM is observed. At higher concentrations (between 15 and 80 μM), the final thickness barely increases. This behavior can be due to the fact that when

the solution is not concentrated enough, all the species near the electrode are reduced and then mostly react with the surface for grafting or with other molecules to form polymers in solution, which creates a local drop of concentration of the species in solution in the vicinity of the electrodes. In order to continue the grafting process, molecules need to diffuse from the solution to the electrochemical double layer where they get reduced and grafted. When the concentration is too low, the process is then limited by the diffusion of **TBPFe** in solution. When the concentration is high enough, the diffusion process is not the limiting factor, but the surface of the working electrode limits the quantity of the **TBPFe** molecules that can be reduced. In the following studies, the concentration of **TBPFe** used is around 28 μM since this concentration is in the plateau and small variations due to solvent evaporation will not impact strongly the resulting thickness.

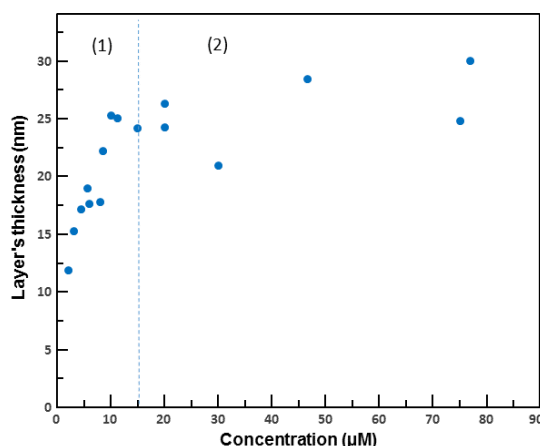


Figure II.19: Final thickness of an electrografted layer of **TBPFe** versus the concentration of **TBPFe** in a solution of 0.1 M TBAPF₆ in ACN using a 120 s CA at -1 V vs Ag/Ag⁺. (1) Grafting limited by diffusion; (2) Grafting limited by the surface of the electrode.

Influence of the potential applied

The influence of the potential of the ECG on the final thickness of **TBPFe** layers is shown figure II.20. Between -0.6 V and -1.5 V, the average thickness of the layer as well as the edge effects, represented by the maximum thickness, increase. The first increase is due to the fact that a higher potential applied gives a higher current, meaning that more species are reduced during the same time, thus giving a thicker layer. In the same way, the increase of edge effects could be due to the fact that, at a higher potential, the local concentration of species to reduce diminishes, until this concentration is close to 0 in the direct vicinity of the electrode. The next molecules to be reduced needs to diffuse from the solution to the surface of the electrode. The sides of the electrode have access to more solution, which leads to the same behavior as the one observed above when studying the impact of concentration.

Below -1.5 V, the thickness and the edge effect decreases. This potential corresponds to the beginning of the reduction peak of the trisbipyridine iron complex. There is then a competition between the reduction of the diazonium part of the molecule and the reduction of its ligands. Below -1.4 V, the reduction of the ligands slowly becomes the most favorable reaction, which explains the decrease of the resulting layer thickness when the potential diminishes.

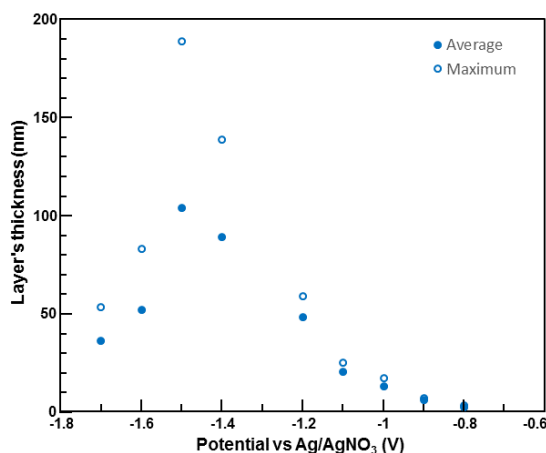


Figure II.20: Final thickness of an electrografted layer of μM **TBPFe** versus the potential applied during a 60s chronoamperometry in a solution of 28 μM **TBPFe** and 0.1 M **TBAPF₆** in ACN.

Influence of the time of the ECG

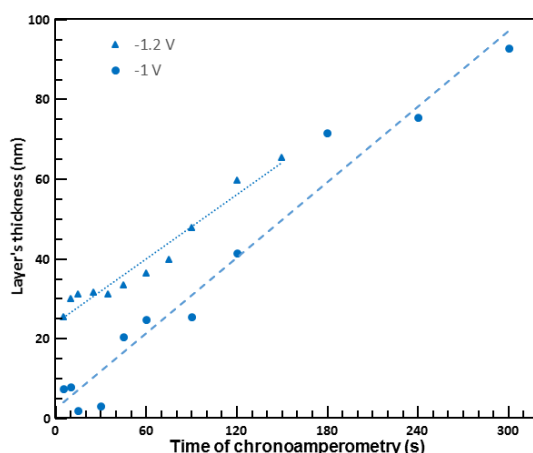


Figure II.21: Final thickness of an electrografted layer of **TBPFe** versus time of the chronoamperometry at -1 V and -1.2 V in a solution of 0.1 M **TBAPF₆** and 28 μM **TBPFe** in ACN.

The influence of time on the final thickness of grafted **TBPFe** layer is shown in figure II.21. The concentration is set at 28 μM , and two grafting potentials are used : -1 V, since it seems the most promising due to the nearly nonexistent edge effects (Figure II.20), and -1.2 V, to see if the grafting can be performed faster at higher potential. The longer the CA is, the thicker the layer. Both curves has a similar slope (18 and 16.2 nm/min respectively), meaning that grafting at higher potential does not increase the grafting speed. In addition, it leads to a higher starting thickness, which is around 5 nm for -1 V and 25 nm for -1.2 V, which is partially due to the fact that there is grafting between -1 V and -1.2 V during the LSV steps. A fine control over the thickness of the **TBPFe** grafted layer between 5 nm and nearly 100 nm on a 1 μm width gold electrode is obtained with a grafting potential of -1 V, which constitutes a major achievement of this study.

Influence of the state of the tip

While a good control over the growth of the **TBPF**e layers was demonstrated in the previous parts, edge effects are still visible even at low potential, especially on samples that have a width of 8 μm . Further studies were conducted to solve this issue. First, electrografting using the best parameters determined above was performed: after the first LSV to -1 V vs Ag/Ag⁺, the potential used during the CA was -1 V vs Ag/Ag⁺ during 20 to 280 s using a tungsten tip in a solution of **TBPF**e 28 μM in acetonitrile. This tip, soaked in the electrolyte and connected to a macroscopic gold electrode was used to graft **TBPF**e by doing 10 CV cycles between -2 V and 1 V on a sacrificial gold sample to passivate it before the electrografting of the electrode of interest. This passivated tungsten tip was then used to electrograft **TBPF**e on patterned electrodes of 8 μm width (figure II.22 left side). This experiment was done with a set of 24 samples, and each showed the edge effects that have been seen during the previous studies.

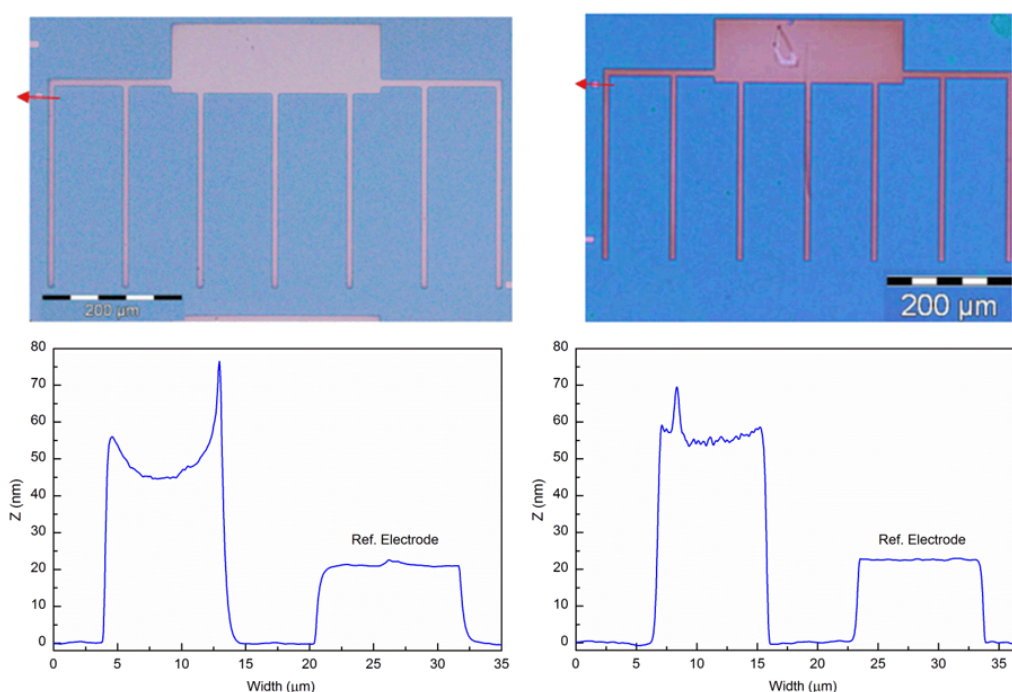


Figure II.22: Optical microscope image of a sample grafted at -1 V vs Ag/Ag⁺ for 85 s with a **TBPF**e passivated tip (up left) and its corresponding profile (down left). Optical microscope image of a sample grafted at -1 V for 280 s with a **DzF8** passivated tip (up right) and its corresponding profile (down right).

Another tip was electrografted with the insulating **DzF8** molecule by using a solution of 0.1 mM of **DzF8** and a non-macroscopic gold sample using 10 CV between -1.3 V and 0 V vs Ag/Ag⁺. Then, the same study as above was conducted. The optical microscope and AFM images of the sample (Figure II.23 and Figure II.22) show that the layer is homogeneous and no edge effects are observed. Also, the resulting layer is homogenous on areas of more than 1000 μm^2 , such as seen in figure II.23 where 150 μm of the electrode shows a homogeneous, smooth and defect-free surface at this scale.

When the final layer thicknesses using a passivated tip or a non-passivated tip are compared (Figure II.24 and II.21 at 2 and 5 min), the results are similar. Thus, the tip

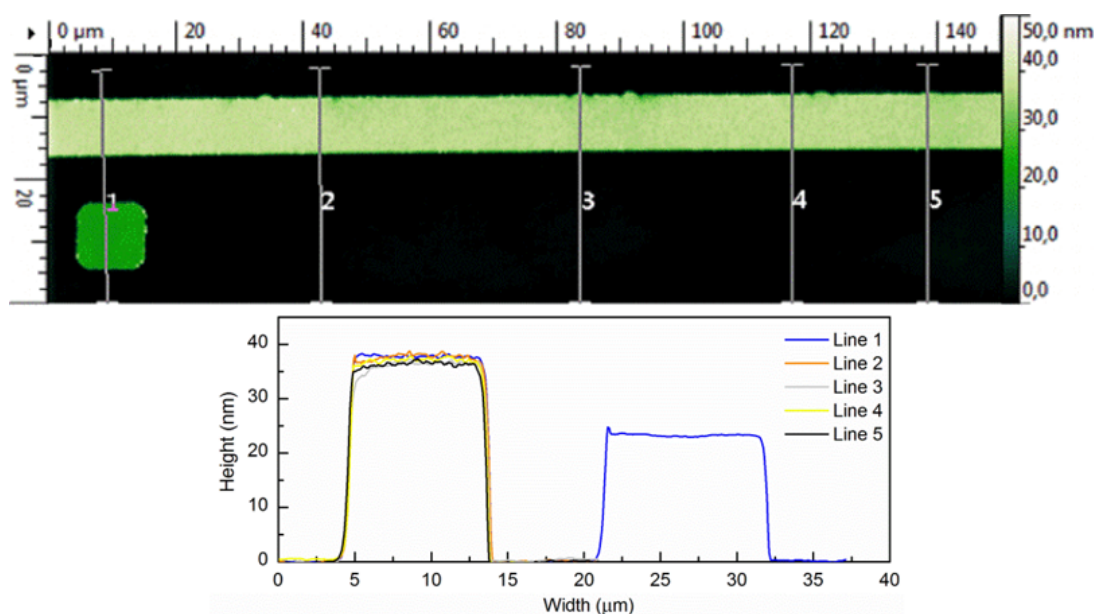


Figure II.23: AFM image of a 150 μm part of an electrode grafted during 120 s with a **TBPFe** passivated tip at -1 V (up) and its corresponding profiles (down).

has only an impact on the quality of the layer and its edge effect, but does not affect its average thickness. The reasons for this phenomenon are being investigated.

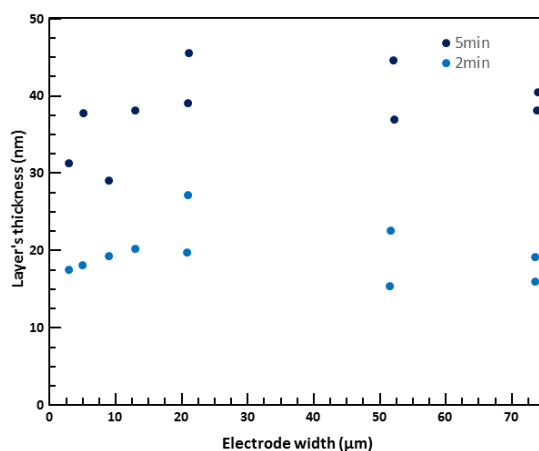


Figure II.24: Final thickness of an electrografted layer of μMTBPFe versus the width of the electrode using a 2 min or 5 min CA at -1 V vs Ag/Ag^+ in a solution of 28 μM **TBPFe** and 0.1 M TBAPF_6 in ACN using a passivated tip.

Since the edge effects are solved, the impact of the size on the electrode on the final thickness of **TBPFe** grafted can be reassessed. The results are shown Figure II.24. Contrary to the previous results, the final thickness of the layer grafted varies between 15 and 23 nm for a 2 min grafting and 30 to 45 nm for a 5 min grafting for a width of the electrode between 2 and 73 μm . When compared to Figure II.17, the results for an electrode between 15 and 75 μm are similar for the grafting with a **DzF8** passivated tip and without one, if what is compared is the average of the grafted layer. However, with an electrode of width <15 μm , the grafting with a non-passivated tip shows a sharp increase up to a layer of 120 nm thickness when the width of the electrode diminishes (Figure II.17). With a **DzF8** passivated tip, the thickness stays around 20 nm for a 2 min

grafting. That means that the effect of the width of the electrode is solved by passivating the tip with the **DzF8**, an insulating molecule. That also confirms the fact that the 120 nm layer that is obtained with the **TBPF** passivated tip is due to the stacking of the edge effects from both sides of the electrode, increasing the average thickness of the layer grafted, as is illustrated in the scheme in the inset of Figure II.17.

II.4.2 DzF8 and Thio electrografting

Influence of the concentration

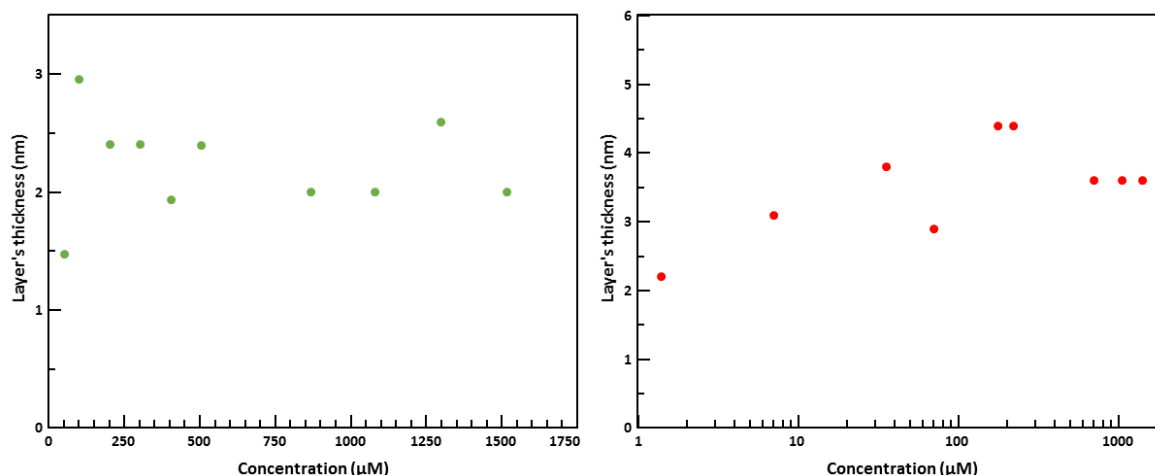


Figure II.25: Final thickness of the electrografted layer of **DzF8** (left) and **Thio** (right) versus the concentration of the active species using a 2 min CA at -1 V and -1.3 V vs Ag/Ag⁺ respectively in a solution of 0.1 M TBAPF₆ in ACN.

The concentration of the active species on the final thickness of the grafted layer is then probed for **DzF8** and **Thio** (figure II.25). The thickness for **DzF8** varies between 1.5 and 3 nm for a concentration between 50 μM and 1600 μM, and between 2 and 4.5 nm for a concentration between 5 and 1050 μM for the **Thio** molecule. The main difference between **TBPF** and these two molecules is that the grafting is self-limited, since the grafted layer can not transfer the electrons from the working electrode to the solution. Whatever the concentration of active species in solution, the molecules of **DzF8** and **Thio** in solution near the working electrode is always sufficient to have the final thickness of the layer without needing the diffusion of the species after depletion of the active molecule in the double layer, hence the fact that the concentration does not have any effect on the final thickness of the layer grafted. Impact of the concentration on the resulting thickness have not been probed for really low concentration for **DzF8**. However, since **Thio** has a similar structure and electrochemical activity, the results should be similar. For the following studies, a concentration of 1 mM for **DzF8** and 0.5 mM for **Thio** is used.

Influence of the potential applied

The influence of the grafting potential on the resulting grafted layer of **DzF8** and **Thio** is shown figure II.26. Both molecules show a similar behavior : the lower the grafting potential is, the thicker the layer is. Since the formed layers do not have any redox centers, the electrons can not be brought to the solution from the working electrode

through the insulating layer. Thus, the only electrons that can reduce the diazonium salts in solution and then increase the thickness of the layers are the electrons that can hop from the working electrode to the solution by tunneling effect. This process exponentially decreases with the layer thickness. Increasing the potential allows the electrons to have more energy to cross the tunneling barrier, which effectively leads to an increase of the layer's thickness. The resulting thickness is around 6 nm for **DzF8** and 4.5 nm for **Thio**, which is way lower than the **TBPF₆** layers. Also, the difference of thickness between **DzF8** and **Thio** can be due to the fact that the **DzF8** molecule is bigger than the **Thio** molecule.

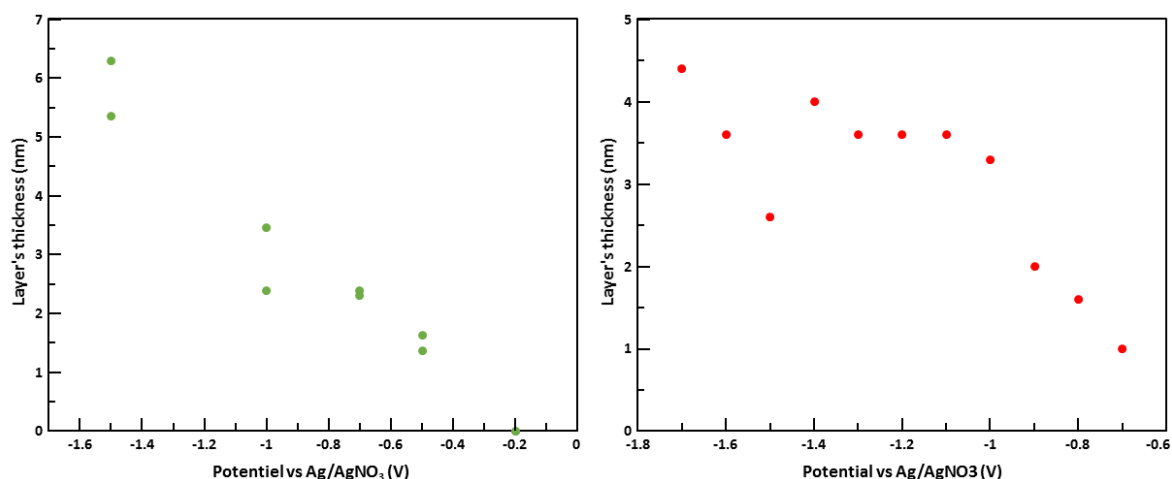


Figure II.26: Final thickness of the electrografted layer of **DzF8** (1 mM) (left) and **Thio** (0.5 mM) (right) versus the potential applied during 2 min in a solution of 0.1 M TBAPF₆ in ACN.

Influence of the time

The influence of the time of the CA on the resulting thickness of **DzF8** and **Thio** layers is shown figure II.27. For **DzF8**, the resulting thickness is between 2 and 3.5 nm for a time between 5 s and 900 s (15 min), which is not surprising considering the fact that the layer formed is insulating. However, for **Thio**, the resulting thickness is between 3.2 and 4 nm for a time between 25 s and 270 s, but increases between 5 and 25 s. **Thio** molecules have a thiol function, which has a great affinity with gold, which would position the molecule with its thiol function close to gold, meaning that the diazo function would be on the opposite side. However, since electrons are on the surface of the working electrode and the molecule is not covalently bonded to the gold electrode with its sulfur atom, it can rotate and thus allowing its diazonium function to be reduced by the electrons at the surface of the electrode. The molecule would then be covalently bonded to the surface with its thiol function on the opposite side of the working electrode on the molecule. This process could explain the time needed to have a fully covered working electrode and then the increase of layer's thickness for short times. However, when the electrode is fully covered, the behavior is the same as the **DzF8** molecule.

In this part, the different molecules used in this PhD were presented : **TBPF₆** has redox properties, **DzF8** has a highly hydrophobic tail and **Thio** has a thiol function that could be used for attaching gold on top of it. Their electrochemical grafting and

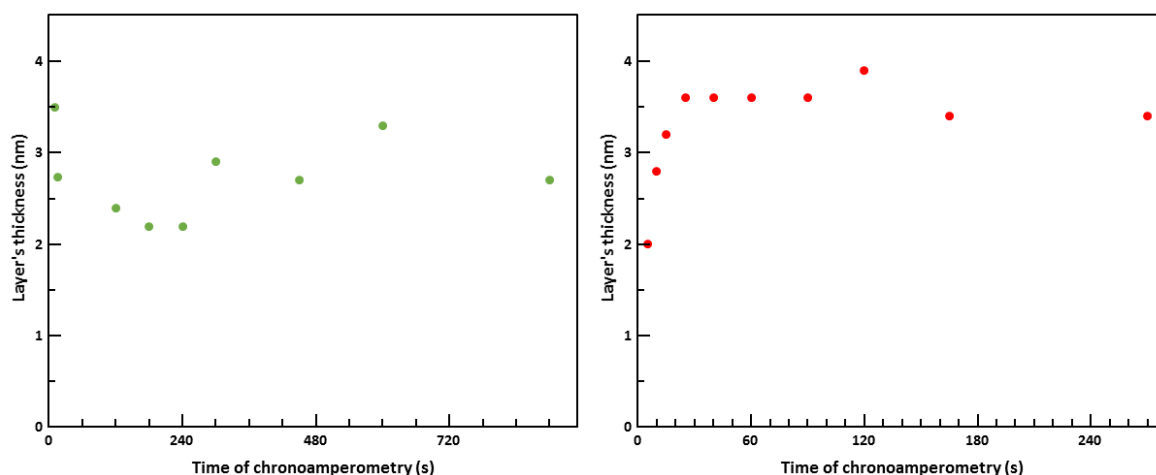


Figure II.27: Final thickness of the electrografted layer of **DzF8** (1 mM) (left) and **Thio** (0.5 mM) (right) versus the time of the CA at -1.3 V vs Ag/Ag⁺ in a solution of 0.1 M TBAPF₆ in ACN.

response have been assessed, and the three molecules have been attributed to two different types : the electroactive type (**TBPFe**) that is not self-limiting when grafted, and the insulating type (**Thio** and **DzF8**) that has a self-limiting grafting. Their structure have been probed by using infrared, which is not enough to conclude on the nature of the grafted layer, and XPS, which confirms that the layers contain only the grafted molecules. Their compacity are also probed by using a redox probe, and the **DzF8** and **Thio** layers were found to be insulating, while the **TBPFe** layer was conductive.

Then, the molecules have been grafted on micro-electrodes made using photolithography and e-beam lithography. A three step process have been developed for an optimal control of the electrografting on these devices. After studying the impact of the geometry on the resulting layers, each molecules have been grafted using different times, grafting potentials and concentrations in order to have a good control over the resulting thickness. Moreover, an upgrade to the electrografting of **TBPFe** has been discovered, allowing this molecule to be grafted as a smooth and apparently defectless layer. In the end, a good control over the electrografting of the three molecules have been achieved : a layer of 5 to 100 nm of **TBPFe** can be made while layers between 2 and 5 nm of **DzF8** and **Thio** can be obtained.

Chapter III

Double layer electrografting

In the previous part, thick layers of electroactive molecules and thin layers of molecules without redox centers have been made. However, having access to organic layers composed of multiple different organic layers could be interesting. In order to do that, electrografting **DzF8** or **Thio** molecules on top of the **TBPFe** layer could work : **TBPFe** layers can be grafted from 5 up to 100 nm, and thus would increase a lot the thickness range for the insulating **DzF8** and **Thio** layers, since those diazonium salts can only be grafted up to 6 nm. This would result in an organic layer of tunable thickness between 10 and 100 nm with an hydrophobic surface, in the case of **DzF8**, or a thiol surface, in the case of **Thio**.

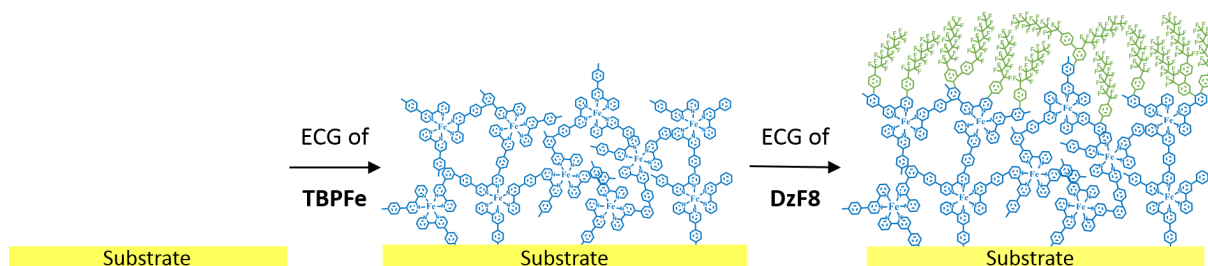


Figure III.1: Scheme of the double layer electrografting (ECG).

This concept, that will be referred in the rest of the document as double layer electrografting, is illustrated on figure III.1. First, the substrate that will be grafted with the double layer is grafted with the **TBPFe** molecule. Then, by using the same electrode as a working electrode in a solution containing another diazonium salt, in this example **DzF8**, the other diazonium salt is electrografted on top of the first organic layer, leading to a thickness increase and a change of the nature of the surface. This leads to a thicker layer with its surface containing no redox active centers in this case.

This idea of polymerizing a molecule on top of an already electrografted layer was shown the first time in 2008 by Santos et al. [107]. In order to do that, a first layer of a molecule, the 4-aminodiphenylamine, is electrografted on a carbon electrode. Since this ECG layer is composed of aniline, oxidation of these molecules are possible and can form a conducting surface, which is then used to electropolymerize polyaniline on top of it. The resulting double layer was found to have better chemical and physical stability than a simple electropolymerized polyaniline film while keeping its electrochemical properties. In the same way, the same group managed to form elongated oligo(EDOT) chains by first electrografting an oligo(BTB) layer and then using it as an organic layer

for electropolymerising EDOT molecules [120]. A scheme presenting both processes is shown in figure III.2.

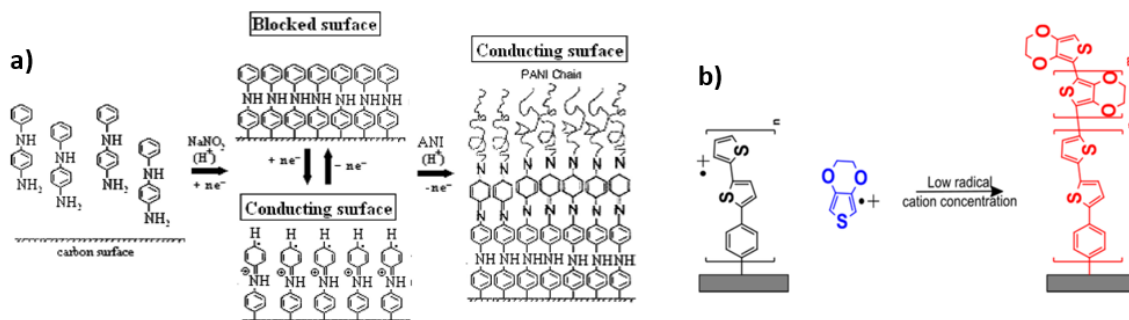


Figure III.2: a) Scheme of 4-aminodiphenylamine grafting and subsequent aniline polymerization on a carbon conducting surface. b) Scheme of a polymerization of EDOT on oligo(BTB) layer. Figures from [107] and [120] respectively.

Thus, this part will present the first double ECG layers consisting of an insulating layer, here **Thio** or **DzF8**, electrografted on top of an electroactive **TBPFe** layer. This could be done thanks to the **TBPFe** layer that exhibits electroactive properties in the reduction potential domain of the diazo function, and thus can reduce the diazonium molecules to electrograft those. The main differences with the works of Lacroix et al. is that the second layer added on the first ECG layer is an electrografted and insulating layer in our case.

III.1 Electrochemical grafting of the double layer

First, the electrochemical behavior of the double layer grafting is studied by using a previously **TBPFe** grafted gold electrode in an electrografting setup. Cyclic voltammetry is done on such gold electrode in a solution containing **DzF8**, and the results are shown figure III.3. Contrary to a normal **DzF8** grafting (figure II.8), the first reduction peak is at -1.2 V, which also corresponds to the reduction peak of the quasi-reversible peaks of grafted **TBPFe**: the **TBPFe** grafted layer could then be insulating in the range of the **DzF8** grafting (between 0 V and -0.6 V). However, as soon as the reduction peak at -1.2 V is met, electrons are exchanged between the working electrode and the molecules in solution, resulting in the reduction of **DzF8** molecules since -1.2 V is below its reduction potential. Then, after the first cycle, the peak at -1.2 V diminishes greatly, since its oxidized counterpart was not met. In the following cycles, the current measured continues to diminish, slower than during a **DzF8** electrografting on a bare gold electrode (II.8), meaning that the ECG process is different on an already grafted electrode. Also, the new electrografted layer is then more and more insulating, as shown by the diminishing measured total current after the first cycle, which is in agreement with the nature of the layer grafted on top of **TBPFe**.

The electrochemical response of the new layer is probed by performing CV in the electrolyte with that electrode as a working electrode (figure III.4). The main differences between the response of the simple **TBPFe** layer and the double layer of **TBPFe**+**DzF8** is the presence or absence of any oxidoreduction peaks. On the CV of **TBPFe**, the peaks of the $\text{Fe}^{2+}/\text{Fe}^{3+}$ and the peaks corresponding to the oxidoreduction of its ligands are visible, which is in agreement with the results seen in the previous chapter. After **DzF8**

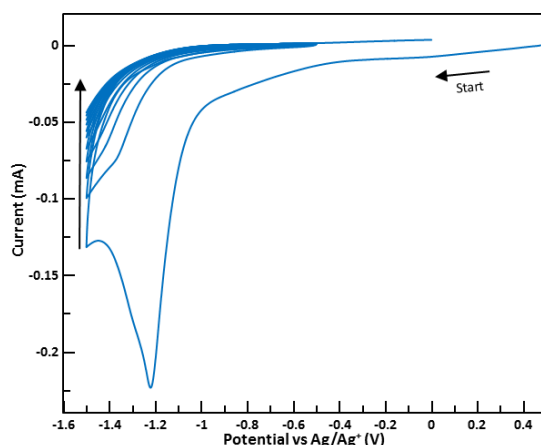


Figure III.3: CV (10 cycles) at 50 mV/s of a solution of 1 mM **DzF8** in 0.1 M TBAPF₆ in ACN using a **TBPF_e** grafted gold electrode as a working electrode.

grafting however, those peaks are barely visible, meaning that the newly grafted layer insulates the **TBPF_e** layer from the solution. The **TBPF_e+DzF8** layer shows a reduction peak around -1.7 V, which could be the reduction peak of the various azo bonds that were made during the grafting.

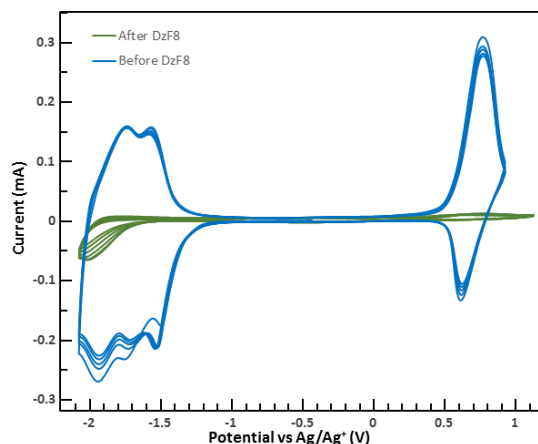


Figure III.4: CV (10 cycles) at 50 mV/s in a solution of 0.1 M TBAPF₆ in ACN with a gold electrode grafted with **TBPF_e** (blue line) and the same electrode after electrografting of **DzF8** (green line).

The insulating properties of the newly made layer is further probed with the same ferrocene test that was made in the previous chapter. The results are shown figure III.5. When the **DzF8** layer is compared with the **TBPF_e+DzF8** double layer, the former is way more passivating than the latter. The **DzF8** of the double layer was grafted on an already grafted **TBPF_e** layer that was not as smooth or dense as a pure gold electrode, which could have made a less compact and insulating layer since the surface was less structured. The **TBPF_e** layer could also have a higher affinity with acetonitrile than **DzF8**, and thus would inflate more than the second layer, which would make it more porous.

The same set of studies are made with a double layer of **TBPF_e+Thio**. First, the electrografting of **Thio** on a **TBPF_e** grafted electrode is shown figure III.6. The behavior is different of the **TBPF_e+DzF8** double layer grafting : instead of disappearing, the

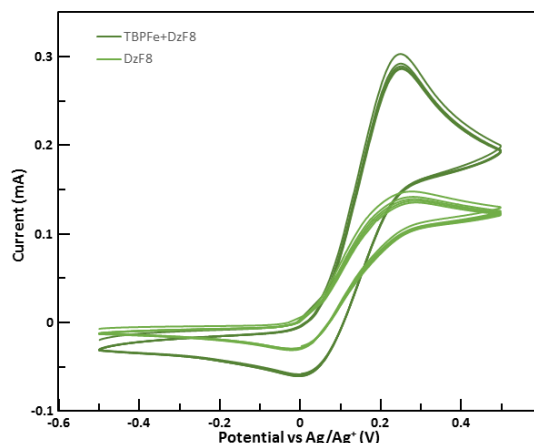


Figure III.5: CV (5 cycles) of a solution of 10 mM ferrocene in 0.1 M TBAPF₆ in ACN on gold grafted with **DzF8** only (light green line) and on gold grafted with a double layer of **TBPFe+DzF8** (dark green line).

peaks corresponding to the azo bonds are shifted and more intense. The oxidation peak of the quasi-reversible peaks of the **TBPFe** layer at +0.7 V is gradually shifted toward higher potential until +0.9 V, while the corresponding reduction peak at -1.3 V is gradually shifted toward lower potentials until -1.4 V. These peaks could be attributed to the oxidoreduction of the various azo bonds of the layers that can be formed during the ECG process of the various diazonium salts.

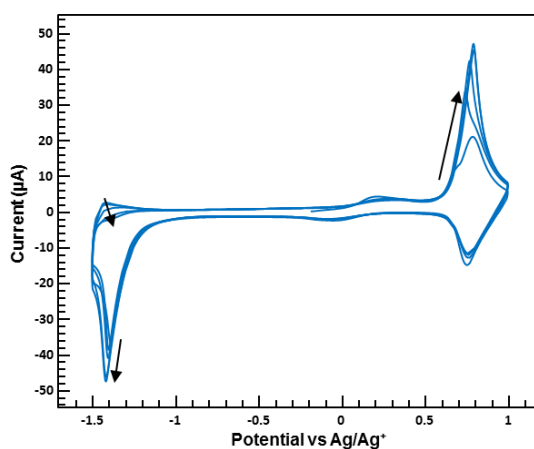


Figure III.6: CV (10 cycles) at 50 mV/s of a solution of 0.5 mM **Thio** in 0.1 M TBAPF₆ in ACN on a **TBPFe** grafted gold electrode.

The **Thio** grafting on top of **TBPFe** could then form more azo bonds on the surface of the electrode, or they could be more accessible for the electrolyte. Also, the peaks corresponding to the oxidoreduction of the iron(II) core of the grafted **TBPFe** does not change at all during the electrografting of **Thio**, meaning that the formed layer is not insulating. This can be explained by the fact that **Thio** is a smaller molecule than **DzF8**, and would then be grafted not on the surface but deeper in the **TBPFe** grafted layer.

The electrochemical response of the **TBPFe+Thio** layer is probed by doing CV with the double layer grafted electrode as a working electrode in the electrolyte (figure III.7). In this case, the second layer of **Thio** was grafted by doing the optimized grafting process at -1.5 V for 5 min. First, this new layer is more insulating than when grafted

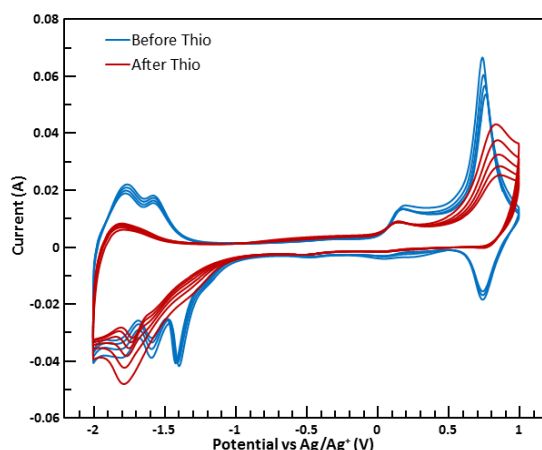


Figure III.7: CV (10 cycles) at 50 mV/s in a solution of 0.1 M TBAPF₆ in ACN with a gold electrode grafted with **TBPFe** (blue line) and the same electrode after electrografting of **Thio** (red line).

with the CV method (figure III.6): the Fe²⁺/Fe³⁺ reduction peak of the **TBPFe** nor the oxidation peaks of the ligands are visible. However, the oxidation peak at +0.9 V is still present, and the reduction peak that was at -1.4 V at the end of the CV electrografting is now at -1.75 V. The LSV-CA-LSV grafting process is then better than the CV process even with double layer electrografting. During cycling, the intensity of these two peaks diminishes. This could mean that the double layer is restructured during the probing CV in order to have most of the **Thio** molecules at the surface, thus giving better insulating properties to the layer, or that the oxidoreduction process associated with these two peaks is slow and not reversible.

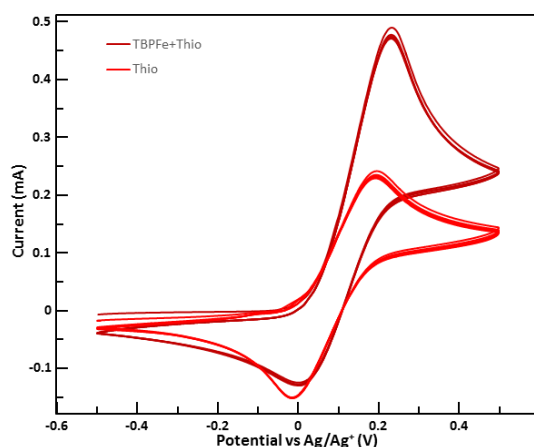


Figure III.8: CV (5 cycles) of a solution of 10 mM ferrocene in 0.1 M TBAPF₆ in ACN on gold grafted with **Thio** only (light red line) and on gold grafted with a double layer of **TBPFe+Thio** (dark red line).

The compacity of the newly made double layer is probed by using a ferrocene redox probe (figure III.8). As with the **TBPFe+DzF8** double layer, the resulting double layer is more insulating than the previous **TBPFe** simple layer. In the same way, the intensity of the ferrocene peaks is higher with the double layer than with the simple layer, and could be due to the same problems than with **TBPFe+DzF8** double layer.

Finally, the ferrocene redox probe results are compared between a simple **TBPFe** layer,

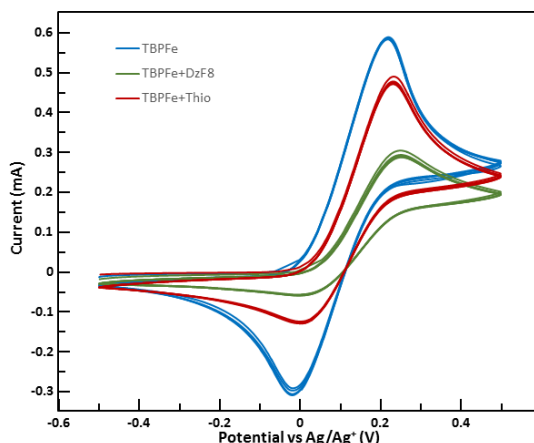


Figure III.9: CV (5 cycles) of a solution of 10 mM ferrocene in 0.1 M TBAPF₆ in ACN on gold grafted with **TBPFe** only (blue line), on gold grafted with a double layer of **TBPFe+DzF8** (green line) and on gold grafted with a double layer of **TBPFe+Thio** (red line).

a **TBPFe+DzF8** double layer and a **TBPFe+Thio** double layer in figure III.9. As seen previously, the passivating behavior is kept for all layers. Also, the **TBPFe+Thio** double layer is more insulating than the **TBPFe** simple layer. However, the **TBPFe+DzF8** layer is by far the most interesting layer in term of insulating properties between these three layers.

III.2 Physical characterization of the grafted double layers

As with the simple layers, the structure of the grafted double layers was probed by using various physical characterization tools. The infrared spectra of each grafted double layer and of a simple **TBPFe** layer are shown figure III.10. The bands corresponding to the aromatic C=C stretching vibration energy at 1600 cm⁻¹ and the bands corresponding to the C-N stretching vibration energy at 1250 cm⁻¹ are present. However, as with the monolayer, the difference between each layers can not be made : no spectra show the low intensity band of the S-H bending vibration at 2550 cm⁻¹. The sharp intense band at 1200 cm⁻¹ corresponding to the C-F bending vibration energy can be observed in the **TBPFe+DzF8** double layer's IR spectra though. Thus, IR can not be used to conclude on the nature of the grafted layer, since it is way too thin to have good spectra.

In order to have a better idea of the composition of the double layer, XPS was done. The results of this analysis on the **TBPFe+DzF8** layer is shown figure III.11 and table III.1. On the survey, peaks for fluor, gold and carbon can be seen. The Au 4f peaks are not visible, meaning that the double layer formed is either compact or thick enough so that the electrode cannot be seen by XPS. The second layer of **DzF8** electrografting then made the layer more porous or less compact than with **TBPFe** simple layer. No peaks are visible for the Fe 2p region, even on the high resolution spectra, which confirms the compacity of the **DzF8** second layer.

However, the peaks corresponding to the **DzF8** are sharp and well resolved. The F 1s peak has only one component corresponding to the C-F atom and represent 45.5% of the atoms measured. The C 1s high resolution spectra can be divided in 3

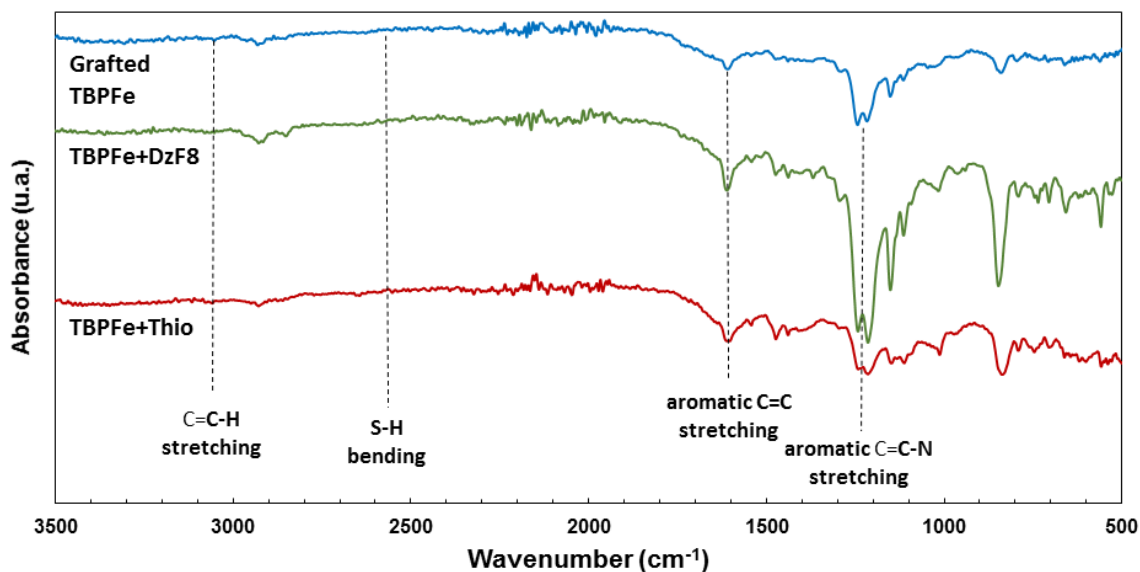


Figure III.10: Infrared spectra of a **TBPFe** grafted layer, a **TBPFe+DzF8** grafted double layer and a **TBPFe+Thio** grafted double layer.

components : the C-F₂ component at 292 eV for a concentration of 24.7%, the C-F₃ component at 294.3 eV for a concentration of 3.2% and the aromatic carbon at 285.7 eV for a concentration of 24.6%. The relative concentrations are what is expected : there is 7.7 times more C-F₂ than C-F₃, which is close than the theoretical 7. The aromatic C concentration is equal to the C-F₂ concentration, while it should be equal to 85% of that. This is due to some of the **TBPFe**'s aromatic carbon being integrated in this peak. The theoretical fluor concentration is 2.43 times higher than the C-F₂ concentration, versus the experimental 1.84 that is observed. The total percentage of the **DzF8** atoms measured is then equal to approximately 94.4% of all the atoms measured, if the quantity of the aromatic carbon at 285.7 eV is considered equal to 85% of the quantity measured of C-F₂. Thus, the second layer of **DzF8** made is pretty thick and dense, which seem to contradict the intensity of the Au 4f peak. Finally, there is the presence of some azo bonds that can be spotted with the N 1s peak at 401.8 eV. The nitrogen peak at 400 eV can be due to the nitrogen presents in the **TBPFe** molecules.

Atom and Orbital	F 1s	C 1s	C 1s	C 1s	N 1s
Peak position (eV)	689.2	294.3	292	285.7	400 / 401.8
Concentration (% atom)	45.5	3.2	24.7	24.6	2
Concentration (Theory)	54.8	3.2	22.6	19.4	0
Attribution					N=N

Table III.1: XPS data table for a grafted double layer of **TBPFe+DzF8** on gold.

The XPS spectra of the **TBPFe+Thio** layer are shown figure III.12 and III.2. The S 2p peak is well defined at 164 eV, and shows the same shape than the **Thio** simple

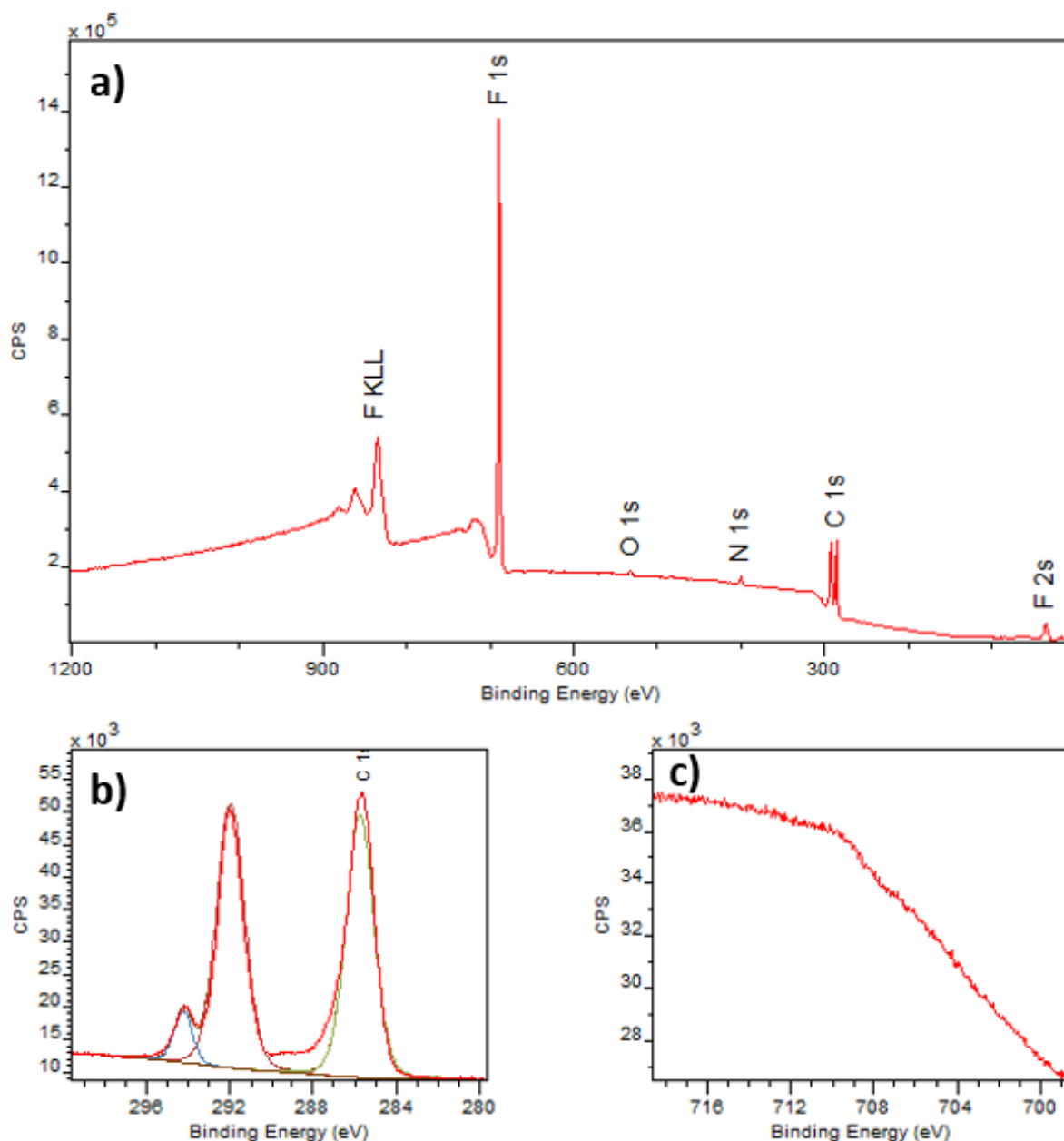


Figure III.11: XPS survey spectra (a) and high resolution spectra of the C 1s region (b) and the Fe 2p region (c) of a double layer of **TBPFe+DzF8** grafted on gold.

layer. Its calculated concentration is 11%, meaning that approximately (since there are 6 times more carbon than sulfur) 77.7% of all atoms measured are from the **Thio** layer. Thus, only 10% of the C 1s measured are from the **TBPFe** bottom layer. The Fe 2p peak is barely visible at 709.3 eV, meaning that the top layer of **Thio** is not as thick or covering as the **DzF8**. The N 1s peaks are also attributed to the various azo bonds.

Peaks corresponding to oxygen, nitrogen, gold and sulfur can be seen. The Au 4f peak at 83.8 and 87.4 eV is visible, but is at a relative lower intensity than in the spectrum of the **TBPFe+DzF8** meaning that the layer is more compact or thicker. However, it is still higher than on the spectrum of the simple **TBPFe** only (figure II.11), meaning that the formed double layer is less compact than its simple layer counterpart.

Both XPS datas prove that a layer of **DzF8** or **Thio** was grafted on top of a **TBPFe** layer.

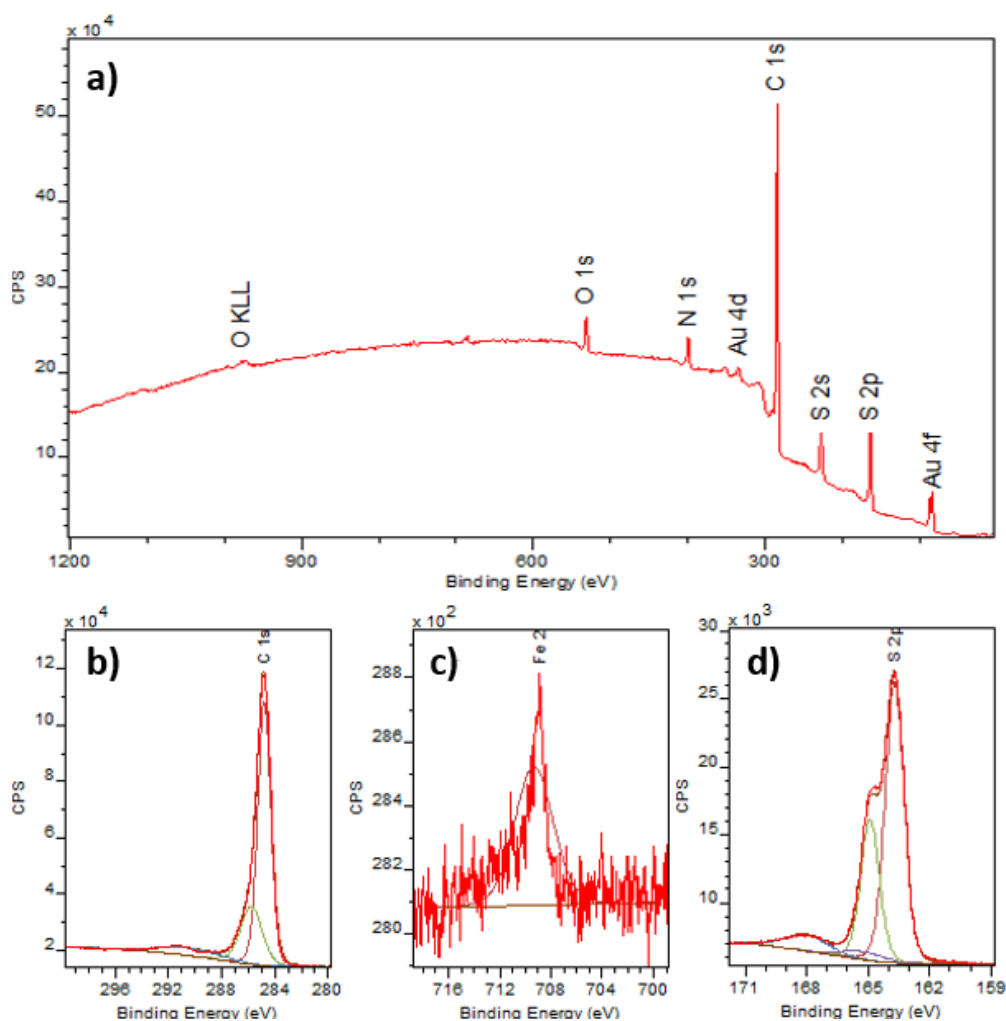


Figure III.12: XPS survey spectra (a) and high resolution spectra of the C 1s region (b), the Fe 2p region (c) and the S 2p region (d) of a double layer of **TBPFfe+Thio** grafted on gold. Theoretical concentrations are not shown due to the presence of the **TBPFfe** in the spectra.

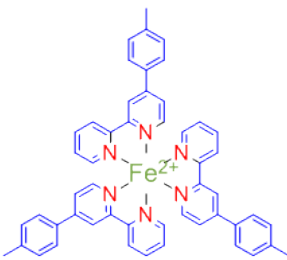
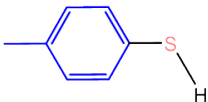
Atom and Orbital	Fe 2p	C 1s	S 2p	N 1s	Au 4f
Peak position (eV)	709.3	284.8/285.8	163.7 / 164.9	399.6 / 401.1	83.8 / 87.4
Concentration (% atom)	<0.1	76.3	11.1	4.5	0.6
Attribution			N=N	Substrate	

Table III.2: XPS data table for a grafted double layer of **TBPFfe+Thio** on gold.

A small notable difference is present : for the **TBPFe+DzF8**, no Fe nor Au signals are visible, meaning that the **DzF8** layer is either thicker or more compact (or both) than the **Thio** layer on top of **TBPFe**. This is confirmed by the fact that, for the **TBPFe+Thio** layer, 0.6% of the atoms measured are gold atoms. Since the LSV-CA-LSV process for the **TBPFe** grafting was the same for both, that means that the **Thio** grafting is probably less covering than the **DzF8** one.

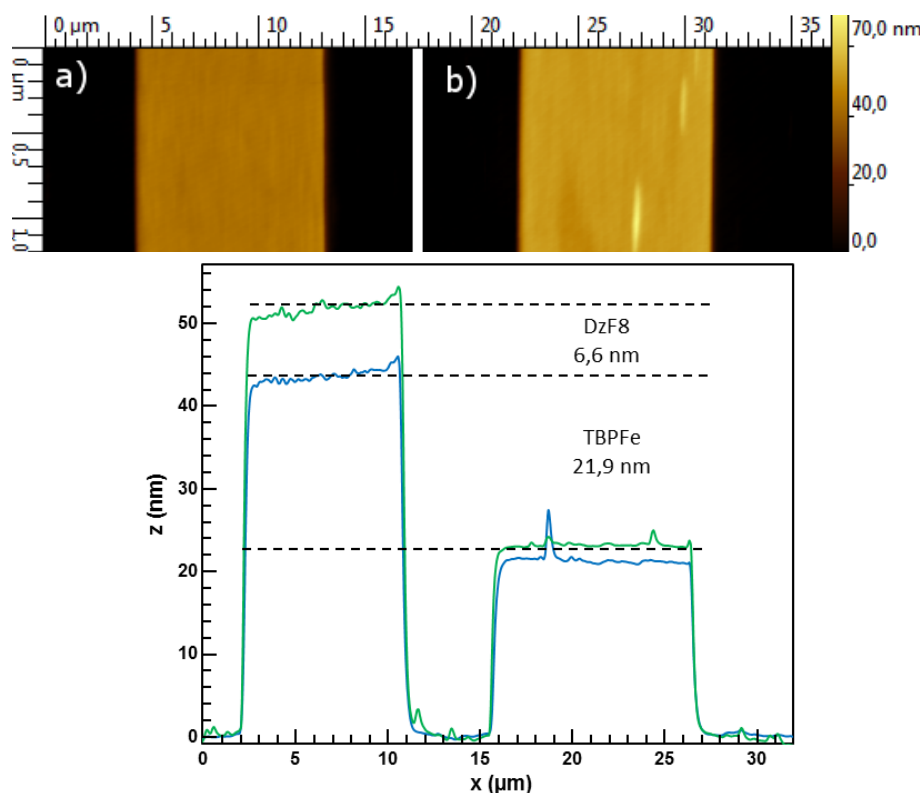


Figure III.13: AFM image of a **TBPFe** grafted electrode before (a) and after (b) electrografting of the second **DzF8** layer (top) and their corresponding profiles (bottom).

In order to check the presence of the second layer, AFM was done on electrodes grafted with **TBPFe** before and after the second layer grafting. The electrodes used are 8 μm width electrodes made using photolithography that were electrografted with **TBPFe** using the optimized parameters. Then, they were put inside a solution of 1 mM of **DzF8** or 0.5 mM of **Thio** and were electrografted using a 2 minutes long process at -1.3 V. The electrodes grafted with the second layer do not show differences when studied using an optical microscope.

However, the AFM images of these electrodes before and after the second layer grafting show that there is a thickness difference. The **DzF8** second layer grafting show an increase of the thickness of the grafted layer of 7 nm. That is higher than the 3-4 nm that should have been grafted at this potential (see figure II.26). Thus, the second layer grafted is thicker than what should have been grafted on an unfunctionalized electrode. This could be explained by the rugosity difference between the **TBPFe** layer and the gold substrate. Also, when **TBPFe** is electrografted with **DzF8**, the electrode is in an acetonitrile solution, meaning that the **TBPFe** layer is inflated by the solvent, and thus does not deflate when the solvent is evaporated since the grafted **DzF8** layer filled the holes during the electrografting.

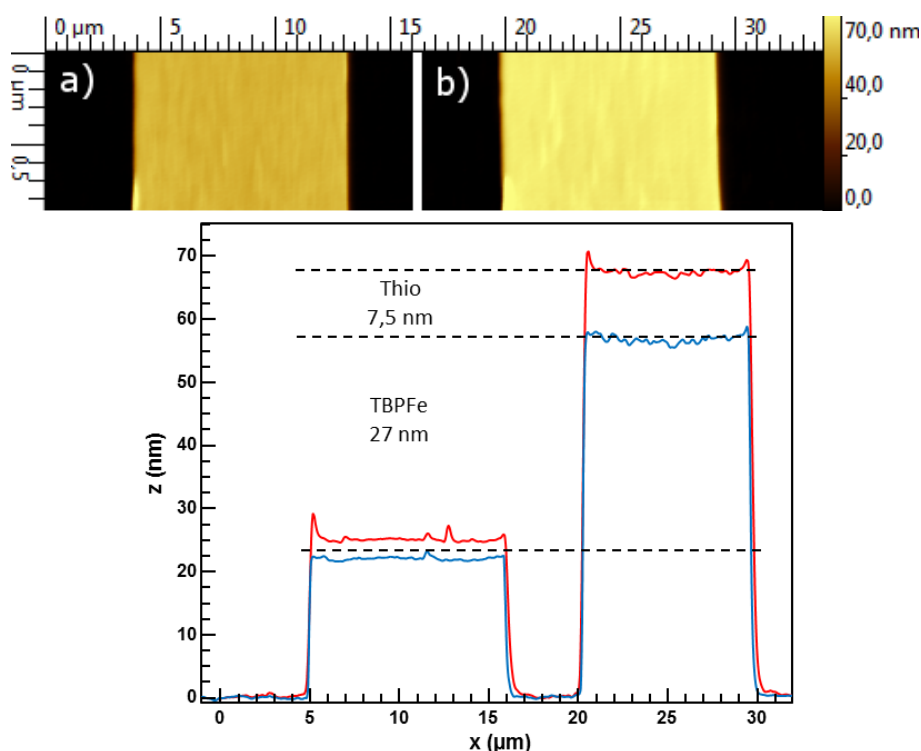


Figure III.14: AFM image of a **TBPFfe** grafted electrode before (a) and after (b) electrografting of the second **Thio** layer (top) and their corresponding profiles (bottom).

In the same way, the second layer of **Thio** grafted on top of a first layer of **TBPFfe** is around 8 nm (figure III.14), which is 3 nm thicker than what can be grafted on bare gold electrode (figure II.26). The difference is a bit bigger than with **DzF8** which can be explained by the fact that the **Thio** molecule is smaller than **DzF8** and thus can access smaller holes in the inflated **TBPFfe** layer during electrografting, and thus the interlayer between a pure **TBPFfe** layer and a pure **Thio** layer is thicker than in the **DzF8** case.

Nature of the layer	Substrate (gold)	TBPFfe	TBPFfe+DzF8	TBPFfe+Thio
Contact angle (°)	48.4	66.5	108.5	74.5

Table III.3: Contact angle measured on gold grafted with **TBPFfe**, **TBPFfe+DzF8** double layer and **TBPFfe+Thio** double layer.

Finally, the hydrophobic behavior of the layer is probed by using contact angle measurement (table III.3). The double layers are more hydrophobic than both gold and **TBPFfe** simple layer. However, while the **TBPFfe+DzF8** double layer has a contact angle similar with the **DzF8** simple layer (108.5° vs 106.8° respectively), the **TBPFfe+Thio** double layer has a much lower contact angle than its simple layer counterpart (74.5° versus 91.5° respectively). Thus, the double layer of **TBPFfe+DzF8** consists on a simple layer of **DzF8** on top of a **TBPFfe** simple layer, while the **TBPFfe+Thio** consists of a really thin layer of simple **Thio** on top of a mixed layer of **Thio+TBPFfe** which would explain the lower hydrophobic behavior (figure III.15).

In this part, a way of making organic thin layers containing two different molecules was developed by using electrografting. A first layer of a redox active molecule is grafted, here **TBPFfe**, which is then used as a working electrode in an electrografting process with another diazonium salt, here **DzF8** or **Thio**. After this electrografting, the resulting

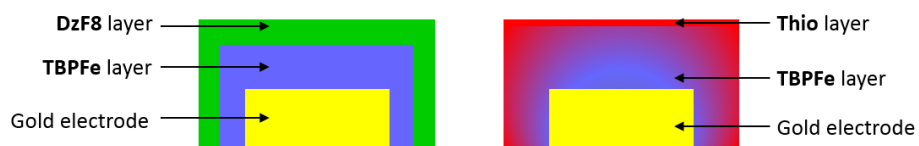


Figure III.15: Scheme of the resulting double layers grafted.

layer has a mix of the properties of the two layers : they are less insulating than the **DzF8** or **Thio** layers but can have a controlled thickness between 10 and 110 nm thanks to their **TBPFe** bottom layer. An article based on the work on the control of the thickness of grafted layer have been published in *Electrochimica Acta* [121] and is available in the supplementary information of this thesis.

Chapter IV

Printed gold nanoparticle top electrode

In this part, the different types of organic layers that were presented in the previous chapters will be used in microsized vertical metal-molecule-metal junctions in order to probe both their compacity and their electrical behavior. First, in order to minimize the risks of seeing memristive behavior due to the nature of the top electrode, titanium will not be used as an anchoring layer. Indeed, when titanium is oxidized, it can lead to TiO₂ layers that can have memristive behavior, as seen in the Chapter one. Thus, pure gold electrodes will be preferred for the top contacts.

Also, as was seen previously in the laboratory for non-optimized grafting conditions, direct metal evaporation on top of ECG layers usually leads to current leakage. Since the ECG process has been studied and optimized on patterned electrodes in chapter 2 and 3, getting efficient top contacts will be probed. In order to maximize the chances of obtaining high quality contacts without atom diffusion in the layer, an alternative to direct metal evaporation is investigated : gold nanoparticles ink printing. This process was developed during this PhD, and will be presented in this chapter. To conclude this chapter, top electrodes made using this process will be printed on top of the ECG layers.

IV.1 State of the art

Printed electronics is an active research domain thanks to various advantages it has over traditional electronics. First, the method is an additive method, and should allow the use of less materials than the subtractive methods. Second, inkjet printing should be compatible with roll to roll processes, which would allow printing on flexible substrate and low cost processes. While the commercially available inks can be costly, they allow the formation of electrodes with conductivity getting closer and closer to the conductivity of their respective bulk material [122].

The principle of metal nanoparticle printing is fairly simple. Metal nanoparticles are synthesized and stabilized by organic additives in order to form a suspension in a solution, usually organic. Then, this solution is printed by various techniques, such as inkjet printing and aerosol jet [123]. It is then heated at high temperature in order for both the organic additives to evaporate and for the nanoparticles to sinter and form a bulk. This process is called the sintering process. It can be done at lower temperature than the melting point of the bulk material, since nanoparticles have a lower melting point. For example, gold nanoparticles of 5 nm diameter have a melting point of 300

°C, as opposed to the bulk gold's melting point of 1064 °C [124, 125]. Figure IV.1 illustrates the whole sintering process.

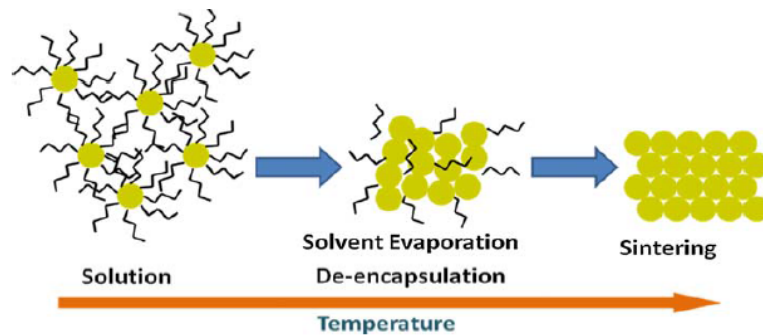


Figure IV.1: Schematic of the sintering process. As temperature increases, encapsulant starts dissociating and the nanoparticles start melting. At some critical temperature, the encapsulant is mostly removed and the particles sinter into a continuous film. Figure and caption from [126].

Various metals can be printed this way. The most common are silver [127, 128] and copper [129, 130, 131]. Silver inks can have sintering temperature as low as 100 °C and resistivity only twice higher than the resistivity of the bulk material [132]. Copper inks can have a conductivity equal to 20 % of bulk copper [133], but needs higher sintering temperature around 350 °C and in a controlled environment to avoid oxidation of the metal [129].

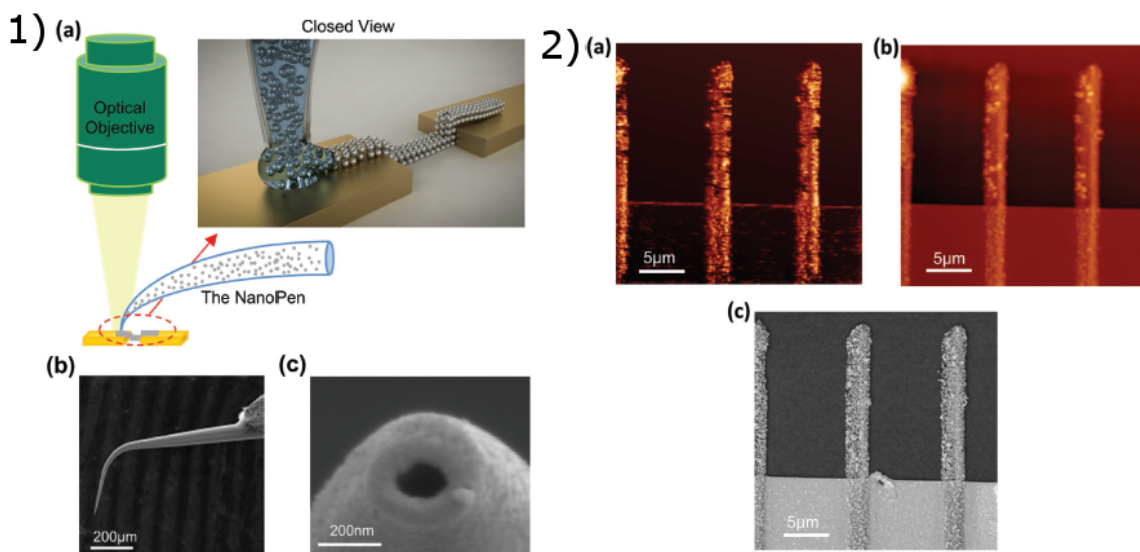


Figure IV.2: 1) Fountain pen nanolithography system. a) A diagrammatic representation of the FPL process depositing a nanoparticle dispersion to connect metallic lines. b) The structure of the probe as seen in a SEM image. c) An image of the nanopen aperture. **2)** Printing electrical lines and interconnections with an Ag nanoparticle dispersion. a-c) Printed silver nanoparticle metallic lines from a gold pad with 80 nm height to an electrically isolated silicon oxide substrate. The width of the lines is 2.2 µm. a) and b) are the C-AFM current and the height images respectively, and c) is the SEM image of the same region. Figures and captions from [134].

Gold nanoparticles printing can also be performed in laboratories, but is not commercialized yet due to its high cost. It has already been used in organic thin films tran-

sistors, for example by Wu et al [135]. The size of the source and drain electrodes printed on the organic PQT-12 semiconductor layer was between 90*2000 μm and 400*5000 μm . Various articles reported high conductivity gold electrodes, but the gold nanoparticle ink was always in organic solvent such as toluene [136], α -terpineol [126] or xylene [137]. Few gold nanoparticle aqueous ink used to print gold electrode has been reported [138]. Also, a sintering process is always used. Reported resistivity of the printed gold electrodes can be as low as 2.7 $\mu\Omega$. cm for a sintering temperature of 300 $^{\circ}\text{C}$ [126] or at 16 $\mu\Omega$.cm with an infra-red sintering process [137].

One of the limitation of metal nanoparticle printing is the resolution of the resulting patterns. Usually, printed electrodes are macroscopic, and have sizes above 100 μm . However, some printing techniques allow the formation of smaller pattern, such as fountain pen lithography (FPL) [134]. The principle of FPL is the following : a bent glass nanopipette is filled with the ink to print, and atomic force feedback is used to control the printing process. By using a specially designed silver ink, Yeshua and al [134] managed to print patterns that are 15 nm wide, while with standard silver ink, the resolution of the printed lines are at 1.5 μm (Figure IV.2).

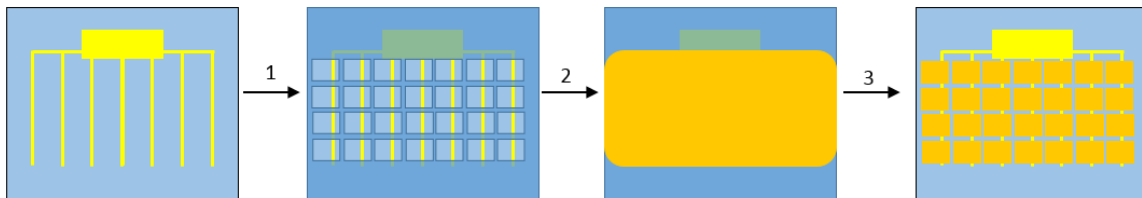


Figure IV.3: Scheme of the gold nanoparticle micro-sized electrodes printing on top of evaporated Cr/Au electrodes made using lithography. (1) Photolithography on the sample. (2) Printing of the gold nanoparticles. (3) Careful lift-off of the photolithography mask.

However, these techniques are fairly specific, and are hard to use due to a particular care taken to have an ink compatible with the special printing processes. Also, these types of printing processes are not accessible in LICSEN. Thus, in order to be able to print micrometer sized electrodes in a patterned ways, printing gold nanoparticles on a lithography mask is studied. The process is shown figure IV.3. This would allow the printing of smaller and well defined patterns. However, since most lithography masks used are organic, the ink used must not solubilize the mask, and thus needs to be aqueous.

IV.2 Printing a gold nanoparticle top electrode

IV.2.1 Printing process and analysis of printed gold nanoparticle electrodes

In this part, the fabrication and printing process of the gold nanoparticle ink is presented. First, the solvent used is a 50/50 mix of ethanol and water in order to have an aqueous solution compatible with the lithography masks. Another interesting point of this mix is that it has a relatively low boiling point, which is compatible with the presence of the ECG organic layer on the electrode's surface.

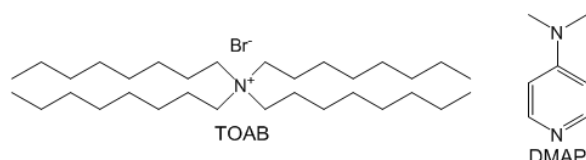


Figure IV.4: Molecular structure of the tetrabutylammonium bromide (TOAB) and the dimethylaminopyridine (DMAP).

The nanoparticles were synthesized using Brust's method [139]. This method consists in diluting a gold salt in an organic solvent, here toluene, in presence of amphiphilic molecules, here tetrabutylammonium bromide (TOAB)(figure IV.4). The reaction is then activated by adding a reducing agent, here sodium borohydride (NaBH_4). The resulting size of the nanoparticles is driven by the concentration of TOAB. The synthesis is further detailed in the experimental section.

After the synthesis, the nanoparticles are stabilized by TOAB in toluene. The charged part of TOAB, the ammonium ion, is stabilizing the charges on the surface of the gold nanoparticle, leaving its long hydrophobic carbonated chains in the solution. In order to have hydrophilic nanoparticles, the stabilizing molecule needs to be water soluble. Thus, a change of the stabilizing molecule is performed, and TOAB is replaced by dimethylaminopyridine (DMAP) (figure IV.4) [139]. Just by adding DMAP in excess in the solution of nanoparticles, the ligands stabilizing the gold nanoparticles are changed, and after a few minutes of stirring, the once opaque toluene solution contains a lot of particles that have precipitated. Contrary to the TOAB, DMAP molecules have their hydrophilic part (the amine function) pointed toward the solution when stabilizing the gold nanoparticles, meaning that the nanoparticles are now hydrophilic [140]. After centrifugation, a clear toluene solution and a black powder is obtained, which means that all gold nanoparticles are effectively hydrophilic and separated from the solvent. The final aqueous solution of gold nanoparticle is obtained by solubilizing the resulting powder in the smallest volume of water possible, which gives a purple solution. The printing solution is obtained by mixing a set volume of ethanol with the same volume of the aqueous nanoparticles solution.

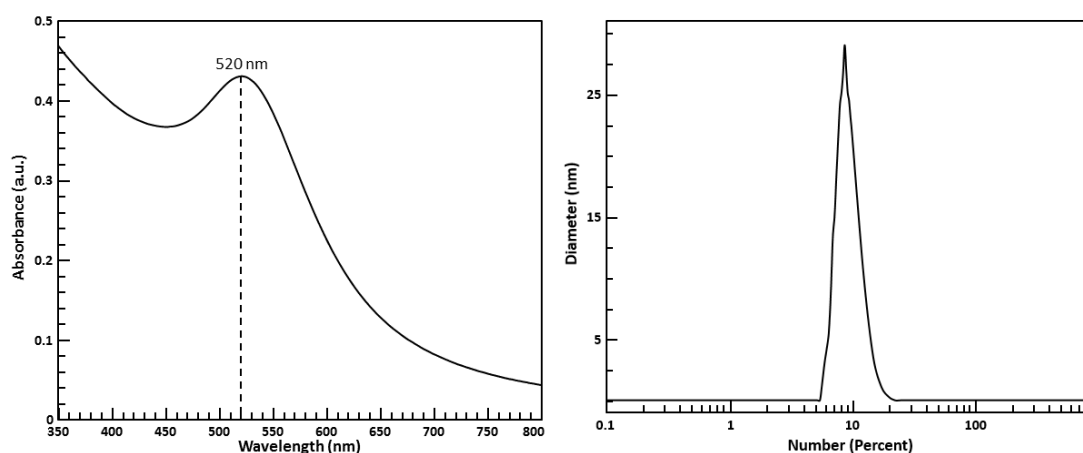


Figure IV.5: UV Spectra (left) and DLS measurements (right) of the gold nanoparticle solution.

The size of the nanoparticles is probed by using two methods : dynamic light scattering

(DLS) and UV-visible spectra (figure IV.5). The first one gives the information about the hydrodynamic radius of the nanoparticle, and thus takes into account the DMAP that stabilizes it and the first layer of water molecules around the nanoparticle, while the second method takes advantage of the shifting of the plasmon band with the size of the gold nanoparticle which is located between 518 nm and 530 nm [141]. The UV-visible spectra of a diluted solution of gold nanoparticles is shown figure IV.5 (left). The measured plasmon band is at 520 nm, which corresponds to an average diameter of 12.5 nm for the nanoparticles. The DLS measurements (figure IV.5 right) gives a radius of 9.5 nm, which is in agreement with the UV-visible measurements. Thus, the nanoparticles have an average radius around 10 nm.

Inkjet printing was done with the gold nanoparticle ink prepared and a Fujifilm Dimatix DMP 2831 inkjet printer system. As mentioned previously, the wanted electrodes are rectangle which sizes are 50 μm per 90 μm , and each electrodes are separated by a 10 μm space, as illustrated in the scheme figure IV.3. However, each droplets made using the printer are of a 10 pL volume, which corresponds to a droplet's diameter of 36 μm . This is in the same order of magnitude than the pattern to print, which means that it cannot be used this way due to a problem of resolution. A photolithography mask (see experimental section) is made on top of the sample in order to have the wanted electrodes. The gold nanoparticle ink solution is printed on top of it using the inkjet printer, which allows in the end the patterning of electrodes that have a size similar to or inferior to the size of the droplets printed on the substrate.

The sample holder is heated at 50 $^{\circ}\text{C}$ in order to facilitate the evaporation of the solvent and thus facilitate the formation of the gold electrode. The printhead of the cartridge is put at 0.5 mm of the sample in order to avoid overheating of the nozzles due to the temperature of the surface on which the solution is printed. If the printhead is too hot, the nozzles can be obstructed by the ink solution that dries during the printing process. For the same reason, even though the printheads have multiple nozzles, only one is used at the same time in order to maximize its lifespan. This also allows a printing precision around 10 μm considering all other experimental difficulties.

Number of printed layers	1	2	3	3	3
Heating temperature ($^{\circ}\text{C}$)	50	50	50	45	35
Resistivity (Ω/\square)	$7.4 \cdot 10^4$	$1.8 \cdot 10^6$	$2.6 \cdot 10^{-2}$	$3.1 \cdot 10^{-2}$	$2.7 \cdot 10^6$

Table IV.1: Data table of various printing parameters and the resulting conductivity of the resulting gold layer.

In order to determine the best printing conditions, the gold nanoparticle ink was printed on a microscope glass without any lithography mask. The pattern was a 4 x 4 mm square. The printing conditions were the ones described in the experimental section, except the number of printed layers and the temperature of the sample holder during the printing process which were studied. The conductivity of the resulting printed pattern was measured by using a four probe measurement. The results are shown table IV.1. When less than 3 layers are printed, the gold electrode is not conducting. However, at 3 printed layers, the resulting electrode has a low resistivity of $3.1 \cdot 10^{-2}$ and $2.6 \cdot 10^{-2}$ Ω/\square when the sample holder is heated at 50 $^{\circ}\text{C}$ or 45 $^{\circ}\text{C}$. When the sample holder is heated at only 35 $^{\circ}\text{C}$, the resulting layer is not conducting. This means that the best parameters for the printing of conducting gold electrodes are heating the sample

holder at 50 °C and printing at least 3 layers. With these parameters in mind, printing the gold electrodes on top of a lithography mask is performed.

The pattern printed on top of the photolithography mask is a simple rectangle which dimensions are 450 μm x 850 μm , which is higher than the 400x800 μm size of the photolithographed area, in order to compensate the experimental errors. After the printing process, lift off of the mask is done by using soft conditions. The sample is put inside an acetone solution pre-heated at 50 °C for a few minutes in order to solubilize the resin. Then the lift-off is performed by doing a mild ultrasonic cleaning. Finally, the sample is washed with acetone and ethanol.

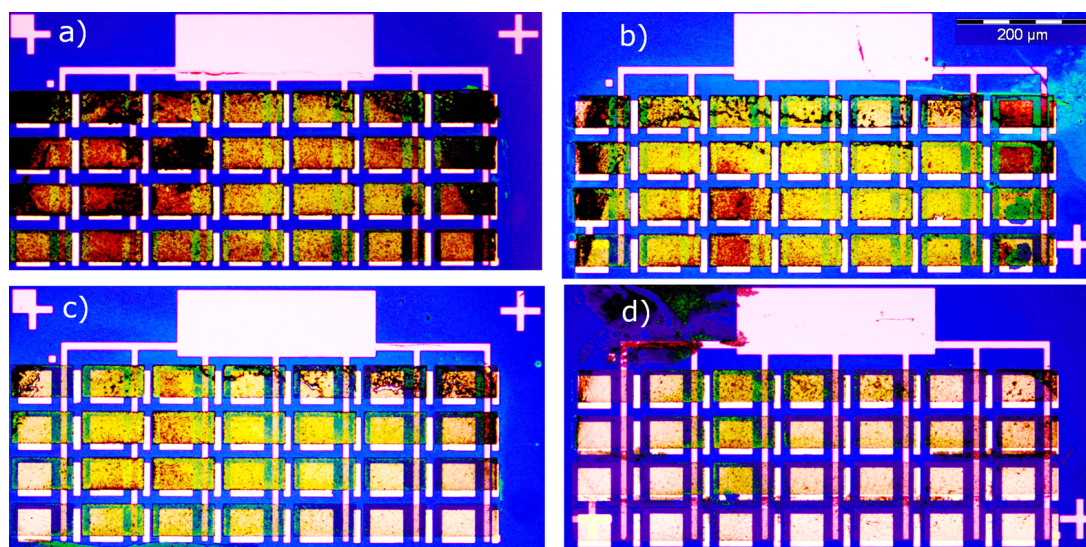


Figure IV.6: Optic Microscope image of a gold electrode printed with 4 layers (a), 3 layers (b), 2 layers (c) and one layer (d) after lift off of the lithography mask. All images have the same scale.

The results of the printing process of different number of layers are shown figure IV.6. Visually, differences are already visible between the different electrodes. For the 1 layer printed electrodes, the patterns look like they are transparent and the bottom electrodes are visible even under the top electrodes. The higher the number of printed layers is, the most opaque the resulting electrode is. However, the 4 layers electrodes look really dark, which could mean that the resulting layer could contain non-sintered nanoparticles. The best looking electrodes are the 3 layers printed ones, with most of its resulting electrodes looking like bulk gold.

Those microscope images also show another problem : the different electrodes on the same electrode do not look like they have the same quantity of gold printed. For example, on the 2 layers sample, electrodes on the middle of the sample look opaque and well done, while the electrodes on the bottom corners are transparent. This phenomenon is probably due to experimental problems, and further experiments with the printer should be made in order to get a homogeneous printing on surfaces bigger than 10 μm . Finally, the 3 layers printed electrodes look like they are the best ones according to the optic microscope measurements.

AFM of one of the central electrodes of each sample is then performed in order to evaluate the rugosity and the thickness of the printed layer (figure IV.7 and table IV.2). The fact that the printing is not homogeneous on the whole pattern printed is well

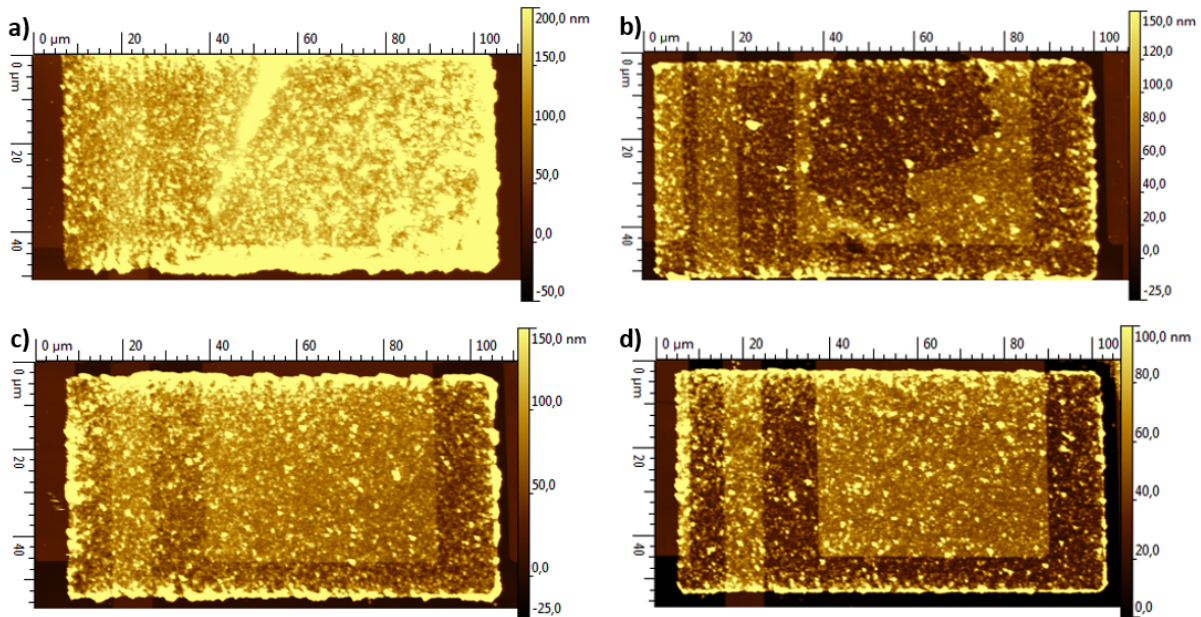


Figure IV.7: AFM image of a gold electrode printed with 4 layers (a), 3 layers (b), 2 layers (c) and one layer (d).

Number of layers	Thickness (nm)	Rugosity (RMS in nm)
1	37	16.8
2	82	26
3	44	24.7
4	120	37.9

Table IV.2: Approximated thickness in nm and root mean squared (RMS) rugosity in nm in a 25 x 25 μm area of the gold electrodes printed using different number of layers.

illustrated by these measurements : the 3 layers printed electrode is thinner than the 2 layers one. The thickness is measured approximately and manually since the rugosity is high, and is roughly the average of what is measured. The thickness of the printed layer increases with the number of layers printed, with the exception of the 3 layers printing. The rugosity also increases. That is expected since printing a new layer on top of another one should combine the thickness and the rugosity of both. Also, the printed layers do not seem to have holes according to AFM.

SEM images of the different samples are performed (figure IV.8 to IV.11). At x11 000, the one layer printed electrodes already do not look homogeneous and covering (figure IV.8). There are also a few aggregates bigger than 300 nm (for example, one aggregate is around 572 nm while another is around 308 nm). However, the side of the electrode where the lift-off was performed is well defined and no nanoparticles can be seen on the part of the bottom electrode that was protected by the mask. At the x150K magnification, a lot of small particles of a diameter between 13 nm and more than 200 nm can be seen. The smaller ones are nanoparticles that did not aggregate at all, while the others are different aggregate states.

The two layers printed electrodes have a similar appearance than the one layer's (figure IV.9). At the x20K magnification, less aggregates can be seen than with the one layer electrode, and the resulting layer seems smoother. However, some holes in the layer

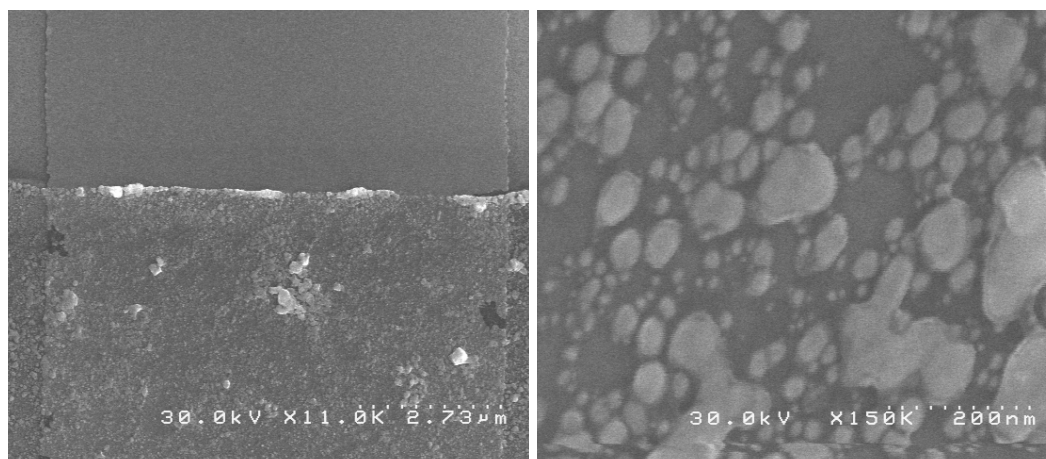


Figure IV.8: SEM images of a one layer printed gold electrode.

are visible, which sizes are between 193 nm in diameter for the smaller one visible and 1.14 μm in width for the biggest one visible. These holes are sufficiently small that they were not seen in AFM, due to a limitation in the resolution of the AFM image (the minimum resolution of what can be seen in these images is roughly 292×292 nm due to numerical limitations). At x150K in the part where the layer is printed, the bottom layer of the sample can be seen. The visible particles' sizes are between 22 nm for the smallest and the biggest is at 83 nm. The size distribution is smaller, and no isolated particles can be seen, showing that printing another layer helps the nanoparticles to aggregate. However, the fact that no single nanoparticles can be seen can be due to the fact that the image is not of the highest quality. This explains why the resulting gold electrode is not conducting when only one or two layers are printed, as was shown in table IV.1.

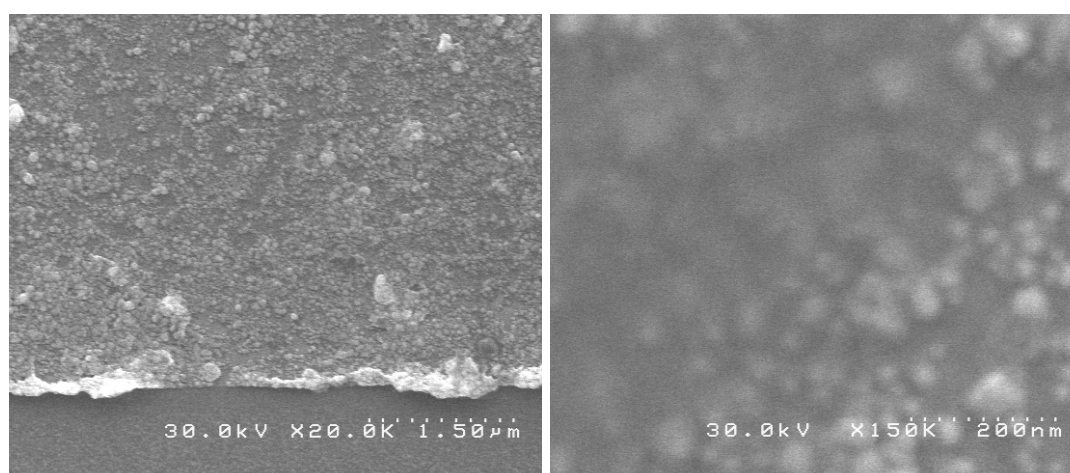


Figure IV.9: SEM images of a 2 layers printed gold electrode.

SEM images of a three layers printed electrode are shown figure IV.10. The most striking difference with the two precedent electrodes is the fact that the bottom electrode cannot be seen through holes on the printed gold electrode, would it be at x30K or at x100K. Also, at x30K, the printed electrode does not look smooth and two big aggregates of 643 nm width and 774 nm width are visible in the middle. At x100K, a big aggregate of 517 nm length and 682 nm width is visible, but also nanoparticles which

sizes range between 14 and 19 nm for the smallest and around 70 nm for the rest. Most of the gold on the electrode is then well aggregated, and consist of an agglomeration of smaller aggregates of gold nanoparticles.

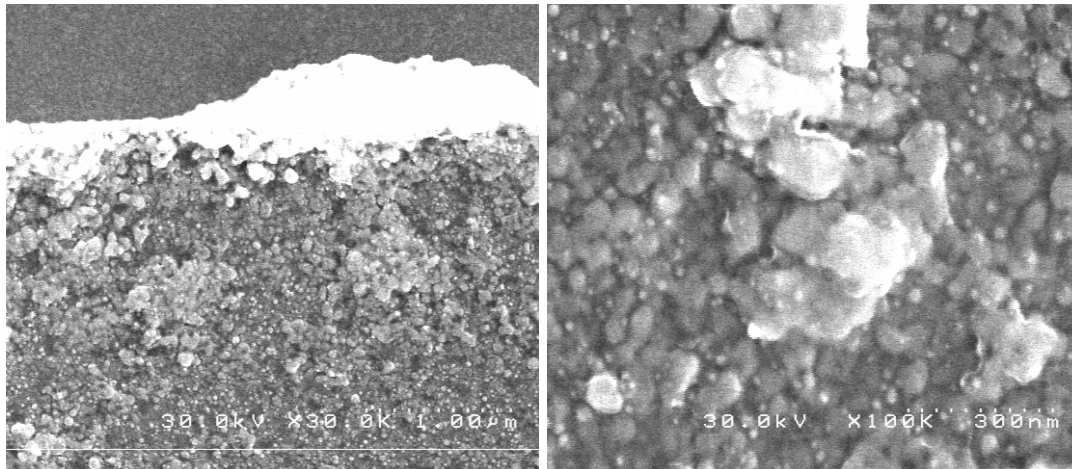


Figure IV.10: SEM images of a 3 layers printed gold electrode.

SEM of a 4 layers printed gold electrode is shown figure IV.11. At x10K magnification, the electrode looks smoother than all the other printed electrodes and shows no sign of holes. Three big aggregates, which size are around 3 μm length and 1.6 μm width, are detached from the electrode in the upper part of the image, which shows that the layer is thick and compact but that the lift-off process did not go as well as with the other electrodes. This can be explained by the fact that, for an efficient lift-off, the deposited material needs to be thinner than the polymer mask. If the thickness deposited is too close to the thickness of the mask, the lift-off is harder to do and can result in not well-defined objects. At x100K magnification, a lot of small aggregates between 50 nm and 90 nm are visible and aggregates with each other to form a porous structure. No single nanoparticles can be seen, contrary to the 3 layers printed electrode. As with the 3 layers printed electrode, sintering could make the quality of the resulting layer better.

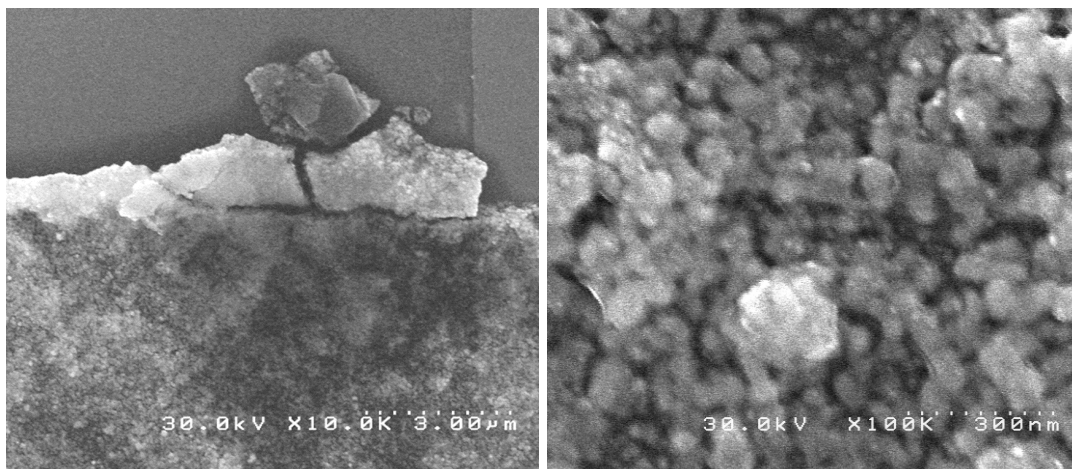


Figure IV.11: SEM images of a 4 layers printed gold electrode.

For the following measurements, the 4 layers printed electrodes will be used. It is the thicker and the most dense layer. Moreover, the lift-off problem is not that problematic,

since it can be solved quite easily by using thicker layers of resin for the mask for example.

In order to check whether DMAP is fully evaporated or still present in the layers, XPS of the printed gold electrodes is performed (figure IV.12, tables IV.3 and IV.4). In the same time, sintered and non sintered process are compared. Sintering was done at 280 °C for 1 hour since the DMAP's boiling point was measured to be around 272 °C at atmospheric pressure [142].

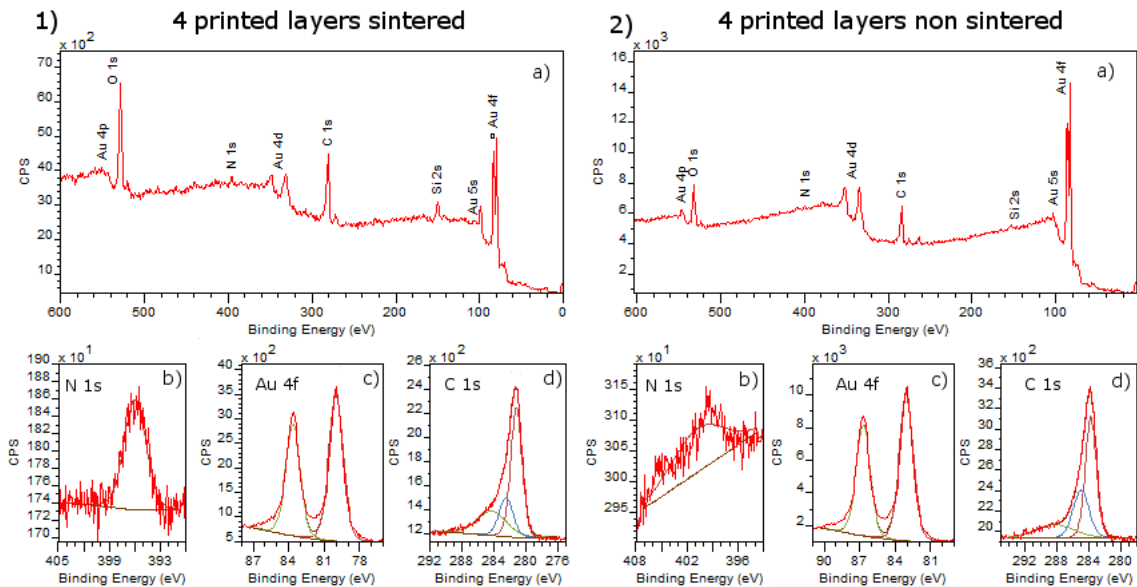


Figure IV.12: XPS survey spectra (a) and high resolution spectra of the N 1s (b), Au 4f (c) and the C 1s (c) region of a 4 printed layers gold electrode sintered (1) and non sintered (2).

Both XPS spectra show the same peaks : gold peaks, oxygen peaks, carbon peaks and nitrogen peaks. Traces of silica peaks are visible, which is due to the fact that the XPS was done on the patterned printed gold electrodes which sizes are 100 x 40 μm which is a bit smaller than the area that the XPS can scan, meaning that the SiO₂ and the evaporated gold electrodes on which the pattern are printed can be seen even though the printed gold layer is thick. The Au 4f peaks of both gold electrodes show only 2 peaks, which is due to the fact that there is the contribution of both the Au 4f 7/2 and the Au 4f 5/2 orbitals. Only one type of gold atom is visible with XPS, meaning that the gold of the printed gold electrode has the same neighbourhood than the evaporated gold electrode. Thus, the resulting printed gold layer is similar to the evaporated one.

Nature of the layer	Sintered			
	Atom and Orbital	N 1s	Au 4f	C 1s
Peak position (eV)	398.7	82.7/86.4	284.0/285.2/287.1	
Concentration (% atom)	5.7	10.2	84.1	
Attribution	DMAP	Gold nanoparticle	DMAP+Contamination	

Table IV.3: XPS data table for a 4 printed layers gold nanoparticle electrode sintered.

The C 1s peaks of both electrodes show 3 contributions. This is due to a lot of contamination, since the carbon contribution for DMAP is 3.5 times the concentration of

Nature of the layer	Non sintered		
	N 1s	Au 4f	C 1s
Peak position (eV)	400.9	83.7/86.8	284.0/285.1/288.3
Concentration (% atom)	5.7	22.6	72.7
Attribution	DMAP	Gold nanoparticle	DMAP+Contamination

Table IV.4: XPS data table for a 4 printed layers gold nanoparticle electrode non sintered.

nitrogen measured, which corresponds to 20 % of atoms measured for both layers. That means that 64.1 % and 54.7 % of the carbon atoms measured correspond to something else than DMAP for the sintered and non sintered sample respectively.

Both spectra also have N 1s peaks, meaning that a molecule containing nitrogen is present on the substrate. The only molecule that contains nitrogen and that could be on the substrate is the DMAP. Thus this nitrogen peak corresponds to this molecule. However, it should show 2 different contributions : for each DMAP molecules, one of the nitrogen should be complexing gold atoms, while the other one would not be influenced by the gold atoms. This peak could then be due to contamination, especially since it's also visible on the sintered gold electrode that was heated at a temperature above the boiling point of the DMAP.

The relative concentration of nitrogen in both electrodes is the same at 5.7 % . However, the Au 4f peaks show a relative concentration of gold in the material at 10.2 % for the sintered electrode and 22.6 % for the non sintered electrode. This means that the relative concentration of nitrogen versus gold is higher for the sintered electrode versus the non sintered electrode, which is not in agreement with the fact that the sintering process should get rid of the DMAP in addition to sinter the nanoparticles for better conductivity. An explanation could be that the sintering process does not get rid of the residual DMAP molecules or produces byproducts.

IV.2.2 Printed gold electrodes deposited on ECG layers

The gold electrodes are then used as top electrodes for vertical metal-molecule-metal junctions. In order to do that, a sample is electrografted with a **TBPFe+DzF8** double layer of 16 nm. Then the printing of the gold nanoparticle microsized electrodes is done according to the previous process by using the 4 layers printed gold electrodes. The resulting sample is shown figure IV.13.

The electrical behavior of the organic layer is then assessed by doing electrical measurements using a probe station with an analyzer. One of the contact is put on the printed gold layer, while the other is put on the bottom electrode. The I-V curves of one of the electrodes are shown figure IV.14 (left). Multiple increase in potential were done starting from +0 V and going to different positive potential. On the first increase, the current measured is low and around 0.5 nA at 2 V. However, as the potential reaches a critical value around 4 V, the current suddenly increases from around 10 nA to 10 μ A. Then the current decreases with a lot of noise until 5 V.

A second increase is done up to 3.5 V. This time, the current is around 5 μ A at 2 V, which is 1000 times more than during the previous increase in potential. At 2.5 V,

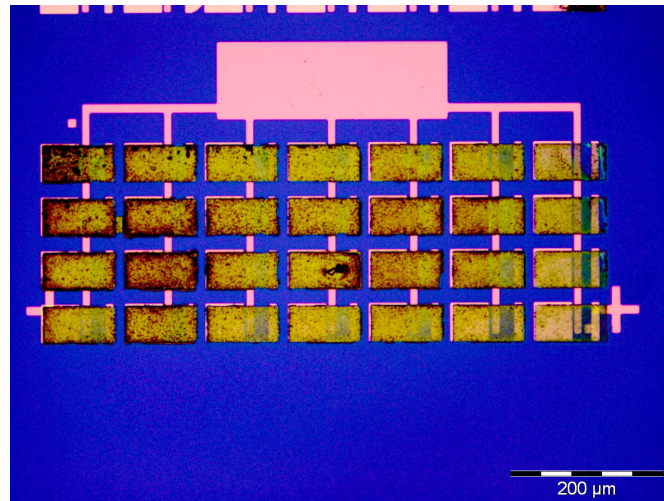


Figure IV.13: Optic Microscope image of a gold electrode printed with 4 layers on an electrografted organic layer.

the current suddenly increases again, and then drops a bit with a lot of noise until 3.5 V. A third increase is done up to 12 V. During this increase in potential, the current is around 80 μA at 2 V, which is 10 times higher than during the second cycle. It then increases suddenly starting at 2.3 V up to 1 mA at 2.9 V. The current then diminishes with a lot of noise until 17 μA at 6 V. It then stabilizes and shows a more traditional conductive behavior until 12 V. During the next increase, a behavior similar to the first measurement is obtained.

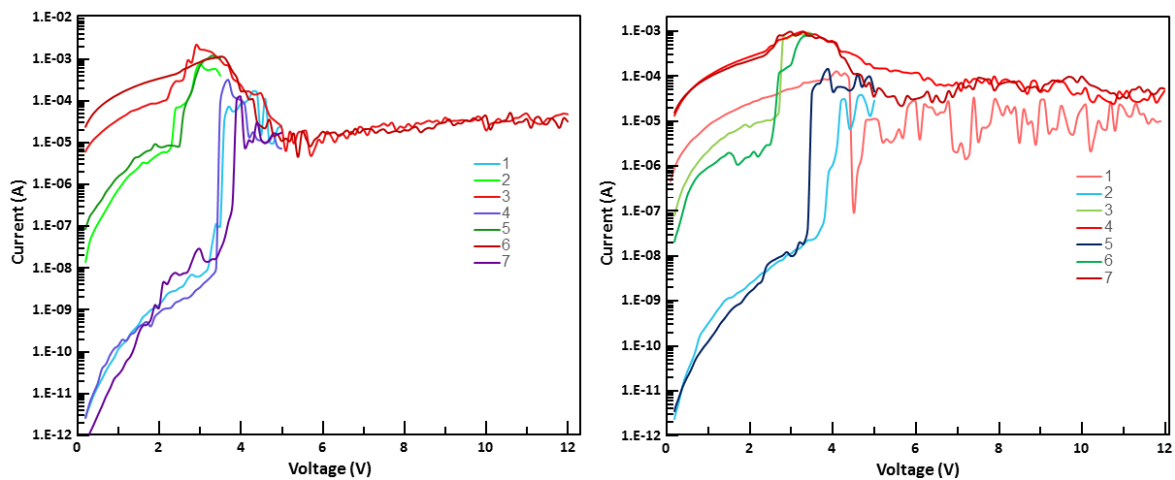


Figure IV.14: Current vs the potential applied for a vertical junction consisting of an evaporated gold-electrografted 16 nm **TBPFe+DzF8** layer-printed gold layer (left) or an evaporated gold-printed gold layer (right). The number associated for each curves correspond to their scanning number. Blue curves are stopped at 5 V, green curves are stopped at 3.5 V and red curves are stopped at 12 V.

Thus these I-V curves show a memristive behavior. This was previously seen in the laboratory by using **TBPFe** layers in a horizontal junction [4]. However, the layers in this article were hundred of nanometers thick and the potentials used to write and erase were lower. Also, the organic layer used in this case were a double layer of **TBPFe+DzF8** while in the article, it was a simple layer of **TBPFe**. Another problem is

that when the potential is reduced from the maximum potential to 0 V in our case, the device is neither written nor erased : it goes back to its original state. That means that the behavior that is being observed is not the memristive behavior of the **TBPFe** layer that was studied in [4].

The electrical properties of the gold electrode without any organic layer were then assessed, in order to check if this strange behavior is due to the gold electrode or to the double layer of **TBPFe+DzF8**. A similar sample as the previous one was made, except that the bottom electrode was not electrografted with anything. The same electrical measurements were then done (figure IV.14 right). These measurements show exactly the same behavior as above except that the device was first conducting at around 0.2 mA at 2 V, and then gets erased and written at the same potentials. That means that the memristive behavior found previously was due to the gold electrode and not the organic layer, and that the organic layer made was not insulating in this setup.

This electrical behavior could be due to the fact that the resulting electrode is not fully sintered, and that the gold nanoparticles are not all aggregated. When the potential increases, so does the current and Joule heating occurs, melting gold and forming micro conducting paths, which leads to a brutal increase in the current measured. However, if the potential is too high, the Joule heating occurs again, but this time in these micro-sized gold wires. They then melt, leading to the destruction of the conductive paths and the formation of an insulating electrode. This explanation seems one of the most logical, but is not verified by our results. In our case, a potential of 12 V is needed to erase our electrode. However, in classic memristive behavior, when the electrode is erased, the measured current diminishes, and stay low when slowly diminishing the potential applied. In our case, if the potential applied is diminished slowly, the electrode stays in its conductive state. The exact behavior of our setup remains unexplained, and further investigation should be done to have a better grasp of the mechanism of the writing and erasing processes of theses printed electrodes.

In this part, a gold patterned electrode was printed using an inkjet printer with a gold nanoparticle hydrophilic ink. This allowed the gold to be printed on top of lithography masks and getting a higher resolution of the final electrode that what could be physically obtained by only using the printer, which was never shown before in the literature. The resulting gold electrode showed a strange electrical behavior that could be probably solved by increasing the sintering temperature (which is not compatible with ECG layers) or upgrading the printing process in order to get rid of the DMAP that is still present after the soft sintering process. Also, the printed electrodes could not be used as top electrodes in vertical metal-molecules-metal junctions where the molecule is an electrografted organic layer. Thus, in order to probe the ECG layers' properties for electronic, a more classical approach is used : direct metal evaporation.

Chapter V

Electronic devices using ECG layers

The ECG thin layers could not be probed using a top contact made by inkjet printing of gold nanoparticle. Thus, classic techniques, such as metal evaporation, will be used in order to first check if the ECG layers can withstand direct metal evaporation without being in short-circuit, then study their electrical behavior. In this chapter, the different types of ECG layers will be used in two different device configurations. The first configuration corresponds to vertical metal-molecules-metal junctions, which are presented in the section V.1. Three different metrics are measured and assessed : the current flowing through these layers, the highest potential that can be applied on these layers before failure, called the breakdown potential, and their capacitance. Then, with these values in mind, transistors using these ECG layers as gate dielectric are fabricated and studied. The channel of these transistors is a single-layer MoS₂ flake, which is a 2D semiconductor synthesized in the laboratory. These results are presented in the section V.2.

V.1 Electrical properties of the ECG layers in vertical metal-molecules-metal junctions with evaporated metal as top electrodes

V.1.1 Conductivity of the ECG layers

The electrical behavior of the ECG layers in vertical metal-molecules-metal configuration is first studied using direct metal evaporation for the top electrode. First, the nature of the top electrode is tested. A 50 nm thick gold electrode is evaporated under vacuum on a sample grafted with 16 nm of **TBPF_e+DzF8** and a 10 nm titanium followed by 50 nm gold electrode is evaporated on another sample grafted with 10 nm of **TBPF_e+DzF8**. An optical microscope image of the resulting sample in the latter case is shown figure V.1.

Then, the current flowing through the organic layers was measured in the 0 to +0.5 V range. Examples of I(V) curves and the statistics of the current measured at V = +0.5 V for different junctions are shown in figure V.2. To facilitate the visualization of the statistics over all the devices, the junctions that could not be measured because their current at +0.5 V was above 100 μA (a value selected as the current compliance in this measurement) are reported in the 100 μA category. These junctions are categorized as being short-circuited. For the top electrode made of pure gold, more than 60 % of the devices are in short-circuit, and the others have a current between 0.1 nA and 0.1

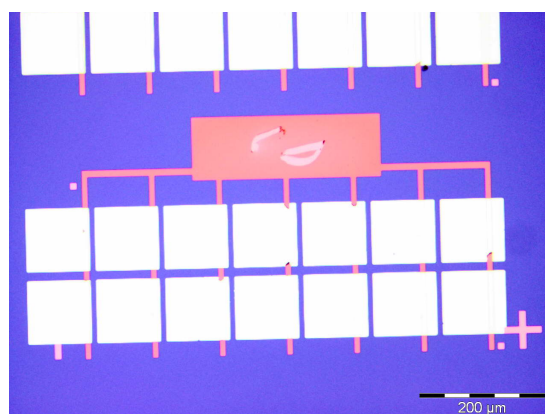


Figure V.1: Optical microscope image of a sample grafted composed of 14 metal-molecules-metal junctions. The global bottom electrode (orange) is grafted with a 15.9 nm **TBPF**e layer. The individual top-electrodes (white squares) are composed of 10 nm of titanium and 50 nm of gold directly deposited by direct evaporation. The surface of each vertical junction is $400 \mu\text{m}^2$.

μA with a large dispersion. However, when the top electrode is composed of Ti/Au, the percentage of short-circuited junctions is less than 5%. Around 70% of the devices drive 10 pA at +0.5 V, meaning that most of the ECG layers behave as thin insulating organic thin layer.

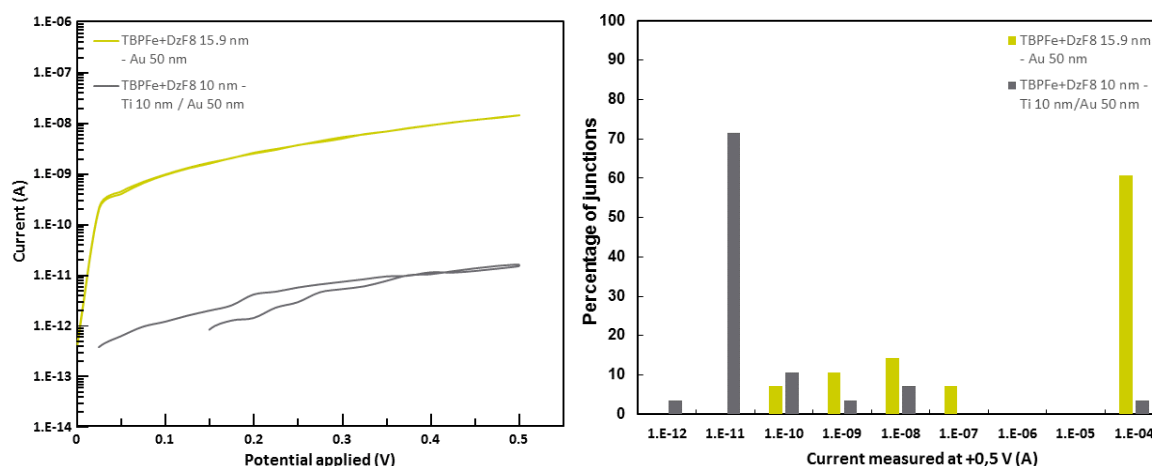


Figure V.2: Example of I(V) measurement for a vertical Au-**TBPF**e+**DzF8**-Au junction and a vertical Au-**TBPF**e+**DzF8**-Ti-Au junction (left). Statistics over the current measured at +0.5 V for a gold top electrode evaporated on top of a 15.9 nm layer of **TBPF**e+**DzF8** (28 junctions) and a titanium/gold top electrode evaporated on top of a 10 nm layer of **TBPF**e+**DzF8** (28 junctions) (right).

The fact that gold only top electrodes lead to a majority of short-circuit could be due to the fact that gold is a softer material than titanium and thus diffuses inside the organic layer. On the other hand, the titanium-gold layers allows the formation of resistive devices with a high yield, which is what was expected from the dual **TBPF**e+**DzF8** layers. Another explanation could be that titanium is more reactive than gold, and that it reacts instantly with the top of the ECG layer and does not diffuse into it. In the following studies, the top electrode used will always be composed of 10 nm of Ti + 50

nm of Au.

The differences between the different layers that can be grafted are then assessed. The five types of layers are studied : the three simple layers consisting of only one diazonium salt electrografted, and the two double layers consisting of a **TBPF**e layer on top of which a **DzF8** or a **Thio** layer is grafted. Then, the top electrodes are evaporated on top of these layers, and the current is measured at ± 1 V. Examples of $I(V)$ curves and the statistical results for 140 junctions (28 of each type) are shown in figure V.3. In the same way as before, the compliance was set at $100 \mu\text{A}$. Thus, when a device reaches the compliance, it is counted in the $100 \mu\text{A}$ category, meaning that devices at $100 \mu\text{A}$ and above are considered as vertical junctions in short-circuit.

The **TBPF**e layer shows only such current leakage in 12 % of the junctions, which is close to what was measured with double layers in figure V.2. The current measured at $+1$ V for the **TBPF**e layers shows a large variability : the majority of the junctions, 35% and 32 %, have a current of 0.1 nA or 1 nA at $+1$ V respectively, but the rest (21 %) of the junctions have a current between 10 nA and $1 \mu\text{A}$. This could be an indication that this ECG layer is not as homogeneous as what was expected from the previous parts or that the quality of the top electrode is not homogeneous on the whole sample. However, the proportion of devices in short-circuit is at 12 %, which is low for this type of devices, especially since no particular care was taken to have a surface of the organic layer that chemically bonds to the evaporated metal.

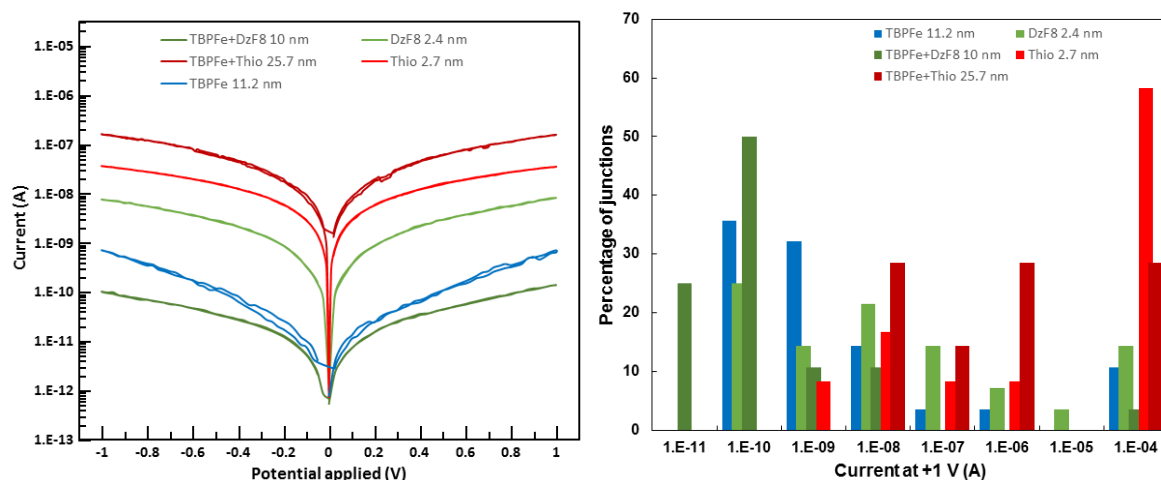


Figure V.3: $I(V)$ characteristic for vertical evaporated Au-ECG layer-Ti+Au junctions for a 5 nm **TBPF**e layer, a 11.2 nm **TBPF**e layer, a 2.4 nm **DzF8** layer, a 10 nm **TBPF**e+**DzF8** layer, a 2.7 nm **Thio** layer and a 25.7 **TBPF**e+**Thio** layer (left). Statistics over the current measured at $+1$ V for 140 vertical metal-molecules-metal junctions (28 of each type) for these samples (right).

The single **DzF8** layer has a similar percentage of junctions showing current leakage as the simple **TBPF**e layer (16 %) while being more than 4 times thinner, showing that the **DzF8** layer produced by our method is really compact and more insulating than the **TBPF**e layer.

The double **TBPF**e+**DzF8** layer has only a percentage of leaking junction of 4 %, which is in agreement with what was measured in the previous part. That means that the layer of **DzF8** adds its insulating properties to the already grafted **TBPF**e. Also, 75 % of the

junctions of the double **TBPF_e+DzF₈** layer drives a current between 10 and 100 pA at +1 V, which is one order of magnitude lower than the **TBPF_e** layer. On the other hand, the simple **DzF₈** layer has a current measured between 100 pA and 1 μ A, which is a large variability. Thus, the final **TBPF_e+DzF₈** has the added insulating properties of both **TBPF_e** and **DzF₈**.

The layers that result in the highest proportion of short-circuited junctions are the simple **Thio** layers and the double **TBPF_e+Thio** layers with respectively 60 % and 32 % of leaky junctions. This confirms the previous results that were indicating the formation of a not so dense layer. The simple layer shows a higher percentage of current leakage for two reasons : it is thinner, which increases the risk of pinholes, and it does not have a **TBPF_e** layer, which means that the resulting layer does not benefit from the insulating properties of the **TBPF_e**. Also, for the insulating junctions, the current measured is between 1 nA and 1 μ A for the **TBPF_e+Thio** double layer, while it is between 10 nA and 1 μ A for the simple **Thio** layer, showing again that the double layer is more insulating than its simple layer counterpart. This also confirms the fact that the **Thio** molecule is not a good choice as insulating material.

Thus, in terms of insulating properties, the double layers are always more interesting than their simple layer counterparts since : (1) the insulating properties of the **TBPF_e** are added to the insulating properties of the second compound, and (2) the non self-limited grafting properties of **TBPF_e** allow the fine tuning of the layer thickness. Between the three molecules, **DzF₈** is the most insulating one, which is in close agreement with what has been shown up to this part. When electrografting in the double layer configuration, it is highly possible that on top of adding another layer of insulating material, it also clogs the pinholes that might be present in the **TBPF_e** layer. On the other side of the insulating spectrum, the **Thio** layer shows high current leakage, and its double layer counterpart is way less interesting than the simple **TBPF_e** layer. This could be due to the fact that, since the **Thio** molecule is smaller than **DzF₈**, it may diffuse inside the **TBPF_e** layer before getting grafted. Then, during ECG, the **Thio** molecules in the **TBPF_e** are grafted both on and in the organic layer. The **TBPF_e** layers probably get expanded, resulting in a more porous layer. Additionally, the fluorinated chains of the **DzF₈** grafted molecules can interact with each other in the film to form a denser layer than the **Thio** molecules, which has only a small thiol group. Finally, the **TBPF_e** layer seems to be a good middle ground with its low percentage of leaking junctions and moderate variability.

V.1.2 Breakdown voltage of the ECG layers

The potential applied on the junctions is then increased in order to probe the potential at which the grafted layers become in short-circuit. These results notably determine the maximum potential that could be applied on the gate electrode of transistors using such ECG layers as gate dielectrics. Layers of **TBPF_e**, **DzF₈** and **TBPF_e+DzF₈** have been studied in this way, as shown in figure V.4. When the potential is increased, the layers show a classic insulating behavior until a certain potential, called the breakdown potential, is met. At this potential, the intensity increases suddenly, and the current measured reaches the compliance (100 μ A). Once the breakdown potential has been exceeded, the layer is irreversibly modified : it becomes highly conductive and is considered to be in short-circuit. The next measurement on the same electrode reaches the compliance as soon as the measurement starts, meaning that its conductivity is

close to the one of a metal. This could be due to the fact that nanoscale filaments were made through the layer, and the top and bottom electrodes are now bridged by metallic pathways [143, 144]. An example of measurements made on a double **TBPF****e**+**DzF8** layer without using a compliance is shown in figure V.4.

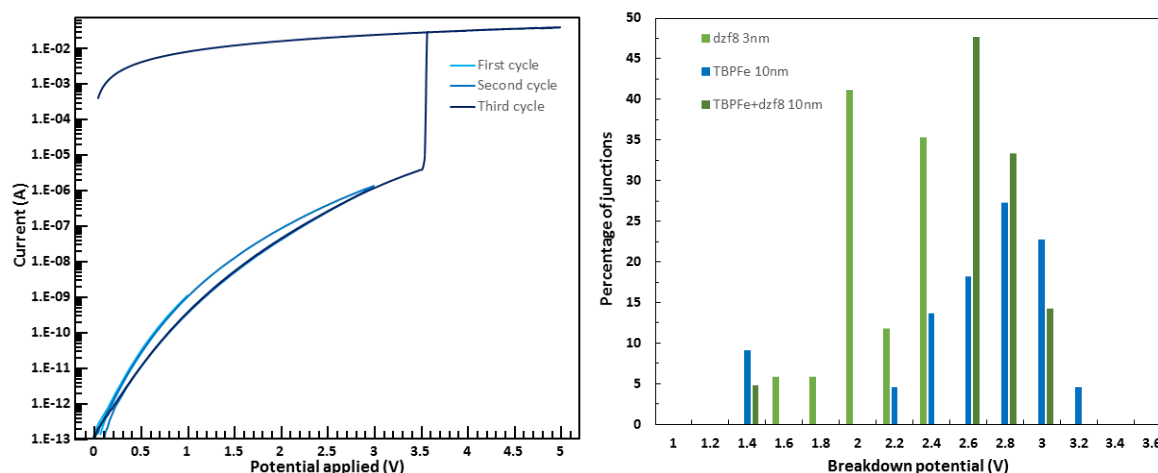


Figure V.4: I(V) characteristic for a vertical metal-molecules-metal junctions with a 10 nm thick **TBPF****e**+**DzF8** organic layer (left) and statistics on the breakdown potential of 84 samples (24 of each types) with a 3 nm **DzF8** layer, a 10 nm **TBPF****e** layer and a 10 nm **TBPF****e**+**DzF8** layer (right).

The statistics on the breakdown potential for the three types of layers are shown in figure V.4 (right). For the thin **DzF8** layer that is only 3 nm thick, more than 80 % of the breakdown potentials are between 2 and 2.4 V (6.6 to 8 MV.cm⁻¹). For the double **TBPF****e**+**DzF8** layer that is 10 nm thick, more than 90 % of the breakdown potentials are between 2.6 and 3 V (2.6 to 3 MV.cm⁻¹), which is higher in terms of potential but lower in terms of electric field. For the simple **TBPF****e** layer that is also 10 nm thick, more than 70 % of the breakdown potentials measured are between 2.6 and 3 V (2.6 to 3 MV.cm⁻¹), which is similar to the double layer case. However, the variability of the breakdown potential is higher since, contrary to the double layer, some junctions have a breakdown potential as high as 3.2 V or as low as 2.2. These results are similar to the previous ones (on conductivity) that indicated a higher variability of the results for the **TBPF****e** layers, meaning that it is most probably less homogeneous than the **TBPF****e**+**DzF8** double layer.

In literature, similar results were achieved with various type of dielectric layers : inorganic layers lead to breakdown field of 4 to 23 MV.cm⁻¹ [145], organic layers lead to breakdown field of 3 to 6 MV.cm⁻¹[146] and SAMs lead to breakdown fields of 9 to 12 MV.cm⁻¹[147]. These results are on par with what can be usually obtained with 3 nm thick SiO₂ or 4 nm thick HfO₂ insulators (23 and 4 MV.cm⁻¹ respectively [145]). It is slightly better than some organic insulators, such as PVP (2-3 MV/cm [148]) or CPS-C_n [60], which are thicker. Thus, in terms of robustness at high electric field, ECG layers are competitive against their counterparts. This constitute a major asset for their use as gate dielectrics in transistors.

V.1.3 Capacitance of the ECG layers

Finally, the third physical property measured for the organic layers is their capacitance. For that purpose, low-frequency dynamic measurements are performed at low bias. A triangular potential signal is applied on the organic layer at a given frequency (typically 1-2 kHz). Since the current is proportional to the capacitance times the derivative of the potential against time, the I-V curves of these measurements allow the extraction of the capacitance according to equation V.1. Equivalently, it can be used to extract the relative permittivity of the organic material, which is adimensional.

$$i(t) = C \frac{dV}{dt} \quad (\text{V.1})$$

$$C = \epsilon_0 \epsilon_r \frac{A}{D} \quad (\text{V.2})$$

The capacitance is frequently used in the literature for the characterization of organic dielectrics, but it is proportional to the inverse of the thickness of the layer, meaning that the thinner the layer is, the higher the capacitance, while the relative permittivity is a material parameter, independent of geometrical factors. The relation between the capacitance to the relative permittivity for a simple planar junction follows the equation V.2 with ϵ_0 the vacuum permittivity ($\epsilon_0=8.85 \cdot 10^{-12}$ F.m⁻¹), ϵ_r the relative permittivity of the material, A the area of the contact and D the thickness of the layer. An example of the measurement of the capacitance of a junction is shown figure V.5 (left).

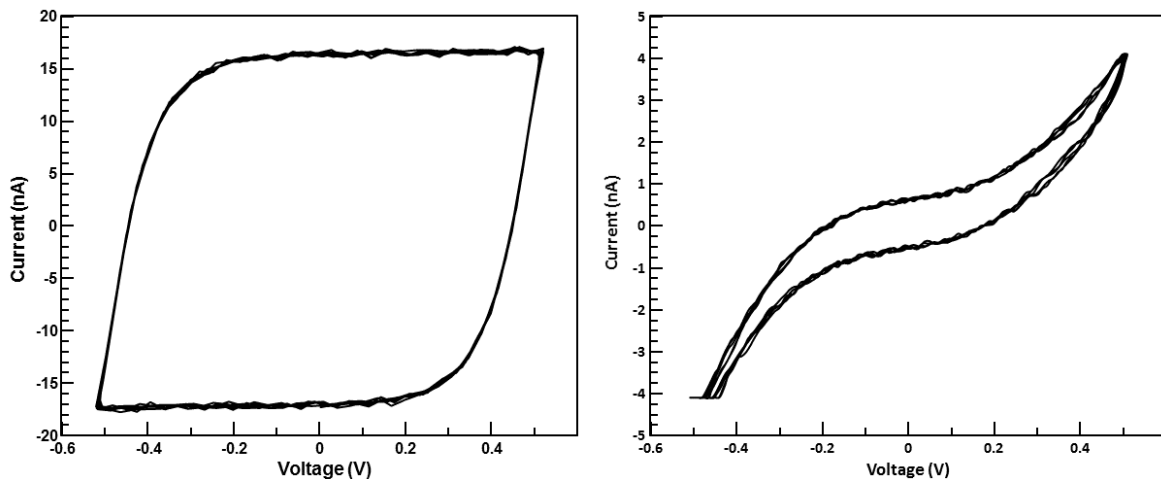


Figure V.5: I(V) characteristic at a frequency of 1500 Hz for a vertical metal-molecules-metal junction where the organic layer is a 5 nm thick **TBPF** layer (left). I(V) characteristic at a frequency of 50 Hz for a vertical metal-molecules-metal junction where the organic layer is a 11.9 nm thick **TBPF** layer (right).

When the layers did not show the expected capacitance behavior illustrated in figure V.5 (left), they showed either a simple resistive behavior or a combination of both a partially conductive and capacitive behavior such as the one shown in figure V.5 (right). The measured capacitance and relative permittivity of different types of junctions are shown in figure V.6. The junctions that did not show a pure capacitive behavior are put in the 0 nF/cm² capacitance and the 0 relative permittivity categories. These results show

however a first problem : the two types of **TBPFe** layers with different thickness do not have the same relative permittivity, while they have the same composition.

The worst capacitors are the junctions with the **Thio** layers, would it be the simple or the double layer. More than 60 % of those have a not-purely capacitive behavior, and the few of them that show a capacitor behavior have a capacitance of 100 nF/cm² or lower. The **DzF8** simple layer is a bit better with 58 % of its junctions that are between 500 and 600 nF/cm².

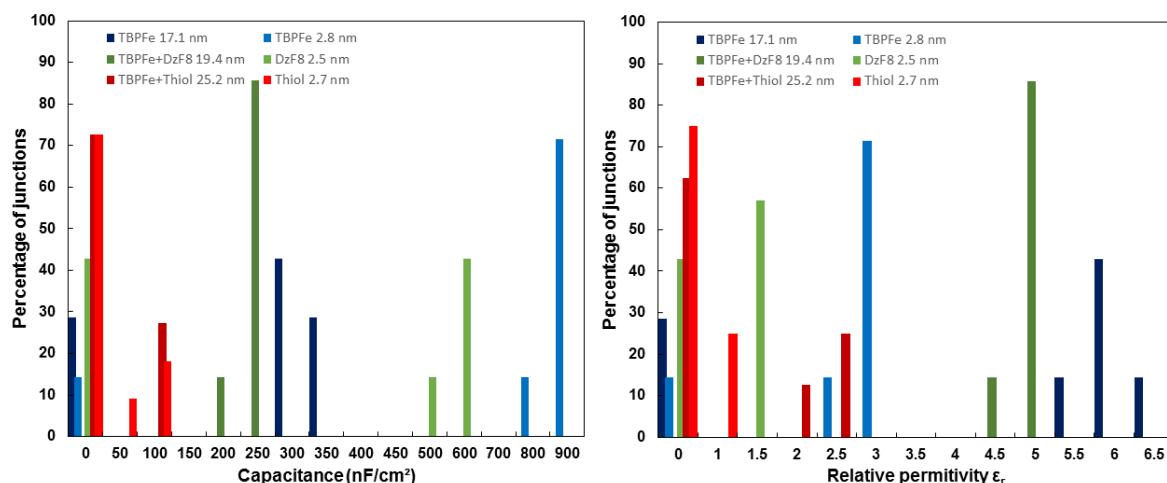


Figure V.6: Statistics over the capacitance measured (left) and the relative permittivity (right) of a 17.1 nm **TBPFe** layer, a 2.8 nm **TBPFe** layer, a 19.4 nm **TBPFe+DzF8** layer, a 2.5 nm **DzF8** layer, a 25.2 nm **TBPFe+Thiol** layer and a 2.7 nm **Thio** layer for a total of 168 junctions (28 of each type).

More than 70 % of the **TBPFe** 17.1 nm layers have a capacitance between 300 and 350 nF/cm² and a relative permittivity between 5.5 and 6.5. However, the most interesting layers in term of capacitance are the thin **TBPFe** layers. Around 85 % of them show the highest capacitance of 800 to 900 nF/cm², which corresponds to a relative permittivity of 2.5 to 3.

Recently, it was shown in the literature that, with more complex hybrid inorganic-organic structures that involve metal layers, capacitance as high as 1 100 nF/cm² can be obtained [61]. Our ECG layers' maximum capacitance is at 80 % of these results while being purely organic layer. It shows that the proposed approach is highly competitive on this aspect. Finally, the **TBPFe+DzF8** double layer is the only one that does not show any resistive behavior, even though its capacitance is only at 200 to 250 nF/cm². This is lower than for thin **TBPFe** alone, but the permittivity values in the 4.5 to 5.5 range and the lower variability are promising

Globally, the values reported here are extremely interesting when compared to more classic strategies : most of the spin-coated organic layers have a very low capacitance between 1 and 10 nF/cm² [64, 33, 34], which is not surprising due to considering high thickness. Even SAMs, with a capacitance up to 900 nF/cm² [149], can attain these capacitance with difficulty. The most impressive contenders, the Hf-SANDs with capacitance up to 1100 nF/cm² [61], are not that far however, and require a particularly long and tedious process to be fabricated. SiO₂ is far behind, with a capacitance of only 104 nF/cm² for a 20 nm thick layer, which justified its progressive replacement by

high-k dielectrics in silicon technologies.

After these three series of measurements (leakage, breakdown and capacitance), we conclude that : ECG metal-molecules-metal junctions can be fabricated with a low short-circuit percentage, 3 % for the best case, even though the surface of such junctions was as high as $400 \mu\text{m}^2$. The most interesting asset of these layers is that they can be finely tuned for their future use both in terms of thickness and chemical composition. Depending on the nature of the layer, the current measured at +1 V can differ by 3 orders of magnitude. The double **TBPFe+DzF8** is the most insulating layer with a current of 100 pA at +1 V and the thin **Thio** layer is the less insulating with 100 nA in the same conditions of surface and potential. The strategy of double layers ECG is extremely interesting, since it allows separating the two adjustable parameters : the first layer is used to tune the thickness while the second one is used to tune the terminal chemical groups. The capacitance values obtained are close to be competitive with the best layers that use more complex structures and metals, such as in Hf-SANDs layers [61]. Altogether, these characteristics make ECG layers extremely interesting for their uses in transistors : they combine low leakage currents, high electrical breakdown fields, competing with those of SiO_2 and HfO_2 and, most importantly, capacitance values which challenge those of high quality SAM or highly structured thin layers made through more complex fabrication processes.

V.2 **MoS₂ transistors with ECG dielectrics**

In the previous parts, it was shown that ECG thin films can behave as robust insulating films with interesting properties : adjustable thickness between 2 and 100 nm, low current leakage, high capacitance, high breakdown voltage, tunable chemical end-groups and compatibility with direct metal evaporation on top of them. Thanks to these qualities, they should behave as efficient gate-dielectric films in FETs. To evaluate the merits of ECG layers in this context, the various ECG layers described above were integrated as gate-dielectric in single-layer MoS₂ FETs.

Single-layer MoS₂ is a direct-bandgap 2D semiconductor that is widely studied as the channel material in FETs since 2011. For a review on this topic, the reader can notably refer to the seminal work by A. Kis and co-workers [48] and to the following review article [150]. For example, top-gated single-layer MoS₂ transistors using HfO₂ as gate dielectrics have been demonstrated to have on/off-current ratios as high as 10^8 , a maximum mobility of $54 \text{ cm}^2 \cdot (\text{V}\cdot\text{s})^{-1}$ and a steep subthreshold slope as low as 74 mV/decade [48]. (Note that the mobility in [48] was most probably overestimated as described in [51], and acknowledged in [52]) Theoretically, the best targetable performances make MoS₂ a remarkable material for low-power electronic applications [27]. In addition to these interesting properties, high-quality single-layer crystalline MoS₂ flakes can be synthesized by CVD in the laboratory. It thus constitutes a good candidate to help evaluating the performances of ECG-based dielectrics.

In a previous work of the laboratory [3], Casademont and co-workers studied bottom-gated MoS₂ transistors in which the dielectric layer was a simple **DzF8** layer of 4-7 nm and the channel material was multi-layers of MoS₂ obtained by mechanical exfoliation of natural MoS₂ using the so-called "scotch-tape method". Top electrodes were evaporated on top of the MoS₂ with a special care taken to avoid direct metal evaporation on

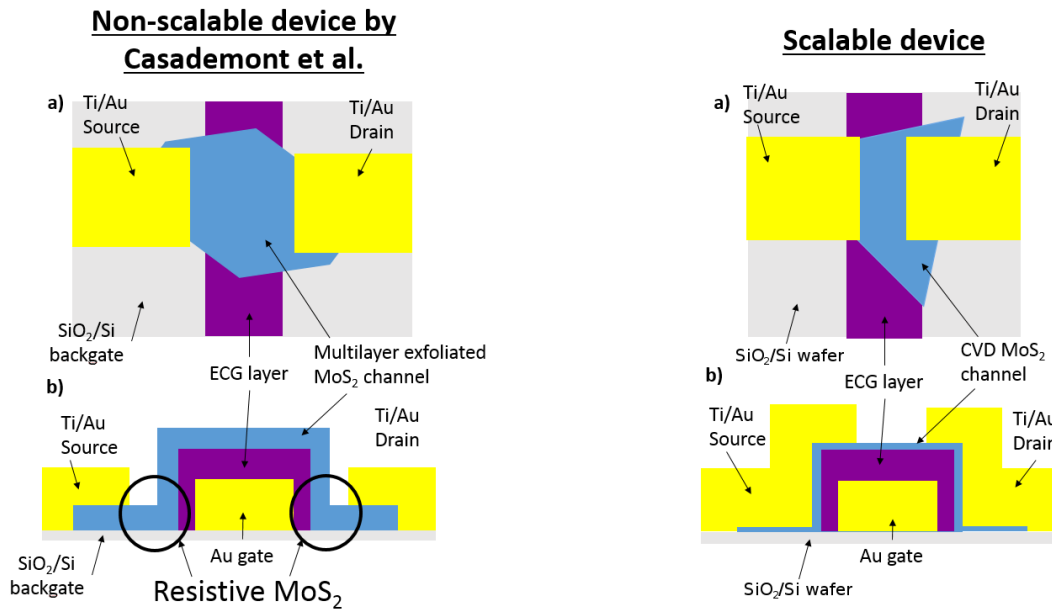


Figure V.7: Two different configurations of MoS₂ transistors with an ECG layer as gate-dielectric : (left) configuration used by Casademont et al. in [3], based on exfoliated MoS₂ and source-drain electrodes not overlapping the gate; (right) the configuration used in this work based on single-layer CVD MoS₂ and source-drain electrodes partly overlapping the channel for improved charge injection. The thickness of the SiO₂ layer is 150 nm.

the organic layer in order to limit the risk of gate current leakage. This configuration, presented in figure V.7, results in four issues :

- Firstly, device miniaturization cannot be performed with this setup, since the space between the gate and the source/drain electrodes strongly increases the channel length at a given gate length.
- Secondly, two parts of the MoS₂ channel are not tuned by the local bottom gate. As seen in figure V.7 (left), the charge-density in the parts of the MoS₂ flakes that are labelled as "Resistive MoS₂" is not controlled by the local gate, and thus these sections are resistive. In order to make these parts of the flake as conductive as possible, the devices were fabricated on a doped silicon wafer covered with 150 nm of SiO₂. The doped substrate was thus used as a global back-gate for the resistive parts of the MoS₂, which means that the device needs 4 electrodes and the continuous application of a high static potential.
- Thirdly, the mechanical exfoliation of MoS₂ has an extremely low yield in particular when very thin flakes are targeted. This issue is not critical for demonstrators such as the one of Kis and co-worker described in [48] because the electrodes of the transistors (including the top gate) are evaporated after MoS₂ deposition, which allows the selection of appropriate flakes located anywhere on the sample. In our case, the very thin only MoS₂ flakes needs to be deposited exactly on top of ECG-modified electrodes. With exfoliated MoS₂ producing almost exclusively multilayers this would result in a very limited number of measurable devices as in [3].
- Finally, the performances of multi-layer MoS₂-FETs are more difficult to analyze

and to compare from device-to-device than the one of single-layer FETs. Indeed, with multi-layers, both the total current and the metal-channel contact quality very much depend on the MoS₂ thickness so that the merits of the gate dielectric itself are more difficult to isolate from the channel effects.

In order to more accurately study the influence of ECG layers as a dielectric in transistors and to get access to scalable devices, direct metal evaporation for the source and drain contacts must be performed partially on top of the gate electrode (with the smallest overlap surface so as to limit as much as possible the gate leakage current). A scheme of the preferable transistor configuration is shown figure V.7 (right). As reported in the previous section, thicker ECG layers lead to lower current leakages and were thus favored here. Three types of scalable MoS₂ FETs are made : (1) devices labelled **TBPF_e-FET**, with a simple 30 nm thick **TBPF_e** ECG layer; (2) devices labelled **(TBPF_e+Thio)-FET**, with a double 28 nm **TBPF_e+Thio** layer; and (3) devices **(TBPF_e+DzF8)-FET**, with a double 32 nm **TBPF_e+DzF8** layer. After the ECG and the MoS₂ deposition on the gate (detailed in the experimental part), direct metal evaporation of Ti 10 nm / Au 50 nm is performed on the sample through a lithography mask. Optical and SEM images of such a device are shown in figure V.8.

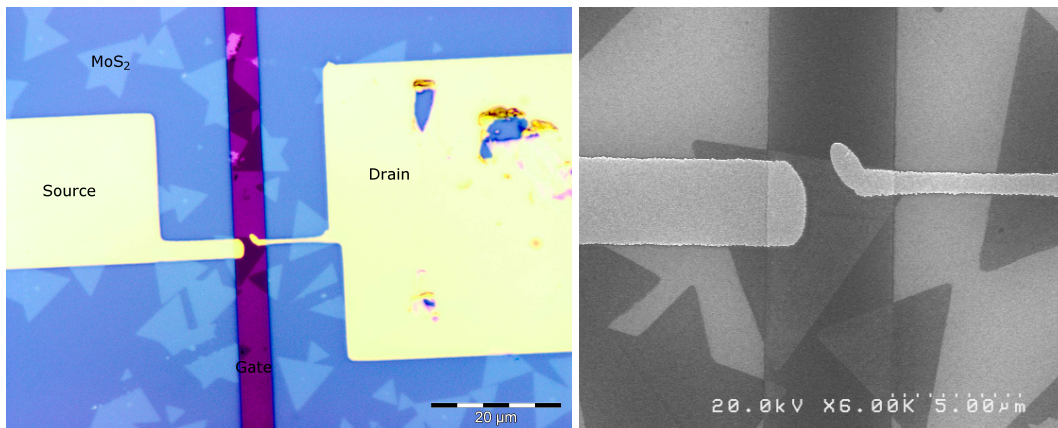


Figure V.8: Optical microscope image (left) and SEM image (right) of a single-layer MoS₂ transistor using a 28 nm thick **TBPF_e+Thio** layer as gate dielectrics and Ti/Au source-drain electrodes.

In total, 16 out of the 18 devices that were fabricated performed as transistors. Only 2 out of the 18 devices showed current leakage through the gate. In some cases, one of the source or drain electrode was slightly shifted outside of the gate, resulting in lower performances due to the same problems as with the devices in the configuration of Casademont et al. In the next part, we concentrate on the 11 devices having the best performances.

First, the best device, a **(TBPF_e+Thio)-FET** is studied. Its $I_D(V_G)$ transfer characteristics measured at $V_D = +1$ V, shown in figure V.9 (up), possesses the expected properties of a particularly good N-type enhancement-mode FET :

- The device fully switches within only 2 V of gate-swing (0-2 V)
- The ON-state current-drive I_D at $V_G = +2$ V and $V_D = +1$ V is 6.5 μ A for a gate-length $L = 2.1$ μ m (considering the channel width $W = 1.8$ μ m this corresponds to a current drive of 3.25 μ A/ μ m), and is a factor 4.10^6 higher than the leakage

current I_G at this bias. This confirms that the ECG layer is a particularly good insulating layer in the useful bias range.

- The I_{ON}/I_{OFF} ratio is $8 \cdot 10^7$, which is nearly 4 orders of magnitude higher than what was reported in [3]. Importantly, such high value exceeds the requirements for digital electronics.

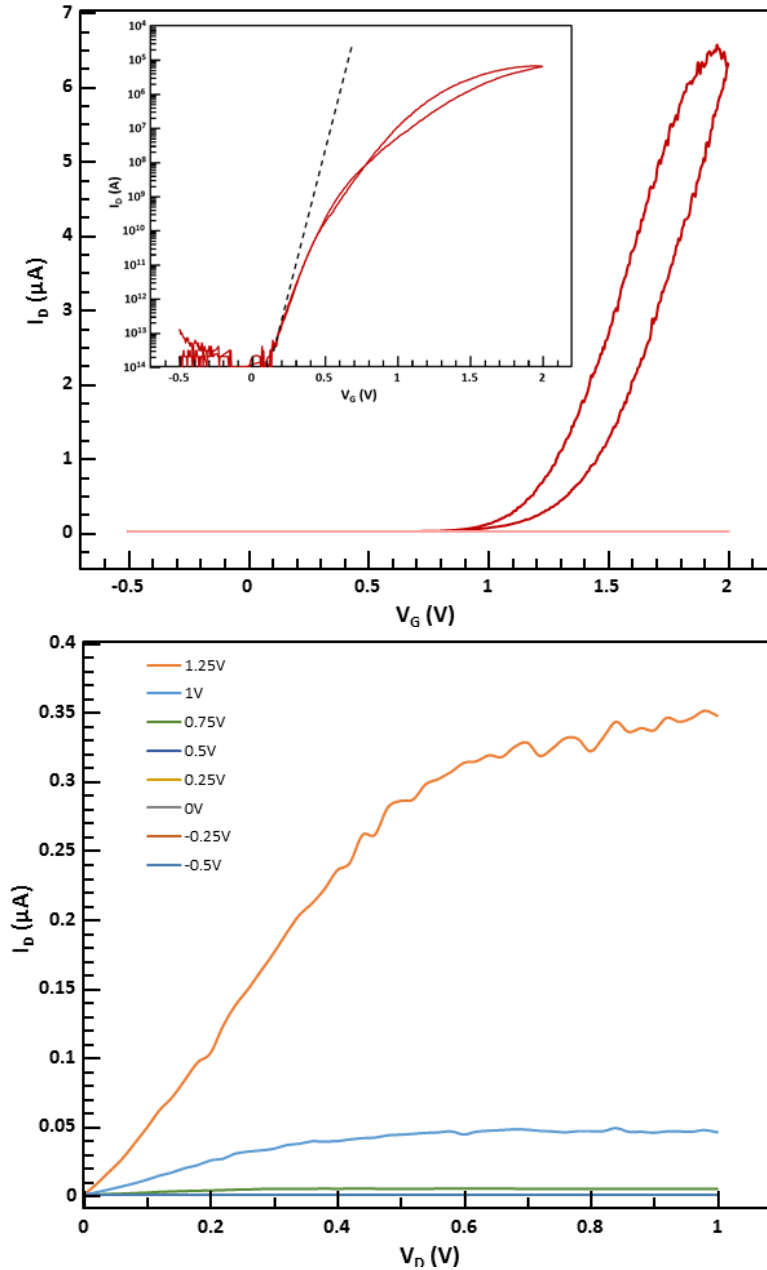


Figure V.9: $I_D(V_G)$ (Dark red) and $I_G(V_G)$ (Light red) transfer characteristics at $V_D = 1$ V. The dotted line is an indicative 60 mV/decade slope (up); $I_D(V_D)$ output characteristics at different V_G for transistors made with MoS₂ as a channel material and a 28 nm thick **TBPFE+Thio** double layer as gate dielectric (bottom).

- The subthreshold slope, measured in its best section (at very low current) is $S = 78$ mV/decade, which is only 18 mV/decade higher than the ideal theoretical value at room temperature (60 mV/decade). We note that the entire subthreshold section of the transfer characteristics does not follow the conventional exponen-

tial shape of typical silicon MOSFETs, in which S is almost constant in the entire OFF-state region. This is however typical of FETs limited by Schottky barriers at the metal-channel interfaces. In such configuration, tunneling current through the Schottky barrier at the source contact is what pilots the ON to OFF-state transition. Only the deep-subthreshold is expected to be limited by thermal emission, and thus concerned by the 60 mV/decade limit [151].

- The field-effect mobility extracted from the maximum transconductance (i.e. from the steepest slope of the transfer characteristics in the ON-state) is $45 \text{ cm}^2 \cdot (\text{V}\cdot\text{s})^{-1}$, which is in the upper range of the reported values in the literature for MoS_2 transistors and significantly better than in previous studies at LICSEN performed with similar CVD-based MoS_2 using SiO_2 as gate-dielectrics.

Then, the $I_D(V_D)$ output characteristics for different V_G are shown figure V.9 (bottom). They mostly confirm the good behavior of such transistor :

- The output curves have a linear behavior at low bias. Despite the fact that these are Schottky-contact FETs, this linear regime indicates that the barrier height for injection of electrons at the source contact is probably very low. This is in agreement with the study by Appenzeller et al. which propose titanium as the second best contact material after scandium for MoS_2 FETs [152].
- The curves start to saturate at low bias ($<0.5 \text{ V}$) which is also typical of conventional FETs with good gate-control over the channel potential [153]
- At $V_D = 1 \text{ V}$, the current is below 1 nA for $V_G = 0.5 \text{ V}$ and above $0.3 \mu\text{A}$ for $V_G = +1.25 \text{ V}$, which confirms the possibility to use such transistor at low bias (in both V_D and V_G) with a high ON-OFF ratio.

$I_D(V_G)$ characteristics for the 11 best devices are shown in figure V.10 with a color-code corresponding to the type of grafted molecules. First, I_G is around 1 pA for all devices at $V_G = +2.5 \text{ V}$, meaning that the ECG layers are good insulators in all the cases. The resulting $I_{\text{ON}}/I_{\text{OFF}}$ are between $5 \cdot 10^6$ and $7.5 \cdot 10^7$ for devices **(TBPFe+Thio)-FETs**, $4.2 \cdot 10^5$ and $8.6 \cdot 10^6$ for the devices **TBPFe-FETs** and $3.1 \cdot 10^6$ and $4.6 \cdot 10^7$ for devices **(TBPFe+DzF8)-FETs**. The mobility is between 11 and $45 \text{ cm}^2 \cdot (\text{V}\cdot\text{s})^{-1}$ for devices **(TBPFe+Thio)-FETs**, 2.5 and $23.1 \text{ cm}^2 \cdot (\text{V}\cdot\text{s})^{-1}$ for devices **(TBPFe+DzF8)-FETs** and between 0.7 and $8 \text{ cm}^2 \cdot (\text{V}\cdot\text{s})^{-1}$ for devices **TBPFe-FETs**. First, these results show that the mobility is widely spread, meaning that the quality of the contacts and the quality of the MoS_2 need to be upgraded. However, all these results also illustrate the fact that the best layer for transistors is the **TBPFe+Thio** layer, followed by the double **TBPFe+DzF8** layer and the **TBPFe** layer.

Finally, the output characteristics of each transistor were compared when the drain potential was applied successively on the left or on the right contact (i.e. $I_D(V_D)$ and $I_S(V_S)$ were compared). All devices presented a lower current in one biasing condition. In some cases, one of the two directions even resulted in a poorly working transistor. This asymmetry results from several factors : (1) MoS_2 flakes are triangular and their orientation respective to the gate electrode is random so that the shape of the channel is not a stripe; (2) the e-beam lithography step usually induces slight shifts from one layer to the next resulting in different drain/gate overlaps; (3) in Schottky-barrier transistors, charge injection is extremely sensitive to the details of the source/channel

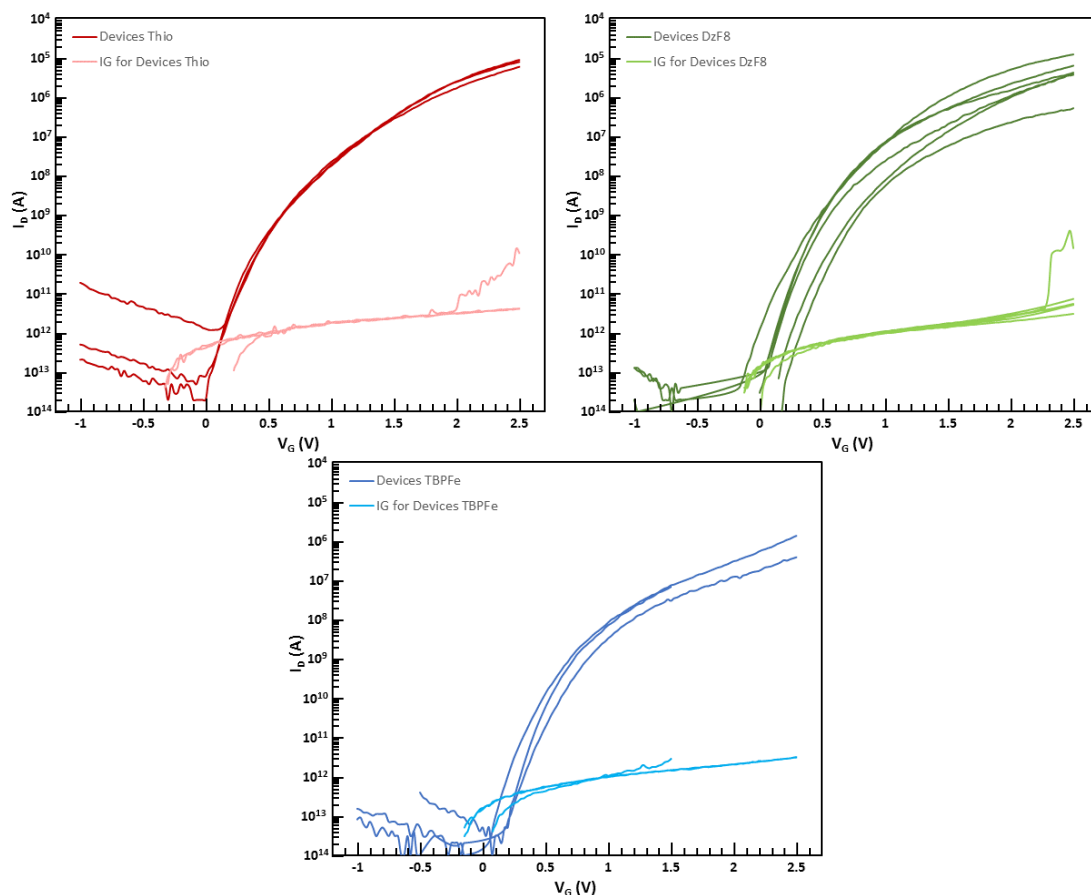


Figure V.10: $I_D(V_G)$ and $I_G(V_G)$ output characteristics of devices **(TBPFfe+Thio)-FETs** (upper left), devices **(TBPFfe+DzF8)-FETs** (upper right) and devices **TBPFfe-FETs** (bottom).

interface. Even when using the same metal and semiconductor materials, a very small difference in the Schottky barrier height can result in a significant difference in current [152, 151].

Then, transistors using these ECG layers as dielectric and monolayers of MoS₂ as channel were studied. While **TBPFfe** and **TBPFfe+DzF8** layers led to good transistors, the best results were obtained with the **TBPFfe+Thio** layers. This could be due to the chemical interaction between the organic and the MoS₂. Indeed, the sulfur atoms on the surface of the thiol terminated layers of the ECG layer can fill the sulfur vacancies that are known to be present in monolayered MoS₂. Such interaction was already observed by different groups and was shown to result in an improvement of the channel quality of the transistors [154, 155]. This constitutes a rather unusual case in the field of electronic devices made from nanomaterials. Indeed, in most cases, chemical reactions on crystalline nanomaterials, such as graphene or carbon nanotubes, can only degrade charge mobility. The reaction of thiols on MoS₂ sulfur vacancies actually brings the material closer to its natural stoichiometry and thus 'heals' the defects.

The studied ECG/MoS₂ transistors have low gate-current leakage, low operating voltage, high charge mobility up to 45 cm².(V.s)⁻¹ and low subthreshold slope down to 78 mV/decade (in the steepest part of the transfer characteristics). Thus, the new generation of MoS₂ transistors constitutes a very significant improvement when compared

with the first generation FET devices made in the laboratory using ECG layers as gate dielectrics [3]. The most promising result is that after careful optimization of the grafting conditions demonstrated in chapter 2 and 3, the source and drain electrodes can now be evaporated directly on top of the organic layers, meaning that the ECG layers are compact and adapted for electronic devices.

When compared with alternative strategies reported in the literature for the integration of thin organic layers as gate-dielectrics in transistors, we note that the potential range for switching between the ON and OFF state is similar to the best results that have been reported in literature for thin organic layers such as SAMs [53] or SANDs [61]. The I_{ON}/I_{OFF} is extremely high at 8.10^7 , and is 2 to 3 orders of magnitude higher than most organic FETs that uses SAM or organic thin layers for the gate [156]. It is however similar to the best devices using SAND gate-dielectric and inorganic semiconductors [157]. In the same way, the subthreshold slope is one of the best reported, being at 78 mV/decade (in its steepest part) while most of organic FETs are above 100 mV/decade [53, 158]. Our result equal the best subthreshold slope obtained with MoS₂ encapsulated with HfO₂ as a gate-dielectric [150]. Finally, the best mobility measured, which is at $45 \text{ cm}^2 \cdot (\text{V} \cdot \text{s})^{-1}$, is one of the highest for MoS₂, with a value close to the work of Kis et al. [48] without having any ambiguities on the final result.

All together, the strategy based on the electrografting of diazonium salts is simple, and leads to robust layers of various properties interesting for electronics. The main illustration of this is the differences between the **TBPF_e+DzF8** and the **TBPF_e+Thio** layer, where the first one is the most resistive layer in simple metal-molecules-metal junctions while the latter is the best gate-dielectric in a MoS₂ transistor. These layers can withstand direct metal evaporation when Ti is used as an anchoring layer, and are highly resistive. Moreover, ECG allows the control of the thickness of the layer, meaning that the resulting organic layer is fully tunable. Another advantage of ECG is that it is possible to graft, on the same chip, different electrodes with different layers (either different thicknesses or different molecules from one electrode to another) with a simple process. Such feature is hardly achievable using most of the other thin layer fabrication processes. That would lead to devices having different properties on the same chip, which makes the fabrication of complex chips easier.

Conclusion and prospects

Conclusion

This PhD thesis work considers an alternative to the deposition of classic organic layers for electronics : electrochemical grafting. The ECG process was studied in details on three different diazonium salts that could be regrouped in two types : salts forming electroactive ECG layers, composed of the tris-bipyridine iron (II) derivative (**TBPFe**), and salts forming non-electroactive ECG layers, composed of the diazonium salt with the long fluorinated chain (**DzF8**) and the one containing a thiol function (**Thio**). The ECG layers were first electrografted using an optimized process (LSV-CA-LSV) on macroscopic gold electrodes and analyzed by various physico-chemical methods : electrochemistry, IR and XPS. The three layers were successfully grafted on the surface and already showed differences, with the **TBPFe** layer being electroactive and the other two layers being insulating in an electrochemical setup.

Then, the ECG was studied on patterned micro-sized gold electrodes made using a combination of optical and e-beam lithography followed by metal evaporation in vacuum. The different parameters of the process were studied in order to precisely control the final thickness of the ECG layer. On one hand, the thickness of ECG layer of **Thio** and **DzF8** was mainly tuned by the potential applied during the ECG, and was explained by the fact that the formed layer is insulating and its growth was driven by current tunneling. A controlled thickness between 2 and 6 nm could be obtained for these diazonium salts. On the other hand, final thickness of **TBPFe** layers was driven by three factors : the concentration of diazonium salt in solution, the potential applied and the time of the process. By choosing the right conditions, a thickness between 5 and 100 nm could be obtained for the **TBPFe** layer [121].

The second part of this work was focused on a novel way to build organic thin layers composed of two different layers : double layer electrografting. This technique consists in using an already grafted electrode as a working electrode in an ECG experiment in order to graft a second ECG layer on top of it. In this thesis, **TBPFe** modified electrodes were grafted with **Thio** and **DzF8** molecules. The nature of the resulting layer was probed by the various physico-chemical measurements used on the previously grafted simple layers : IR, XPS and electrochemistry. An interesting result is that, in cyclic voltammetry, the double layers formed showed a more insulating behavior than the simple layer of **TBPFe**, meaning that the response of the whole double layer is mostly controlled by its top layer. Thus, this process allows the formation of double layer of organic molecules. In this thesis, it was used mostly to tune the thickness of insulators between 10 and 100 nm by using the double **TBPFe+DzF8** and **TBPFe+Thio** layers.

Then, the electrical behavior of the ECG layers were probed by integrating them in vertical metal-molecules-metal junctions. First, the top gold electrodes were deposited

using a process developed during this thesis : printing an aqueous solution of gold nanoparticles on top of a lithography mask. The printing process was optimized in order to get conductive gold electrodes. The first results of junctions using a **TBPF**e thin layer between an evaporated gold bottom electrode and a printed gold top electrode showed a memristive behavior, which is what was expected for this ECG layer. However, after verification, the memristive properties were intrinsic to the printed gold electrodes. While highly conductive printed gold electrodes were successfully made, their operating bias range was only between 0 and +2 V. Thus, further studies are needed in order to use them for probing the electrical properties of ECG layers.

Direct metal evaporation was then performed on the ECG layers to make vertical metal-molecules-metal junctions. A first short study on the influence of the nature of the top electrode was used to determine that a small layer of evaporated Ti under a thicker Au layer was needed to have a high percentage of non-leaking devices. Then, various parameters of all ECG layers made during this thesis were measured : the current measured at +1 V is between 10 and 100 pA for the most insulating **TBPF**e+**DzF8** layer; the breakdown field measured, between 2.6 to 6 MV.cm⁻¹, is competitive against silica and other organic thin layers; and finally, the maximum capacitance measured (between 800 and 900 nF/cm² for the best **TBPF**e layer) is also competitive against most organic thin layers and HF-SANDs or SAMs. All these results indicate that ECG layers could behave as good gate-dielectrics for transistors. Also, it also illustrates quite well the power of ECG : each layers had a different electrical behavior, with **TBPF**e layers having higher capacitance and **DzF8** being more resistive than the other layers. The interest of double layer grafting was also highlighted by the fact that each double layer had better insulating properties than their simple layers counterpart.

Finally, the potential of ECG layers for electronics was shown by using them as gate-dielectric in a transistor where the channel material is a single-layer MoS₂ flake. In the case of the **TBPF**e+**Thio** layer, the measured mobility (45 cm².(V.s)⁻¹), subthreshold slope (79 mV/decade) and I_{ON}/I_{OFF} (8.10⁷) ratios are all better than what was already measured in the laboratory for related devices in a less optimal configuration. The compactness and thickness adjustment of the ECG that allowed the direct metal evaporation were thus key to the performance improvement. Such transistor is also competitive against other transistors made using MoS₂ from the literature [48, 150]. Then, the importance of the chemical nature of the gate-dielectrice top surface was illustrated by comparing these results with similar transistors made using **TBPF**e only or **TBPF**e+**DzF8** layers as gate-dielectric. Surprisingly, while **TBPF**e+**DzF8** was the best insulator in simple vertical metal-molecules-metal junctions, the transistors made using **TBPF**e+**Thio** as gate-dielectric had better characteristics, probably due to the fact that the sulfur atoms on the surface of the ECG layers could fill some of the sulfur vacancies of the MoS₂ and improve its semiconducting properties.

To summarize, the most significant contribution of this thesis to organic electronics and diazonium electrografting are the following :

- The controlled ECG of micrometer sized patterned gold electrodes
- The control over the thickness of ECG layers of different types
- The development of double layer grafting using only ECG process, which allows controlling the chemical nature of the top-surface independantly from the thickness

- The formation of highly resistive, robust (high breakdown voltage) vertical metal-molecules-metal junctions with high capacitance by using various ECG layers
- The formation of transistors using ECG layers as efficient gate dielectric, and the tuning of their properties by using different types of ECG layers

This PhD thesis showed only a small part of what could be achieved with electrografting for organic electronics. It highlighted the main advantages this process has over more classical processes : it can functionalize selectively huge patterned surfaces of one chip, which allows for different functions to be made on the same chip; the thickness of the resulting layer is controllable and fills the gap between SAMs and spin-coated or evaporated molecular layers; the nature of the layer is easily tunable by changing the grafted diazonium salt; and by forming double layers of diazonium salts, properties of the resulting ECG layers can be enhanced. Therefore, ECG process seems to be a promising process for the future of organic electronics.

Prospects

While this PhD thesis showed the potential of ECG layers for electronics, a lot of work can still be done to exploit the full potential of this technique. The most straightforward prospect is to use different organic molecules than the ones used in this thesis for electronics. For example, most of the molecular gate-dielectric presented in literature could be grafted on electrodes by adding an aryl-diazonium function to the molecule. This would lead to better defined gate-dielectric layer, and should potentially allow for a fine tuning of its capacitance through the control of the permittivity and the thickness of the ECG layers.

Double layer grafting also opened a new way of designing organic electronic devices. It could lead to the formation of new functions by combining two different organic layers. For example, rectifying diode could be realized this way by grafting first an electroattractive molecule and then by adding on top of it a molecule that repulses electron in order to form a push-pull system. It could also be used to form a transistor configuration simply by electrografting first an extremely thin dielectric, then by electrografting on top of it a semiconducting layer.

Experimental

Wash sequence for the samples

Before doing any photolithography, e-beam lithography or electrografting, the samples are always washed with the following process :

- ultrasonic bath for 10 min in water+Decon® then washed with water
- ultrasonic bath for 10 min in acetone then washed with acetone
- ultrasonic bath for 10 min in ethanol then washed with ethanol
- dried under nitrogen flux

Photolithography

Silica wafers (Si P++ with 150 nm of SiO₂) are always washed according to the wash sequence described above before doing photolithography. If the sample was not electrografted, a step of Reactive Ion Etching (RIE) was performed with a Plassys MG200 used at 130 V and 50 µbar of O₂ for 20 s. Photolithography was done in a clean room environment. After the washing process, Microposit S1805 G2 was spin coated on a wafer (60 s at 400 rpm) and dried at 115 °C for 60 s. It was then exposed through a mask to a 405 nm UV light using a MJB3 Karl Suss Photomask Aligner. The sample was then developed during 40s in a solution of Microposit MF-319 and thoroughly rinsed water. If the sample was not electrografted, the same step of RIE as before is done.

E-beam lithography

Silica wafers are always washed according to the wash sequence described above before doing E-Beam lithography. MAA EL10 was spin-coated (60 s at 4000 rpm) and dried at 100 °C for 60s. After that, a layer of PMMA is spin-coated at 4000 rpm during 60 s on top of the MAA layer and dried at 100 °C for 60 s. E-beam lithography was performed using a JEOL SEM controlled by a Raith e-beam setup. The sample was developed in a solution of ethanol/methylisobutylketone (1:3 in volume) for 5 s, rinsed with ethanol and dried under nitrogen. The lift-off was performed by putting the sample in a heated acetone bath and using an ultrasonic bath.

DzF8 and Thio synthesis

For this PhD, **TBPFe** was previously synthesized according to [4]. However, **DzF8** and **Thio** were synthesized during this PhD. Since the protocol is similar for both, it will only be described once with a table showing the differences between both processes.

Diazonium synthesized	m_{Amine} (mg)	m_{NOBF_4} (mg)
DzF8	1256	316
Thio	75.6	110

Table E.1: Concentrations of the compounds used in the synthesis of **DzF8** and **Thio**

First, a mass m_{Amine} of amine derivative of the diazonium salt is solubilized in ACN. It is then put in a bath of ACN cooled with liquid nitrogen. A mass m_{NOBF_4} of NOBF_4 is added to the solution, which is stirred for 30 minutes. Diethyl ether is then added to the solution. A precipitate appears. The solution is filtered with a microfiltering setup. Finally, the powder obtained is dried. The final color of the compound is white for **DzF8** and light brown for **Thio**. The ^1H NMR of the compounds are shown in figure E.2, E.1 and E.3. The IR spectra can be found in the main text in figure II.7.

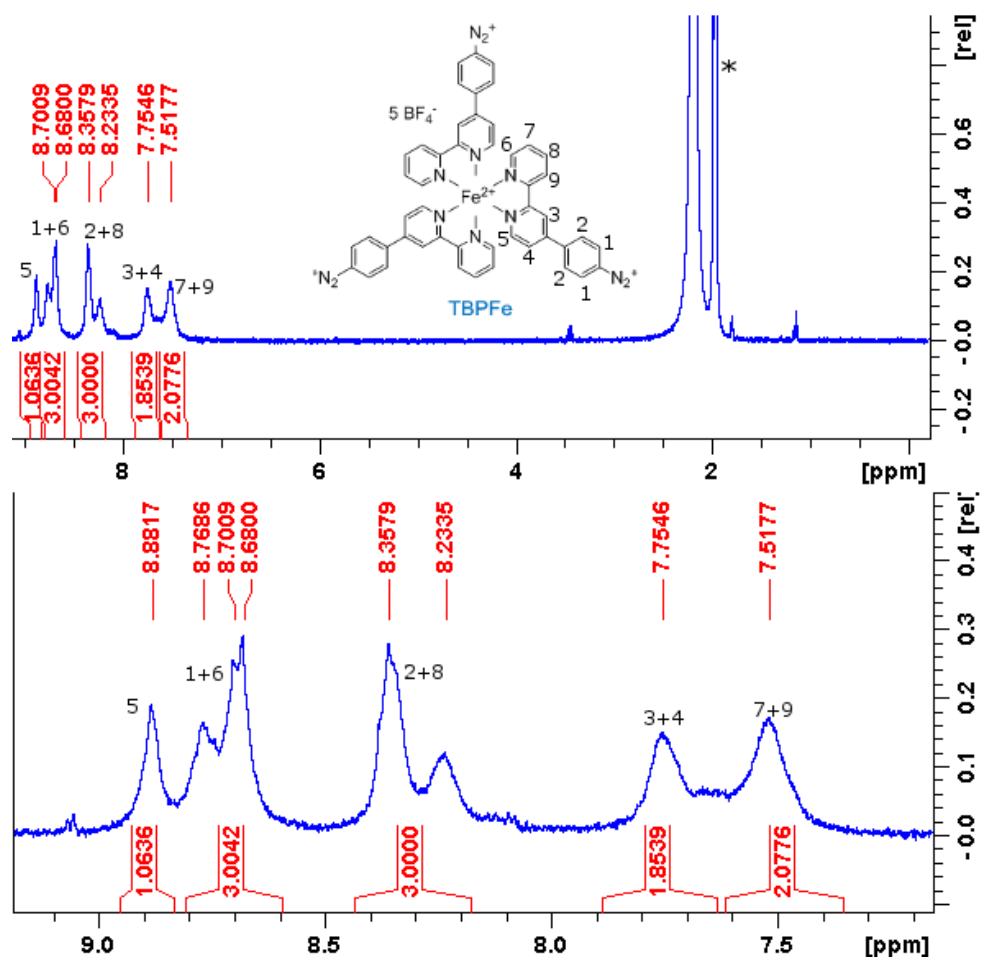


Figure E.1: ^1H NMR of **TBPFe** in CD_3CN . The solvent peak is marked by a *. The peak at 2.25 ppm is from residual ethanol.

Metal evaporation

The bottom electrodes of all samples are composed of 1 nm Cr and 20 nm Au evaporated under vacuum.

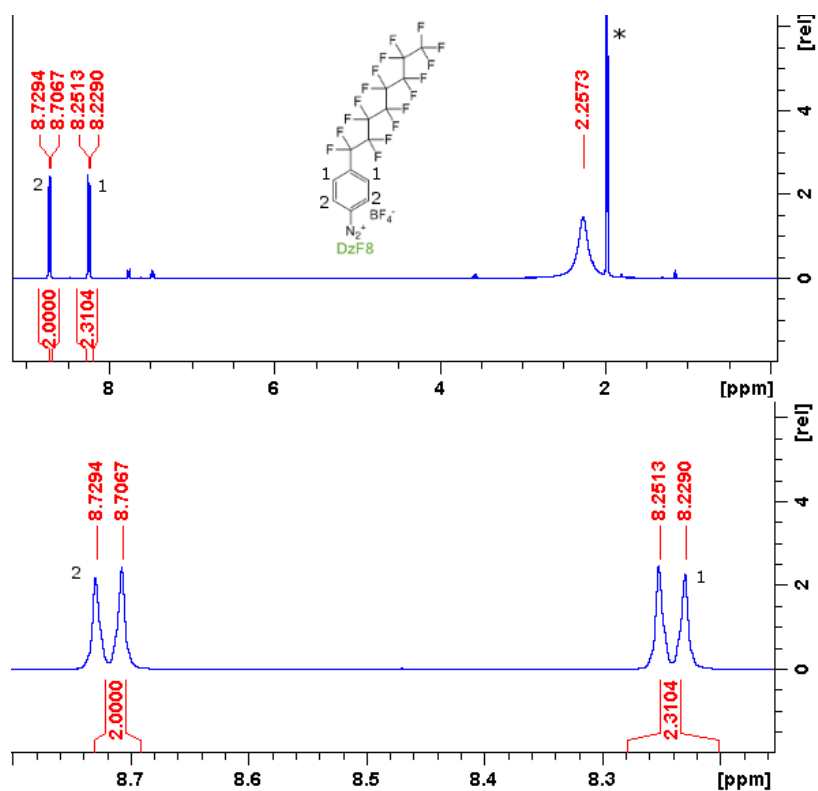


Figure E.2: ^1H NMR of **DzF8** in CD_3CN . The solvent peak is marked by a *. The peak at 2.25 ppm is from residual ethanol.

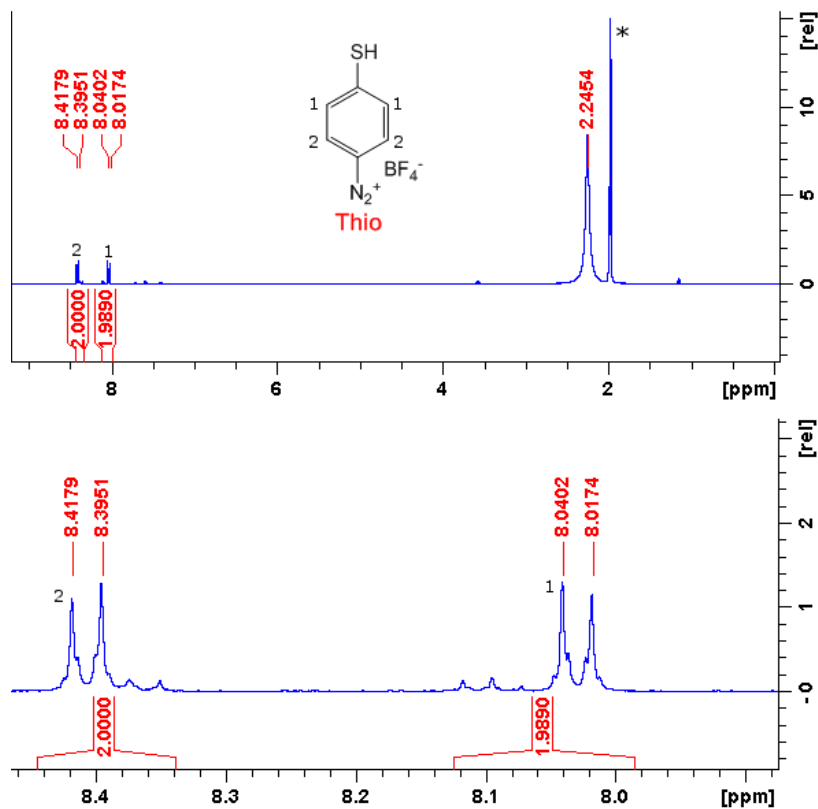


Figure E.3: ^1H NMR of **Thio** in CD_3CN . The solvent peak is marked by a *. The peak at 2.25 ppm is from residual ethanol.

Gold nanoparticle ink synthesis

Gold nanoparticle ink is fabricated in two parts : first, the gold nanoparticles are growth in an organic solvent, then they are fonctionnalized by the dimethylamminopyridine (DMAP) according to the process described in [140].

The gold nanoparticles are synthesized using the Brust method [139]. First, 82 mg of gold(III) chloride HAuCl_4 is solubilized in 33 mL of deionized water. 342 mg of tetraoctylammonium bromide TOAB is solubilized in 100 mL of toluene. Then, the aqueous solution is added to the organic solution, and the resulting solution is stirred until the aqueous phase is transparent. Then, a solution of 77 mg NaBH_4 in 27 mL of water is added to the organic phase, and the solution becomes black. After stirring 2 hours, the organic phase is washed with aqueous solutions of HCl 1 M, then NaHCO_3 saturated and finally with NaCl saturated. The washed organic phased is then dried with dry Na_2SO_4 and filtered. A dark opaque homogeneous solution of gold nanoparticles is obtained.

509 mg of DMAP is added to the toluene solution. After solubilizing all the DMAP, the solution is not opaque anymore and contain small black particles in suspension. After centrifugation at 15 000 rpm for 10 min, a black powder is obtained. It is then solubilized in the lowest volume of water possible, and a black aqueous solution is obtained. From that, the ink is made by adding ethanol in order to have a 50/50 water/ethanol solution.

Gold nanoparticle ink printing

Gold nanoparticle ink printing was done using a Fujifilm Dimatix DMP 2831 inkjet printer system. The ink was put as prepared in a 10 μL cartridge, meaning that each droplets that the cartridge prints has a volume of 10 μL . The printing parameters were a resolution of 7 μm and a height of the cartridge of 0.5 mm above the surface. Most of the times, multiple layers are printed. Between each layer, the nozzles of the cartridge are washed. For the best gold printed electrodes, the tray was heated to 50 $^\circ\text{C}$.

ECG setup

ECG of every samples was done inside a glovebox. The setup is shown figure II.15. The solution are 1 mM for **DzF8**, 28 μM for **TBPFe** or 0.5 mM for **Thio** in a $\text{TBAPF}_6/\text{ACN}$ electrolyte, except when specified. Before grafting, the sample was washed by an ultrasonic treatment : first, 10 min in water and Decon; then, 10 min in acetone ; finally, 10 min in ethanol, followed by drying with nitrogen. A homemade Teflon electrochemical cell is filled with the diazonium salt's solution. Then, the sample is plunged in the cell and electrically connected with a tungsten tip fixed on a micromanipulator. The counter electrode is a platinum wire and the reference electrode is an Ag wire in a solution of AgNO_3 in $\text{TBAPF}_6/\text{ACN}$ electrolyte. Then, ECG is done using the various conditions described in the main text. After the ECG process, the sample is washed again using a shorter ultrasonic bath sequence : 10 min in acetone followed by 10 min in ethanol, then dried with a nitrogen flow.

AFM

AFM is done using a PicoLE AFM with a Picoscan software. Most of the AFM measurements are used for determining the thickness of the layer grafted. This is done by measuring both the grafted electrode and a non grafted reference gold spot on the sample, and then by doing a profile with the two patterns.

Electrical measurements

The electrical properties of the organic layers were measured in vacuum (10^{-3} mbar), except when specified, in a Lakeshore TTP6 probe station using an Agilent 4156C Precision Semiconductor Parameter Analyzer with a detection limit in the sub-100 fA range.

SEM

The SEM images were taken with a Field-Emission SEM Hitachi S-4500.

IR spectroscopy

IR measurements were done using a FTIR spectrometer Bruker Alpha-II.

^1H NMR

The ^1H NMR spectra were recorded on a Bruker DPX 200 MHz instrument.

Contact angle measurement

Contact angle measurements were done using an OCA 15EC contact angle meter.

XPS

X-ray photoelectron spectroscopy (XPS) was performed with a Kratos Analytical Axis Ultra DLD spectrometer, using an Al $K\alpha$ source monochromatized at 1486.6 eV and a charge compensation system. A hemispheric analyzer working at pass energy of 160 eV was used for the global spectrum and 40 eV for core levels.

Optical microscopy

Optical microscopy was used using an Olympus BX61 microscope with an Olympus BX-UCB controller.

Fabrication of the MoS_2 transistor

MoS_2 transistors were fabricated using the following steps. First, the gate electrodes were fabricated on oxidized silicon wafers by photolithography, metal evaporation and lift-off. Then, these electrodes were electrografted with the selected thickness of an ECG layer. In parallel, single-layer MoS_2 domains were synthesized by Chemical Vapor Deposition (CVD) on a separate oxidized silicon wafer, through the co-annealing of

sulfur and MoO_3 in a 2-zones tubular oven. The temperatures for these two solid precursors were respectively adjusted in the 180-220 °C and in the 650-720 °C. The growth was conducted in a nitrogen flow of controlled pressure and flux. All the parameters were adjusted to achieve the required MoS_2 domain morphology for the project (namely triangular single-layer only domains with a size $>7 \mu\text{m}$ and a distance between domains $>5 \mu\text{m}$). The quality of the MoS_2 grown at Licsen with this method was previously assessed by SEM, AFM, BALM and XPS at Licsen, by μ -Raman and photoluminescence mapping at CEA Leti, and by high-resolution TEM at CEA Inac (H. Okuno).

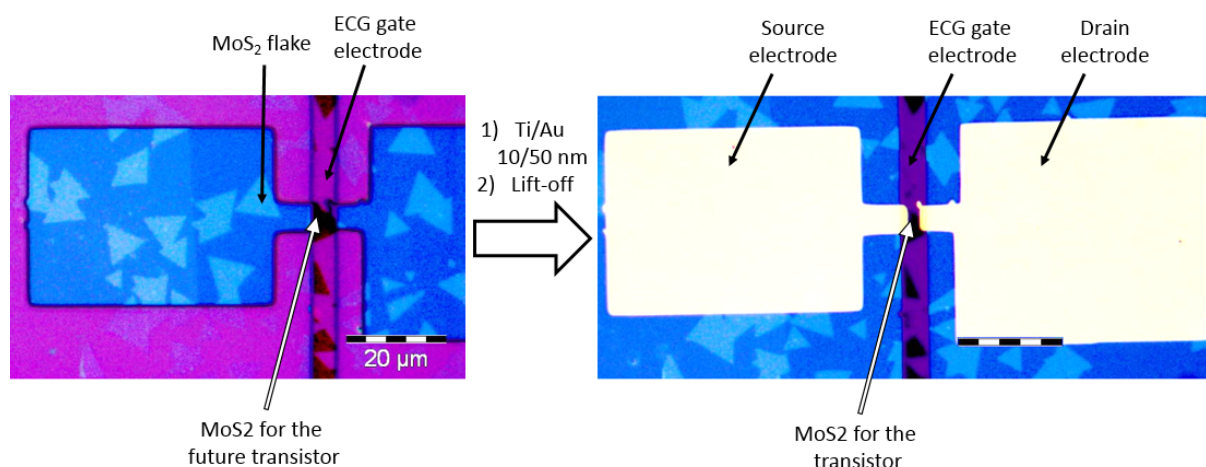


Figure E.4: Optic image of a sample on which MoS_2 is deposited after e-beam lithography (left) and after lift off (right). The scale bar is at $20 \mu\text{m}$ for both images.

A sample with the appropriate size, shape and density of MoS_2 domains was then covered with PMMA by spin-coating, diced and placed in KOH (30% KOH in DI water) with the PMMA facing upward. The sample was initially floating. After a few hours, the SiO_2 layer had been etched away and the silicon wafer piece lied at the bottom of the solution. The remaining PMMA membrane with MoS_2 domains attached to it remained floating on the KOH/water solution. It was cautiously transferred twice to a clean DI water solution, and finally transferred a third time directly on top of the target sample containing the grafted electrodes. This last transfer step was critical to place the best MoS_2 areas resulting from the CVD growth precisely on top of the grafted electrodes and to limit as much as possible any folding of the PMMA/ MoS_2 membrane which would result in damaged MoS_2 domains.

After this transfer step, individual MoS_2 domains bridging grafted electrodes were located by optical microscopy and an e-beam lithography mask was designed for the source and drain electrodes. Special care was taken to limit the size of the source and drain overlap with the gate electrode and to avoid the crossing of other MoS_2 domains not located on bottom electrodes. The source and drain contacts composed of Ti (10 nm) + Au (60 nm) were finally prepared by evaporation and lift-off.

References

- [1] G. Moore, "Moore's law," Electronics Magazine, vol. 38, no. 8, p. 114, 1965.
- [2] M. M. Waldrop, "The chips are down for Moore's law," Nat. News, vol. 530, p. 144, Feb. 2016.
- [3] H. Casademont, L. Fillaud, X. Lefèvre, B. Jousselme, and V. Derycke, "Electrografted Fluorinated Organic Ultrathin Film as Efficient Gate Dielectric in MoS₂ Transistors," J. Phys. Chem. C, vol. 120, pp. 9506–9510, May 2016.
- [4] Y.-P. Lin, C. H. Bennett, T. Cabaret, D. Vodenicarevic, D. Chabi, D. Querlioz, B. Jousselme, V. Derycke, and J.-O. Klein, "Physical Realization of a Supervised Learning System Built with Organic Memristive Synapses," Sci. Rep., vol. 6, p. 31932, Sept. 2016.
- [5] B. Mann and H. Kuhn, "Tunneling through Fatty Acid Salt Monolayers," J. Appl. Phys., vol. 42, pp. 4398–4405, Oct. 1971.
- [6] A. Aviram and M. A. Ratner, "Molecular rectifiers," Chem. Phys. Lett., vol. 29, pp. 277–283, Nov. 1974.
- [7] H. Shirakawa, E. J. Louis, A. G. MacDiarmid, C. K. Chiang, and A. J. Heeger, "Synthesis of electrically conducting organic polymers: Halogen derivatives of polyacetylene, (CH)_x," J. Chem. Soc. Chem. Commun., vol. 0, no. 16, pp. 578–580, 1977.
- [8] E. E. Polymeropoulos and J. Sagiv, "Electrical conduction through adsorbed monolayers," J. Chem. Phys., vol. 69, pp. 1836–1847, Sept. 1978.
- [9] R. H. Friend, R. W. Gymer, A. B. Holmes, J. H. Burroughes, R. N. Marks, C. Taliani, D. D. C. Bradley, D. A. D. Santos, J. L. Brédas, M. Lögdlund, and W. R. Salaneck, "Electroluminescence in conjugated polymers," Nature, vol. 397, p. 121, Jan. 1999.
- [10] M. A. Baldo, D. F. O'Brien, Y. You, A. Shoustikov, S. Sibley, M. E. Thompson, and S. R. Forrest, "Highly efficient phosphorescent emission from organic electroluminescent devices," Nature, vol. 395, p. 151, Sept. 1998.
- [11] L. S. Roman, M. Berggren, and O. Inganäs, "Polymer diodes with high rectification," Appl. Phys. Lett., vol. 75, pp. 3557–3559, Nov. 1999.
- [12] S. Steudel, K. Myny, V. Arkhipov, C. Deibel, S. D. Vusser, J. Genoe, and P. Heremans, "50 MHz rectifier based on an organic diode," Nat. Mater., vol. 4, p. 597, Aug. 2005.

REFERENCES

- [13] A. Pierre, I. Deckman, P. B. Lechêne, and A. C. Arias, "High Detectivity All-Printed Organic Photodiodes," *Adv. Mater.*, vol. 27, no. 41, pp. 6411–6417, 2015.
- [14] Y. Noda, T. Yamada, K. Kobayashi, R. Kumai, S. Horiuchi, F. Kagawa, and T. Hasegawa, "Few-Volt Operation of Printed Organic Ferroelectric Capacitor," *Adv. Mater.*, vol. 27, no. 41, pp. 6475–6481, 2015.
- [15] L. Qi, L. Petersson, and T. Liu, "Review of Recent Activities on Dielectric Films for Capacitor Applications," *Journal of International Council on Electrical Engineering*, vol. 4, pp. 1–6, Jan. 2014.
- [16] B. S. Ong, Y. Wu, P. Liu, and S. Gardner, "High-Performance Semiconducting Polythiophenes for Organic Thin-Film Transistors," *J. Am. Chem. Soc.*, vol. 126, pp. 3378–3379, Mar. 2004.
- [17] L. A. Agapito, S. Alkis, J. L. Krause, and H.-P. Cheng, "Atomistic Origins of Molecular Memristors," *J. Phys. Chem. C*, vol. 113, pp. 20713–20718, Dec. 2009.
- [18] J. Lee, H. Chang, S. Kim, G. S. Bang, and H. Lee, "Molecular Monolayer Non-volatile Memory with Tunable Molecules," *Angew. Chem. Int. Ed.*, vol. 48, no. 45, pp. 8501–8504, 2009.
- [19] A. Tsumura, H. Koezuka, and T. Ando, "Macromolecular electronic device: Field-effect transistor with a polythiophene thin film," *Appl. Phys. Lett.*, vol. 49, pp. 1210–1212, Nov. 1986.
- [20] C. D. Dimitrakopoulos and P. R. L. Malenfant, "Organic Thin Film Transistors for Large Area Electronics," *Adv. Mater.*, vol. 14, no. 2, pp. 99–117, 2002.
- [21] P. Avouris, J. Appenzeller, R. Martel, and S. J. Wind, "Carbon nanotube electronics," *Proceedings of the IEEE*, vol. 91, pp. 1772–1784, Nov. 2003.
- [22] C. Rutherglen, D. Jain, and P. Burke, "Nanotube electronics for radiofrequency applications," *Nat. Nanotechnol.*, vol. 4, pp. 811–819, Dec. 2009.
- [23] F. Schwierz, "Graphene transistors," *Nat. Nanotechnol.*, vol. 5, pp. 487–496, July 2010.
- [24] S. J. Tans, A. R. M. Verschueren, and C. Dekker, "Room-temperature transistor based on a single carbon nanotube," *Nature*, vol. 393, pp. 49–52, May 1998.
- [25] R. Martel, T. Schmidt, H. R. Shea, T. Hertel, and P. Avouris, "Single- and multi-wall carbon nanotube field-effect transistors," *Appl. Phys. Lett.*, vol. 73, pp. 2447–2449, Oct. 1998.
- [26] H. Liu, A. T. Neal, Z. Zhu, Z. Luo, X. Xu, D. Tománek, and P. D. Ye, "Phosphorene: An Unexplored 2D Semiconductor with a High Hole Mobility," *ACS Nano*, vol. 8, pp. 4033–4041, Apr. 2014.
- [27] Y. Yoon, K. Ganapathi, and S. Salahuddin, "How Good Can Monolayer MoS₂ Transistors Be?," *Nano Lett.*, vol. 11, pp. 3768–3773, Sept. 2011.
- [28] X. Duan, Y. Huang, Y. Cui, J. Wang, and C. M. Lieber, "Indium phosphide nanowires as building blocks for nanoscale electronic and optoelectronic devices," *Nature*, vol. 409, p. 66, Jan. 2001.

- [29] Y. Cui and C. M. Lieber, "Functional Nanoscale Electronic Devices Assembled Using Silicon Nanowire Building Blocks," *Science*, vol. 291, pp. 851–853, Feb. 2001.
- [30] F. Ebisawa, T. Kurokawa, and S. Nara, "Electrical properties of polyacetylene/polysiloxane interface," *J. Appl. Phys.*, vol. 54, pp. 3255–3259, June 1983.
- [31] K. Kudo, M. Yamashina, and T. Moriizumi, "Field Effect Measurement of Organic Dye Films," *Jpn. J. Appl. Phys.*, vol. 23, pp. 130–130, Jan. 1984.
- [32] G. Horowitz, D. Fichou, X. Peng, Z. Xu, and F. Garnier, "A field-effect transistor based on conjugated alpha-sexithienyl," *Solid State Commun.*, vol. 72, pp. 381–384, Oct. 1989.
- [33] Y. Kato, S. Iba, R. Teramoto, T. Sekitani, T. Someya, H. Kawaguchi, and T. Sakurai, "High mobility of pentacene field-effect transistors with polyimide gate dielectric layers," *Appl. Phys. Lett.*, vol. 84, pp. 3789–3791, May 2004.
- [34] W. Wang, D. Ma, S. Pan, and Y. Yang, "Hysteresis mechanism in low-voltage and high mobility pentacene thin-film transistors with polyvinyl alcohol dielectric," *Appl. Phys. Lett.*, vol. 101, p. 033303, July 2012.
- [35] O. D. Jurchescu, M. Popinciuc, B. J. van Wees, and T. T. M. Palstra, "Interface-Controlled, High-Mobility Organic Transistors," *Adv. Mater.*, vol. 19, no. 5, pp. 688–692, 2007.
- [36] M. Yamagishi, J. Takeya, Y. Tominari, Y. Nakazawa, T. Kuroda, S. Ikehata, M. Uno, T. Nishikawa, and T. Kawase, "High-mobility double-gate organic single-crystal transistors with organic crystal gate insulators," *Appl. Phys. Lett.*, vol. 90, p. 182117, Apr. 2007.
- [37] R. J. Chesterfield, J. C. McKeen, C. R. Newman, P. C. Ewbank, D. A. da Silva Filho, J.-L. Brédas, L. L. Miller, K. R. Mann, and C. D. Frisbie, "Organic Thin Film Transistors Based on N-Alkyl Perylene Diimides: Charge Transport Kinetics as a Function of Gate Voltage and Temperature," *J. Phys. Chem. B*, vol. 108, pp. 19281–19292, Dec. 2004.
- [38] R. Schmidt, J. H. Oh, Y.-S. Sun, M. Deppisch, A.-M. Krause, K. Radacki, H. Braunschweig, M. Könemann, P. Erk, Z. Bao, and F. Würthner, "High-Performance Air-Stable n-Channel Organic Thin Film Transistors Based on Halogenated Perylene Bisimide Semiconductors," *J. Am. Chem. Soc.*, vol. 131, pp. 6215–6228, May 2009.
- [39] M. Ichikawa, T. Kato, T. Uchino, T. Tsuzuki, M. Inoue, H.-G. Jeon, T. Koyama, and Y. Taniguchi, "Thin-film and single-crystal transistors based on a trifluoromethyl-substituted alternating (thiophene/phenylene)-co-oligomer," *Org. Electron.*, vol. 11, pp. 1549–1554, Sept. 2010.
- [40] F. Zhang, Y. Hu, T. Schuettfort, C.-a. Di, X. Gao, C. R. McNeill, L. Thomsen, S. C. B. Mannsfeld, W. Yuan, H. Sirringhaus, and D. Zhu, "Critical Role of Alkyl Chain Branching of Organic Semiconductors in Enabling Solution-Processed N-Channel Organic Thin-Film Transistors with Mobility of up to $3.50 \text{ cm}^2 \text{ V}^{-1} \text{ s}^{-1}$," *J. Am. Chem. Soc.*, vol. 135, pp. 2338–2349, Feb. 2013.

- [41] S. Iijima and T. Ichihashi, "Single-shell carbon nanotubes of 1-nm diameter," *Nature*, vol. 363, p. 603, June 1993.
- [42] D. S. Bethune, C. H. Kiang, M. S. de Vries, G. Gorman, R. Savoy, J. Vazquez, and R. Beyers, "Cobalt-catalysed growth of carbon nanotubes with single-atomic-layer walls," *Nature*, vol. 363, p. 605, June 1993.
- [43] T. Dürkop, S. A. Getty, E. Cobas, and M. S. Fuhrer, "Extraordinary Mobility in Semiconducting Carbon Nanotubes," *Nano Lett.*, vol. 4, pp. 35–39, Jan. 2004.
- [44] S. J. Kang, C. Kocabas, T. Ozel, M. Shim, N. Pimparkar, M. A. Alam, S. V. Rotkin, and J. A. Rogers, "High-performance electronics using dense, perfectly aligned arrays of single-walled carbon nanotubes," *Nat. Nanotechnol.*, vol. 2, pp. 230–236, Apr. 2007.
- [45] K. S. Novoselov, A. K. Geim, S. V. Morozov, D. Jiang, Y. Zhang, S. V. Dubonos, I. V. Grigorieva, and A. A. Firsov, "Electric Field Effect in Atomically Thin Carbon Films," *Science*, vol. 306, pp. 666–669, Oct. 2004.
- [46] A. S. Mayorov, R. V. Gorbachev, S. V. Morozov, L. Britnell, R. Jalil, L. A. Ponomarenko, P. Blake, K. S. Novoselov, K. Watanabe, T. Taniguchi, and A. K. Geim, "Micrometer-Scale Ballistic Transport in Encapsulated Graphene at Room Temperature," *Nano Lett.*, vol. 11, pp. 2396–2399, June 2011.
- [47] R. Fivaz and E. Mooser, "Mobility of Charge Carriers in Semiconducting Layer Structures," *Phys. Rev.*, vol. 163, pp. 743–755, Nov. 1967.
- [48] B. Radisavljevic, A. Radenovic, J. Brivio, V. Giacometti, and A. Kis, "Single-layer MoS₂ transistors," *Nat. Nanotechnol.*, vol. 6, pp. 147–150, Mar. 2011.
- [49] A. K. Geim and I. V. Grigorieva, "Van der Waals heterostructures," *Nature*, vol. 499, pp. 419–425, July 2013.
- [50] H. Wang, L. Yu, Y.-H. Lee, Y. Shi, A. Hsu, M. L. Chin, L.-J. Li, M. Dubey, J. Kong, and T. Palacios, "Integrated Circuits Based on Bilayer MoS₂ Transistors," *Nano Lett.*, vol. 12, pp. 4674–4680, Sept. 2012.
- [51] M. S. Fuhrer and J. Hone, "Measurement of mobility in dual-gated MoS₂ transistors," *Nat. Nanotechnol.*, vol. 8, pp. 146–147, Mar. 2013.
- [52] B. Radisavljevic and A. Kis, "Reply to 'Measurement of mobility in dual-gated MoS₂ transistors'," *Nat. Nanotechnol.*, vol. 8, pp. 147–148, Mar. 2013.
- [53] J. Collet, O. Tharaud, A. Chapoton, and D. Vuillaume, "Low-voltage, 30 nm channel length, organic transistors with a self-assembled monolayer as gate insulating films," *Appl. Phys. Lett.*, vol. 76, pp. 1941–1943, Apr. 2000.
- [54] J. Collet and D. Vuillaume, "Nano-field effect transistor with an organic self-assembled monolayer as gate insulator," *Appl. Phys. Lett.*, vol. 73, pp. 2681–2683, Nov. 1998.
- [55] Y. D. Park, D. H. Kim, Y. Jang, M. Hwang, J. A. Lim, and K. Cho, "Low-voltage polymer thin-film transistors with a self-assembled monolayer as the gate dielectric," *Appl. Phys. Lett.*, vol. 87, p. 243509, Dec. 2005.

- [56] U. Zschieschang, F. Ante, M. Schlörholz, M. Schmidt, K. Kern, and H. Klauk, "Mixed Self-Assembled Monolayer Gate Dielectrics for Continuous Threshold Voltage Control in Organic Transistors and Circuits," *Adv. Mater.*, vol. 22, no. 40, pp. 4489–4493, 2010.
- [57] S. Kobayashi, T. Nishikawa, T. Takenobu, S. Mori, T. Shimoda, T. Mitani, H. Shimotani, N. Yoshimoto, S. Ogawa, and Y. Iwasa, "Control of carrier density by self-assembled monolayers in organic field-effect transistors," *Nat. Mater.*, vol. 3, p. 317, May 2004.
- [58] K. P. Pernstich, S. Haas, D. Oberhoff, C. Goldmann, D. J. Gundlach, B. Batlogg, A. N. Rashid, and G. Schitter, "Threshold voltage shift in organic field effect transistors by dipole monolayers on the gate insulator," *J. Appl. Phys.*, vol. 96, pp. 6431–6438, Nov. 2004.
- [59] U. Kraft, M. Sejfić, M. J. Kang, K. Takimiya, T. Zaki, F. Letzkus, J. N. Burghartz, E. Weber, and H. Klauk, "Flexible Low-Voltage Organic Complementary Circuits: Finding the Optimum Combination of Semiconductors and Monolayer Gate Dielectrics," *Adv. Mater.*, vol. 27, no. 2, pp. 207–214, 2015.
- [60] M.-H. Yoon, H. Yan, A. Facchetti, and T. J. Marks, "Low-Voltage Organic Field-Effect Transistors and Inverters Enabled by Ultrathin Cross-Linked Polymers as Gate Dielectrics," *J. Am. Chem. Soc.*, vol. 127, pp. 10388–10395, July 2005.
- [61] K. Everaerts, J. D. Emery, D. Jariwala, H. J. Karmel, V. K. Sangwan, P. L. Prabhumirashi, M. L. Geier, J. J. McMorrow, M. J. Bedzyk, A. Facchetti, M. C. Hersam, and T. J. Marks, "Ambient-Processable High Capacitance Hafnia-Organic Self-Assembled Nanodielectrics," *J. Am. Chem. Soc.*, vol. 135, pp. 8926–8939, June 2013.
- [62] Y. Baek, S. Lim, E. J. Yoo, L. H. Kim, H. Kim, S. W. Lee, S. H. Kim, and C. E. Park, "Fluorinated Polyimide Gate Dielectrics for the Advancing the Electrical Stability of Organic Field-Effect Transistors," *ACS Appl. Mater. Interfaces*, vol. 6, pp. 15209–15216, Sept. 2014.
- [63] M. E. Roberts, N. Queraltó, S. C. B. Mannsfeld, B. N. Reinecke, W. Knoll, and Z. Bao, "Cross-Linked Polymer Gate Dielectric Films for Low-Voltage Organic Transistors," *Chem. Mater.*, vol. 21, pp. 2292–2299, June 2009.
- [64] J. Li, J. Du, J. Xu, H. L. W. Chan, and F. Yan, "The influence of gate dielectrics on a high-mobility n-type conjugated polymer in organic thin-film transistors," *Appl. Phys. Lett.*, vol. 100, p. 033301, Jan. 2012.
- [65] J. Lee, M. J. Panzer, Y. He, T. P. Lodge, and C. D. Frisbie, "Ion Gel Gated Polymer Thin-Film Transistors," *J. Am. Chem. Soc.*, vol. 129, pp. 4532–4533, Apr. 2007.
- [66] D. B. Strukov, G. S. Snider, D. R. Stewart, and R. S. Williams, "The missing memristor found," *Nature*, vol. 453, pp. 80–83, May 2008.
- [67] S. H. Jo, T. Chang, I. Ebong, B. B. Bhadviya, P. Mazumder, and W. Lu, "Nanoscale Memristor Device as Synapse in Neuromorphic Systems," *Nano Lett.*, vol. 10, pp. 1297–1301, Apr. 2010.
- [68] J. J. Yang, D. B. Strukov, and D. R. Stewart, "Memristive devices for computing," *Nat. Nanotechnol.*, vol. 8, pp. 13–24, Jan. 2013.

- [69] R. Waser, R. Dittmann, G. Staikov, and K. Szot, "Redox-Based Resistive Switching Memories – Nanoionic Mechanisms, Prospects, and Challenges," *Adv. Mater.*, vol. 21, no. 25-26, pp. 2632–2663, 2009.
- [70] D. S. Jeong, R. Thomas, R. S. Katiyar, J. F. Scott, H. Kohlstedt, A. Petraru, and C. S. Hwang, "Emerging memories: Resistive switching mechanisms and current status," *Rep. Prog. Phys.*, vol. 75, p. 076502, June 2012.
- [71] F. Argall, "Switching phenomena in titanium oxide thin films," *Solid-State Electron.*, vol. 11, pp. 535–541, May 1968.
- [72] D.-H. Kwon, K. M. Kim, J. H. Jang, J. M. Jeon, M. H. Lee, G. H. Kim, X.-S. Li, G.-S. Park, B. Lee, S. Han, M. Kim, and C. S. Hwang, "Atomic structure of conducting nanofilaments in TiO₂ resistive switching memory," *Nat. Nanotechnol.*, vol. 5, pp. 148–153, Feb. 2010.
- [73] L. D. Bozano, B. W. Kean, V. R. Deline, J. R. Salem, and J. C. Scott, "Mechanism for bistability in organic memory elements," *Appl. Phys. Lett.*, vol. 84, pp. 607–609, Jan. 2004.
- [74] M. Carloti, S. Soni, S. Kumar, Y. Ai, E. Sauter, M. Zharnikov, and R. C. Chiechi, "Two-Terminal Molecular Memory through Reversible Switching of Quantum Interference Features in Tunneling Junctions," *Angew. Chem. Int. Ed.*, vol. 57, no. 48, pp. 15681–15685, 2018.
- [75] K. Seo, A. V. Konchenko, J. Lee, G. S. Bang, and H. Lee, "Molecular Conductance Switch-On of Single Ruthenium Complex Molecules," *J. Am. Chem. Soc.*, vol. 130, pp. 2553–2559, Feb. 2008.
- [76] T. Miyamachi, M. Gruber, V. Davesne, M. Bowen, S. Boukari, L. Joly, F. Scheurer, G. Rogez, T. K. Yamada, P. Ohresser, E. Beaurepaire, and W. Wulfhekel, "Robust spin crossover and memristance across a single molecule," *Nat. Commun.*, vol. 3, p. 938, Jan. 2012.
- [77] B. Pradhan and S. Das, "Role of New Bis(2,2'-bipyridyl)(triazolopyridyl)ruthenium(II) Complex in the Organic Bistable Memory Application," *Chem. Mater.*, vol. 20, pp. 1209–1211, Feb. 2008.
- [78] B. K. Barman, M. M. Guru, G. K. Panda, B. Maji, and R. K. Vijayaraghavan, "Pyrene-affixed triazoles: A new class of molecular semiconductors for robust, non-volatile resistive memory devices," *Chem. Commun.*, vol. 55, no. 32, pp. 4643–4646, 2019.
- [79] H. Yan, A. J. Bergren, R. McCreery, M. L. D. Rocca, P. Martin, P. Lafarge, and J. C. Lacroix, "Activationless charge transport across 4.5 to 22 nm in molecular electronic junctions," *Proc. Natl. Acad. Sci. U.S.A.*, vol. 110, pp. 5326–5330, Apr. 2013.
- [80] A. J. Bergren, K. D. Harris, F. Deng, and R. L. McCreery, "Molecular electronics using diazonium-derived adlayers on carbon with Cu top contacts: Critical analysis of metal oxides and filaments," *J. Phys.: Condens. Matter*, vol. 20, p. 374117, Aug. 2008.

- [81] T. Fluteau, C. Bessis, C. Barraud, M. L. Della Rocca, P. Martin, J.-C. Lacroix, and P. Lafarge, "Tuning the thickness of electrochemically grafted layers in large area molecular junctions," *J. Appl. Phys.*, vol. 116, p. 114509, Sept. 2014.
- [82] A. Bayat, J.-C. Lacroix, and R. L. McCreery, "Control of Electronic Symmetry and Rectification through Energy Level Variations in Bilayer Molecular Junctions," *J. Am. Chem. Soc.*, vol. 138, pp. 12287–12296, Sept. 2016.
- [83] V.-Q. Nguyen, D. Schaming, D. L. Tran, and J.-C. Lacroix, "Ordered Nanoporous Thin Films by Nanosphere Lithography and Diazonium Electroreduction: Simple Elaboration of Ultra-Micro-Electrode Arrays," *ChemElectroChem*, vol. 3, no. 12, pp. 2264–2269, 2016.
- [84] Q. V. Nguyen, P. Martin, D. Frath, M. L. Della Rocca, F. Lafalet, S. Bellinck, P. Lafarge, and J.-C. Lacroix, "Highly Efficient Long-Range Electron Transport in a Viologen-Based Molecular Junction," *J. Am. Chem. Soc.*, vol. 140, pp. 10131–10134, Aug. 2018.
- [85] M. Supur, C. Van Dyck, A. J. Bergren, and R. L. McCreery, "Bottom-up, Robust Graphene Ribbon Electronics in All-Carbon Molecular Junctions," *ACS Appl. Mater. Interfaces*, vol. 10, pp. 6090–6095, Feb. 2018.
- [86] D.-A. Roşca, J. A. Wright, and M. Bochmann, "An element through the looking glass: Exploring the Au–C, Au–H and Au–O energy landscape," *Dalton Trans.*, vol. 44, pp. 20785–20807, Dec. 2015.
- [87] B. Barbier, J. Pinson, G. Desarmot, and M. Sanchez, "Electrochemical Bonding of Amines to Carbon Fiber Surfaces Toward Improved Carbon-Epoxy Composites," *J. Electrochem. Soc.*, vol. 137, pp. 1757–1764, Jan. 1990.
- [88] G. Herlem, C. Goux, B. Fahys, F. Dominati, A. M. Gonçalves, C. Mathieu, E. Sutter, A. Trokourey, and J. F. Penneau, "Surface modification of platinum and gold electrodes by anodic oxidation of pure ethylenediamine," *J. Electroanal. Chem.*, vol. 435, pp. 259–265, Sept. 1997.
- [89] C. P. Andrieux, F. Gonzalez, and J.-M. Savéant, "Derivatization of Carbon Surfaces by Anodic Oxidation of Arylacetates. Electrochemical Manipulation of the Grafted Films," *J. Am. Chem. Soc.*, vol. 119, pp. 4292–4300, May 1997.
- [90] P. D. Astudillo, A. Galano, and F. J. González, "Radical grafting of carbon surfaces with alkylic groups by mediated oxidation of carboxylates," *J. Electroanal. Chem.*, vol. 610, pp. 137–146, Dec. 2007.
- [91] C. Jérôme, N. Willet, R. Jérôme, and A.-S. Duwez, "Electrografting of Polymers onto AFM Tips: A Novel Approach for Chemical Force Microscopy and Force Spectroscopy," *Chem. Phys. Chem.*, vol. 5, no. 1, pp. 147–149, 2004.
- [92] G. Lecayon, Y. Bouizem, C. Le Gressus, C. Reynaud, C. Boiziau, and C. Juret, "Grafting and growing mechanisms of polymerised organic films onto metallic surfaces," *Chem. Phys. Lett.*, vol. 91, pp. 506–510, Oct. 1982.
- [93] S. Leroy, C. Boiziau, J. Perreau, C. Reynaud, G. Zalczer, G. Lécayon, and C. Le Gressus, "Molecular structure of an electropolymerized polyacrylonitrile film and its pyrolyzed derivatives," *J. Mol. Struct.*, vol. 128, pp. 269–281, May 1985.

- [94] S. Baranton and D. Bélanger, "Electrochemical Derivatization of Carbon Surface by Reduction of in Situ Generated Diazonium Cations," *J. Phys. Chem. B*, vol. 109, pp. 24401–24410, Dec. 2005.
- [95] S. Cuenot, S. Gabriel, C. Jérôme, R. Jérôme, and A.-S. Duwez, "Are Electrografted Polymers Chemisorbed or Physisorbed onto their Substrate?," *Macromol. Chem. Phys.*, vol. 206, pp. 1216–1220, June 2005.
- [96] C. Combellas, F. Kanoufi, J. Pinson, and F. I. Podvorica, "Sterically Hindered Diazonium Salts for the Grafting of a Monolayer on Metals," *J. Am. Chem. Soc.*, vol. 130, pp. 8576–8577, July 2008.
- [97] E. Ahlberg, B. Helgee, and V. D. Parker, "The reaction of aryl radicals with metallic electrodes," *Acta Chem. Scand. B*, vol. 34, pp. 181–186, 1980.
- [98] D. Bélanger and J. Pinson, "Electrografting: A powerful method for surface modification," *Chem. Soc. Rev.*, vol. 40, no. 7, p. 3995, 2011.
- [99] J. Charlier, S. Ameer, J. P. Bourgoin, C. Bureau, and S. Palacin, "Mask-free Localized Grafting of Organic Polymers at the Micrometer or Submicrometer Scale on Composite Conductors or Semiconductor Substrates," *Adv. Funct. Mater.*, vol. 14, pp. 125–132, Feb. 2004.
- [100] C. Combellas, F. Kanoufi, and S. Nunige, "Surface Modification of Halogenated Polymers. 10. Redox Catalysis Induction of the Polymerization of Vinylic Monomers. Application to the Localized Graft Copolymerization of Poly(tetrafluoroethylene) Surfaces by Vinylic Monomers," *Chem. Mater.*, vol. 19, pp. 3830–3839, July 2007.
- [101] R. Pazo-Llorente, C. Bravo-Diaz, and E. Gonzalez-Romero, "pH Effects on Ethanolytic of Some Arenediazonium Ions: Evidence for Homolytic Dediazotiation Proceeding through Formation of Transient Diazo Ethers," *European J. Org. Chem.*, vol. 2004, no. 15, pp. 3221–3226, 2004.
- [102] P. Doppelt, G. Hallais, J. Pinson, F. Podvorica, and S. Verneyre, "Surface Modification of Conducting Substrates. Existence of Azo Bonds in the Structure of Organic Layers Obtained from Diazonium Salts," *Chem. Mater.*, vol. 19, pp. 4570–4575, Sept. 2007.
- [103] L. Lee, P. A. Brooksby, P. Hapiot, and A. J. Downard, "Electrografting of 4-Nitrobenzenediazonium Ion at Carbon Electrodes: Catalyzed and Uncatalyzed Reduction Processes," *Langmuir*, vol. 32, pp. 468–476, Jan. 2016.
- [104] A. Benedetto, M. Balog, P. Viel, F. Le Derf, M. Sallé, and S. Palacin, "Electroreduction of diazonium salts on gold: Why do we observe multi-peaks?," *Electrochim. Acta*, vol. 53, pp. 7117–7122, Oct. 2008.
- [105] K. K. Cline, L. Baxter, D. Lockwood, R. Saylor, and A. Stalzer, "Nonaqueous synthesis and reduction of diazonium ions (without isolation) to modify glassy carbon electrodes using mild electrografting conditions," *J. Electroanal. Chem.*, vol. 633, pp. 283–290, Aug. 2009.
- [106] C. Cannizzo, M. Wagner, J.-P. Jasmin, C. Vautrin-UI, D. Doizi, C. Lamouroux, and A. Chaussé, "Calix[6]arene mono-diazonium salt synthesis and covalent im-

- mobilization onto glassy carbon electrodes," *Tetrahedron Lett.*, vol. 55, pp. 4315–4318, July 2014.
- [107] L. M. Santos, J. Ghilane, C. Fave, P.-C. Lacaze, H. Randriamahazaka, L. M. Abrantes, and J.-C. Lacroix, "Electrografting Polyaniline on Carbon through the Electroreduction of Diazonium Salts and the Electrochemical Polymerization of Aniline," *J. Phys. Chem. C*, vol. 112, pp. 16103–16109, Oct. 2008.
- [108] A. C. Cruickshank, E. S. Q. Tan, P. A. Brooksby, and A. J. Downard, "Are redox probes a useful indicator of film stability? An electrochemical, AFM and XPS study of electrografted amine films on carbon," *Electrochem. Commun.*, vol. 9, pp. 1456–1462, July 2007.
- [109] T. Menanteau, E. Levillain, and T. Breton, "Electrografting via Diazonium Chemistry: From Multilayer to Monolayer Using Radical Scavenger," *Chem. Mater.*, vol. 25, pp. 2905–2909, July 2013.
- [110] S. Baranton and D. Bélanger, "In situ generation of diazonium cations in organic electrolyte for electrochemical modification of electrode surface," *Electrochim. Acta*, vol. 53, pp. 6961–6967, Oct. 2008.
- [111] A. Adenier, N. Barré, E. Cabet-Deliry, A. Chaussé, S. Griveau, F. Mercier, J. Pinson, and C. Vautrin-UI, "Study of the spontaneous formation of organic layers on carbon and metal surfaces from diazonium salts," *Surface Science*, vol. 600, pp. 4801–4812, Nov. 2006.
- [112] V. Mévellec, S. Roussel, L. Tessier, J. Chancolon, M. Mayne-L'Hermite, G. Deniau, P. Viel, and S. Palacin, "Grafting Polymers on Surfaces: A New Powerful and Versatile Diazonium Salt-Based One-Step Process in Aqueous Media," *Chem. Mater.*, vol. 19, pp. 6323–6330, Dec. 2007.
- [113] A. Mesnage, S. Esnouf, P. Jégou, G. Deniau, and S. Palacin, "Understanding the Redox-Induced Polymer Grafting Process: A Dual Surface-Solution Analysis," *Chem. Mater.*, vol. 22, pp. 6229–6239, Dec. 2010.
- [114] M. Ceccato, A. Bousquet, M. Hinge, S. U. Pedersen, and K. Daasbjerg, "Using a Mediating Effect in the Electroreduction of Aryldiazonium Salts To Prepare Conducting Organic Films of High Thickness," *Chem. Mater.*, vol. 23, pp. 1551–1557, Mar. 2011.
- [115] H. Randriamahazaka and J. Ghilane, "Electrografting and Controlled Surface Functionalization of Carbon Based Surfaces for Electroanalysis," *Electroanalysis*, vol. 28, no. 1, pp. 13–26, 2016.
- [116] X. Lefèvre, F. Moggia, O. Segut, Y.-P. Lin, Y. Ksari, G. Delafosse, K. Smaali, D. Guérin, V. Derycke, D. Vuillaume, S. Lenfant, L. Patrone, and B. Joussemme, "Influence of Molecular Organization on the Electrical Characteristics of π -Conjugated Self-Assembled Monolayers," *J. Phys. Chem. C*, vol. 119, pp. 5703–5713, Mar. 2015.
- [117] C. Celle, C. Suspène, J.-P. Simonato, S. Lenfant, M. Ternisien, and D. Vuillaume, "Self-assembled monolayers for electrode fabrication and efficient threshold voltage control of organic transistors with amorphous semiconductor layer," *Org. Electron.*, vol. 10, pp. 119–126, Feb. 2009.

REFERENCES

- [118] W. Jing Yang, K.-G. Neoh, E.-T. Kang, S. L.-M. Teo, and D. Rittschof, "Stainless steel surfaces with thiol -terminated hyperbranched polymers for functionalization via thiol -based chemistry," *Polym. Chem.*, vol. 4, no. 10, pp. 3105–3115, 2013.
- [119] K. L. Knoche, C. Hettige, P. D. Moberg, S. Amarasinghe, and J. Leddy, "Cyclic Voltammetric Diagnostics for Inert, Uniform Density Films," *J. Electrochem. Soc.*, vol. 160, pp. H285–H293, Jan. 2013.
- [120] V. Stockhausen, V. Q. Nguyen, P. Martin, and J. C. Lacroix, "Bottom-Up Electrochemical Fabrication of Conjugated Ultrathin Layers with Tailored Switchable Properties," *ACS Appl. Mater. Interfaces*, vol. 9, pp. 610–617, Jan. 2017.
- [121] F. Lebon, R. Cornut, V. Derycke, and B. Joussetme, "Fine growth control of electrografted homogeneous thin films on patterned gold electrodes," *Electrochim. Acta*, vol. 318, pp. 754–761, Sept. 2019.
- [122] H. W. Tan, J. An, C. K. Chua, and T. Tran, "Metallic Nanoparticle Inks for 3D Printing of Electronics," *Adv. Electron. Mater.*, vol. 5, no. 5, p. 1800831, 2019.
- [123] Y. Jo, J. Young Kim, S.-Y. Kim, Y.-H. Seo, K.-S. Jang, S. Yeon Lee, S. Jung, B.-H. Ryu, H.-S. Kim, J.-U. Park, Y. Choi, and S. Jeong, "3D-printable, highly conductive hybrid composites employing chemically-reinforced, complex dimensional fillers and thermoplastic triblock copolymers," *Nanoscale*, vol. 9, no. 16, pp. 5072–5084, 2017.
- [124] G. L. Allen, R. A. Bayles, W. W. Gile, and W. A. Jesser, "Small particle melting of pure metals," *Thin Solid Films*, vol. 144, pp. 297–308, Nov. 1986.
- [125] E. Roduner, "Size matters: Why nanomaterials are different," *Chem. Soc. Rev.*, vol. 35, no. 7, pp. 583–592, 2006.
- [126] T. Bakhishev and V. Subramanian, "Investigation of Gold Nanoparticle Inks for Low-Temperature Lead-Free Packaging Technology," *J. Electron. Mater.*, vol. 38, pp. 2720–2725, Dec. 2009.
- [127] H.-H. Lee, K.-S. Chou, and K.-C. Huang, "Inkjet printing of nanosized silver colloids," *Nanotechnology*, vol. 16, pp. 2436–2441, Sept. 2005.
- [128] C. Gaspar, S. Passoja, J. Olkkonen, and M. Smolander, "IR-sintering efficiency on inkjet-printed conductive structures on paper substrates," *Microelectron. Eng.*, vol. 149, pp. 135–140, Jan. 2016.
- [129] B. K. Park, D. Kim, S. Jeong, J. Moon, and J. S. Kim, "Direct writing of copper conductive patterns by ink-jet printing," *Thin Solid Films*, vol. 515, pp. 7706–7711, July 2007.
- [130] J. Ryu, H.-S. Kim, and H. T. Hahn, "Reactive Sintering of Copper Nanoparticles Using Intense Pulsed Light for Printed Electronics," *J. Electron. Mater.*, vol. 40, pp. 42–50, Jan. 2011.
- [131] J. S. Kang, J. Ryu, H. S. Kim, and H. T. Hahn, "Sintering of Inkjet-Printed Silver Nanoparticles at Room Temperature Using Intense Pulsed Light," *J. Electron. Mater.*, vol. 40, pp. 2268–2277, Nov. 2011.

- [132] D. J. Lee, S. H. Park, S. Jang, H. S. Kim, J. H. Oh, and Y. W. Song, "Pulsed light sintering characteristics of inkjet-printed nanosilver films on a polymer substrate," *J. Micromech. Microeng.*, vol. 21, p. 125023, Nov. 2011.
- [133] J. Niittynen, E. Sowade, H. Kang, R. R. Baumann, and M. Mäntysalo, "Comparison of laser and intense pulsed light sintering (IPL) for inkjet-printed copper nanoparticle layers," *Sci. Rep.*, vol. 5, p. 8832, Mar. 2015.
- [134] T. Yeshua, M. Layani, R. Dekhter, U. Huebner, S. Magdassi, and A. Lewis, "Micrometer to 15 nm Printing of Metallic Inks with Fountain Pen Nanolithography," *Small*, vol. 14, p. 1702324, Jan. 2018.
- [135] Y. Wu, Y. Li, B. S. Ong, P. Liu, S. Gardner, and B. Chiang, "High-Performance Organic Thin-Film Transistors with Solution-Printed Gold Contacts," *Adv. Mater.*, vol. 17, no. 2, pp. 184–187, 2005.
- [136] F. Basarir and T.-H. Yoon, "Preparation of gold patterns on polyimide coating via layer-by-layer deposition of gold nanoparticles," *J. Colloid Interface Sci.*, vol. 352, pp. 11–18, Dec. 2010.
- [137] A. Määttänen, P. Ihalainen, P. Pulkkinen, S. Wang, H. Tenhu, and J. Peltonen, "Inkjet-Printed Gold Electrodes on Paper: Characterization and Functionalization," *ACS Appl. Mater. Interfaces*, vol. 4, pp. 955–964, Feb. 2012.
- [138] W. Cui, W. Lu, Y. Zhang, G. Lin, T. Wei, and L. Jiang, "Gold nanoparticle ink suitable for electric-conductive pattern fabrication using in ink-jet printing technology," *Colloids Surf A Physicochem Eng Asp*, vol. 358, pp. 35–41, Apr. 2010.
- [139] M. Brust, J. Fink, D. Bethell, D. J. Schiffrin, and C. Kiely, "Synthesis and reactions of functionalised gold nanoparticles," *J. Chem. Soc., Chem. Commun.*, no. 16, p. 1655, 1995.
- [140] D. I. Gittins and F. Caruso, "Spontaneous Phase Transfer of Nanoparticulate Metals from Organic to Aqueous Media," *Angew. Chem. Int. Ed.*, vol. 40, no. 16, pp. 3001–3004, 2001.
- [141] Y. Q. He, S. P. Liu, L. Kong, and Z. F. Liu, "A study on the sizes and concentrations of gold nanoparticles by spectra of absorption, resonance Rayleigh scattering and resonance non-linear scattering," *Spectrochim. Acta A Mol. Biomol. Spectrosc.*, vol. 61, pp. 2861–2866, Oct. 2005.
- [142] "Dimethylamminopyridine chemical properties." <http://www.chemspider.com/Chemical-Structure.13646.html>.
- [143] W.-J. Joo, T.-L. Choi, J. Lee, S. K. Lee, M.-S. Jung, N. Kim, and J. M. Kim, "Metal Filament Growth in Electrically Conductive Polymers for Nonvolatile Memory Application," *J. Phys. Chem. B*, vol. 110, pp. 23812–23816, Nov. 2006.
- [144] S. Gao, C. Song, C. Chen, F. Zeng, and F. Pan, "Dynamic Processes of Resistive Switching in Metallic Filament-Based Organic Memory Devices," *J. Phys. Chem. C*, vol. 116, pp. 17955–17959, Aug. 2012.
- [145] C. Sire, S. Blonkowski, M. J. Gordon, and T. Baron, "Statistics of electrical breakdown field in HfO₂ and SiO₂ films from millimeter to nanometer length scales," *Appl. Phys. Lett.*, vol. 91, p. 242905, Dec. 2007.

- [146] Y.-Y. Noh and H. Sirringhaus, "Ultra-thin polymer gate dielectrics for top-gate polymer field-effect transistors," *Org. Electron.*, vol. 10, pp. 174–180, Feb. 2009.
- [147] P. Fontaine, D. Goguenheim, D. Deresmes, D. Vuillaume, M. Garet, and F. Rondelez, "Octadecyltrichlorosilane monolayers as ultrathin gate insulating films in metal-insulator-semiconductor devices," *Appl. Phys. Lett.*, vol. 62, pp. 2256–2258, May 1993.
- [148] H. Klauk, M. Halik, U. Zschieschang, G. Schmid, W. Radlik, and W. Weber, "High-mobility polymer gate dielectric pentacene thin film transistors," *J. Appl. Phys.*, vol. 92, pp. 5259–5263, Nov. 2002.
- [149] M. Halik, H. Klauk, U. Zschieschang, G. Schmid, C. Dehm, M. Schütz, S. Maisch, F. Effenberger, M. Brunnbauer, and F. Stellacci, "Low-voltage organic transistors with an amorphous molecular gate dielectric," *Nature*, vol. 431, p. 963, Oct. 2004.
- [150] D. Lembke, S. Bertolazzi, and A. Kis, "Single-Layer MoS₂ Electronics," *Acc. Chem. Res.*, vol. 48, pp. 100–110, Jan. 2015.
- [151] J. Appenzeller, J. Knoch, V. Derycke, R. Martel, S. Wind, and P. Avouris, "Field-Modulated Carrier Transport in Carbon Nanotube Transistors," *Phys. Rev. Lett.*, vol. 89, p. 126801, Aug. 2002.
- [152] S. Das, H.-Y. Chen, A. V. Penumatcha, and J. Appenzeller, "High Performance Multilayer MoS₂ Transistors with Scandium Contacts," *Nano Lett.*, vol. 13, pp. 100–105, Jan. 2013.
- [153] S. Sze and K. N. Kwok, *Physics of Semiconductor Devices*. Wiley-Interscience, 2006.
- [154] D. M. Sim, M. Kim, S. Yim, M.-J. Choi, J. Choi, S. Yoo, and Y. S. Jung, "Controlled Doping of Vacancy-Containing Few-Layer MoS₂ via Highly Stable Thiol-Based Molecular Chemisorption," *ACS Nano*, vol. 9, pp. 12115–12123, Dec. 2015.
- [155] Z. Yu, Y. Pan, Y. Shen, Z. Wang, Z.-Y. Ong, T. Xu, R. Xin, L. Pan, B. Wang, L. Sun, J. Wang, G. Zhang, Y. W. Zhang, Y. Shi, and X. Wang, "Towards intrinsic charge transport in monolayer molybdenum disulfide by defect and interface engineering," *Nat. Commun.*, vol. 5, p. 5290, Dec. 2014.
- [156] A. Facchetti, M.-H. Yoon, and T. J. Marks, "Gate Dielectrics for Organic Field-Effect Transistors: New Opportunities for Organic Electronics," *Adv. Mater.*, vol. 17, no. 14, pp. 1705–1725, 2005.
- [157] H.-S. Kim, S. M. Won, Y.-G. Ha, J.-H. Ahn, A. Facchetti, T. J. Marks, and J. A. Rogers, "Self-assembled nanodielectrics and silicon nanomembranes for low voltage, flexible transistors, and logic gates on plastic substrates," *Appl. Phys. Lett.*, vol. 95, p. 183504, Nov. 2009.
- [158] J. E. McDermott, M. McDowell, I. G. Hill, J. Hwang, A. Kahn, S. L. Bernasek, and J. Schwartz, "Organophosphonate Self-Assembled Monolayers for Gate Dielectric Surface Modification of Pentacene-Based Organic Thin-Film Transistors: A Comparative Study[†]," *J. Phys. Chem. A*, vol. 111, pp. 12333–12338, Dec. 2007.

Notations

ACN	Acetonitrile
AFM	Atomic Force Microscopy
C-AFM	Conductive AFM
CA	Chronoamperometry
CV	Cyclic Voltammetry
DLS	Dynamic Light Scattering
DMAP	4-Dimethylaminopyridine
DzF8	4-heptadecafluorobenzene diazonium
ECG	Electrografting or Electrografted
FET	Field Effect Transistor
FPL	Fountain Pen Lithography
IR	Infrared
LICSEN	Laboratoire d'Innovation en Chimie des Surfaces Et Nanoscience
LSV	Linear Sweep Voltammetry
NIMBE	Nanosciences et Innovation pour les Matériaux, la Biomédecine et l'Énergie
OCP	Open Circuit Voltage
OFET	Organic Field Effect Transistor
PVD	Physical Vapor Deposition
SEM	Scanning Electron Microscope
TBAPF₆	Tetrabutylammonium hexafluorophosphate
TBPFe	Tris-bipyridine iron (II) diazonium derivative
TOAB	Tetraoctylammonium bromide
Thio	4-thiophenol diazonium
XPS	X-Ray photoelectron spectroscopy

Résumé

Le travail de cette thèse s'inscrit dans le domaine de l'électronique organique. Il vise à proposer une alternative aux différentes couches organiques utilisées dans ce domaine, notamment les couches minces déposées par évaporation ou spin-coating, d'épaisseur supérieure à 100 nm en général, ou les monocouches moléculaires auto-assemblées (SAMs), d'épaisseur inférieure à 5 nm. La technique utilisée ici est le greffage électrochimique de sels de diazonium, qui permet de former des couches d'épaisseur comprise entre 5 et 100 nm. Ce résumé présentera succinctement les différentes avancées faites sur l'électrogreffage de trois différentes molécules sur des électrodes patternées, ainsi que leur utilisation dans des dispositifs électroniques micro-métriques basés sur des jonctions verticales métal-molécules-métal. Un transistor à effet de champ utilisant ces couches électrogreffées comme diélectrique de grille sera notamment étudié.

Électrogreffage de sels de diazonium sur électrodes patternées

Présentation des sels de diazonium

Durant cette thèse, trois sels de diazonium sont utilisés : un dérivé de la tris-bipyridine fer (II) (**TBPFe**), le 4-heptadecafluorobenzène diazonium (**DzF8**) et le 4-thiophenol diazonium (**Thio**) (figure R.1). Ces molécules ont été choisies pour les différentes propriétés qu'elles apporteraient une fois électrogreffées : les couches électrogreffées de **TBPFe** ont des propriétés memristives, comme montré dans le travail de Lin et al. [4] et les couches électrogreffées de **DzF8** peuvent être utilisées comme diélectrique de grille dans des transistors, comme montré dans le travail de Casademont et al. [3]. Les couches électrogreffées de **Thio** ont une surface présentant des fonctions thiol, qui pourraient être utilisées notamment pour fixer l'or déposé par-dessus et éviter sa diffusion dans la couche.

L'électrogreffage consiste à réduire les fonctions diazonium afin de former des radicaux qui réagiront avec l'électrode de travail dans une cellule électrochimique. L'électrogreffage du **TBPFe** et du **DzF8** par voltamétrie cyclique (CV) sont présentés figure R.2. Dans le cas du **DzF8**, deux pics de réduction irréversibles à 0 V et -0.6 V vs Ag/Ag⁺ lors du premier cycle sont présents, signes de la réduction de la fonction diazonium. Durant les cycles suivants, ces pics de réduction ont disparus et le courant diminue, signe qu'il y a formation d'une couche isolante sur l'électrode de travail. Le sel de diazonium **Thio** montre un comportement similaire.

L'électrogreffage du **TBPFe** montre un comportement différent. Lors de la voltamétrie cyclique, plusieurs pics réversibles sont présents : un couple à +0.9 V correspondant

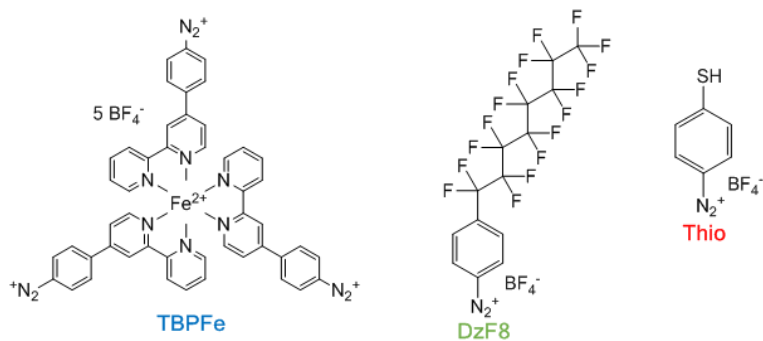


Figure R.1: Structures chimiques des sels de diazonium du complexe de tris-bipyridine fer (II) (**TBPFe**), de 4-heptadecafluorobenzenearyldiazonium (**DzF8**) et de 4-thiophenaryldiazonium (**Thio**).

au couple Fe(II)/Fe(III) et deux couples entre -1.5 et -2 V correspondant à l'oxydoréduction successive des différents ligands. Le pic de réduction à -1 V et le pic d'oxydation à +0.7 V forment un couple avec une large surtension, et peuvent être attribué à l'oxydoréduction des différentes liaisons azo formées dans la couche électrogreffée. Durant l'électro-greffage du **TBPFe**, les intensités de tous ces pics augmentent, ce qui est un signe de la croissance d'une couche électroactive sur l'électrode de travail. L'analyse par spectroscopie de photoélectrons induits par rayon X (XPS) et par spectroscopie infrarouge (IR) des différentes électrode de travail électrogreffées confirme la présence d'une couche électrogreffée par ces sels de diazonium.

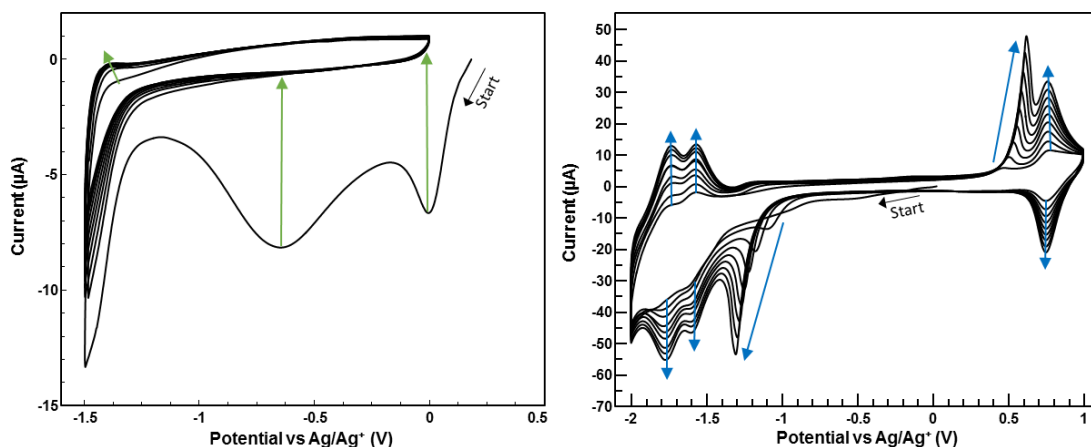


Figure R.2: CV (10 cycles) à 50 mV/s d'une solution à 1 mM **DzF8** (gauche) ou 28 μM **TBPFe** (droite) dans 0.1M TBAPF₆ dans ACN sur une électrode d'or.

Contrôle de l'épaisseur de la couche électrogreffée

L'électrogreffage de ces sels de diazonium est ensuite mené sur des électrodes micrométriques patternées fabriquées par évaporation de métal sous vide à travers un masque de lithographie optique ou électronique. Afin de contrôler finement l'épaisseur de la couche électrogreffée sur ces électrodes, l'électrogreffage est réalisé en utilisant un procédé différent de la voltamétrie cyclique : une première étape de voltamétrie à balayage linéaire (LSV) est suivie d'une étape de chronoampérométrie au potentiel de greffage voulu (CA), pour terminer par une étape de LSV qui se termine à 0

V. L'influence des différents paramètres (potentiel appliqué pendant la phase de CA, temps de cette phase, concentration en sel de diazonium de la solution) sur l'épaisseur finale de la couche électrogreffée est étudiée.

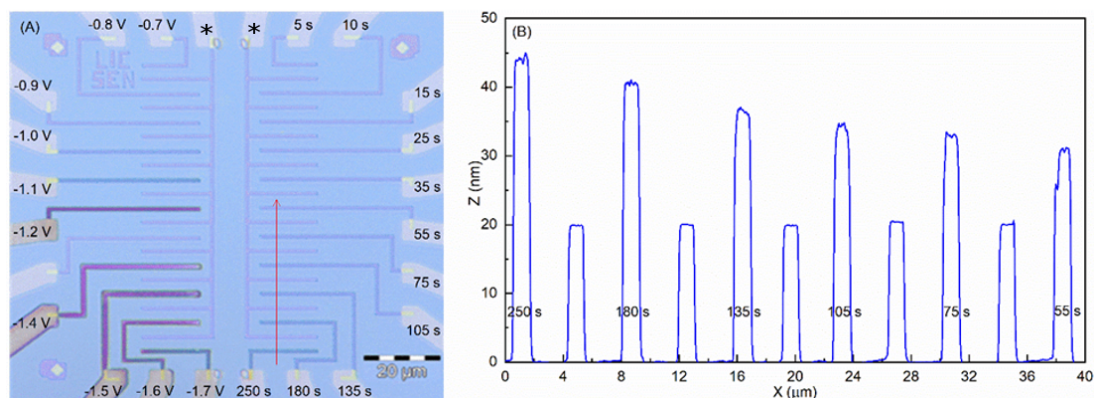


Figure R.3: Image de microscopie optique (gauche) et profil AFM (droite) selon la flèche rouge d'un échantillon électrogreffé avec du **TBPF₆** en utilisant différents potentiels pour la partie gauche et différents temps pour la partie droite. Les électrodes non greffées sont marquées d'une astérisque.

Un exemple d'une étude sur le contrôle de l'épaisseur de la couche de **TBPF₆** greffée est montré figure R.3. Sur cet échantillon, l'influence du potentiel et du temps sont étudiées, et chaque électrode est électrogreffée individuellement dans des conditions différentes. L'épaisseur finale de la couche électrogreffée est mesurée en comparant l'épaisseur des électrodes greffées avec des électrodes non greffées, comme illustré dans le profil de la figure R.3.

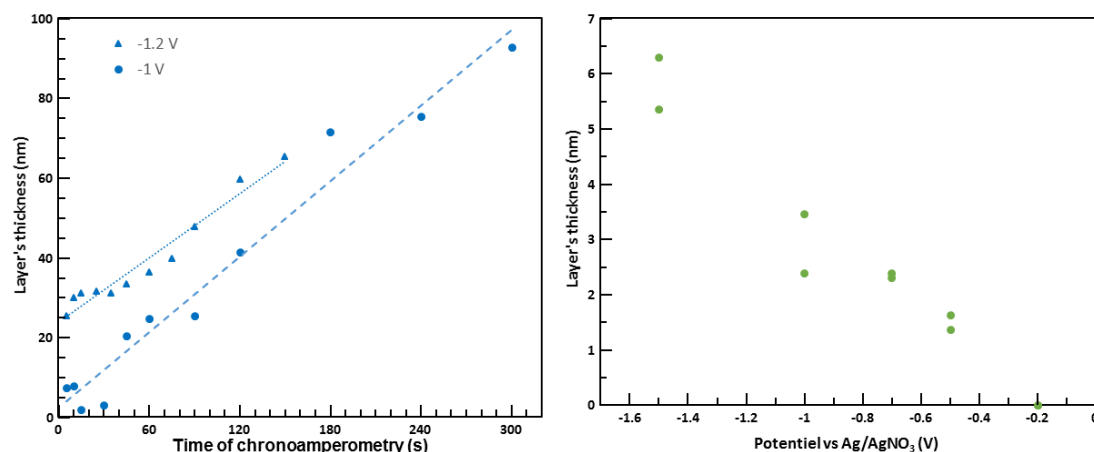


Figure R.4: Épaisseur finale d'une couche électrogreffée dans une solution à 28 μM **TBPF₆** en fonction du temps de la chronoampérométrie pour un potentiel appliqué de -1 ou -1.2 V vs Ag/AgNO₃ (gauche); épaisseur finale d'une couche électrogreffée dans une solution à 1 mM **DzF₈** en fonction du potentiel appliqué pendant une chronoampérométrie de 60 s (droite). L'électrolyte utilisé est une solution à 0.1 M de TBAPF₆ dans l'acétonitrile.

Pour le contrôle de l'épaisseur greffée de **TBPF₆**, les trois paramètres étudiés sont importants. En effet, l'épaisseur finale greffée de **TBPF₆** augmente avec la concentration, jusqu'à atteindre un plateau; celle-ci atteint un maximum pour un potentiel appliqué de

-1.5 V vs Ag/Ag⁺; enfin, elle a un comportement affine en fonction du temps de la CA, comme illustré sur la figure R.4. Une couche organique d'épaisseur comprise entre 5 et 100 nm de **TBPFe** peut donc être obtenue de façon précise en jouant sur la durée du procédé.

Les couches électrogreffées de **DzF8** et **Thio** sont quant à elles uniquement contrôlées par le potentiel appliqué durant l'étape de CA. Des épaisseurs comprises entre 2 et 6 nm peuvent ainsi être obtenues de façon reproductible.

Électrogreffage de doubles couches

Une façon innovante de former des couches organiques composées de différentes molécules est ensuite étudiée : l'électrogreffage de doubles couches. Ceci consiste à utiliser une électrode déjà électrogreffée, de préférence par une molécule électroactive, comme électrode de travail dans une solution contenant un deuxième sel de diazonium à électrogreffer. Le procédé est illustré figure R.5. Durant cette thèse, des électrodes greffées par différentes épaisseurs de **TBPFe** sont greffées avec des molécules de **DzF8** ou de **Thio**, afin d'obtenir les propriétés de surface de ces deux molécules sur une couche organique d'épaisseur contrôlée supérieure à 5 nm.

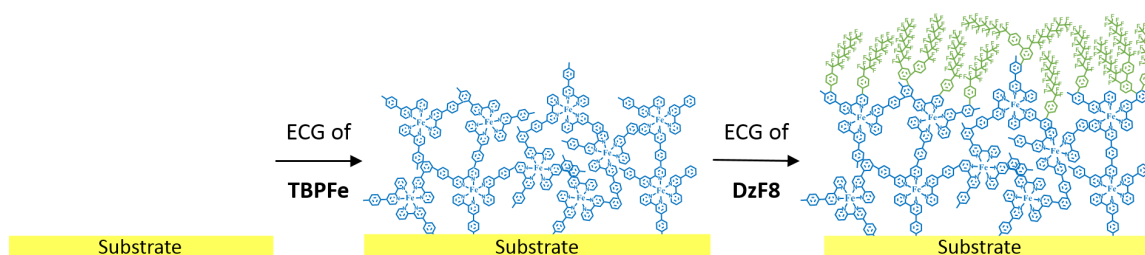


Figure R.5: Schéma de l'électrogreffage de double couches.

L'électrogreffage par voltamétrie cyclique du **DzF8** ou du **Thio** sur une électrode fonctionnalisée par du **TBPFe** montre une passivation de celle-ci. Afin d'illustrer ceci, les CV d'une électrode greffées par du **TBPFe** avant et après passivation avec le **DzF8** sont présentées figure R.6 gauche. On observe une très forte diminution des pics d'oxydoréduction liés au **TBPFe**, ce qui montre bien l'effet passivant de la couche de **DzF8**. Ceci est confirmé par des mesures électrochimiques utilisant une sonde électrochimique, le ferrocène, et les électrodes greffées comme électrodes de travail. Les résultats de cette étude (figure R.6 droite) montrent que la double couche de **TBPFe+DzF8** semble plus passivante que la double couche de **TBPFe+Thio**, et que ces deux doubles couches sont effectivement plus passivantes que la couche de **TBPFe**.

Des mesures d'XPS et d'IR ont été réalisées sur les doubles couches électrogreffées, et confirment leur formation. Ces doubles couches ont ensuite été greffées sur des électrodes patternées, et une étude comparative de l'épaisseur finale de ces couches avant et après greffage de la seconde épaisseur ont montré une augmentation de l'épaisseur totale de la couche entre 7 et 8 nm. Conformément aux objectifs, cette partie de l'étude permet donc la réalisation de double couches organiques fines et robustes dont l'épaisseur et la fonction chimique de surface sont ajustables.

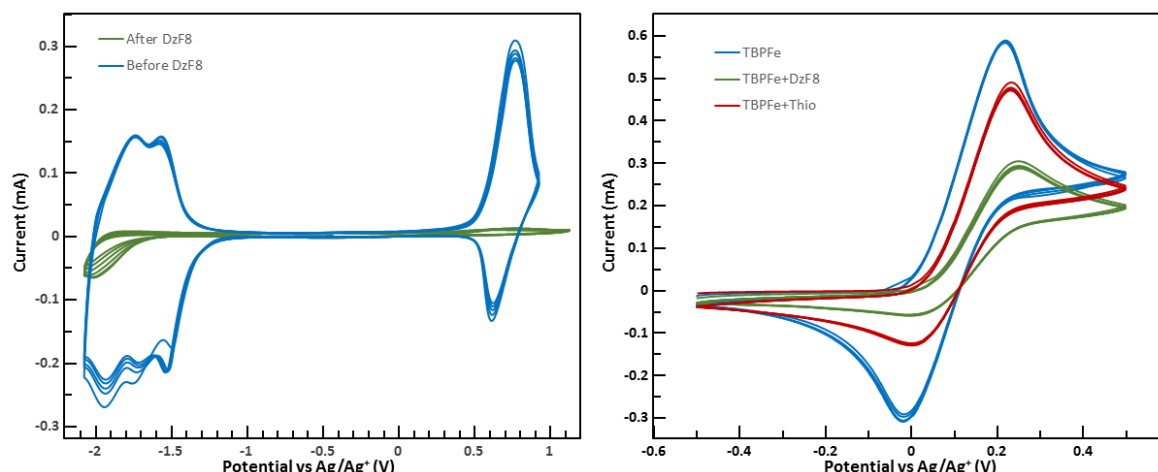


Figure R.6: CV (10 cycles) à 50 mV/s d'une solution à 0.1 M TBAPF₆ dans ACN avec une électrode greffée par du **TBPFe** avant (bleu) et après électrogreffage de **DzF8** (vert) comme électrode de travail (gauche); CV (5 cycles) d'une solution à 10 mM en ferrocène et 0.1 M TBAPF₆ d'une électrode d'or électrogreffée par du **TBPFe** uniquement (bleu), par une double couche de **TBPFe+DzF8** (vert) ou par une double couche de **TBPFe+Thio** (rouge).

Impression de nanoparticules d'or pour la formation d'une électrode supérieure

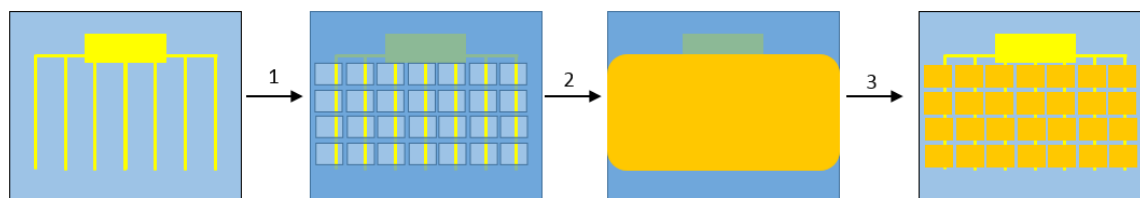


Figure R.7: Schéma de l'impression d'une solution aqueuse de nanoparticules d'or à travers un masque de photolithographie. (1) Ouverture de motifs par lithographie au-dessus de l'échantillon. (2) Impression des nanoparticules. (3) Retrait du masque de lithographie (Lift-off).

Afin de mesurer les propriétés électriques des différentes couches électrogreffées, des mesures électriques de celles-ci intégrées dans des jonctions verticales métal-molécules-métal doivent être menées. La réalisation de contacts supérieurs sur des couches organiques fines n'entraînant pas de dégradation de celle-ci est un défi important du domaine. En premier lieu, la possibilité de réaliser les électrodes supérieures de telles jonctions par impression jet d'encre d'une solution aqueuse de nanoparticules d'or est évalué, selon un procédé développé durant cette thèse. Celui-ci consiste à imprimer cette solution sur des masques de photolithographie afin d'avoir accès à une meilleure résolution de motifs que ce qu'une impression classique peut donner. Le procédé est illustré figure R.7.

Après optimisation du processus d'impression des nanoparticules, une conductivité de l'électrode imprimée de $3 \cdot 10^{-2} \Omega / \square$ est mesurée. Ces électrodes optimisées sont ensuite imprimées sur une électrode électrogreffée par du **TBPFe** selon le procédé

décrit précédemment. Un exemple d'un dispositif final est montré figure R.8 gauche. Des mesures électriques sont menées sur ces dispositifs, et montrent la présence d'un comportement memristif, comme présenté sur la figure R.8 droite. Cependant, après vérification, ce comportement est lié aux électrodes d'or imprimées et n'est pas intrinsèque au film de **TBPFE**.

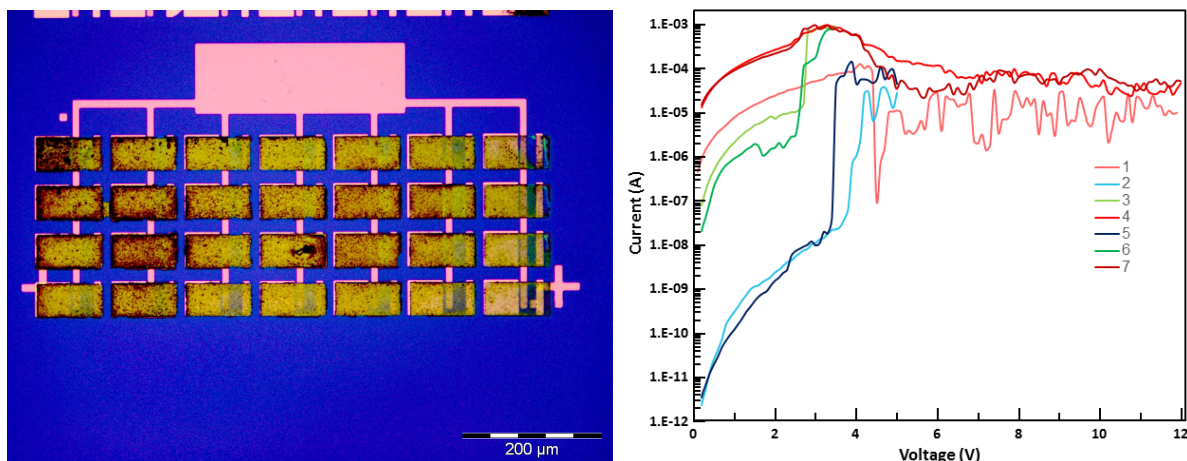


Figure R.8: Image de microscopie optique d'une électrode d'or imprimée composée de 4 couches sur une électrode électrogréffée (gauche); $I(V)$ d'une jonction or évaporé-or imprimé (droite). Le nombre indiqué correspond au numéro de la mesure. Les courbes bleues s'arrêtent à 5 V, les vertes à 3.5 V et les rouges à 12 V.

Des électrodes d'or imprimées sont ainsi réalisées avec succès à travers un masque de lithographie, et permettent donc d'avoir accès à une résolution supérieure à ce qu'une imprimante jet d'encre peut proposer. Cependant, le domaine d'utilisation de ces électrodes dans le cadre de mesures électriques est trop limité, entre 0 et +2 V, et des études supplémentaires afin d'optimiser le procédé pourraient être menées.

Dispositifs électroniques à base de couches électrogréffées

Jonctions verticales métal-molécules-métal

Afin d'évaluer le potentiel des couches électrogréffées, des jonctions verticales métal-molécules-métal sont réalisées en utilisant l'évaporation de métaux sous vide pour la formation des électrodes supérieures. Après avoir déterminé que l'utilisation de titane comme couche d'accroche sur les couches électrogréffées est nécessaire, des mesures électriques de ces jonctions, de surface $400 \mu\text{m}^2$, sont menées. Des résultats de ces études sont montrés figure R.9.

Les différentes mesures ont permis de déterminer les caractéristiques des couches électrogréffées :

- Le pourcentage de jonctions en court-circuit est le plus bas pour les doubles couches de **TBPFe+DzF8** de 10 nm (4%) et le plus haut pour les simples couches de **Thio** de 2.7 nm (60%), avec des résultats intermédiaires entre 10 et 20% pour les autres types de couches.
- Le courant mesuré à +1 V dépend de la nature de la couche électrogréffée. Les doubles couches de **TBPFe+DzF8** de 10 nm sont notamment les plus isolantes.

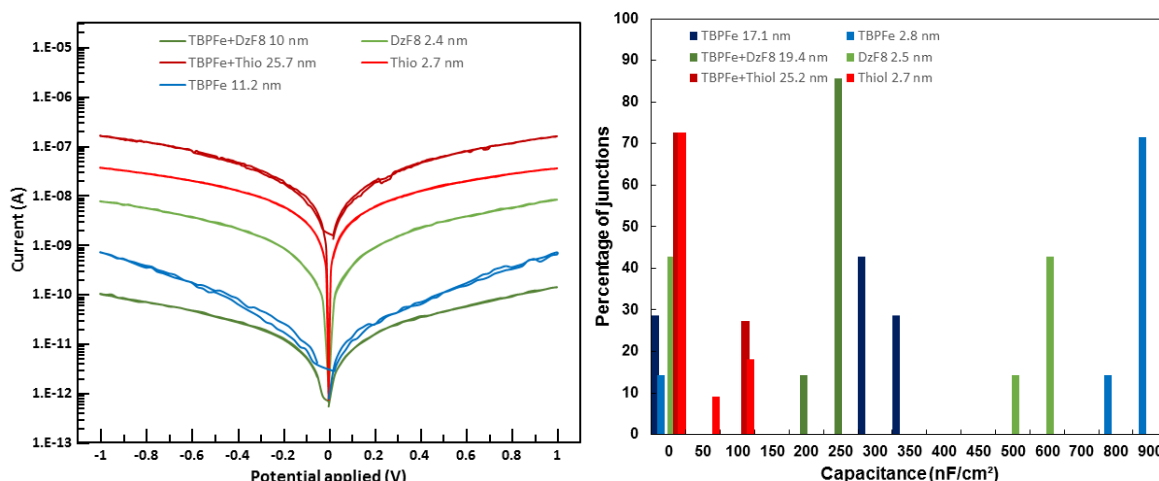


Figure R.9: $I(V)$ caractéristiques pour des jonctions verticales Au-couche ECG-TiAu pour une couche ECG de 5 nm **TBPFfe**, de 18 nm **TBPFfe**, de 3 nm **DzF8**, de 10 nm **TBPFfe+DzF8**, de 2.7 nm **Thio** et de 23.7 **TBPFfe+Thio** (gauche). Statistiques sur la capacitance mesurée d'une couche de 17 nm **TBPFfe**, de 2.8 nm **TBPFfe**, de 19.4 nm **TBPFfe+DzF8**, de 2.5 nm **DzF8**, de 25.2 nm **TBPFfe+Thio** et de 2.7 nm **Thio**. (droite).

- Les doubles couches sont plus isolantes et ont moins de court-circuits que leurs équivalents simple couche.
- La tension de claquage des couches dépend essentiellement de leur épaisseur et non de leur nature. Celles-ci sont compétitives vis-à-vis de la littérature (2.6 à 8 MV/cm).
- Les meilleures capacitances mesurées sont celles de la simple couche de **TBPFfe** de 2.8 nm, avec des valeurs comprises entre 800 et 900 nF/cm². Ces valeurs élevées sont proches de ce que d'autres stratégies plus complexes de couches minces organiques et hybrides organiques/inorganiques proposent dans la littérature.

Les couches électrogréffées ont donc des propriétés intéressantes pour l'électronique, et montrent un degré d'ajustement de leurs propriétés via leur épaisseur ou leur nature.

Couches électrogréffées comme diélectrique de grille pour des transistors

Les mesures précédentes ont montré que la méthode développée peut produire des films organiques minces, isolants et de forte capacitance. Ils présentent donc les qualités requises pour être utilisés en tant que diélectriques de grille dans les transistors. Nous avons ainsi étudié l'intégration des couches ECG en tant que diélectriques de grilles de FETs en utilisant comme canal semiconducteur des domaines de MoS₂ monocouche produits par CVD au laboratoire. Un exemple de transistor utilisant une couche de 28 nm de **TBPFfe+Thio** est présenté figure R.10. Les propriétés résultantes du meilleur transistor étudié sont les suivantes :

- Le courant source-drain est supérieur d'un facteur $4 \cdot 10^6$ au courant source-grille, signe d'une couche organique particulièrement isolante.

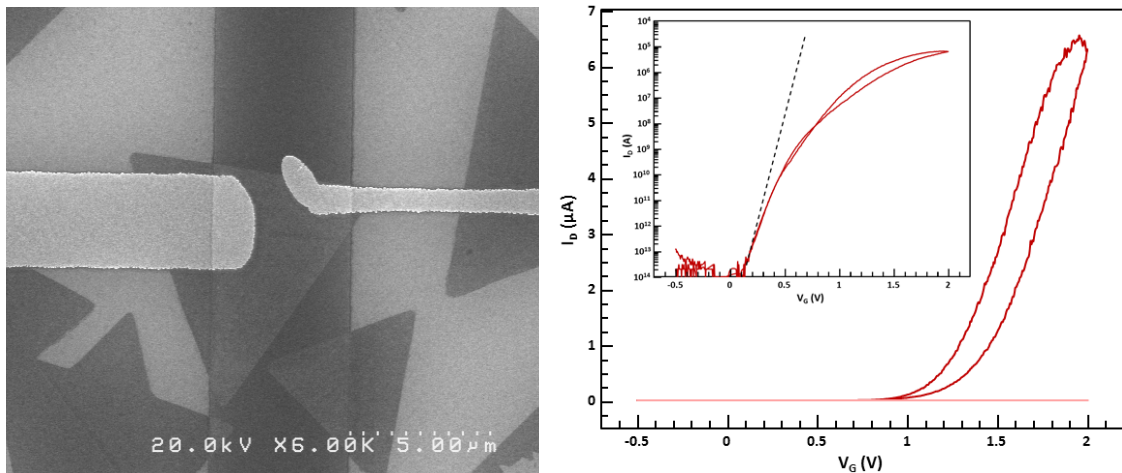


Figure R.10: Image MEB d'un cristal monocouche de MoS₂ utilisé comme canal dans un transistor avec une couche de 28 nm de **TBPFé+Thio** comme diélectrique de grille (gauche). Caractéristiques de transfert I_D(V_G) (rouge sombre) et I_G(V_G) à V_D = 1 V du transistor. La ligne en pointillée correspond à une pente de 60mV/decade ajoutée pour comparaison(droite).

- Le dispositif commute totalement avec une différence de tension de grille de seulement 2 V à V_D = 1 V. Ces couches permettent donc un fonctionnement à base tension.
- Le rapport I_{ON}/I_{OFF} est très élevé : 8.0.10⁷.
- La pente sous le seuil est de 78 mV/decade (dans sa partie la plus raide), qui est extrêmement proche du minimum théorique de 60 mV/decade à température ambiante.
- Les courbes I_D(V_D)aturent à bas potentiel, signe d'un bon contrôle de la grille sur le matériau de canal.
- La mobilité des porteurs de charge est estimée entre 11 et 45 cm².(V.s)⁻¹ pour tous les dispositifs utilisant un diélectrique de **TBPFé+Thio**, ce qui est une valeur élevée pour un canal de MoS₂.
- Seuls 2 dispositifs sur 18 fabriqués de cette façon présentent un court-circuit entre la grille et le drain ce qui valide le protocole de contact direct sur les couches ECG en configuration de dispositifs.

Des mesures similaires ont été menées sur huit transistors utilisant le même matériau de canal mais avec deux autres types de diélectrique de grille : une simple couche de **TBPFé** de 30 nm et une double couche de **TBPFé+DzF8** de 32 nm. Même si ces dispositifs sont moins performants que celui présenté ci-dessus, ils présentent des mobilités de porteurs de charge comprises entre 0.7 et 23.1 cm².(V.s)⁻¹. Les couches électrographées présentées durant cette thèse ont donc pu être utilisées avec succès en tant que diélectrique de grille dans des transistors.

Conclusion

Dans cette thèse, le potentiel des couches électrogreffées pour l'électronique a pu être déterminé. Tout d'abord, un contrôle fin de l'épaisseur de ces couches sur des électrodes patternées fabriquées par lithographie et évaporation de métal sous vide a été prouvé. Ensuite, une méthode d'électrogreffage séquentiel de double couches permettant de régler séparément l'épaisseur et les fonctions chimiques de surface a été démontrée. Ces couches ont ensuite été utilisées dans des jonctions verticales métal-molécules-métal avec succès, et leurs propriétés électriques ont pu être sondées. Enfin, des transistors à base de MoS₂ monocouche les utilisant en tant que diélectriques de grille ont été fabriqués, et présentent des performances témoignant d'une grande qualité du diélectrique de grille.

Les couches organiques électrogreffées sont donc une alternative prometteuse aux différentes méthodes actuelles à base d'organique pour l'électronique. En plus de la variété des molécules utilisables avec cette méthode, l'électrogreffage permet d'accéder à de nouvelles épaisseurs de couches organiques robustes avec un contrôle fin, ainsi qu'à la formation de doubles couches aux fonctions chimiques de surface modulable. Ces avantages procurent une grande capacité d'ajustement des propriétés électroniques des couches formées. De même, la possibilité de greffer sélectivement sur différentes électrodes de la même puce permet d'obtenir différentes fonctions sur un même support avec un procédé de fabrication versatile.

Supplementary information



Fine growth control of electrografted homogeneous thin films on patterned gold electrodes

F. Lebon, R. Cornut, V. Derycke, B. Joussetme*

LICSEN, NIMBE, CEA, CNRS, Université Paris-Saclay, CEA Saclay, 91191, Gif-sur-Yvette, Cedex, France



ARTICLE INFO

Article history:

Received 28 January 2019

Received in revised form

13 June 2019

Accepted 18 June 2019

Available online 20 June 2019

Keywords:

Electrochemical grafting

Patterned electrodes

Control thickness

ABSTRACT

Electrochemical grafting of two different diazonium salts was performed on patterned gold electrodes of micrometric size. One of the molecules, a tris-bipyridine iron (II) derivative (**TBPFe**) enables a fine control over the final thickness of the electrografted layer thanks to its redox centers that acts as intermediate for charge transfers between the solution and the working electrode. The other one, an aromatic cycle with a fluorinated carbon chain (**DzF8**), forms an insulating layer that stops the charge transfer from the working electrode to the solution and thus limits the thickness of the resulting organic layer. Grafting parameters (concentration, time, tip passivation, etc.) were investigated in details. Their precise control leads to compact and homogeneous thin films. Smooth **TBPFe** layers with an adjustable thickness in the 5–100 nm range are obtained, while the thickness is limited to 2–6 nm in the **DzF8** case. With the achieved film quality, direct metal evaporation on top of these electrodes is possible and yields 85% of working devices. Electrical measurements for the two molecules are compared for different thicknesses.

© 2019 Elsevier Ltd. All rights reserved.

1. Introduction

While Self-Assembled Monolayers (SAMs) were proposed as a potential alternative to inorganic materials for electronics [1], important improvements are needed before industrial uses can be considered. First, even though the monolayers' fabrication is well controlled, their integration in metal-SAM-metal type of electronic devices is still a challenge since direct metal evaporation usually leads to current leakage (except in some rare and specific cases) [2,3]. Some methods give interesting results but are not suitable for high density integration, such as on-edge molecular junctions [4], while others can lead to high density chips but can hardly be used in an industrial process, such as lift-and-float approaches [5,6] or nanotransfer printing techniques [7]. Electrochemical grafting (ECG) of diazonium salts leads to thin films with the deposition of multilayers of molecules. The layers are thicker than SAMs and allow potentially the use of more classic top electrodes fabrication techniques, such as metal evaporation. Moreover the electrical behavior of the thin film issue from the cumulative effect of all the molecules in the layer allows to avoid long statistical measurements. Macroscopic metal-molecules-metal junctions (with a

surface in the 400 μm^2 range) made using electrografting have already been studied [8,9]. While our recent contributions showed interesting results on using electrografted layers as thin gate dielectrics in transistors [10] or as the active part of memristive devices [11], a better control over the formation of the electrografted layers is needed to optimize the performances and develop new functionalities.

ECG also brings other interesting advantages. Firstly, many different types of molecules can be electrografted, since only one specific electroactive function on the molecules is needed, such as a diazonium function [12]. All the compounds have different properties, and can be grafted on many different conductors or semiconductors, such as copper, cobalt, iron [13], gold [14], silicon [15] or even on some insulators like PTFE [16]. Moreover, the strong covalently bonded organic thin films ($D_{\text{C-Au}} \approx 262$ kJ/mol, comparable to $D_{\text{S-Au}} = 254$ kJ/mol typical for SAMs on gold) [17] allow their compatibility with the techniques for fabricating microelectronic devices. ECG can also be used to graft selectively different electrodes on the same chip, by using different conditions or different molecules for example.

Most ECG studies focused on the electrochemical properties of the reaction [12,18]. Few studies showed that the layer thickness of a diazonium grafted layer can be controlled [19–21]. While these studies show that different thickness of layers can be grafted, the control of that aspect was not detailed and the substrates that were

* Corresponding author.

E-mail address: bruno.joussetme@cea.fr (B. Joussetme).

used were bulky electrodes. None of them have studied in details the influence of the different parameters on the ECG for different molecules and on patterned electrodes of micrometer size.

The main objectives of this study is to demonstrate the level of control that ECG can achieve in terms of thickness adjustment and compacity for organic layers with different structures and to show that such compact thin films can be used in vertical metal-molecules-metal junctions. To achieve this, two different molecules were electrografted (Fig. 1): the tris-bipyridine iron(II) diazonium derivate (**TBPFe**), which is redox-active, and the 4-heptadecafluorobenzene diazonium salt (**DzF8**), which forms insulating layers. The important parameters for the control of the final thickness of ECG films of these molecules are determined and studied, and the differences between ECG of the two molecules is discussed. Finally, vertical metal-molecules-metal junctions incorporating both types of electrografted layers are made, in order to prove the compacity of the layers as well as their potential for future applications in electronics.

2. Materials and methods

2.1. Fabrication of the patterned gold electrodes

The patterned gold electrodes were made using optical and e-beam lithography. A wafer of oxidized Si(100) (150 nm SiO₂) (Siltronix) was thoroughly washed in an ultrasonic bath using successively water and Decon, acetone and ethanol. It was then cleaned in an oxygen plasma using reactive-ion etching (Plassys MG200 used at 130 V and 50 μbar of O₂ for 20 s). For optical lithography of the bottom electrodes, Microposit S1805 G2 was spin-coated on a wafer (60 s at 4000 rpm) and dried at 115 °C for 60 s. It was then exposed through a mask to a 405 nm UV light using an MJB3 Karl Suss Photomask Aligner. The sample was then developed during 40 s in a solution of Microposit MF-319 and thoroughly rinsed with water. A final step of RIE was performed using the same conditions as previously.

The electrodes used to study the impact of the width of the electrodes on the resulting thickness of the grafted layers were made by e-beam lithography. For this, MAA EL10 was spin-coated (60 s at 4000 rpm) and dried at 100 °C for 60 s. A layer of PMMA was then spin-coated (60 s at 4000 rpm) on top of it and dried at 100 °C for 60 s. E-beam lithography was performed using a JEOL SEM controlled by a Raith e-beam setup. The sample was developed in a solution ethanol/methylisobutylketone (1:3 in volume) for 5 s, rinsed with ethanol and dried under nitrogen.

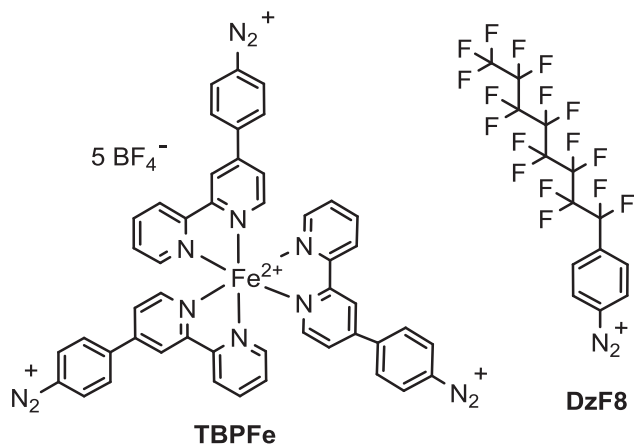


Fig. 1. Chemical structures of the tris-bipyridine iron(II) diazonium derivate (**TBPFe**) and the 4-heptadecafluorobenzene diazonium salt (**DzF8**).

1 nm of chromium and 20 nm of gold were evaporated under vacuum on the lithographed samples. Lift-off was performed in acetone using mild sonication. The sample was rinsed thoroughly with acetone then ethanol, and dried with nitrogen. The top contact electrodes for the electrical measurements were fabricated by optical lithography (using LOL2000/S1805 double layer resist). The resist was exposed to UV during 15 s through a mask. The sample was developed in Microposit MF-319 for 30 s, and rinsed thoroughly with water. The next step consists in evaporation under high vacuum of 10 nm of titanium then 50 nm of gold at $\pm 5^\circ$ using a MEB 450 e-gun PLASSYS. The final sample was then put in a solution of N-methyl pyrrolidone at 50 °C inside an ultrasonic bath for 3 min, rinsed thoroughly with acetone and ethanol, and dried with nitrogen.

2.2. ECG of diazonium salts

The diazonium salts **DzF8** and **TBPFe** were synthesized according to the literature.^{10,11} Electrografting was performed in a glove box in a setup depicted in Fig. 2. The solution concentration were 1 mM for **DzF8** and 28 μM for **TBPFe** in a tetrabutylammonium hexafluorophosphate/acetonitrile (TBAPF₆/ACN) electrolyte, except when the influence of the concentration was studied. Before grafting, the sample was washed by an ultrasonic treatment, 10 min in acetone and 10 min in ethanol, followed by drying with nitrogen. A homemade Teflon electrochemical cell was filled with the solution of the diazonium salt. The sample was then plunged in the cell and electrically connected with a tungsten tip fixed on a micro-manipulator (Fig. 2). The counter electrode was a platinum wire and the reference electrode was an Ag wire inside a solution of AgNO₃ at 10 mM in TBAPF₆/ACN electrolyte. The range of the cyclic voltammetry was -2 V to 1 V vs Ag/Ag⁺ at 50 mV/s for **TBPFe** and between -1 and 0 V at 50 mV/s for **DzF8**, both starting at open circuit voltage. To graft the molecules on patterned electrodes a three steps process was applied: (i) linear sweep voltammetry (LSV) at 50 mV/s from the open circuit voltage to the given potential, (ii) chronoamperometry (CA) at the given potential, (iii) LSV at 50 mV/s to 0 V. After grafting, the sample was washed again using an ultrasonic bath, 10 min in acetone followed by 10 min in ethanol, then dried with nitrogen flow.

2.3. Layer thickness measurements

Layer thickness measurements were performed by atomic force microscopy (AFM) with a PicoLE AFM by comparison between

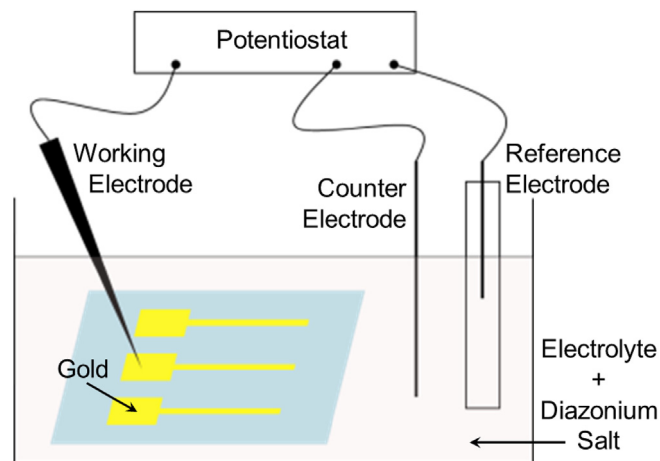


Fig. 2. Scheme of the ECG setup for the functionalization of patterned gold electrodes.

grafted and non-grafted electrode.

2.4. Electrical measurements

The electrical properties of the organic layers were measured in vacuum (10^{-3} mbar) in a Lakeshore TTP6 probe station using an Agilent 4156C Precision Semiconductor Parameter Analyzer with a detection limit in the sub-100 fA range.

3. Results and discussion

3.1. Electrochemical properties of diazonium salts

Cyclic voltammetry (CV) of the two (**TBPFe** and **DzF8**) molecules in TBAPF₆/ACN electrolyte on gold electrodes in a classic electrochemical cell was performed (Fig. 3) to study their ECG. Concerning **DzF8** (Fig. 3A), during the first reduction cycle, two irreversible peaks are observed at -0.07 V and -0.57 V. These peaks are associated with the reduction of the diazonium function. When the diazonium function (N_2^+) is reduced, it forms a radical that reacts at the beginning with the surface of the working electrode, and after on the already grafted layer to form a covalent bond. In literature, the presence of two peaks was tentatively ascribed to different effects: the reduction of the diazonium function on different crystalline orientation of gold [22], the pretreatment of the substrate [23] or two different reactions, one catalyzed and another uncatalyzed [24]. During the next cycle, the two reduction peaks can't be seen, and the current diminishes greatly, meaning that the layer formed is more and more insulating and that the reduction process of the **DzF8** is stopped. This result is coherent with the fact that **DzF8** layers were observed to be insulating [10].

CV of **TBPFe** (Fig. 3B) shows a very different behavior. During the first cycle, a peak around -0.30 V can barely be seen, which is attributed to the reduction of the diazonium part of **TBPFe**. Then, this peak vanishes and moves to lower potential for the next cycles, hidden by the other reduction peaks of the metal complexes. During the grafting, the intensity of all the peaks increases upon cycling, which shows that more and more active species are close to the gold electrode. Multiple reversible redox couples are present: one at $+0.76$ V corresponding to the reversible oxidation of the iron(II) core, and two at -1.57 V and -1.77 V corresponding to the successive reversible reduction of two bipyridine ligands. Two additional peaks: one starting from -1.00 V up to -1.29 V and the other from $+0.46$ V up to $+0.64$ V can also be seen on the CV. These two peaks, still under investigation and dependent on each other as previously shown on ruthenium complexes [25], can be attributed to charges trapped in the growing film or to the redox properties of

the various azo bonds that are formed during the formation of the layer.

Compared to **DzF8**, the intensity of all the peaks increases during the electrografting of **TBPFe** because charges can be exchanged between the working electrode and the solution thanks to the redox properties that allow the transmission of the charges [25]. Secondly, the quantity of active species that are oxidized or reduced increases during the cycles, potential indication of the formation of a thicker layer. Finally, the CV of electrografted electrodes used as a working electrode after washing and rinsing in acetonitrile containing 0.1 M TBAPF₆ shows the same peaks than the last cycle of the CV obtained during the electrografting (Fig. S1). It confirms that the redox properties of the metal complex are maintained in its electrografted form.

Thus, the two different diazonium salts with different electrochemical properties have been successfully grafted. The first one, **DzF8**, forms an insulating film and its grafting is self-limited. The second one, **TBPFe**, contains electrochemical active parts, which makes its grafting continuous. These properties have been then assessed on patterned electrodes.

3.2. Influence of the geometry of the electrodes on the thickness of electrografted **TBPFe**

TBPFe was grafted on patterned gold electrodes made by photolithography. The electrografting conditions used in the following part are described in the materials and methods part, with a CA time of 90 s at -1 V. The working electrode (Fig. 4A) is composed of different segments of different length with a width varying from $4 \mu\text{m}$ to $107 \mu\text{m}$. AFM measurements give the final layer thickness shown in Fig. 4B. The results show that the wider the electrode is, the thinner the average grafted layer. The AFM height-profile also reveals that the layer presents an edge effect: the layer is thicker near the edges of the electrode and thinner in the middle. This effect could be explained by the fact that the side of the electrode have access to a higher quantity of diazonium salts to be reduced, since the solution that is near this part and above the SiO₂ substrate can also provide diazonium salts. Both, the average thickness (evaluated in the middle of the grafted electrode by comparison with the height of the non-grafted reference electrodes) and the thickness of the edge effect increase when decreasing the width of the electrode. The relative intensity of the edge effect, shown in Fig. 4C, is approximately the same as the average thickness for the $107 \mu\text{m}$ width electrode and the $7 \mu\text{m}$ width. However, for the $4 \mu\text{m}$ width electrode, this effect is 35% of the average thickness of the grafted layer versus a 100% increase for larger electrodes. This means that after a critical width, the average

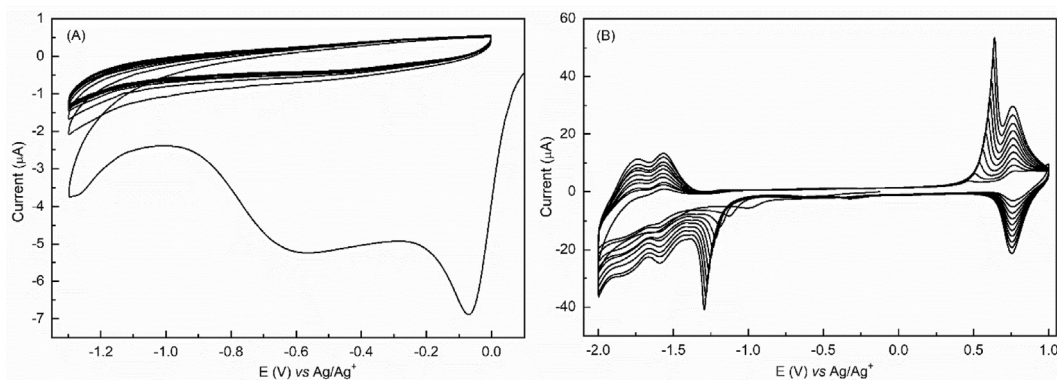


Fig. 3. CV at 50 mV/s of a solution of 1 mM **DzF8** (A) and 28 μM **TBPFe** (B) in 0.1M TBAPF₆ in ACN on gold.

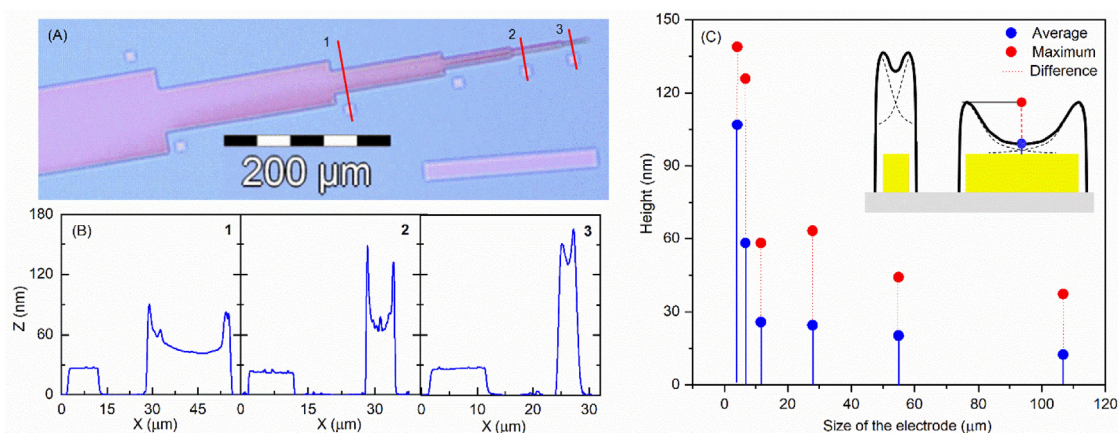


Fig. 4. (A) Optical microscope image of a **TBPF** electrografted electrode (CA -1 V 45 s with a non-passivated tip and $[C_{\text{TBPF}}] = 23\ \mu\text{M}$) and (B) profile along the red lines corresponding to an electrode width of $28\ \mu\text{m}$ (1), $7\ \mu\text{m}$ (2) and $4\ \mu\text{m}$ (3) respectively. (C) Results of the different layers' thickness and illustration of the impact of the edge effect (black curves) on the final thickness of the grafted **TBPF** layer (dotted black line) with the reduction of the width of the patterned gold electrode (yellow). (For interpretation of the references to colour in this figure legend, the reader is referred to the Web version of this article.)

height of the grafted layer continues to increase but the intensity of the edge effect is lower when the width of the electrode diminishes. One explanation could be the following: as seen in the profile in Fig. 4C, the edge effects have a sharp increase near the outer part of the electrode, and then have a slow decrease in the inner part of the electrode. When the electrode is thin enough, instead of being inexistent in the middle of it, the edge effects combine themselves to get a higher thickness in the middle and less “edge effect” on the outside, as shown in Fig. 4C.

In summary, the geometry of the electrode can drastically change the homogeneity and thus the final thickness of the layer of **TBPF**. Thus, in the following studies we fixed the width at $1\ \mu\text{m}$ (which is more relevant than large electrodes in the perspective of developing scaled electronic devices) to determine the keys parameters involved in the control of the film thickness and solve this edge effect issue.

3.3. Influence of ECG parameters on the thickness of electrografted diazonium salts

The impact of different parameters was evaluated in the following way: different electrodes of $1\ \mu\text{m}$ width on the same chip were grafted separately using various conditions such as concentration of the solution, time and potential of the chronoamperometry, state of the tip (see below), etc. An example of final results after **TBPF** electrografting using different potentials or different time of grafting are depicted in Fig. S2.

3.3.1. Influence of the diazonium concentration

The concentration of the diazonium active molecule on the final thickness of the grafted layer was first investigated. The grafting process was performed at -1 V vs Ag/Ag^+ for 120s. Fig. 5 displays the final thickness of **TBPF** (determined by AFM) as a function of the concentration of **TBPF** in solution. A sharp increase between $1\ \mu\text{M}$ and $15\ \mu\text{M}$ is observed. At higher concentrations (15 and $80\ \mu\text{M}$), the final thickness barely increases. This behavior can be due to the fact that when the solution is not concentrated enough, all the species near the electrode are reduced and then mostly react with the surface for grafting or with other molecules to form polymers in solution, which creates a local drop of concentration of the species in solution in the vicinity of the electrodes. In order to continue the grafting process, molecules need to diffuse from the solution to the electrochemical double layer where the complexes

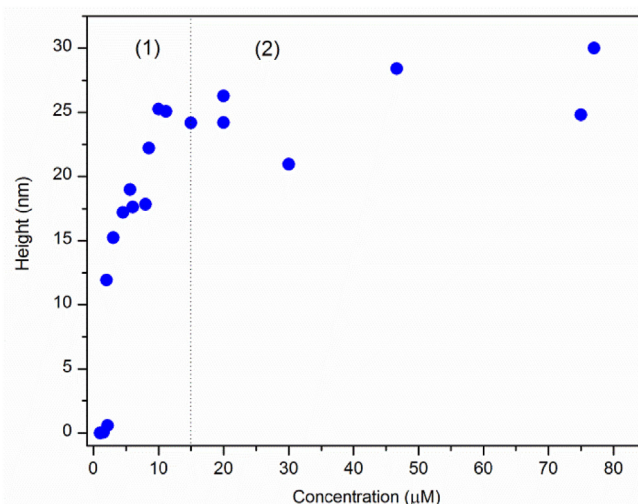


Fig. 5. Final thickness of an electrografted layer of **TBPF** versus the concentration of the active species in a solution of $0.1\ \text{M}$ **TBAPF**₆ in acetonitrile using a 120s CA at -1 V vs Ag/Ag^+ with a non-passivated tip. (1) Grafting limited by the local concentration of species; (2) Grafting not limited by the diffusion.

get reduced and grafted. When the concentration is too low, the process is then limited by the diffusion of **TBPF** in solution. When the concentration is high enough, the diffusion process is not the limiting factor, but the surface of the working electrode limits the quantity of the **TBPF** molecules that can be reduced.

On the other hand, the final thickness of **DzF8** grafted does not vary with the concentration of the diazonium salt in solution (Fig. S3) in the tested range (Note that at very low concentration, this parameter could play a role but thickness evolution in the sub-2nm range is both beyond our resolution and of limited relevance from a device perspective). The thickness is between 2 and 4 nm. The main difference with the **TBPF** grafting is that the grafting is self-limited. Whatever the concentration of the solution, the quantity of **DzF8** in solution near the working electrode is always sufficient to have the final thickness of the layer without needing the diffusion of the species after depletion of **DzF8** in the double layer, hence the fact that the concentration doesn't have any effect on the final thickness of the layer grafted.

In the following, a concentration of diazonium salts around

1 mM will be used for **DzF8**. Since the concentration of **TBPF** has a huge effect on its resulting layer, the concentration that will be used for the next studies is selected on the plateau, where a small variation of concentration would not impact the resulting thickness. Thus, a concentration of 28 μM of **TBPF** is used in the following.

3.3.2. Influence of the ECG potential

The influence of the potential of the CA on the final thickness of the grafted layer was then studied. The influence of the potential of the ECG on the final thickness of **TBPF** layers is shown Fig. 6. Between -0.8 V and -1.4 V , the average thickness of the layer as well as the edge effects, represented by the maximum thickness, increase. The first increase is due to the fact that a higher potential applied gives a higher current, meaning that more species are reduced during the same time, thus giving a thicker layer. In the same way, the increase of edge effects could be due to the fact that, at a higher potential, the local concentration of species to reduce diminishes, until this concentration is close to 0 in the direct vicinity of the electrode. The next molecules to be reduced need to diffuse from the solution to the surface of the electrode, which leads to the same behavior as the one observed above when studying the impact of concentration.

Below -1.4 V , the thickness decreases. At this potential the reduction of the ligands becomes possible and induces the formation of radical anions of metal complexes in the electrolyte. These radicals are able to decrease the resulting layer thickness as previously described [26,27].

The results of the grafting of **DzF8** at 1 mM versus the applied potential (Fig. 7B) show that the lower the potential is, the thicker the layer. The final thickness of the layers are lower than those with **TBPF** with a maximum thickness of 6 nm. The formed layers have no redox center and thus can't bring the electrons from the electrode to the surface. It means that during the layer's formation, the only electrons that can reduce new **DzF8** molecules in solution are the one that can pass through the formed layer by tunneling (a process that exponentially decreases with the layer thickness). Increasing the potential allows the electrons to have more energy to cross the tunneling barrier, which effectively lead to an increase of the thickness of the layer.

3.3.3. Influence of time

The influence of time on the final thickness of grafted **TBPF** layer is shown in Fig. 7. The concentration is set at 28 μM , and two grafting potentials are used: 1 V , since it seems the most promising due to the nearly nonexistent edge effects (Fig. 6A), and -1.2 V , to

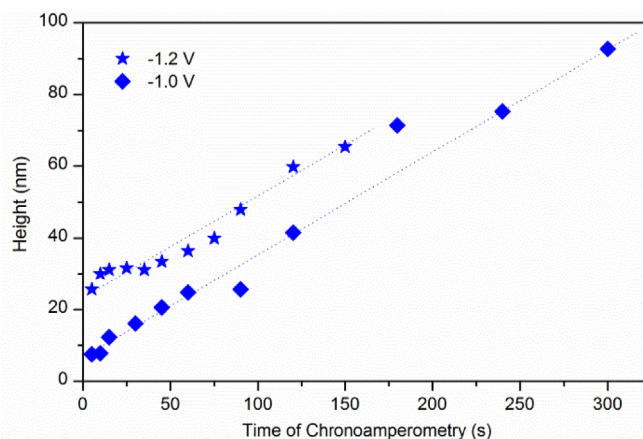


Fig. 7. Final thickness of an electrografted layer of **TBPF** versus time of the chronoamperometry at -1 V and -1.2 V in a solution of 0.1 M TBAPF₆ and 28 μM **TBPF** in acetonitrile with a non passivated tip.

see if the grafting can be performed faster at higher potential. The longer the CA is, the thicker the layer. Both curves have a similar slope (18.0 and 16.2 nm/min respectively), meaning that grafting at higher potential does not increase the grafting speed. In addition, it leads to a higher starting thickness (measured at the start of the CA step by extrapolating the obtained curves), which is around 5 nm for -1 V and 25 nm for -1.2 V , which is partially due to the fact that there is grafting between -1 V and -1.2 V during the LSV step. A fine control over the thickness of the **TBPF** grafted layer between 5 nm and nearly 100 nm on a 1 μm width gold electrode is obtained with a grafting potential of -1 V which constitute a major achievement of this study.

The influence of the time on the electrografting of **DzF8**, shown Fig. S4, is not surprising. All the thicknesses obtained between 10 s and 300 s of grafting are between 2.2 nm and 3.6 nm, which shows that the insulating layer is formed nearly instantly. Even with leaving the potential applied during longer time, the layer doesn't grow further.

These studies show how a good control over the growth of the **TBPF** can be obtained. Layers as thin as 5 nm or thicker than 50 nm can be obtained in a controlled manner only by changing the time of the procedure. On the other hand, **DzF8** layer's thickness can be controlled between 3 and 6 nm by changing the grafting potential, which illustrates the difference between the grafting of two different types of molecules.

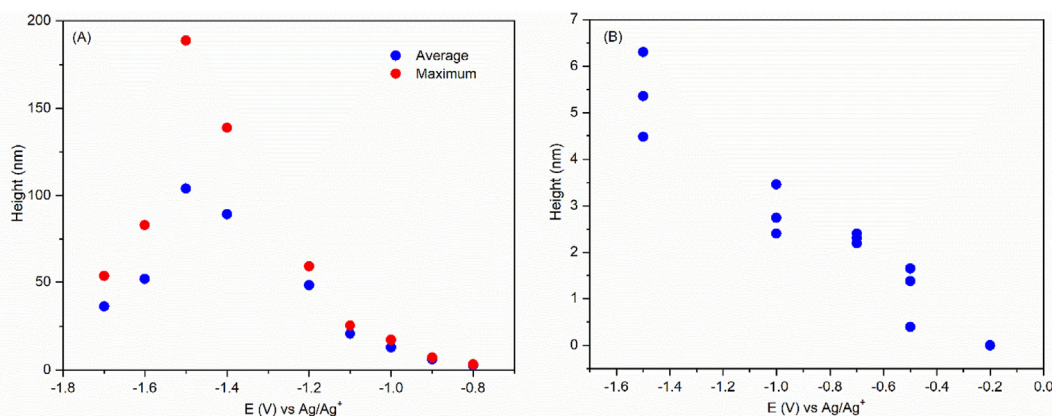


Fig. 6. Final thickness of the electrografted layer of **TBPF** (28 μM) (A) and **DzF8** (1 mM) (B), versus the potential applied during a 60s chronoamperometry in a solution of 0.1 M TBAPF₆ in acetonitrile with a non passivated tip.

3.3.4. Control over the edge effects of **TBPFe**

While a good control over the growth of the **TBPFe** layers was demonstrated in the previous parts, edge effects are still visible even at low potential, especially on samples that have a width of 8 μm . Further studies were conducted to solve this issue. First, electrografting using the best parameters determined above was performed: after the first LSV to -1 V vs Ag/Ag^+ , the potential used during the CA was -1 V vs Ag/Ag^+ during 20–280 s using a tungsten tip (see Fig. 2 Working Electrode) in a solution of **TBPFe** 28 μM in acetonitrile. To passivate the surface of the tungsten tip before the electrografting of the electrode of interest, the tip was soaked in the electrolyte, connected to a unpatterned gold electrode and electrografted with **TBPFe** by doing 10 CV cycles between -2 V and 1 V . The aim of this step is to passivate the body of the tip while letting the part in contact with the surface of the tip non-functionalized. This passivated tungsten tip was then used to electrograft **TBPFe** on patterned electrodes (Fig. S5). This experiment was done with a set of 24 samples, and each showed the edge effects that have been seen during the previous studies.

Another tip was electrografted with the insulating **DzF8** molecule by using a solution of 1 mM of **DzF8** and a gold sample using 10 CV between -1.3 V and 0 V vs Ag/Ag^+ . Then, the same study as above was conducted. The optical microscope images of the sample (Fig. 8A and Fig. S5) show that the layer is homogeneous and no edge effects are observed. Also, the resulting layer is homogenous on areas of more than $1000\text{ }\mu\text{m}^2$, such as seen in Fig. 8 where 130 μm of the electrode shows a homogeneous, smooth and defect-free surface at this scale.

When the final layer thicknesses using a passivated tip or a non-passivated tip are compared (Fig. S5), the results are similar. Thus, the tip has only an impact on the quality of the layer and its edge effect, but does not affect its average thickness. The reasons for this phenomenon are being investigated. This could be due to the fact that **TBPFe** passivated tip can generate radicals which would induce the edge effects, while the **DzF8** passivated tip does not since its only conducting part is the part where it is connected with the gold electrode, and thus no radical species are formed near the

tip. Another possible explanation involves the equilibration of electronic states of the tip and the substrate upon contact, which could lead to enhanced short time grafting with the non-passivated probe, leading to high edge effect. In any case, as the passivated probe removed the edge effect, we went further into the investigation to evaluate the extend of control we could achieve regarding electrografting.

Since the edge effects are solved, the impact of the size on the electrode on the final thickness of **TBPFe** grafted can be reassessed. The results are shown Fig. S6. Contrary to the previous results, the final thickness of the layer grafted varies between 15 and 28 nm for a 2 min grafting and 30–45 nm for a 5 min grafting for a width of the electrode between 2 and 73 μm . When compared to Fig. 4, the results for an electrode between 15 and 75 μm are similar for the grafting with a **DzF8** passivated tip and without one, if what is compared is the average of the grafted layer. However, with an electrode of width $<15\text{ }\mu\text{m}$, the grafting with a non-passivated tip shows a sharp increase up to a layer of 120 nm thickness (Fig. 4) when the width of the electrode diminishes. With a **DzF8** passivated tip, the thickness stays around 20 nm for a 2 min grafting. That means that the effect of the width of the electrode is solved by passivating the tip with the **DzF8**, an insulating molecule. That also confirms the fact that the 120 nm layer that is obtained with the first method is due to the stacking of the side effects from both sides of the electrode, increasing the average thickness of the layer grafted, as is illustrated in the scheme in the inset of Fig. 4.

These studies showed that a control of the electrografting of thin layers can be achieved. The layer is smooth and without defects when using classic surface characterization tools such as AFM and optical microscopy. In order to check their real potential in electronics and confirm their compactness, their electric properties were investigated.

3.4. Electrical measurements of the **DzF8** and **TBPFe** layers

Vertical devices using **TBPFe** or **DzF8** electrografted organic layers were fabricated using 8 μm as the width of the bottom

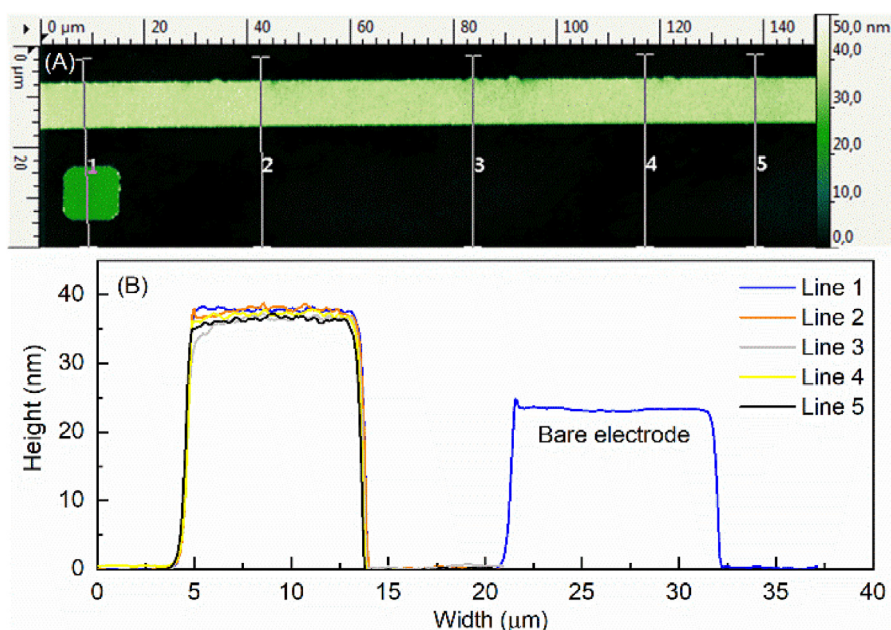


Fig. 8. (A) AFM image of a 150 μm part of an electrode grafted with **TBPFe** during a 120 s CA with a **DzF8** passivated tip at -1 V in a solution of 28 μM **TBPFe** and 0.1 M **TBAPF₆** in ACN and (B) its corresponding profiles.

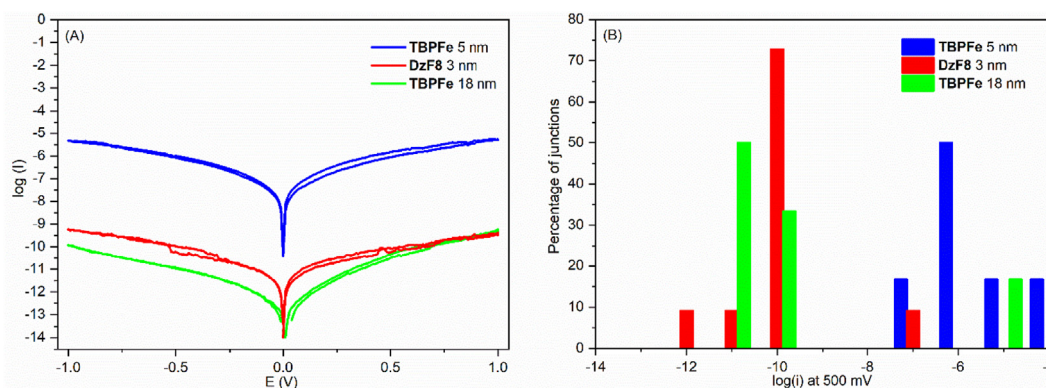


Fig. 9. (A) $\log(i)$ versus the potential applied for three selected junctions of $2000 \mu\text{m}^2$ and (B) statistics over the $\log(i)$ measured at 500 mV for various junctions.

electrodes. These electrodes are electrografted using the optimized parameters determined previously and the **DzF8** passivated tip. For **TBPF**, electrografting was performed during 10 s and 120 s to obtain 5 nm and 18 nm respectively (at -1 V vs Ag/Ag^+ in $28 \mu\text{M}$ **TBPF** in the $\text{TBAPF}_6/\text{ACN}$ electrolyte). For **DzF8**, electrografting was performed during 180 s at -1.3 V vs Ag/Ag^+ in 0.1 mM in the $\text{TBAPF}_6/\text{ACN}$ electrolyte, which leads to a 3 nm thick layer. Then, top electrodes composed of 10 nm of Ti and 50 nm of gold were evaporated on top through a mask made by photolithography (Fig. S7). The junction area was $2000 \mu\text{m}^2$. Electrical measurements were performed in vacuum. The results are shown in Fig. 9.

The current flowing through the layer is less than 0.1 nA at 500 mV for most of the devices constituted of a layer of **DzF8** 3 nm thick (red) or a layer of **TBPF** 18 nm thick (green). However, the devices made using a 5 nm thick layer of **TBPF** (blue) typically drive current four orders of magnitude higher (average current around $1 \mu\text{A}$ at 500 mV). The difference of conductivity between a **TBPF** layer and a **DzF8** layer of similar thickness can be explained since electrografting the **DzF8** is a self-limited process and thus creates a denser layer than the grafting of **TBPF**. The **TBPF** layer also shows electron transport in solution, meaning that the resulting layer of **TBPF** is more likely to conduct electrons in the solid state. Also, the $\log(i)$ versus V of all junctions are stable and does not show any abnormal behavior (memory or breakdown effects for example) during the measurements in this bias range, excepted for the moderate hysteresis displayed in Fig. 9A.

Only few junctions show current leakage. Less than 15% of the **TBPF** 18 nm junctions and **DzF8** 3 nm junctions have an intensity 5 decades higher than their average, which can be attributed to the current leaking through the layer, probably through a defect. However, as Fig. 8 shows, even on more than $130 \mu\text{m}$ of one electrode, no defects or holes on the electrografted layer can be found at the micron scale. This means that by fabricating scaled-down devices of reduced area, the current leakage ratio is reduced.

These results show that the conducting behavior of the electrografted layer can be controlled both by changing the thickness (5 nm **TBPF** versus 18 nm **TBPF**) and/or changing its nature (**TBPF** versus **DzF8**). These layers can be used on vertical metal-molecules-metal junctions of large area of contact, here $2000 \mu\text{m}^2$.

4. Conclusion

In this article, we showed that electrochemical grafting of diazonium salts can be controlled to obtain different grafted layer thickness. On one hand, ECG of **TBPF**, a redox active molecule, can be controlled by changing the time of the chronoamperometry and fixing the concentration of the solution and the potential of the

chronoamperometry, and lead to accurately tuned thickness of grafted layers between 5 and 100 nm. On the other hand, **DzF8**, a molecule without redox properties except from its diazonium part, can be grafted and yields layer thickness of 3–6 nm by controlling the potential applied during the ECG. This technique is particularly adapted to functionalize patterned electrodes and keep the properties of the molecule used, which show great promises for future use in electronics or sensors. The optimization of the grafting was further studied by changing the experimental conditions. Thanks to that, smooth edge-less layers of **TBPF** can be grafted over very large areas. However the final thickness is highly dependent of the geometry and the size of the patterned electrodes.

After optimizing the grafting of the two diazonium molecules, large areas of vertical metal-molecule-metal junctions have been successfully fabricated. In these devices, less than 15% of each type showed short-circuit for a surface of $2000 \mu\text{m}^2$.

Notes

The authors declare no competing financial interest.

Acknowledgment

This work was supported by the French National Research Agency (REMIND project – ANR-15-CE09-0001). The authors thank Olivier Segut, Laure Fillaud, Théo Cabaret, Hugo Casademont and Yu-Pu Lin for the initial developments of the setup and protocols.

Appendix A. Supplementary data

Supplementary data to this article can be found online at <https://doi.org/10.1016/j.electacta.2019.06.115>.

References

- [1] J.C. Love, L.A. Estroff, J.K. Kriebel, R.G. Nuzzo, G.M. Whitesides, Self-Assembled monolayers of thiolates on metals as a form of nanotechnology, *Chem. Rev.* 105 (2005) 1103–1170.
- [2] H. Haick, O. Niiitsoo, J. Ghabboun, D. Cahen, Electrical contacts to organic molecular films by metal evaporation: effect of contacting details, *J. Phys. Chem. C* 111 (2007) 2318–2329.
- [3] Y. Tai, A. Shaporenko, W. Eck, M. Grunze, M. Zharnikov, Abrupt change in the structure of self-assembled monolayers upon metal evaporation, *Appl. Phys. Lett.* 85 (2004) 6257–6259.
- [4] W. Chen, X. Liu, Z. Tan, K.K. Likharev, J.E. Lukens, Fabrication and characterization of novel cross point structures for molecular electronic integrated circuits, *J. Vac. Sci. Technol., B: Microelectron. Nanometer Struct.–Process., Meas., Phenom.* 24 (2006) 3217–3220.
- [5] A. Vilan, A. Shanzler, D. Cahen, Molecular control over Au/GaAs diodes, *Nature* 404 (2000) 166.
- [6] Y. Selzer, D. Cahen, Fine tuning of Au/SiO₂/Si diodes by varying interfacial

- dipoles using molecular monolayers, *Adv. Mater.* 13 (2001) 508–511.
- [7] Y.-L. Loo, D.V. Lang, J.A. Rogers, J.W.P. Hsu, Electrical contacts to molecular layers by nanotransfer printing, *Nano Lett.* 3 (2003) 913–917.
- [8] A. Bayat, J.-C. Lacroix, R.L. McCreery, Control of electronic symmetry and rectification through energy level variations in bilayer molecular junctions, *J. Am. Chem. Soc.* 138 (2016) 12287–12296.
- [9] V. Rabache, J. Chaste, P. Petit, M.L. Della Rocca, P. Martin, J.-C. Lacroix, R.L. McCreery, P. Lafarge, Direct observation of large quantum interference effect in anthraquinone solid-state junctions, *J. Am. Chem. Soc.* 135 (2013) 10218–10221.
- [10] H. Casademont, L. Fillaud, X. Lefèvre, B. Jousset, V. Derycke, Electrografted fluorinated organic ultrathin film as efficient gate dielectric in MoS₂ transistors, *J. Phys. Chem. C* 120 (2016) 9506–9510.
- [11] Y.-P. Lin, C.H. Bennett, T. Cabaret, D. Vodenicarevic, D. Chabi, D. Querlioz, B. Jousset, V. Derycke, J.-O. Klein, Physical realization of a supervised learning system built with organic memristive synapses, *Sci. Rep.* 6 (2016) 31932.
- [12] D. Bélanger, J. Pinson, Electrografting: A powerful method for surface modification, *Chem. Soc. Rev.* 40 (2011) 3995–4048.
- [13] G. Lecayon, Y. Bouizem, C. Le Gressus, C. Reynaud, C. Boiziau, C. Juret, Grafting and growing mechanisms of polymerised organic films onto metallic surfaces, *Chem. Phys. Lett.* 91 (1982) 506–510.
- [14] S. Cuenot, S. Gabriel, C. Jérôme, R. Jérôme, A.-S. Duwez, Are electrografted polymers chemisorbed or physisorbed onto their substrate? *Macromol. Chem. Phys.* 206 (2005) 1216–1220.
- [15] J. Charlier, S. Ameer, J.P. Bourgoin, C. Bureau, S. Palacin, Mask-free localized grafting of organic polymers at the micrometer or submicrometer scale on composite conductors or semiconductor substrates, *Adv. Funct. Mater.* 14 (2004) 125–132.
- [16] C. Combellas, F. Kanoufi, S. Nunige, Surface modification of halogenated polymers. 10. Redox catalysis induction of the polymerization of vinylic monomers. Application to the localized graft copolymerization of poly(-tetrafluoroethylene) surfaces by vinylic monomers, *Chem. Mater.* 19 (2007) 3830–3839.
- [17] P. Doppelt, G. Hallais, J. Pinson, F. Podvorica, S. Verneyre, Surface modification of conducting substrates. Existence of azo bonds in the structure of organic layers obtained from diazonium salts, *Chem. Mater.* 19 (2007) 4570–4575.
- [18] M. Ceccato, A. Bousquet, M. Hinge, S.U. Pedersen, K. Daasbjerg, Using a mediating effect in the electroreduction of aryldiazonium salts to prepare conducting organic films of high thickness, *Chem. Mater.* 23 (2011) 1551–1557.
- [19] F. Anariba, S.H. DuVall, R.L. McCreery, Mono- and multilayer formation by diazonium reduction on carbon surfaces monitored with atomic force microscopy "Scratching", *Anal. Chem.* 75 (2003) 3837–3844.
- [20] J. Pinson, F. Podvorica, Attachment of organic layers to conductive or semi-conductive surfaces by reduction of diazonium salts, *Chem. Soc. Rev.* 34 (2005) 429–439.
- [21] P. Allongue, M. Delamar, B. Desbat, O. Fagebaume, R. Hitmi, J. Pinson, J.-M. Savéant, Covalent modification of carbon surfaces by aryl radicals generated from the electrochemical reduction of diazonium salts, *J. Am. Chem. Soc.* 119 (1997) 201–207.
- [22] A. Benedetto, M. Balog, P. Viel, F. Le Derf, M. Sallé, S. Palacin, Electro-reduction of diazonium salts on gold: Why do we observe multi-peaks? *Electrochim. Acta* 53 (2008) 7117–7122.
- [23] L. Lee, P.A. Brooksby, P. Hapiot, A.J. Downard, Electrografting of 4-nitrobenzenediazonium ion at carbon electrodes: Catalyzed and uncatalyzed reduction processes, *Langmuir* 32 (2016) 468–476.
- [24] K.K. Cline, L. Baxter, D. Lockwood, R. Saylor, A. Stalzer, Nonaqueous synthesis and reduction of diazonium ions (without isolation) to modify glassy carbon electrodes using mild electrografting conditions, *J. Electroanal. Chem.* 633 (2009) 283–290.
- [25] B. Jousset, G. Bidan, M. Billon, C. Goyer, Y. Kervella, S. Guillerez, E.A. Hamad, C. Goze-Bac, J.-Y. Mevellec, S. Lefrant, One-step electrochemical modification of carbon nanotubes by ruthenium complexes via new diazonium salts, *J. Electroanal. Chem.* 621 (2008) 277–285.
- [26] T. Menanteau, E. Levillain, A.J. Downard, T. Breton, Evidence of monolayer formation via diazonium grafting with a radical scavenger: Electrochemical, AFM and XPS monitoring, *Phys. Chem. Chem. Phys.* 17 (2015) 13137–13142.
- [27] L. Pichereau, I. López, M. Cesbron, S. Dabos-Seignon, C. Gautier, T. Breton, Controlled diazonium electrografting driven by overpotential reduction: A general strategy to prepare ultrathin layers, *Chem. Commun.* 55 (2019) 455–457.

Titre : Nano-composants à base de films minces organiques électrogreffés : Fabrication, caractérisation, étude du transport électronique et intégration

Mots clés : Electrochimie, sels de diazonium, électronique moléculaire, films minces, transistors

Résumé : Le principal objectif de cette thèse est de montrer le potentiel pour l'électronique organique de films moléculaires minces liés de façon covalente au substrat et déposés par greffage électrochimique. Ces couches organiques de 5 à 100 nm d'épaisseur visent à proposer une alternative aux films minces organiques d'épaisseur supérieure à 100 nm et aux couches mono-moléculaires autoassemblées d'épaisseur comprise entre 1 et 5 nm.

Ce travail a d'abord permis d'établir les conditions optimales de greffage de trois différents sels de diazonium : un dérivé de la tris-bipyridine fer (II), un sel de diazonium comportant une longue chaîne fluorée et un autre comportant une fonction thiol. En particulier, un contrôle fin de l'épaisseur des films est démontré sur des électrodes patternées micrométriques adaptées à la réalisation de dispositifs.

L'électrogreffage de doubles couches est ensuite étudié. Il consiste à utiliser une électrode électrogreffée par des molécule électroactives, ici le dérivé de la tris-bipyridine fer (II), comme électrode de travail

pour l'électrogreffage d'un second sel de diazonium. Cette technique permet de former des couches organiques d'épaisseur contrôlée par la première couche et présentant des fonctions terminales contrôlées par le choix du second composé (ici, fonctions thiols ou chaînes fluorées). L'intérêt de ces couches fonctionnelles est ensuite évalué dans des jonctions verticales métal-molécules-métal utilisant différents types d'électrodes supérieures : des électrodes imprimées à partir d'une solution de nanoparticules d'or, suivant un procédé élaboré dans cette thèse, et des électrodes fabriquées à partir de métaux évaporés sous vide. Enfin, des transistors à base de MoS₂ utilisant 30 nm de ces couches greffées comme diélectrique de grille sont fabriqués et étudiés. Leurs performances (mobilité électronique de 46 cm².(V.s)⁻¹, rapport I_{ON}/I_{OFF} de 9.10⁷, etc.) confirment la qualité de ces isolants organiques électrogreffés. La méthode s'avère ainsi efficace et versatile pour la préparation de couches organiques robustes d'épaisseur contrôlée et aux propriétés de surface ajustables.

Title: Organic electrografted thin films based nano-devices

Keywords: Electrochemistry, diazonium salts, molecular electronic, thin films, field-effect transistors

Abstract: The main objective of this PhD thesis is to show the potential for organic electronics of molecular thin films covalently bounded and formed by electrochemical grafting. These 5 to 100 nm thick layers aim to propose an alternative to organic thin films of thickness above 100 nm and to self-assembled monolayers of thickness between 1 and 5 nm.

This work first establishes the optimal electrografting conditions of three diazonium salts : a derivative from the tris-bipyridine iron (II), a diazonium salt with a long fluorinated chain and another with a thiol function). In particular, a fine tuning of the thickness of the resulting layers is demonstrated on micrometric patterned electrodes.

Double layer electrografting is then studied. It consists in using an electrode electrografted with electroactive molecules, here the tris-bipyridine iron (II) derivative, as a working electrode for the electrografting of a sec-

ond diazonium salt. This technique allows the formation of organic double-layers of thickness controlled by the first layer and presenting terminal functions controlled by the choice of the second compound (here, thiol functions or fluorinated chains).

The potential of these layers is then evaluated in vertical metal-molecules-metal junctions using various top electrodes : electrodes printed from an aqueous gold nanoparticle ink through a method developed in this thesis, and electrodes made by metal evaporation in vacuum. To conclude, field-effect transistors based on MoS₂ using these electrografted thin layers as gate-dielectric are fabricated and studied. Their performances (electronic mobility of 46 cm².(V.s)⁻¹, I_{ON}/I_{OFF} ratio of 9.10⁷, etc.) confirm the quality of these organic electrografted insulators. The method is thus efficient and versatile for the preparation of robust organic layers with adjustable surface properties and thickness.

